

Open Research Online

The Open University's repository of research publications and other research outputs

pH Regulatory Molecules In The Tumour Microenvironment: Modulators Of Aggressiveness And Immune Profile Of Human Hepatocellular Carcinoma

Thesis

How to cite:

Tuccitto, Alessandra (2018). pH Regulatory Molecules In The Tumour Microenvironment: Modulators Of Aggressiveness And Immune Profile Of Human Hepatocellular Carcinoma. PhD thesis The Open University.

For guidance on citations see [FAQs](#).

© 2018 The Author

Version: Version of Record

Copyright and Moral Rights for the articles on this site are retained by the individual authors and/or other copyright owners. For more information on Open Research Online's data [policy](#) on reuse of materials please consult the policies page.

oro.open.ac.uk



FONDAZIONE IRCCS
ISTITUTO NAZIONALE
DEI TUMORI



Alessandra Tuccitto

Degree in Biological Sciences

OU personal identifier: E4142132

**pH regulatory molecules in the tumour microenvironment: modulators
of aggressiveness and immune profile of human hepatocellular
carcinoma**

Thesis presented for the Degree of Doctor of Philosophy

The Open University, Milton Keynes (UK)

Faculty of Science Technology Engineering and Mathematics (STEM)

School of Life, Health and Chemical Sciences

Date of submission: May 2018

Affiliated Research Centre:

Fondazione IRCCS Istituto Nazionale dei Tumori, Milan (Italy)

Director of studies: Dr. Chiara Castelli

Internal supervisor: Dr. Chiara Castelli

External supervisor: Prof. Malcolm Ronald Alison

Table of contents

Abstract	1
1.Introduction and aims of the study	
1.1.1 Metabolism and cancer	4
1.1.2 The Warburg effect	4
1.1.3 Metabolic reprogramming	6
1.1.4 Hypoxia, acidity and cancer metabolism	8
1.1.5 Hypoxia, acidity are pro-tumorigenic: influence on tumour aggressiveness and immunosuppression	10
1.1.5.1 Proliferation, invasion and metastasis	12
1.1.5.2 Epithelial-to-mesenchymal transition (EMT) and cancer stem cells (CSCs)	13
1.1.5.3 Macrophages and tumour-associated macrophages (TAMs)	14
1.1.5.4 Myeloid-derived suppressor cells (MDSCs)	15
1.1.5.5 Regulatory T cells (Tregs)	16
1.2 Hepatocellular carcinoma: role of hypoxia, immunosuppression, cancer stem cells in the biology of the tumour	17
1.2.1 Hepatocellular carcinoma (HCC)	17
1.2.2 Chronic inflammation and HCC	19
1.2.3 Molecular mechanisms and pathogenesis of HCC	21
1.2.4 Stem cells and cancer stem cells in HCC	22
1.2.5 Hypoxia as metabolic condition in HCC affecting immune infiltrating cells	25
1.3 pH regulatory molecules as therapeutic strategy for hypoxic and acidic microenvironment	30
1.3.1 V-ATPase complex	31

1.3.2 Carbonic anhydrase IX and XII	36
1.4 Aims od the study	40
2. Materials and Methods	
2.1 <i>Ex vivo</i> experiments	42
2.1.1 Ethical statement	42
2.1.2 Patients, tissue samples and clinical data	42
2.1.3 HCC tissue explants: generation and treatment	43
2.1.4 RNA extraction, reverse transcription, pre-amplification and quantitative real-time PCR on HCC tissues	43
2.1.5 Immunohistochemistry analysis on HCC tissues	49
2.1.6 Confocal microscopy analysis on HCC tissues	53
2.1.7 Single-cell suspensions from HCC tissues	55
2.1.7.1 Multiparametric flow cytometry on single cell-suspensions from HCC tissues	55
2.1.8 Generation of the index score	58
2.2 <i>In vitro</i> experiments	59
2.2.1 Cell lines and culture conditions	59
2.2.2 RNA extraction, reverse transcription and quantitative real-time PCR on HCC cell lines	60
2.2.3 Western blotting on HCC cell lines	60
2.2.4 Flow cytometry on HCC cell lines	61
2.2.5 Pharmacological inhibitors and cell viability assay	62
2.2.6 Cell proliferation assay	65
2.2.7 Apoptosis assays	65
2.2.8 Necrosis assay	66
2.2.9 Confocal microscopy analysis on HCC cell lines	66

2.3 Statistical analysis	67
3, 4, 5 and 6. Results and Discussion	
3. pH regulatory molecules, intrinsic features and aggressiveness of HCC	68
3.1 mRNA expression of pH regulators in HCC patients	69
3.2 Evaluation of genes related to HCC aggressiveness in HCC patients	78
3.3 Correlation between pH regulators and genes related to HCC aggressiveness	81
3.4 The development of a prognostic index score	85
4. Expression of pH regulatory molecules at the tumour site: IHC analysis	96
4.1 Protein expression of CAs in HCC patients	97
4.2 Protein expression of V-ATPase in HCC patients	101
5. pH regulators as a target for pharmacological intervention in HCC: <i>in vitro</i> data	108
5.1 <i>In vitro</i> characterisation of CAs in HCC cell lines	108
5.2 <i>In vitro</i> characterisation of V-ATPase in HCC cell lines	115
5.3 Effect of pH regulatory molecule inhibitors on the cell viability of HCC cell lines	116
5.4 Mechanisms of cell death induced by pH regulatory molecule inhibitors	120
6. V-ATPase as modulator of the tumour microenvironment	130
6.1 Expression of V-ATPase in the immune components of the HCC microenvironment	131
6.2 In the tumour microenvironment, V-ATPase inhibition modulated cancer and immune cell features: <i>ex vivo</i> analysis	135
7. General Discussion	
7.1 Overall summary	142

7.2 Conclusions	147
7.3 Future perspectives	149
References	152
List of abbreviations	169
List of figures	176
List of tables	179
Publications	180
Acknowledgements	181
Appendix	182

Abstract

Background: Hepatocellular carcinoma (HCC) arises in an inflammatory, hypoxic/acidic microenvironment that favours tumour progression and fosters immunosuppression. Tumour cells survive this hostile environment by over-expressing pH regulatory molecules such as carbonic anhydrase (CA) IX, XII and V-ATPase complex, but the relevance of these molecules in HCC is poorly defined.

Aim: The aim of this study was to dissect the relationships between pH regulatory molecules and the aggressive behaviour of malignant hepatocytes, and to evaluate how pH regulatory molecules influence the immune microenvironment of HCC.

Methods: HCC, non-tumour and normal liver tissue samples were analysed by qRT-PCR for the expression of genes encoding the pH regulatory molecules (CAIX, CAXII and V-ATPase), of genes associated to epithelial-to-mesenchymal-transition (EMT) (*TWIST*, *CDH1*, *VIM*) and those encoding for HCC stem cell-associated markers (*CD13*, *CD24*, *CD44*, *CD90*, *EpCAM*, *CD133*, *KRT19*, *OCT4*, *NANOG* and *SOX2*). Selected HCC, non-tumour and normal liver tissue samples were evaluated by immunohistochemistry (IHC) to detect the presence and localization of CAIX, CAXII and V-ATPase and to assess the distribution of macrophages and T cells. Confocal microscopy and flow cytometry were implemented to assess the co-expression of selected markers. HCC cell lines, characterised for the expression of pH regulators, were tested for the sensitivity to the CAIX, CAXII, and V-ATPase specific inhibitors. The effects of V-ATPase specific drug were also studied *ex vivo* in primary human HCC tumour explants by qRT-PCR and by flow cytometry in

HCC single cell suspensions obtained by the enzymatic digestion of HCC specimens.

Results: Our mRNA analysis showed that the expression of CA9 was significantly correlated with the expression of the hypoxia-inducible factor 1 α -related gene (*HIF1A*) and of the stem cell-associated markers CD24, CD133, EpCAM and KRT19. Moreover, mRNA for CA9 and for the different CA12 isoforms were associated with tumour grading, thus indicating their possible role in tumour malignancy. Applying a machine learning tool known as the 'Adaptive Index Model' the combined expression of different CA12 isoforms, *CD209* and *CDH1* defined a 'signature' classifying HCC patients in groups at different risk of recurrence, thus indicating a link between pH regulators, myeloid and EMT markers likely influencing HCC prognosis. IHC analysis indicated that HCC displays a complex expression pattern for the pH regulatory proteins. Both CAIX and CAXII were detected in transformed, but not in normal hepatocytes. CAIX protein had a focal distribution in the tumour, thus supporting its possible association with hypoxic and the most aggressive tumour area. Conversely, CAXII was homogeneously expressed by all tumour hepatocytes, but mainly retained in the endoplasmic reticulum (ER). The majority of HCC expressed V-ATPase which, importantly, was also present in immune infiltrating cells. This expression pattern qualified the CAIX, CAXII and V-ATPase as possible targetable molecules. Our *in vitro* data indicated that blockage of their enzymatic activities by specific drugs affected the viability of HCC cell lines in a dose dependent fashion, although with the CAXII specific inhibitor showing low efficacy, likely related to the preferential ER localization of CAXII molecules inside the HCC cells.

Ex vivo experiments with HCC tissue explants and HCC cellular suspensions showed that inhibition of V-ATPase modulated the epithelial/mesenchymal features of HCC cells and the levels of pro- and anti-tumour cytokines expressed by M2 macrophages and T cells infiltrating HCC.

Conclusions: Herein, our data demonstrated that the pH regulatory molecules, CAIX, CAXII and V-ATPase are over expressed in the HCC microenvironment and interfering with their pathways exerted anti-tumour activities, although these data also lead to the conclusion that more effective CAXII specific drugs should be designed. The results of this thesis also suggest that pH regulatory molecules might have a role in HCC aggressiveness and prognosis. Importantly, one of these pH regulators, namely V-ATPase complex, influences the mesenchymal features of tumour cells and the immunosuppressive tumour microenvironment (TME). Interfering with tumour metabolism is an emerging strategy for treating cancers that are resistant to standard therapies. Thus, targeting the unique crosstalk between tumour cells and the microenvironment, played by the pH regulatory molecules, can be considered as a new option for HCC treatment and the blockage of the V-ATPase complex might represent a multi-task strategy for the treatment of HCC patients.

1. Introduction

1.1.1 Metabolism and cancer

Metabolism can be described as series of chemical reactions at a cellular level aimed at converting fuel into energy to carry out cellular processes within a living cell. In metabolism, complex organic molecules (such as polysaccharides, lipids, nucleic acids and proteins) are broken down into smaller units that are either oxidized to release energy (catabolism) or used in anabolic reactions that construct complex molecules from smaller units (such as monosaccharides, fatty acids, nucleotides, and amino acids) using energy (anabolism). Monosaccharides, fatty acids and amino acids are transformed into acetyl-Coenzyme A (acetyl-CoA), which is used in the mitochondrial tricarboxylic acid (TCA) cycle releasing carbon dioxide (CO₂). During cellular respiration, the electrons removed from organic molecules in the oxidative reactions are transferred to oxygen through a series of enzymes associated with the electron transport chain of the oxidative phosphorylation. The energy released by electron transport is used to make adenosine triphosphate (ATP) coupled with the production of protons (H⁺). The produced ATP is then used both in the catabolic and anabolic reactions, being also a precursor for DNA and RNA synthesis. Normal differentiated tissues, proliferating tissues and cancer cells differ in their metabolic pathways [1].

1.1.2 The Warburg effect

In the presence of oxygen (O₂), normal differentiated cells mainly rely on oxidative phosphorylation for their energy production. Glucose is first

metabolized to pyruvate *via* glycolysis and most of it is then completely oxidized to CO₂ in the mitochondria during the TCA cycle. This is a highly efficient process, which produces 36 mol ATP per mol glucose. Only in the absence of oxygen, the normal differentiated cells skip the mitochondrial oxidative phosphorylation of pyruvate which instead is fully converted into lactate through anaerobic glycolysis, although with minimal ATP production of 2 mol ATP per glucose molecule. In 1924 Otto Warburg discovered that proliferative cells and cancer cells generate energy mainly using aerobic glycolysis and, despite the presence of O₂, most of the pyruvate (about 85%) is converted into lactate. With only a minor fraction of pyruvate entering the TCA cycle, the energy efficiency is that of 4 mol ATP production per glucose molecule. Afterwards, “the Warburg effect” is the enhanced conversion of glucose to lactate even in the presence of normal levels of O₂ [1]. The Warburg effect is summarised in Figure 1.1.2.

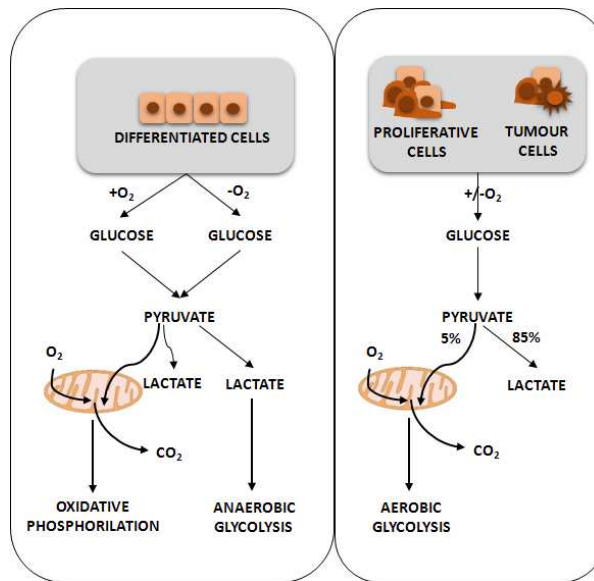


Figure 1.1.2. Schematic representation of oxidative phosphorylation, anaerobic glycolysis, and aerobic glycolysis (Warburg effect) in differentiated tissue, proliferating tissue and tumour. Differentiated tissues use oxidative phosphorylation to metabolize glucose to pyruvate and carbonic dioxide (CO₂) in the mitochondria in the presence of oxygen (O₂). In limiting O₂ conditions, differentiated tissues convert the pyruvate into lactate by anaerobic glycolysis, without the participation of the mitochondria. Proliferative and tumour tissues mainly convert pyruvate into lactate even in the presence of normal levels of O₂ through aerobic glycolysis. This phenomenon is known as the Warburg effect. *This figure is taken from reference [1].*

This metabolic reprogramming is as a hallmark of cancer [1] and it is directly linked to the presence of activated oncogenes and inactivated tumour suppressors in cancer cells. Thus, aberrant cancer metabolism certainly results from the intrinsic genetic features of cancer cells. The influence of oncogene driven pathways on cellular metabolism is discussed in the following paragraph.

1.1.3 Metabolic reprogramming

Among the different signaling pathways altered in cancer cells, PI3K/Akt/mTOR/mTORC1 and Myc pathways have been shown to be

important regulators of carbohydrate, lipid, protein and amino acid metabolism in several tumours. Specifically, PI3K/Akt controls the uptake of glucose increasing the expression of the glucose transporter (GLUT1) on the cell surface. Akt is involved in the conversion of citrate into acetyl-CoA which is used for lipid synthesis, while protein synthesis is enhanced by mTORC1, a downstream molecule of the PI3K/Akt pathway. Moreover, Myc is linked to lactate production through the increased expression of lactate dehydrogenase A (LDHA), and it is involved in the promotion of glutamine uptake and in the conversion of glutamine into acetyl-CoA in the mitochondria [2, 3]. The PI3K/Akt/mTOR and Myc pathways are involved in the constitutive activation of hypoxia-inducible factor 1 α (HIF-1 α), the master regulator of the hypoxic response. Under normoxic conditions, the activation of PI3K/Akt/mTOR signaling stimulates protein synthesis of HIF-1 α [4], while Myc induces the stabilization of HIF-1 α and the transcription of enzymes involved in the glycolysis [5]. The reprogramming of cancer metabolism is schematised in the Figure 1.1.3.

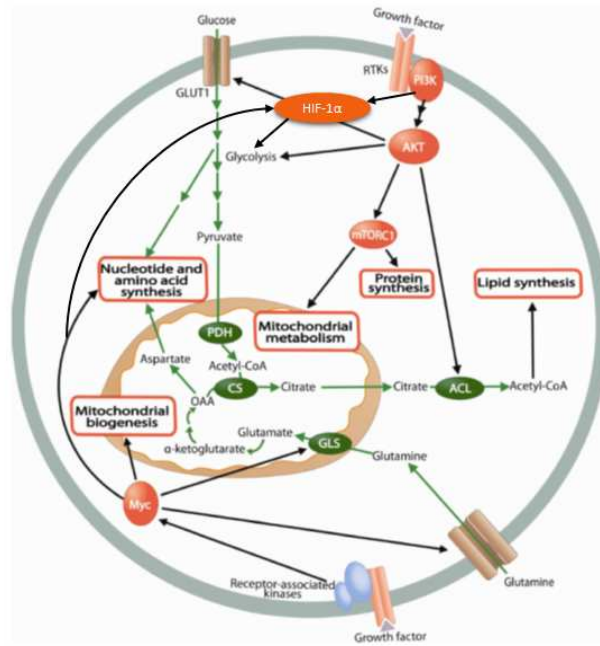


Figure 1.1.3. Signaling pathways and oncogenes involved in the metabolic reprogramming of cancer cells. PI3K/Akt pathway is responsible for the increased glycolysis. Akt regulates lipid synthesis through the conversion of citrate into acetyl-CoA. Protein synthesis is regulated by mTORC1. PI3K stimulates the synthesis of HIF-1 α that activates glycolytic genes. HIF-1 α and dysregulated Myc promote glycolysis. The conversion of glutamine to glutamate involves Myc. *This figure is taken from reference [2].*

The stabilization of HIF-1 α can be also mediated by the establishment of hypoxic conditions due to the fast proliferation of cancer cells [6]. This will be discussed in the next paragraph.

1.1.4 Hypoxia, acidity and cancer metabolism

During tumour development, cancer cells proliferate rapidly, oxygen and nutrients supplied from normal vasculature are not sufficient to support their high metabolic rate and low O₂ availability (hypoxia) characterises fast growing tumours. The hypoxic tumour cells release angiogenic factors that drive the formation of new vasculature in a process known as angiogenesis. The new vessels are not well organised and are not very functional, thus they contribute to exacerbate the already existent hypoxia at the tumour site. The

low O_2 tension induces the stabilization of HIFs through the inactivation of a family of HIF prolyl hydroxylases (PHDs) [7]. Hypoxia restricts oxidative phosphorylation, thus hypoxia further pushes the tumour cell metabolism toward the conversion of pyruvate to lactate in an O_2 independent manner. The production of lactate, CO_2 and H^+ during the metabolic reactions are the main causes of acidity in the tumour. The large amounts of acidic metabolites increase intracellular and extracellular acidosis that is associated with changes in intracellular pH (pHi) and extracellular pH (pHe). The optimal pHi for cell proliferation in tissues is around 7.4, but it decreases when cells are exposed to metabolic acidosis. To maintain neutral pHi cancer cells overexpress several types of pH regulators that will be discussed in detail in chapter 1.3 of this thesis. The pH regulators are responsible for extruding acid metabolites out of the cells, thus establishing an acidic extracellular microenvironment. The acidic and hypoxic microenvironment supports the pro-tumourigenic functions of cancer cells and cells composing the TME [8]. The following paragraph will examine the effect of acidity and hypoxia at the tumour site.

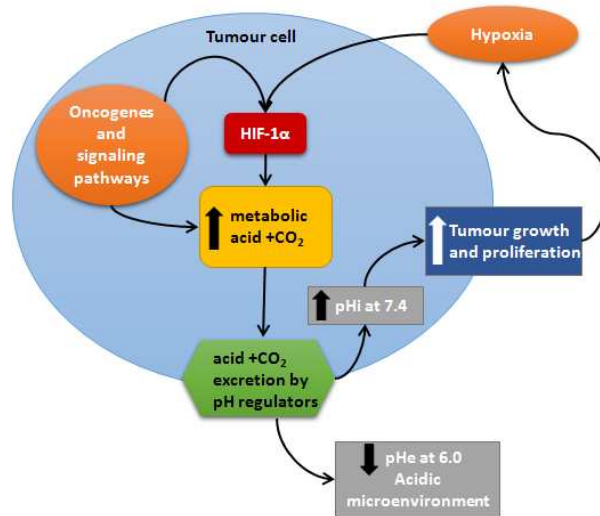


Figure 1.1.4. Model of hypoxia, cancer metabolism and acidity in tumour cells. Oncogenes, signaling pathways and hypoxia can reprogram cellular metabolism by the stabilization of HIF-1 α dependently or independently from O₂. The metabolic reprogramming contributes to the generation of metabolic acid and carbonic dioxide (CO₂). Cancer cells extrude acidic elements out of the cells by pH regulators reducing the extracellular pH (pHe) and generating an acidic microenvironment, while increasing the intracellular pH (pHi). This condition favours the growth and proliferation of cancer cells. *This figure is adapted from reference [8].*

1.1.5 Hypoxia and acidity are pro-tumourigenic: influence on tumour aggressiveness and immunosuppression

The combinatorial effects of hypoxia and poor vasculature perfusion increase flux of carbons induce the acidosis of the TME. Hypoxia and acidity have been also involved in the regulation of aggressive behaviour of malignant cells such as proliferation, migration and invasion [9, 10] and in the support of cancer stem cells (CSCs), a tumourigenic subpopulation of tumour cells able to perpetuate the tumour [11].

In addition to transformed, malignant cells, the tumour mass also includes stromal and immune cells which communicate with each other and compose

the TME. A tumour mass highly enriched by innate and adaptive immune cells is defined as a 'hot' or 'inflamed' tumour [12]. Tumours and inflammation share a decreased O₂ tension that causes the induction of HIFs. Nuclear factor of kappa light polypeptide gene enhancer in B cells (NF-κB), a master regulator of inflammation, is also a direct transcriptional regulator of HIF-1α [13]. Hypoxia regulates the secretion of chemokines from cancer cells that contribute to the recruitment of immune cells at the tumour site thus further boosting local inflammation [14]. The immune and stromal cells, such as stellate cells in HCC, secrete factors that, by remodelling the extracellular matrix (ECM) and contributing to the development of fibrosis, further hamper the delivery of oxygen and nutrients from vessels and limit the elimination of lactate from the extracellular milieu. Thus, lactate produced by the high proliferating cancer cells accumulates at the tumour site and it is in part responsible for the local acidification of the TME. Lactate accumulation leads to the setting of a pro-tumour and immune suppressed environment [15]. In fact, lactate serves as nutriment for cancer-associated fibroblasts (CAFs), which generally exert pro-tumour activities. It also inhibits the T cell anti-tumour response in part by feeding tumour-associated macrophages (TAMs) which in turn suppress T cell activity [16]. T regulatory cells (Tregs) are also attracted to the hypoxic and acidic tumour areas [15, 17]. Figure 1.1.4 illustrates the role of hypoxia and acidity in tumour aggressiveness and immunosuppression. In the next sections, will be described additional details on the effect of hypoxia and acidity on proliferation, invasion and metastasis, EMT, CSCs and in immunosuppression.

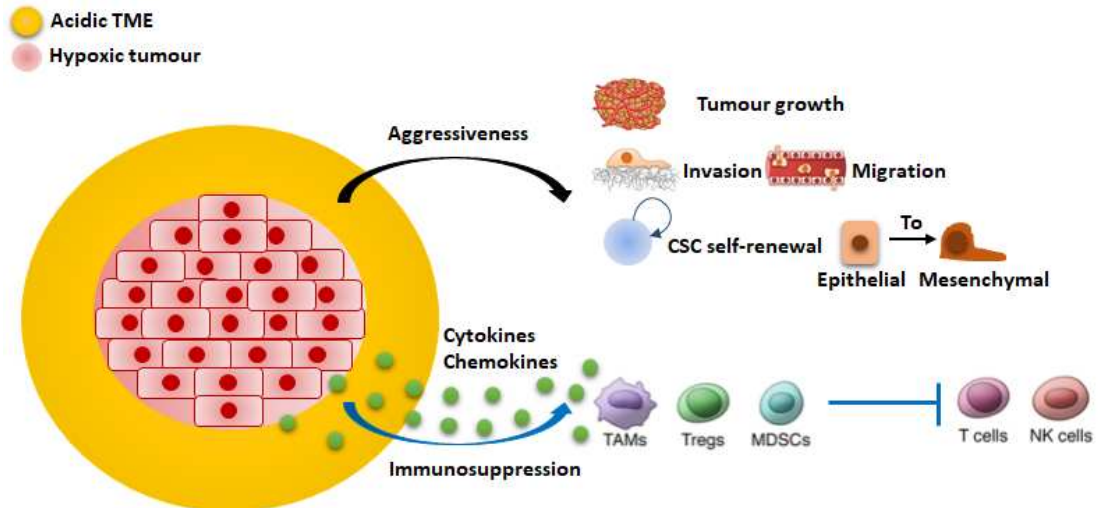


Figure 1.1.5. Tumour hypoxia and acidic tumour microenvironment can influence tumour aggressiveness and immunosuppression. Hypoxia and acidity can increase tumour growth, invasion and migration capacity of cancer cells, promote the self-renewal of cancer stem cells (CSCs) and induce epithelial-to-mesenchymal transition (EMT). Furthermore, hypoxia and acidity can promote the aggressiveness of cancer cells by the induction of immunosuppression. Hypoxic and acidic cells release immune factors (cytokines and chemokines) that recruit immunosuppressive cells such as tumour-associated macrophages (TAMs), T regulatory cells (Tregs) and myeloid-derived suppressor cells (MDSCs), which in turn suppress the anti-tumour activity of T and NK cells. *Figure adapted from reference [13].*

1.1.5.1 Proliferation, invasion and metastasis

Recently, it has been shown that hypoxia-mediated extracellular acidification sustains the growth and proliferation of cancer cells [18]. Moreover, an acidic pH also contributes to resistance to apoptosis through the activation of signalling pathways that are also implicated in the regulation of tumour aggressiveness such as the mitogen-activated protein kinase (MAPK) and Mek/ERK pathway [19]. It has been reported that an acidic pH increases the invasive and metastatic ability of tumour cells [20] by favouring the enzymatic degradation and remodelling of the ECM operated by the matrix metalloproteinases [21, 22]. Through the induction of lysyl oxidases (LOX),

hypoxia promotes the formation of the premetastatic niche in several organs including liver [23]. Furthermore, hypoxia and acidosis induce the release of proangiogenic factors, such as interleukin 8 (IL-8) [24] and vascular endothelial growth factor A (VEGF-A) and vascular endothelial growth factor C (VEGF-C) involved in the development of lymphangiogenesis [25, 26] and thus, they promote metastasis formation.

1.1.5.2 Epithelial-to-mesenchymal transition (EMT) and cancer stem cells (CSCs)

EMT is a process characterised by diminished proliferation, induced expression of mesenchymal markers, increased resistance to apoptosis and increased invasiveness associated with metastasis formation and CSCs [27]. In renal cell carcinoma, a highly hypoxic tumour, hypoxia promotes EMT through the downregulation of E-cadherin and by the induction of nuclear transcription factors such as Snail family transcriptional repressor 1 (SNAIL1) and Twist family BHLH transcription factor (TWIST) [28]. EMT can also be promoted by the acid pH in melanoma and breast cancer cells [20, 29] CSCs (also known as tumour-initiating cells, TICs) are a subpopulation of cancer cells in the tumour mass that are able to self-renew. Division of CSCs produces one CSC that maintains the pool of cells that propagate the tumour, and one differentiated cell that forms the tumour mass. It has been recently shown that adult epithelial and embryonic stem cells have a lower pH_i compared to the differentiated cells, thus opening the possibility that also TICs might have a lower pH_i than the cells composing the bulk of the tumour mass [30]. Mathieu and colleagues found that, through HIF-1 α , hypoxia

promotes the expression of embryonic stem cell markers such as Nanog, OCT4 and SOX2 [31]. The relationship between hypoxia/acidity, EMT and CSCs has been reported in several studies. For example, the inhibition of vacuolar ATPase (V-ATPase), a complex responsible for the extrusion of the H⁺ out of the cells, reduces the self-renewal of mammospheres and decreases the EMT phenotype of immortalized human mammary epithelial cells [32]. In glioma, hypoxia and acidosis maintain the pool of CSCs through the induction of HIF [33]. Moreover, Hjelmeland and collaborators demonstrated that without the concomitant setting of hypoxia, low pHe *per se*, acts as an inductor of the cancer stem cell phenotype in glioma stem cells (GSCs), by promoting the HIF-2 α and VEGF-A expression [34].

1.1.5.3 Macrophages and tumour-associated macrophages (TAMs)

In general, all tumours are infiltrated by macrophages, a subpopulation of myeloid cells recruited to the tumour site from the circulation by soluble factors actively released by cancer cells. Macrophages are subdivided into classically activated, pro-inflammatory and anti-tumour M1 or alternatively activated and pro-tumourigenic M2 (TAMs) [35]. M2 macrophages are enriched in tumour zones with a low O₂ tension, while the M1 type is mainly localized in tumour areas with a normal O₂ level [36]. Laoui and colleagues showed that hypoxia does not drive the differentiation of macrophages into TAMs, but it regulates the pro-angiogenic phenotype of M2 cells [37]. Macrophages migrate to the hypoxic zones of the tumour responding to signals mediated by VEGF, endothelin A, C-X-C chemokine receptor type 4 (CXCR4) and Semaphorin 3A [38, 39]. TAMs are involved in tumour

invasion and metastasis. In particular, TAMs located in low oxygen areas of the tumour release VEGF-A stimulating angiogenesis, exacerbating hypoxia and promoting the migration of cancer cells [40]. Tripathi and collaborators showed that Oncostatin M and Eotaxin produced by hypoxic breast cancer cells are essential factors to recruit M2 macrophages. The blockade of Oncostatin M and Eotaxin reduced the recruitment of M2 cells and increased the efficacy of the anti-angiogenic drug Bevacizumab [41]. HIF-1 α alone [42] or in combination with an acidic TME rich in lactic acid [43] increases the immunosuppressive capacity of TAMs by the production of VEGF, arginase 1 (Arg1) and nitric oxide synthase (iNos) [42, 43]. Hypoxia induces also the “don’t eat me signal” through the expression of CD47 mediated by HIF-1 in tumour cells that thus are protected from macrophage-derived phagocytosis [44].

1.1.5.4 Myeloid-derived suppressor cells (MDSCs)

MDSCs are an immature myeloid cell population and two main types of MDSC have been described: monocytic MDSCs (mMDSC) and granulocytic MDSCc (gMDSC). In healthy conditions, MDSCs present in the bone marrow differentiate into macrophages or neutrophils. MDSCs exert their immunosuppressive function in tumours by inhibiting T and NK cell functions. MDSCs are associated with increased tumour burden in several cancer types [45] and are recruited to the tumour site in response to tumour-derived factors such as the macrophage migration inhibitory factor (MIF) produced by tumour cells expressing HIF-1 α and HIF-2 α in response to hypoxia. The migration of MDSCs to the tumour site can be reduced by the inhibition of the

axis HIF-1 α /2 α and NF- κ B/IL-6 [46]. Low O₂, by promoting the stabilization of HIF-1 α , induces the differentiation of MDSCs into TAMs [47]. In addition, in hypoxic conditions, HIF-1 α leads to the expression of the immune-checkpoint PD-L1 (programmed cell death ligand 1) on MDSCs. These cells inhibit T cells by interleukin 10 (IL-10) and the suppressive activity of MDSCs is abrogated by the usage of anti-PD-L1 and a neutralizing antibody against IL-10 [48]. Hypoxia contributes to the formation of pre-metastatic niche in lung by inducing the production of C-C motif chemokine 2 (CCL-2), tumour necrosis factor α (TNF), VEGF, metalloprotease 9 (MMP-9), metalloproteinase inhibitor 1 (TIMP-1), granulocyte colony-stimulating factor (G-CSF) in murine breast cancer cell lines. CCL-2 works by recruiting MDSCs and its neutralization using a specific antibody restores the anti-tumour activity of NK cells in lung metastasis [49]. Another example of the significance of hypoxia in the pre-metastatic niche formation, which involved MDSC recruitment, comes from the study published by Chafe and collaborators. They showed that carbonic anhydrase IX, induced by hypoxia, promotes MDSC mobilization and the establishment of a metastatic niche by stimulating G-CSF production in breast cancer cells [50].

1.1.5.5 Regulatory T cells (Tregs)

Tregs are another important component of the TME that are frequently increased in cancer and that support tumour progression. Tregs are CD4⁺ cells identified by the expression of forkhead box transcription factor 3 (Foxp3). In physiological conditions, Tregs are required to prevent autoimmune diseases [51]. Treg formation is promoted by hypoxia through

the expression of Foxp3 induced by HIF-1 α [52]. Moreover, the production of TGF- β 1 mediated by hypoxic conditions in gastric cancer cells also boosts the expression of Foxp3 in Tregs [53]. In turn, Foxp3 expression favours Tregs survival with respect to T cells in an acid pH rich in lactate [54]. Furthermore, hypoxia likely potentiates also the Treg effector functions. In fact, HIF-1 α induction mediated by hypoxia induces the expression of CD39 and CD73, molecules involved in the conversion of ATP to adenosine, a crucial pathway of immune suppression mediated by Tregs and MDSCs [55, 56]. Hypoxia not only favours the induction/generation and effector functions of Treg as described above, but also it is involved in Treg recruitment by inducing C-C motif chemokine 28 (CCL-28) expression in cancer cells as shown for ovarian and liver cancer cells. CCL-28 works as chemoattractant for C-C chemokine receptor type 10 (CCR10)-positive Treg [57, 58]. In line with all these observations, Pilon-Thomas and colleagues demonstrated that neutralizing the acidity of the TME in several models improved the efficacy of the checkpoint-based immunotherapy by restoring the anti-tumour function of T cells [59].

1.2 Hepatocellular carcinoma: role of hypoxia, cancer stem cells and immunosuppression in the biology of the tumour

1.2.1 Hepatocellular carcinoma

Hepatocellular carcinoma (HCC) is the sixth most prevalent cancer and the second most common cause of cancer-related deaths worldwide [60]. HCC constitutes 85–90% of all primary liver cancers. HCC generally occurs in a chronically inflamed liver showing hepatocyte necrosis and regeneration

together with fibrosis. Risk factors for HCC include hepatitis virus B (HBV) or C (HCV) and aflatoxin B1 infections, alcohol abuse, obesity and visceral adiposity that can result in non-alcoholic fatty liver disease (NAFLD) and non-alcoholic steatohepatitis (NASH) and haemochromatosis. All these viral and metabolic insults cause inflammation and can progress into a chronic status establishing cirrhosis in the liver of 70-80% of patients.

The stage and treatment strategy of HCC patients is based on the Barcelona Clinic Liver Cancer (BCLC) classification that takes into account the number and the size of the tumour nodules, the chronic liver disease and cirrhosis status (Child-Pugh score). Patients affected by HCC with localised disease are subjected to curative surgery with surgical resection and ablation. Unfortunately, about 70% of HCC patients relapse in approximately five years after the treatment [61]. Liver transplantation is applicable to patients with early-stage tumours, but patients with poor outcomes are not treated with liver transplantation. Few systemic therapies are available which include treatment with anti-angiogenic drugs such as sorafenib and regorafenib [62]. Sorafenib and regorafenib are inhibitors of the receptor for VEGF or for platelet-derived growth factor (PDGF) expressed by tumour cells. In addition, sorafenib can control the proto-oncogene serine/threonine-protein kinase c-RAF that participates in the MAPK cascade, while regorafenib can inhibit the angiopoietin-1 receptor (TIE2) present on TAMs [63]. Recently, immunotherapy trials based on immune checkpoint inhibitors (ICIs) have demonstrated that HCC patients could derive benefit from immunotherapy based on ICIs [64] and the usage of nivolumab (anti-PD-1), one of the ICIs, has been recently approved by the FDA in advanced HCC patients. However,

the major obstacles for the complete response to these therapies are the establishment of tumour-intrinsic and -extrinsic resistance which certainly includes the emergence of dysmetabolism and immunosuppressive pathways [65].

1.2.2 Chronic inflammation and HCC

Complex molecular events link chronic liver damage and cell death with inflammation and HCC development. Figure 1.2.2 summarises the key steps leading to HCC development in the setting of a chronic inflammation. Different damaging agents, which include viral infection, alcohol abuse, high fat, induce cell death in hepatocytes. Different types of cell death occur in liver disease including caspase-mediated apoptosis and also necroptosis, a highly regulated form of necrosis involving receptor-interacting protein kinases 1 and 3 (RIPK1-3) [66]. Dying hepatocytes release damage-associated molecular patterns (DAMPs) including high mobility group box 1 (HMGB1), S100, which induce a sterile inflammation by activating macrophages through the triggering of advanced glycation end product (RAGE) and Toll-like receptors [67]. This chronic 'wound healing response' drives HCC development. M1 macrophages are early players in the TME and they work by recruiting other inflammatory cells including Th17 and Th1 cells. The local production of TNF, interleukin 1 β (IL1 β) and importantly interleukin 6 (IL-6) induce anti-apoptotic signals and compensatory proliferation in hepatocytes. Reactive oxygen species (ROS) and reactive nitrogen species (RNS) produced by the activated inflammatory/immune cells induce DNA damage and mutations that then accumulate in the proliferating hepatocytes, thus constituting the basis for HCC carcinogenesis and promoting the

appearance of pre-malignant cells. Of note, IL-6, present in the inflammatory milieu, helps malignant hepatocyte progenitor cells to survive in the early phase until they became self-sufficient by acquiring an autocrine production of IL-6 (see chapter 1.2.3) [68]. At later stages of tumour progression the immune microenvironment becomes more suppressive with the accumulation of pro-tumour M2 macrophages (see paragraph 1.2.2), Th2 cells and MDSCs. Th1 cytotoxic anti-tumour response is then blocked and completely ineffective unless immunosuppressive factors are eliminated [69]. Overcoming immune suppressive pathways by the usage of ICIs is one of the promising strategies in cancer treatment (see below).

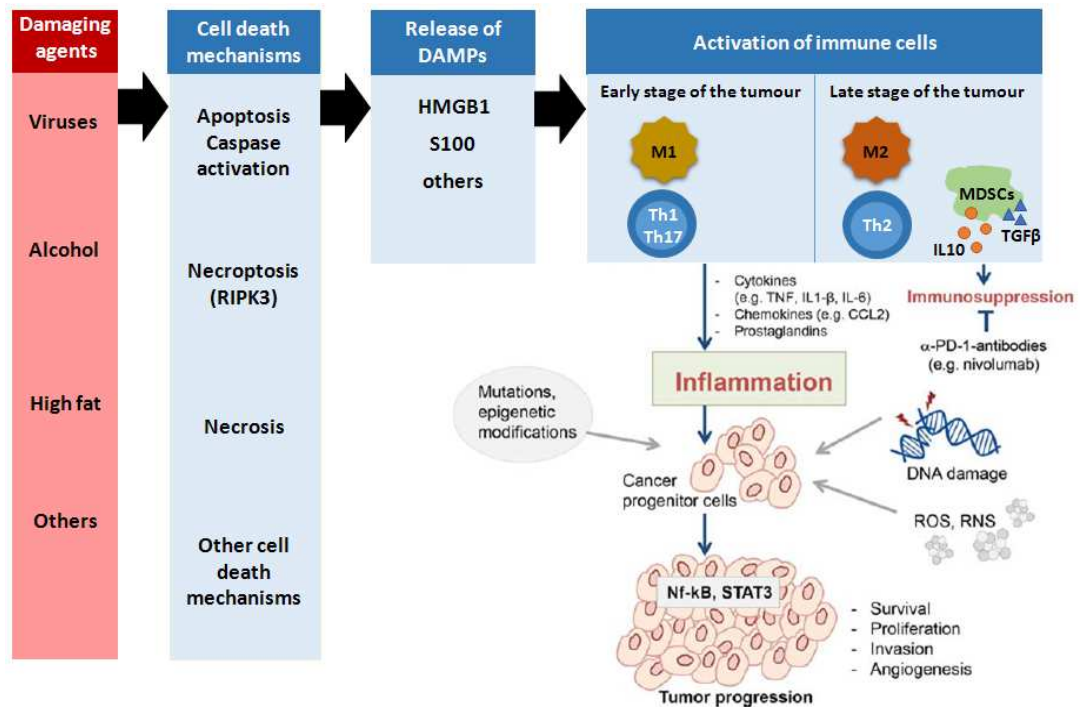


Figure 1.2.2. HCC development in the setting of a chronic inflammation. Virus infections, alcohol abuse, high fat induce injury in the liver that leads to death of hepatocytes through several mechanisms of cell death. Dying hepatocytes release damage-associated molecular patterns (DAMPs) including HMGB1 and S100 that induce inflammation. The early stage of the tumour inflammation process is mediated by M1 macrophages that by the release of cytokines recruit Th1 and Th17 cells. The latter cells produce TNF and IL-6 which activate anti-apoptotic and proliferative signals such as NF-κB and STAT3 in hepatocytes. Activated inflammatory/immune cells produce ROS/RNS that cause genetic alterations in hepatocytes that acquire the ability to survive and proliferate. In the late stage of tumour development, M2 macrophages recruit Th2 cells leading to immunosuppression. MDSCs participate to immunosuppression producing IL-10 and TGFβ and inducing angiogenesis. *Figure taken from reference [69].*

1.2.3 Molecular mechanisms and pathogenesis of HCC

HCC derives from the malignant transformation of different liver resident cells, including hepatocytes and stem or progenitor cells (see paragraph 1.2.4 for further details) occurring in a setting of inflammation (see paragraph 1.2.2). The development of the tumour starts with the formation of low-grade dysplastic nodules (LGDNs) that progress into high-grade dysplastic nodules (HGDNs), and then into early-stage HCC which finally progresses into

advanced HCC. This is a complex multistep process driven by the progressive accumulation of alterations at the molecular and cellular levels resulting in the loss of tumour suppressor genes or in the activation of oncogenes and their related molecular pathways. These genetic modifications contribute to proliferation, progression, invasion and immune escape of HCC [63] and depict for HCC a highly heterogeneous molecular landscape. However, inside this enormous complexity, genomic studies performed on a large set of primary HCC surgical specimens identified different molecular subclasses of HCC and new targetable genomic alterations, such as MDM4 or IDH1 and 2 have been recently identified [70]. Although the full translation into clinical management of this molecular classification still needs to be achieved, these new findings possibly open fresh approaches of precision medicine for this deadly disease for which few effective therapeutic options are currently available (see paragraph 1.2.1) [70-72].

1.2.4 Stem cells and cancer stem cells in HCC

The liver is composed by hepatocytes and cholangiocytes together with non-parenchymal cells which include fibroblasts, hepatic stellate cells, Kupffer cells and endothelial cells. Hepatocytes constitute about the 60-80% of the liver mass. Adult stem cells are specialised cells able to sustain tissue turnover because of their self-renewal potential and capacity to differentiate. While this is well accepted for skin or intestine, the situation in the liver is more complex. Hepatocytes, which are quiescent in the liver steady state condition, became highly proliferative following liver injury and it is believed

that liver regeneration relies also on the replication capacity of differentiated hepatocytes. In line with these data is the recent finding that a few hepatocytes, highly positive for telomerase reverse transcriptase (TERT) expression, are distributed along the liver lobule. These hepatocytes self-renew and differentiate to maintain the liver mass during homeostasis. This finding is well in agreement with the notion that activation of TERT is associated with cirrhosis, and that activation of the TERT promoter is the most frequent molecular event in HCC [73]. However, additional evidence on the existence of cells with features of hepatic stem or progenitors cells do exist in the adult liver although no definitive consensus about their location and nature has been reached yet. Oval cells, which can differentiate both into hepatocytes and into cholangiocytes are supposed to be located in the canals of Hering, the most terminal branches of the biliary duct. However other studies have indicated the presence of highly proliferating self-renewing duct-like cells responsible for liver reconstitution located in the portal zone of the hepatic lobule. Finally, it has been suggested that epigenetic programming might be involved in the transdifferentiation of mature hepatocytes into oval like cells [74].

Given this complex background, several hypotheses on the cells of origin of HCC have been formulated. Indeed, HCC are heterogeneous and some HCC display strong stem cell features, suggesting their origin from stem cell like cells. Other studies in animal models strongly support this hypothesis [75]. However, several lines of evidence exist that support the origin of HCC from adult differentiated hepatocytes, mainly based on their extraordinary plasticity and their capacity to dedifferentiate and acquire a progenitor phenotype [75-

77]. Several molecular pathways are associated to this dedifferentiation including loss of TP53, activation of WNT and NOTCH. But, irrespective of the origin of HCC, HCC displaying stem cell-like features have the worse prognosis [78].

As in other solid tumours, the population of CSCs of the liver has been prospectively identified as cells expressing several different markers [76], but a unique definition of CSCs for HCC has not yet been defined. The HCC CSC-associated markers include epithelial cell adhesion molecule (EpCAM), cytokeratin 19 (KRT19), prominin 1 (CD133), sialoglycoprotein (CD24), thymocyte differentiation antigen 1 (CD90) and cell-surface glycoprotein (CD44) [76].

Regarding the origin of CSCs in HCC, as for the 'normal' liver stem cells, several hypothesis have been formulated which include: - CSCs originate from transformation of normal liver stem cells; - mature hepatocytes and biliary cells might be transformed into CSCs by genetic/ epigenetic alteration; - mature hepatocytes and biliary cells might acquire CSCs feature by dedifferentiation processes [76]. An additional important concept in HCC is that chronic inflammation seems to be crucial in sustaining, at least at the initial disease phases, the growth and expansion of the putative HCC CSCs by providing the inflammatory cytokine IL-6. With disease progression, HCC CSCs acquire an autonomous IL-6 production, as shown in a murine model [68]. In humans, gene expression analysis partially confirmed this finding/hypothesis by showing that late recurrence in surgically resected HCC patients was associated with the presence of an IL-6 driven inflammatory signature [79].

Indeed, an important crosstalk between the immunosuppressive TAMs and CSCs has been reported for HCC. In HCC, CD44⁺ CSCs are expanded and maintained by IL-6-producing TAMs. IL-6 enhances the tumourigenic potential of CSCs in immunocompromised mice [80]. In addition, hypoxia plays a role in increasing the CSC marker expression and the tumourigenic potential of these cells. For example, CD133⁺ HCC stem cells displayed a preferential survival in a TME with low oxygen and nutrients by the activation of an autophagy pathway [81].

1.2.5 Hypoxia as a metabolic condition in HCC affecting immune infiltrating cells

To prevent an aberrant immune response to gut-derived microbes, the liver displays an inherent tolerogenicity. Tolerogenicity is mediated by Tregs, dendritic cells (DCs) and macrophages resident in the liver (Kupffer cells) that suppress the activity of T cells [82]. This tolerogenic setting is further exacerbated during chronic inflammation and the development of HCC by contribution of Tregs, TAMs and MDSCs newly and actively recruited to the tumour site through the stimulation of hypoxia and acidity [83].

When HCC is growing, cancer cells suffer from a reduced level of O₂. O₂ supply becomes limiting due to the high metabolic rate of the cancer cells and the increased tumour size [84]. Although there are no studies that measure the exact extent of hypoxia in human HCC, it is well-known that in normal human liver the partial pressure of oxygen (pO₂) is about 5% and in patients with liver metastasis from colorectal cancer the pO₂ is 0.8% [85]. Moreover, in an orthotopic rat HCC model, the pO₂ inside the tumour ranges

from about 0-1% [86]. Furthermore, hypoxia is implicated in the lipid accumulation, inflammation and fibrosis of the damaged liver [87]. Liver fibrosis is a wound-healing response to the persistent injury in liver parenchyma, characterised by the deposition of collagen type I by the activated hepatic stellate cells (HSCs) [88]. The activation of HSCs contributes also to the setting of immunosuppression by inducing the differentiation of monocytes into MDSCs [89]. It was recently reported from Chiu and collaborators that the C-C motif chemokine ligand 26 (CCL-26) is produced by hypoxic HCC cell lines and attracts CX₃CR1+MDSCs *in vitro* and *in vivo*. The blockade of CCL-26 inhibits MDSCs recruitment [90]. Further work from the same group showed that a metabolic regulator ectonucleoside triphosphate diphosphohydrolase 2 (ENTPD2) that transforms ATP into 5'-AMP is induced in hypoxic HCC tumours and maintains the pool of MDSCs [91]. Hypoxia promotes the release of the C-C motif chemokine ligand 20 (CCL-20) by tumour hepatocytes and induces the production of indoleamine-pyrrole 2,3-dioxygenase (IDO) by immunosuppressive macrophages. The IDO suppresses T cells and promotes the expansion of Tregs [92]. The recruitment of Tregs to the tumour site is also due to the release of CCL-28 by hypoxic malignant hepatocytes and it is essential for tumour growth *in vivo* [58].

Among the molecular factors implicated in the pathogenesis of HCC, the activation of Wnt/ β -catenin and Akt-mTOR-MAPK signalling and the amplification of VEGF-A can be found in advanced HCC [63]. The contribution of hypoxia and acidity in the regulation of these pathways was extensively described in the previous section. For the specific field of HCC, it

is already known that hypoxic conditions induce the stabilization of β -catenin through the reduction of GSK-3 β associated with the increased phosphorylation of Akt. This signalling pathway regulates *in vitro* EMT, migration and the metastatic potential of malignant hepatocytes [93]. Furthermore, HIF-1 α enhances the gene transcription of β -catenin through the co-activator B-cell lymphoma 9 (BCL9). BCL9 acts as a *bonafide* oncogene and its loss contributes to a reduction of tumour growth, angiogenesis and the gene targets of β -catenin in immunocompromised mice [94].

Recently, it was reported that transarterial chemoembolization (TACE), a therapy used for the intermediate stage of HCC without vascular invasion, induces a hypoxic microenvironment associated with an increased expression of carbonic anhydrase IX in cells expressing CSC markers such as KRT19 and EpCAM [95]. These data collectively suggest that the hypoxic and acidic microenvironment in the liver is an important driver for tumourigenesis exacerbating inflammation, inducing the activation/maintenance of CSCs and immunosuppression. Thus, targeting hypoxia alone or in combination with other factors might contribute to reduce the aggressiveness of HCC. In this regard, a recent study performed on HCC showed that limiting the acidity of the TME by the usage of bicarbonate improves the survival of HCC patients undergoing TACE [96]. Mechanisms implicated in HCC development and discussed in this chapter are summarised in Figure 1.2.5.

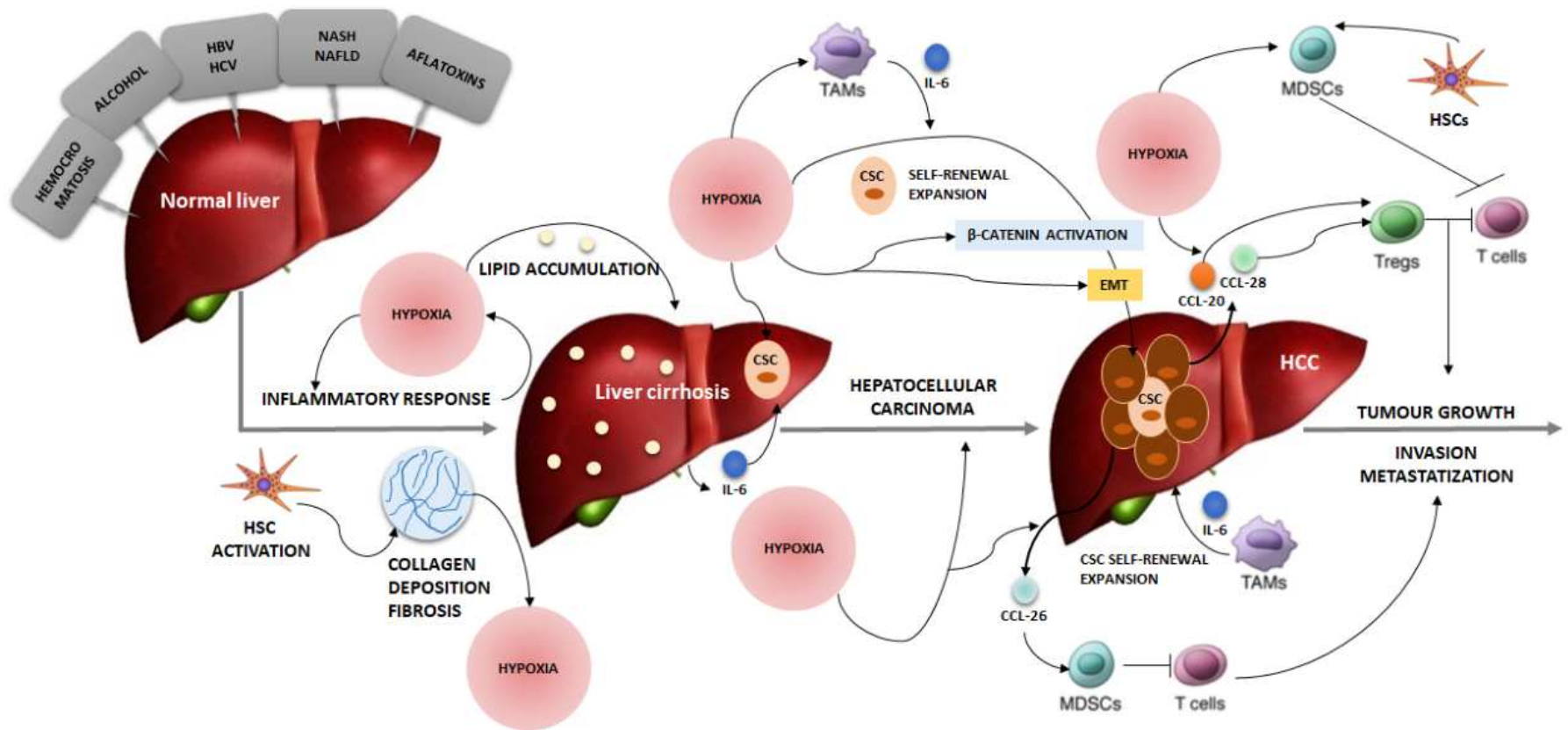


Figure 1.2.5. The main players in the development of HCC. Normal hepatocytes undergo cell death induced by different damaging agents (hemochromatosis, alcohol, HBV or HCV or aflatoxin infections, NASH or NAFLD). An inflammatory response is then initiated together with the activation of hepatic stellate cells (HSCs) that produce collagen ending with fibrosis. Inflammation and fibrosis promote hypoxia which leads to lipid accumulation in the liver and the establishment of cirrhosis. In the cirrhotic liver, macrophages and hepatocytes produce IL-6, which supports the self-renewal and expansion of CSCs. The development of HCC is driven by hypoxia that activates the β -catenin pathway, epithelial-to-mesenchymal transition (EMT). Hypoxia also contributes to immunosuppression by further recruiting tumour-associated macrophages (TAMs), myeloid-derived suppressor cells (MDSCs) and regulatory T cells (Tregs) responding to the chemokines (CCL-20, CCL-26, CCL-28) produced by hypoxic tumour cells. The immunosuppressive cells inhibit the anti-tumour cytotoxic immune response and contribute to tumour expansion, invasion and metastasis.

1.3 pH regulatory molecules as a therapeutic strategy for the hypoxic and acidic tumour microenvironment

As described in the previous paragraphs, metabolic reprogramming, hypoxia, acidity and inflammation lead to the acidification of the pH_i. To preserve the alkaline pH_i, cells express many pH regulators such as monocarboxylate transporters (MCTs), Na⁺/H⁺ exchanger 1 (NHE1), G-protein coupled receptors (GPCR), non-G-protein coupled receptors (GPCR), including vacuolar ATPase (V-ATPase) and carbonic anhydrases (CAs) [15, 97].

These pH regulators are expressed by immune cells, in which they regulate physiological functions, but they have gained increasing attention, because of their expression in tumour cells. Therefore, cancer cells expressing pH regulators in a hypoxic and acidic microenvironment have a great advantage in growth with respect to normal cells. Thus, pH regulators represent interesting therapeutic targets, alone or in combination, across many cancer types [98]. In Figure 1.3 we provide a graphic explanation of the function of V-ATPase and the most studied cancer-related carbonic anhydrases (CAIX and CA XII). V-ATPase extrudes H⁺ out of the cells, while carbonic anhydrases catalyse the reversible hydration of CO₂ and water to bicarbonate and H⁺. In the following paragraphs we describe in detail their role in cancer.

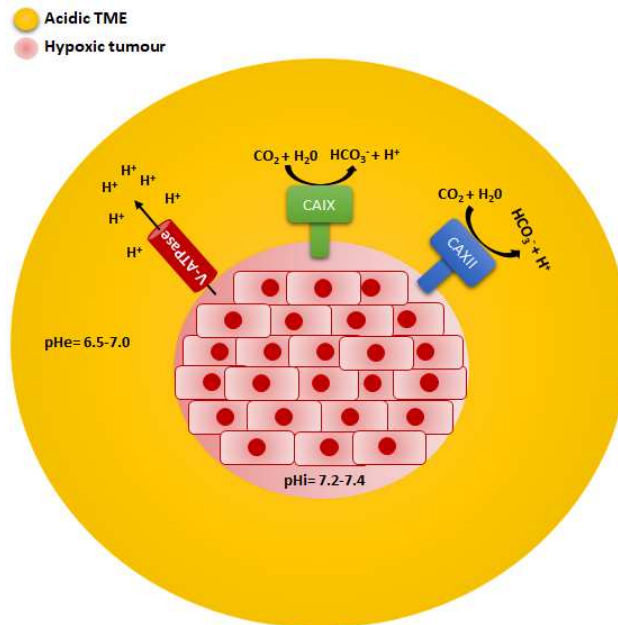


Figure 1.3. Hypoxic and acidic cancer cells express pH regulators. V-ATPase and carbonic anhydrases (CAIX and CAXII) are expressed on the cell surface of hypoxic and acidic tumour cells. The V-ATPase combines the energy released from ATP hydrolysis to the extrusion of protons (H⁺) out of cells into the extracellular space. CAIX and CAXII convert carbonic dioxide (CO₂) and water (H₂O) into bicarbonate (HCO₃⁻) and protons. These reactions contribute to increase the pHi acidifying the pHe.

1.3.1 V-ATPase complex

V-ATPase is composed of many subunits organized into the V₁ and the V₀ domains. The V₁ is composed of eight subunits A₃B₃CDE₃FG₃H, it is localized on the cytoplasmic side of the cells and it is responsible for the hydrolysis of ATP. Five subunits ac₉c''de constitute the integral V₀ domain assigned to the extrusion of the protons out of cells. The binding site for the proton pump inhibitors (PPIs) resides in a subunit. This unidirectional proton transport is due to ATP hydrolysis at the interface of A and B subunits that cause a rotation of subunits D and F of V₁ and subunits d, c and c'' of the V₀ domain. The inactivation of V-ATPase is due to the separation between the V₁ and the V₀ domain, while the activation of the complex is regulated by

either a high glucose level, growth factor exposure, amino acid starvation or viral infection. V-ATPase is localised in the membranes of lysosomes, endosomes and secretory vesicles, but also in the plasma membrane of specialised cells such as osteoclasts or cancer cells. The NH₂-terminal domain is implicated in the localization of the complex in the plasma membrane of the cells [99]. The structure and function of V-ATPase is schematised in Figure 1.3.1.1.

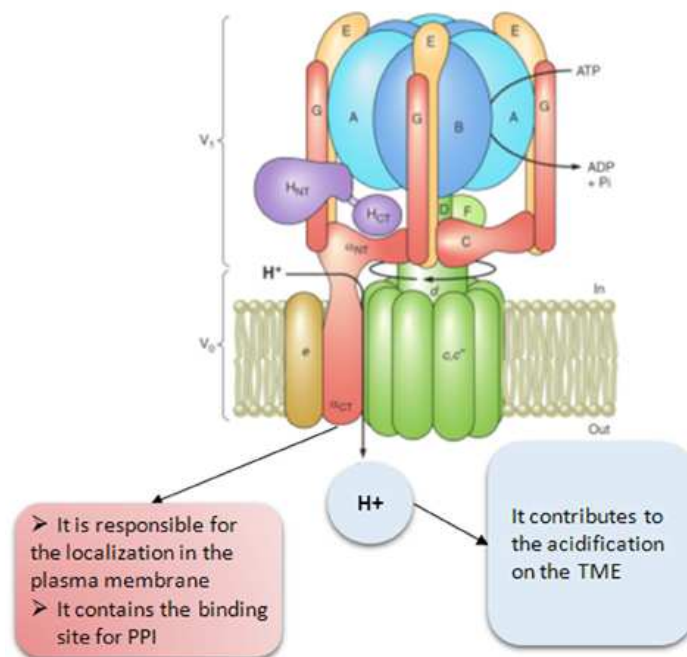


Figure 1.3.1.1. Graphic representation of structure and mechanism of the V-ATPase complex. Two domains, the V₀ and the V₁ compose the V-ATPase complex. On the cytoplasmic side of the cells resides the V₁ domain that carry out the hydrolysis of ATP generating a rotation of the central part of the complex which includes D and F subunits of the V₁ and c, c' subunits of the V₀ domain. The V₀ is a transmembrane domain and it is responsible for the extrusion of the protons (H⁺) out of the cells. The extrusion of H⁺ contributes to the acidification of the extracellular microenvironment, while maintaining the neutral intracellular pH (pHi) of the cells. a subunit of V₁ domain binds proton pump inhibitors (PPIs). *This figure is adapted from reference [100].*

Although the expression of V-ATPase is increased in hypoxic tumour cells, its expression is not dependent on HIF-1 α , but it has been demonstrated that V-ATPase promotes the degradation of HIF-1 α through its binding to VHL and lysosomal degradation [101]. Moreover, the iron depletion mediated by V-ATPase inhibition leads to HIF-1 α degradation. This mechanism is reversed by iron supplementation in ovarian cancer cells [102]. Recent work has shown that V-ATPase has important roles in cancer cells [100]. Some subunits of this large complex are overexpressed in breast cancer [103, 104], gastric cancer [105], HCC [106-108], melanoma [109], colon cancer [110], ovarian cancer cells [111], oral squamous cell carcinoma [112], sarcomas [113] and prostate cancer [114].

V-ATPase controls directly or indirectly pathways implicated in the growth and survival of tumour cells and CSCs. For example, the prorenin receptor (PRR), an additional accessory protein of the V-ATPase, is important for the activation of Wnt/ β -catenin signalling, the stabilization of β -catenin and it allows β -catenin to continue the transcription of its target genes. Specifically, PRR permits communication between the complex LPR6 and Frizzled of the β -catenin pathway and the internalization of the complex mediated by V-ATPase. Notch signalling requires V-ATPase for enhancing the cleavage of the Notch receptor dependent on the acidification of endosomes after the internalization of the receptor and the consequent increase of Notch target gene transcription [100]. These pathways are also involved in the maintenance of CSCs, thus it is conceivable that V-ATPase is implicated in the regulation of CSCs. In support of this concept, it is already known that murine neuronal stem cells are preserved by Notch signalling through the

function of V-ATPase [115]. Furthermore, Di Cristofori and colleagues demonstrated that V-ATPase is also active in CSCs. Specifically, the expression of the G1 subunit regulates the self-renewal of glioblastoma stem cells and this subunit is also associated with poor prognosis of glioblastoma patients [116]. It is well known that cancer cells rely on the expression and activity of V-ATPase to increase their survival and evade apoptosis in an acidic environment and this complex regulates the migration and invasive capacity of cancer cells [117]. Moreover, the expression of V-ATPase was also studied in immune cells, in which it is implicated in the regulation of their physiological functions see reference [15] for further details. Interestingly, it was recently reported that the polarization of TAMs requires the activation of the mTOR pathway in combination with V-ATPase [118].

For all the reasons described in this section, the inhibition of V-ATPase has become an interesting strategy to fight cancer. Specific inhibitors of V-ATPase are known. In particular, compounds of microbial origin such as concanamycin A, bafilomycin A1 and archazolid bind the c subunit of the V_0 domain. The anti-tumour activity of these drugs has been studied *in vitro* and *in vivo* [32, 107,119-121]. For example, concanamycin A reduces the cell migration ability and invasiveness of melanoma and breast cancer cells [119]. Archazolid inhibits *in vitro* and *in vivo* tumour growth of breast cancer cells through the blockade of iron metabolism [120]. Furthermore, archazolid reduces the invasiveness of breast cancer cells [122] and the metastatic capacity of several metastatic cancer cells [123]. Archazolid is also able to restrain TIC generation affecting EMT [32]. Another class of compounds that inhibit H^+/K^+ ATPase expressed in gastric parietal cells are the PPIs that are

able to cross-react with V-ATPase. These compounds could be selective for cancer cells, because their activation is mediated by acidic conditions [124]. Among the PPIs we found omeprazole and esomeprazole. Omeprazole and esomeprazole are able to delay tumour growth *in vivo* of melanoma and B-cell tumours, displaying a low toxicity [125-127]. Remaining in the field of melanoma, Calcinotto and collaborators showed that esomeprazole, the S-enantiomer of omeprazole, reconstitutes the anti-tumour activity of T cells [128]. Figure 1.3.1.2 summarises the effects of targeting V-ATPase in cancer cells.

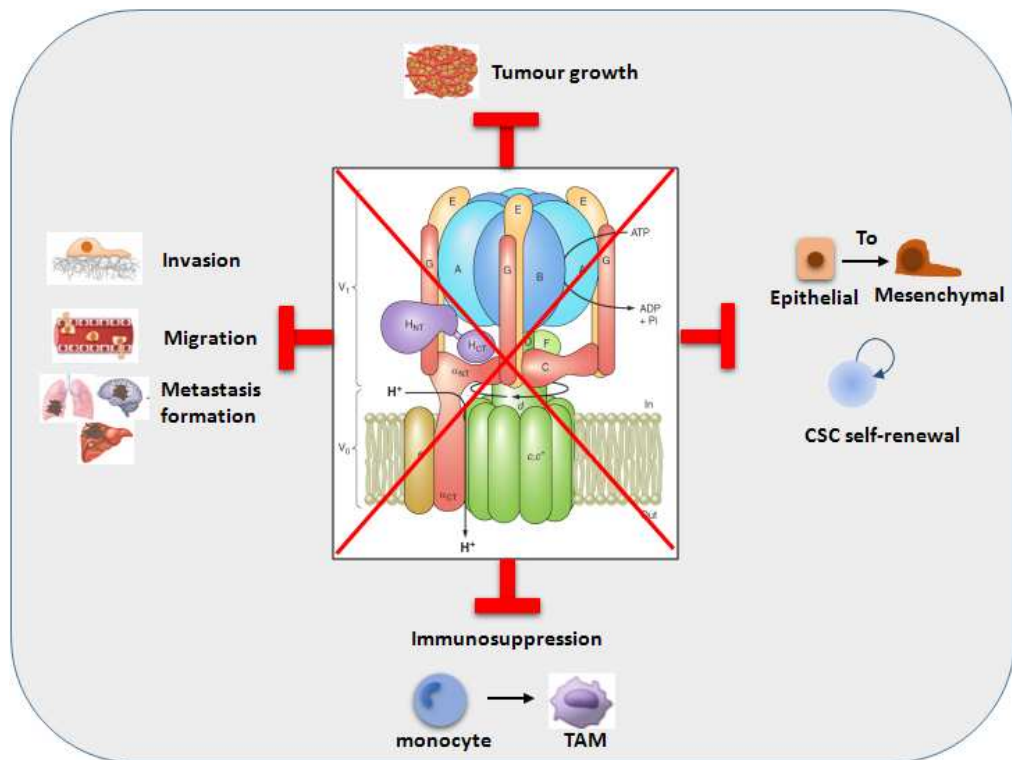


Figure 1.3.1.2. The role of V-ATPase inhibition in cancer. Targeting V-ATPase contributes to reduce tumour growth, invasion, migration, metastasis formation, epithelial-to-mesenchymal transition, cancer stem cell (CSC) self-renewal and immunosuppression. *Figure adapted from reference [100].*

1.3.2 Carbonic anhydrase IX and XII

CAs are a big family of metalloenzymes, which contain zinc in their active site and comprise 15 isoforms in humans. These members are membrane-associated, cytosolic, secreted and mitochondrial. The two transmembrane proteins identified to be important for cancers are CAIX and CAXII [129]. They are organised into the catalytic domain (CA) on the extracellular side, the transmembrane domain (TM) and the intracellular C-terminal tail (IC) on the cytoplasmic side of the cells. CAIX has also a proteoglycan domain (PG) in the N-terminus CA domain and this part is important for conferring aggressive features to cancer cells [130]. Interestingly, CAIX and CAXII are up-regulated in tumour hypoxic areas [131], but only CAIX contains in its promoter the hypoxia-response element (HRE) for HIF-1 α [132].

The distribution of CAIX and CAXII has been investigated across several normal and tumour tissues [133], but the impact of these molecules on the prognosis of cancer patients is tissue-dependent [134]. The presence of CAIX is associated with poor prognosis in a variety of cancers, such as breast [135], non-small cell lung cancer (NSCLC) [136], adrenocortical tumours [137], ovarian cancer [138] and HCC [139-141]. In renal cell cancer (RCC) a high level of CAIX is a predictor of a good prognosis [142]. Conversely, the relationship of CAXII with the outcome of cancer patients is controversial and remains to be fully clarified. CAXII is associated with better clinical outcomes in breast cancer [143], cervical cancer [144] and NSCLC [145, 146]. While CAXII presence has a worse prognostic value in infiltrating astrocytic gliomas [147]. Ilie and colleagues demonstrated also that the combined expression of high level CAIX and low level CAXII has a bad

impact for the prognosis of patients with NSCLC. They showed that CAIX is the most sensitive molecule to re-oxygenation, which maintains a stable expression when the lung cell lines were shifted from hypoxic to normoxic conditions. On the contrary, in lung cancer cell lines CAXII was slightly up-regulated by hypoxia, but down-regulated after the re-oxygenation [148].

CAIX and CAXII are involved in the aggressiveness of cancer cells by regulating the spreading of cancer cells. Recently, Dedhar's group demonstrated that the enzymatic activity of CAIX is required for collagen degradation mediated by metalloprotease 14 (MMP-14) [149]. Moreover, CAIX and CAXII are able to enhance cell migration and invasion through the activation of important signalling pathways for cancers. Specifically, CAIX activates the FAK/PI3K/mTOR pathway in ovarian and cervical cancer cell lines [150], and induces mTORC1, which is implicated in the expansion of CD44⁺CD24^{-/low} breast CSCs [151]. CAXII enhances the migration and invasive capacity of tumour cells by increasing the expression of MMP-2 and 9 induced by the activation of p38 MAPK signalling pathway [152].

Several compounds belonging to the sulfonamide/sulfamate and coumarin families have been developed by Supuran's group [129] and the generation of more selective drugs specific for CAIX and CAXII is on-going [153]. Among all the compounds for CAs only a few have been investigated in animal models and only the CAIX inhibitor called SLC-0111 has entered in a clinical trial for solid tumours (NCT02215850). Several studies have shown that the inhibition of CAIX and CAXII by these small molecules inhibits the growth of breast cancer cells and have an anti-metastatic effect [154-157]. Moreover, interfering with CAXII also reduces cell proliferation and induces

apoptosis in T-cell lymphomas [158]. In addition to pharmacological inhibition, anti-CAXII monoclonal antibodies have been developed. The systemic administration of a CAXII blocking antibody delays the *in vivo* tumour growth of several human cancer cell lines in xenograft models [159, 160].

The inhibition of CAIX and CAXII can also display synergistic activity when administered in combination with other anti-tumour treatments. For example, CAIX inhibition by specific drugs improves the effect of temozolomide in glioblastomas [161] and potentiates the effect of rapamycin in the down-regulation of the mTOR pathway. Moreover, the gene silencing of CAIX in combination with bevacizumab (anti-VEGF-A) reduces the tumour growth and induces necrosis in colon cancer and glioblastoma cells [162]. Finally, the efficacy of radiotherapy in colon adenocarcinomas is boosted by the reduction of CAIX and CAXII activity [163, 164]. The anti-cancer effects of CAIX and CAXII inhibition are summarised in Figure 1.3.2.

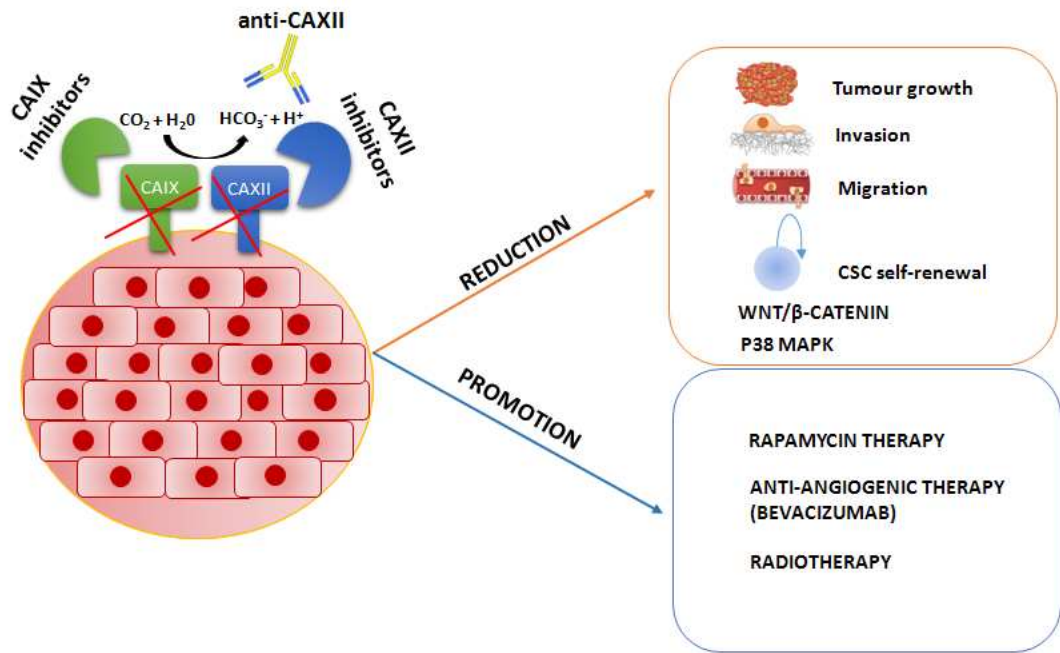


Figure 1.3.2. Anti-cancer effect of CAIX and CAXII inhibition. The inhibition of CAIX and CAXII by specific antibody or inhibitors reduces tumour growth, invasion, migration, cancer stem cell (CSC) self-renewal also interfering with the wnt/β-catenin and p38 MAPK pathways. Furthermore, inhibiting CAIX and CAXII increases the effect of common therapies such as rapamycin, anti-angiogenic treatments and radiotherapy.

1.4 Aims of the study

Featuring a rapid proliferation rate and exacerbated glycolysis, HCC creates a highly hypoxic and acidic microenvironment, which promotes disease aggressiveness and cancer-related immunosuppression. This thesis had the final aim of assessing whether interfering with tumour metabolism could represent a potential new therapeutic strategy for HCC patients.

To achieve this goal, this project was focused on pH regulators. These molecules, with their enzymatic activities, work as a bridge between tumour cells and their surrounding milieu and are directly involved in the setting of the TME acidity. In HCC cell lines and *ex vivo* in patient's tumours, we investigated the expression and the role of these molecules in shaping tumour properties and in modulating the immunological features of HCC. Specifically, we evaluated:

- a) the expression of genes encoding for the pH regulatory molecules in patient-derived HCC tissues, their relationship with markers related to aggressiveness and immunosuppression in HCC, evaluating any potential influence on patient prognosis
- b) the distribution and cellular localization of the pH regulatory molecules in HCC tissues to assess whether, on the basis of their *ex vivo* expression profile, they represented targetable molecules
- c) the effects of inhibition of the pH regulatory molecule on cell viability of HCC cell lines and dissect also the mechanisms of cell death

d) the expression of the pH regulator V-ATPase in the HCC immune infiltrating cells and the effects of blocking V-ATPase activity on the HCC TME.

2. Materials and Methods

2.1 *Ex vivo* experiments

2.1.1 Ethical statement

This study was conducted in compliance with the Declaration of Helsinki 1975. The research protocol was approved by the review board of Fondazione IRCCS Istituto Nazionale dei Tumori of Milan (protocol number: INT 110/13). Patients with HCC who underwent curative resection at Fondazione IRCCS Istituto Nazionale dei Tumori of Milan signed a written informed consent form for the collection of their liver tissue specimens for research purposes.

2.1.2 Patients, tissue samples and clinical data

Tumour (T) and adjacent non-tumour liver tissue (NT), sampled within two cm proximal to the tumour margin, were collected from patients with well-compensated cirrhosis (n=57) undergoing curative resection from 2011 to 2015 at the Gastrointestinal Surgery and Liver Transplantation Unit of Fondazione IRCCS Istituto Nazionale dei Tumori of Milan headed by the Professor Mazzaferro. Nine non-cirrhotic, normal (N) liver tissue samples were obtained from patients who underwent operations unrelated to cancer (cholecystectomy). The liver specimens were collected in the operating room and to maintain RNA integrity of cells in the tissue, under sterile conditions, the fresh tissues were cut in small pieces (≤ 0.5 cm) and then they were placed in five-ten volumes of *RNAlaterTM* solution (Thermo Fisher Scientific), stored at 4°C for overnight (ON) and then placed at -80°C until use. The characteristics and medical information of patients, including sex, age, aetiology of chronic liver disease, alpha-fetoprotein (AFP) serum levels,

number and size of tumour nodules, grade of tumour differentiation and presence or not of micro vascular invasion and recurrence, were obtained from the patients' medical records (see Table 3.1.1 in Chapter 3.1). The impact of the clinicopathological parameters on the recurrence of the tumour was assessed by univariate Cox proportional hazards regression analysis (see Table 3.1.2 in Chapter 3.1). Formalin-fixed, paraffin-embedded (FFPE) samples corresponding to the liver tissues stored in the RNA*later*TM solution were also prepared for immunostaining. Breast cancer samples were used as a control (n=3) and were obtained from a pathology archive of Fondazione IRCCS Istituto Nazionale dei Tumori of Milan.

2.1.3 HCC tissue explants: generation and treatment

Culturing of the *ex vivo* HCC tissue explants was adapted from reference [165]. The fresh HCC tissues (n=12) were cut into three mm pieces using a biopsy punch under sterile conditions and were cultured for 24h in a 48-well plate (Corning) in the presence of 300 µl RPMI 1640 with 1% FCS (Lonza) and 100 µg/ml omeprazole (Sigma-Aldrich) or drug vehicle (dimethylsulfoxide, DMSO, Sigma-Aldrich). Tumours treated with the drug or with control medium were then frozen in RNA*later*TM solution for qRT-PCR analysis.

2.1.4 RNA extraction, reverse transcription and quantitative real-time PCR on HCC tissues

Total RNA from frozen liver tissues was extracted using a NucleoSpin miRNA kit (Macherey-Nagel). The RNA*later*TM solution was removed and, to maintain the RNA integrity and to enhance the yield, the specimens were placed in liquid nitrogen and then homogenized with a TissueLyser Homogenizer

(Qiagen) in the presence of lysis buffer ML (provided in the NucleoSpin miRNA kits) and tungsten carbide beads (Qiagen) for 2 min at a frequency of 30 oscillations/sec. After the addition of ethanol, DNA and RNA were bound to the NucleoSpin RNA columns. The DNA was digested on the columns by RNase-free recombinant DNase. Subsequently, the RNA was washed and eluted with RNase-free water pre-warmed at 95°C. The purity of the RNA samples was assessed by measuring the OD_{260}/OD_{280} ratio on a Picodrop spectrometer (Picodrop). The RNA with a ratio of 1.8-2.0 was considered pure and further processed. The total RNA (2.5 µg) was used to synthesize cDNA using the High-Capacity cDNA Reverse Transcription kit (Thermo Fisher Scientific) and the reverse transcription polymerase chain reaction (RT-PCR) was carried out in the GeneAmp PCR System 9700 instrument (Thermo Fisher Scientific) using the following settings: 25 °C for 10 min and 60 °C for 120 min. cDNA obtained from the HCC tissue explants was pre-amplified using the TaqMan[®] Preamp Master Mix Kit (Thermo Fisher Scientific) by combining 188 ng cDNA with TaqMan[®] Preamp Master Mix and pooling the TaqMan[®] gene expression assays (Thermo Fisher Scientific) at a final concentration of 0.2X, according to the manufacturer's instructions. cDNA was used to perform real-time PCR (qRT-PCR) with TaqMan[®] gene expression assays and the primers/probes reported in Table 2.1.4. qRT-PCR assays were run in the ABI 7900HT instrument (Thermo Fisher Scientific) with the standard qRT-PCR settings: 50 °C for 2 min, 95 °C for 10 min, and 40 cycles of 95 °C for 15 s and 60 °C for 1 min. Data analysis was performed with SDS 2.2.2 software (Thermo Fisher Scientific). The relative levels of templates in each sample were determined through relative quantification

(RQ) using the comparative Ct ($\Delta\Delta\text{CT}$) method ($\text{RQ}=2^{-\Delta\Delta\text{CT}}$, where $\Delta\text{CT}=\text{CT}_{\text{target gene}}-\text{CT}_{\text{GAPDH}}$, and $\Delta\Delta\text{CT}=\Delta\text{CT}_{\text{sample}}-\Delta\text{CT}_{\text{calibrator}}$).

Table 2.1.4. Panel of TaqMan[®] gene expression assays					
Gene name	Gene symbol	RefSeq (NM)	Assay ID^a	Amplicon length	Protein name
Alanyl Aminopeptidase, Membrane	<i>ANPEP</i> (<i>CD13</i>)	NM_001150.2	Hs00174265_m1	64	Aminopeptidase N
ATPase H+ transporting V0 subunit a1	<i>ATP6V0A1</i>	NM_001130020.1 NM_001130021.1 NM_005177.3	Hs00193110_m1	62	V-ATPase subunit a isoform 1
ATPase H+ Transporting V0 Subunit C	<i>ATP6V0C</i>	NM_001198569.1 NM_001694.3	Hs00798308_sH	100	V-type proton ATPase 16 kDa proteolipid subunit
ATPase H+ transporting V1 subunit A1	<i>ATP6V1A1</i>	NM_001690.3	Hs01097169_m1	66	V-ATPase subunit A isoform 1
ATPase H+ transporting V1 subunit C1	<i>ATP6V1C1</i>	NM_001695.4	Hs00940702_m1	67	V-ATPase subunit C isoform 1
ATPase H+ transporting V1 subunit H	<i>ATP6V1H</i>	NM_015941.3 NM_213619.2 NM_213620.2	Hs00977521_m1	103	V-ATPase subunit H
Carbonic anhydrase 9	<i>CA9</i>	NM_001216.2	Hs00154208_m1	78	CAIX
Carbonic anhydrase 12	<i>CA12 1</i>	NM_001218.4	Hs01080910_m1	51	CAXII
Carbonic anhydrase 12	<i>CA12 2/3</i>	NM_206925.2 NM_001293642.1	Hs01080911_m1	64	CAXII
C-c motif chemokine ligand 22	<i>CCL22</i>	NM_002990.4	Hs01574247_m1	88	C-C motif chemokine 22
CD24 Molecule	<i>CD24</i>	NM_001291737.1 NM_001291738.1 NM_013230.3	Hs03044178_g1	146	Signal transducer CD24
CD44 Molecule (Indian Blood Group)	<i>CD44</i>	NM_000610.3 NM_001001389.1 NM_001001390.1 NM_001001391.1 NM_001001392.1 NM_001202555.1 NM_001202556.1	Hs01075861_m1	70	CD44 antigen

CD209 Molecule	<i>CD209</i>	NM_001144893.1 NM_001144894.1 NM_001144895.1 NM_001144896.1 NM_001144897.1 NM_001144899.1 NM_021155.3	Hs01588349_m1	131	CD209 antigen
Cadherin 1	<i>CDH1</i>	NM_001317184.1 NM_001317185.1 NM_001317186.1 NM_004360.4	Hs01023894_m1	61	cadherin 1
Epithelial Cell Adhesion Molecule	<i>EpCAM</i>	NM_002354.2	Hs00901885_m1	95	Epithelial cell adhesion molecule
Glyceraldehyde-3-phosphate dehydrogenase	<i>GAPDH</i>	NM_001289746.1 NM_002046.5	Hs99999905_m1	122	Glyceraldehyde-3-phosphate dehydrogenase
Hypoxia Inducible Factor 1 Alpha Subunit	<i>HIF1A</i>	NM_001530.3 NM_181054.2	Hs00936371_m1	62	Hypoxia-inducible factor 1-alpha
Interleukin 6	<i>IL6</i>	NM_000600.4	Hs00985639_m1	66	interleukin-6
interferon gamma	<i>IFNG</i>	NM_000619.2	Hs00989291_m1	73	Interferon gamma
Keratin 19	<i>KRT19</i>	NM_002276.4	Hs00761767_s1	116	Keratin, type I cytoke ra tin 19
V-myc avian myelocytomatosis viral oncogene homolog	<i>MYC</i>	NM_002467.4	Hs00153408_m1	107	Myc proto-oncogene protein
Nanog Homeobox	<i>NANOG</i>	NM_001297698.1 NM_024865.3	Hs02387400_g1	109	Homeobox protein NANOG
POU Class 5 Homeobox 1B	<i>POU5F1B (OCT4)</i>	NM_001159542.1	Hs01596605_s1	113	Putative POU domain, class 5, transcription factor 1B
Prominin 1	<i>PROM1 (CD133)</i>	NM_001145847. NM_001145848.1 NM_001145849.1 NM_001145850.1 NM_001145851.1 NM_001145852.1	Hs01009250_m1	75	Prominin-1

		NM_006017.2			
SRY-Box 2	<i>SOX2</i>	NM_003106.3	Hs01053049_s1	91	Transcription factor SOX-2
Thy-1 Cell Surface Antigen	<i>THY1 (CD90)</i>	NM_001311160.1 NM_001311162.1 NM_006288.4	Hs00264235_s1	99	Thy-1 membrane glycoprotein
Tumour necrosis factor	<i>TNF</i>	NM_000594.3	Hs00174128_m1	80	tumour necrosis factor
Twist Family BHLH Transcription Factor 1	<i>TWIST</i>	NM_000474.3	Hs01675818_s1	85	Twist-related protein 1
Vimentin	<i>VIM</i>	NM_003380.3	Hs00958111_m1	65	vimentin
Note: ^a TaqMan [®] Gene Expression Assays purchased from Thermo Fisher Scientific					

2.1.5 Immunohistochemistry on HCC tissues

Serial sections of 1-2- μm -thickness FFPE HCC (n=23) and normal liver (n=9) samples were processed for immunohistochemical staining. For each HCC case, the FFPE section slides of non-tumour, (NT) tumour (T) and peritumour (PT) tissues were analysed. PT corresponds to the FFPE HCC sections, which include areas enriched in immune infiltrating cells adjacent to tumour nodules. After xylene deparaffinization and rehydration, the sections were incubated in a 3% H_2O_2 solution for 10 min to block endogenous peroxidase. Antigen retrieval was performed by heating the sample in 1 mM EDTA at pH 8 or 5 mM citrate buffer solution in a high pressure cooker for 10-15 or 20 min and cooled for 15 min prior to immunostaining. A peroxidase-labeled polymer (UltraVision Quanto Detection System HRP Polymer, Thermo Fisher Scientific) was used for detection according to the manufacturer's instructions and was visualized using 3,3'-diaminobenzidinetetrahydrochloride (DAB)/ H_2O_2 . The immunostaining intensity was evaluated with a scoring system performed by the pathologist Massimo Milione of Fondazione IRCCS Istituto Nazionale dei Tumori of Milan. The intensity of the nuclear or membrane/cytoplasmic staining was scored as I = 0 negative, I = 1 lower than the internal or experimental control, and I = 2 equal to the internal or experimental control. The extent of the cell staining was scored as 0 (0-<5%), 1 (<10%), 2 (10-50%), and 3 (>50%). The score categories are shown in Table 4.1.1 and 4.2.1 in chapter 4. Bile duct cells were used as positive internal control for CAIX staining, while the glandular and superficial foveolar compartment in the stomach tissue were used as positive experimental control for and CAXII staining. The islets of

Langerhans in the human pancreas and the glandular compartment in stomach tissues were used as positive experimental controls for a1 and H staining, respectively. The antibodies used are reported in Table 2.1.5. Stained whole-section slides were scanned using the Aperio Scanscope Cs (Aperio Technologies). Images were visualized and annotated with ImageScope software (Aperio Technologies).

Table 2.1.5. Antibodies used for immunohistochemistry (IHC) analysis									
Antibody	Catalogue number	Company	Clone	Host species	Isotype	Staining platform	Dilution	Antigen retrieval	Visualization system
β-catenin	#9582	Cell Signaling	6B3	rabbit	monoclonal IgG	Manual staining	1:200	EDTA buffer pH 8, pressure cooker 15 min at 110 °C	Ultravision Quanto Detection System HRP Thermo + Liquid DAB substrate chromogen System DAKO
CAIX	/	BioScience	M75	mouse	monoclonal IgG2b	Manual staining	1:100	EDTA buffer pH 8, pressure cooker 15 min at 110 °C	Ultravision Quanto Detection System HRP Thermo + Liquid DAB substrate chromogen System DAKO
CAXII	sc-374314	Santa Cruz Biotechnology	D-2	mouse	monoclonal IgG1	Manual staining	1:50	EDTA buffer pH 8, pressure cooker 15 min at 110 °C	Ultravision Quanto Detection System HRP Thermo + Liquid DAB substrate chromogen System DAKO
CD3	ab699	Abcam	PS1	mouse	monoclonal IgG2a	Manual staining	1:50	Citrate buffer pH 6, pressure cooker 20 min at 110 °C	Ultravision Quanto Detection System HRP Thermo + Liquid DAB substrate chromogen System DAKO
CD14	MS-1080	Thermo Fisher Scientific	7	mouse	monoclonal IgG2a	Manual staining	1:50	EDTA buffer pH 8, pressure cooker 15 min at 110 °C	Ultravision Quanto Detection System HRP Thermo + Liquid DAB substrate chromogen System DAKO
CD34	M7165	Dako	QBEnd-10	mouse	monoclonal IgG1	Manual staining	1:100	Citrate buffer pH 6, pressure cooker 20 min at 110 °C	Ultravision Quanto Detection System HRP Thermo + Liquid DAB substrate chromogen System DAKO
CD68	NCL-CD68-KP1	Leica Microsystems	KP1	mouse	monoclonal IgG1 k	Manual staining	1:200	EDTA buffer pH 8, pressure cooker 15 min at 110 °C	Ultravision Quanto Detection System HRP Thermo + Liquid DAB substrate chromogen System DAKO
CD163	NCL-L-CD163	Leica Microsystems	10D6	mouse	monoclonal IgG1	Manual staining	1:100	Citrate buffer pH 6, pressure	Ultravision Quanto Detection System HRP Thermo + Liquid DAB substrate chromogen

								cooker 20 min at 110 °C	System DAKO
CD209	551186	BD	DCN46	mouse	monoclonal IgG2b	Manual staining	1:20	Citrate buffer pH 6, pressure cooker 20 min at 110 °C	Ultravision Quanto Detection System HRP Thermo + Liquid DAB substrate chromogen System DAKO
V- ATPase subunit a isoform 1	HPA0221 44	Sigma-Aldrich	/	rabbit	polyclonal	Manual staining	1:200	EDTA buffer pH 8 and 0.5% Triton, pressure cooker 15 min at 110 °C	Ultravision Quanto Detection System HRP Thermo + Liquid DAB substrate chromogen System DAKO
V- ATPase subunit C isoform 1	HPA0239 43	Sigma-Aldrich	/	rabbit	polyclonal	Manual staining	1:200	EDTA buffer pH 8, pressure cooker 15 min at 110 °C	Ultravision Quanto Detection System HRP Thermo + Liquid DAB substrate chromogen System DAKO
V- ATPase subunit H	NBP1- 85668	Novus Biological	/	rabbit	polyclonal	Manual staining	1:50	EDTA buffer pH 8, pressure cooker 15 min at 110 °C	Ultravision Quanto Detection System HRP Thermo + Liquid DAB substrate chromogen System DAKO
Note: /, not available									

2.1.6 Confocal microscopy analysis of HCC tissues

Serial sections of 1-2- μm -thick FFPE paired tumour and adjacent non-tumour liver tissues ($n = 3$) and breast cancer tissues ($n = 3$) were processed for deparaffinization and antigen retrieval. The sections were treated briefly with 0.1 M glycine in PBS, pH 7.4 followed by 0.3% Triton X-100 in 1x PBS (Sigma-Aldrich) and incubated overnight at 4 °C with the primary antibodies. The samples were washed and incubated for 1 h with dye-conjugated secondary antibodies (see Table 2.1.6). Following a final wash, the stained tissue sections were mounted on glass slides with 95% glycerol in 1x PBS. Confocal microscopic analyses were performed using FFPE samples and HCC cell lines that were exposed or not to hypoxia (1% O₂) for 72h. The antibodies used are reported in Table 2.1.6. The nuclei were stained with Toto-3 (Thermo Fisher Scientific). Confocal microscopy was performed using a Radiance 2100 microscope (Bio-Rad Laboratories) equipped with a krypton/argon laser and a red laser diode.

Table 2.1.6. Antibodies used for immunofluorescence (IF) analysis									
Antibody	Catalogue number	Company	Clone	Host species	Isotype	Staining platform	Dilution	Antigen retrieval	Visualization system
β-catenin	#9582	Cell Signaling	6B3	rabbit	monoclonal IgG	Manual staining	1:20	EDTA buffer pH 8, pressure cooker 15 min at 110 °C	anti-rabbit 488 Alexa Fluor®
Calnexin	NBP2-36570	Novus Biological	1C2.2D11	mouse	monoclonal IgG2b k	Manual staining	1:200	EDTA buffer pH 8, pressure cooker 15 min at 110 °C	anti-IgG2b 488Alexa Fluor®
CAXII	sc-374314	Santa Cruz Biotechnology	D-2	mouse	monoclonal IgG1	Manual staining	1:5	EDTA buffer pH 8, pressure cooker 15 min at 110 °C	anti-IgG1 568Alexa Fluor®
CD3	ab699	Abcam	PS1	mouse	monoclonal IgG2a	Manual staining	1:10	Citrate buffer pH 6, pressure cooker 20 min at 110 °C	anti-IgG2b 488Alexa Fluor®
CD163	NCL-L-CD163	Leica Microsystems	10D6	mouse	monoclonal IgG1	Manual staining	1:10	Citrate buffer pH 6, pressure cooker 20 min at 110 °C	anti-IgG1 568Alexa Fluor®
CD209	551186	BD	DCN46	mouse	monoclonal IgG2b	Manual staining	1:10	Citrate buffer pH 6, pressure cooker 20 min at 110 °C	anti-IgG2b 488Alexa Fluor®
V- ATPase subunit a isoform 1	HPA022144	Sigma-Aldrich	/	rabbit	polyclonal	Manual staining	1:20	EDTA buffer pH 8 and 0.5% Triton, pressure cooker 15 min at 110 °C	anti-rabbit 488 Alexa Fluor®
V- ATPase subunit H	NBP1-85668	Novus Biological	/	rabbit	polyclonal	Manual staining	1:50	EDTA buffer pH 8, pressure cooker 15 min at 110 °C	anti-rabbit 488 Alexa Fluor®
Note: /, not available									

2.1.7 Single-cell suspensions from HCC tissues

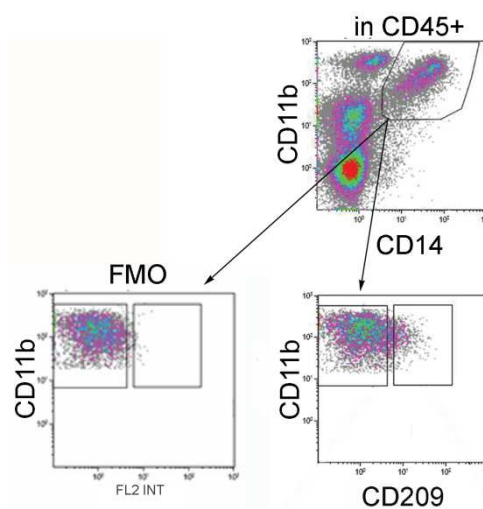
To obtain single-cell suspensions, the HCC tissues were enzymatically and mechanically digested using the gentleMACS Dissociator (Miltenyi Biotec) and were stored in liquid nitrogen until use. Briefly, the tumour liver tissue specimens were minced under sterile conditions into small pieces and digested for 1h at 37°C in the incubator following the gentleMACS Dissociator protocol (Miltenyi Biotec). The obtained cell suspension was filtered through a 70 µm mesh (BD Biosciences), the red blood cells were lysed, and the cell suspension was washed with RPMI 1640 (Lonza). The cells were stained with trypan blue and counted, then were stored in liquid nitrogen until use.

2.1.7.1 Flow cytometry on single-cell suspensions from HCC tissues

Multiparametric flow cytometry was carried out on single-cell suspensions obtained from the HCC liver tissues. The antibodies used in flow cytometry are reported in Table 2.1.7.1. Dead cells were identified using the LIVE/DEAD Fixable Violet Dead Cell Stain Kit (ThermoFisher Scientific) and were excluded from the analysis.

Intracellular staining was performed to detect CCL22, IFN γ and TNF in the single-cell suspensions treated with 100 µg/ml omeprazole or with the vehicle of the drug (DMSO) for 24h. Golgi Stop (0.7 µl/ml) was added after 1.5h of treatment. Briefly, the samples were stained with the antibodies recognising the cell surface markers (see Table 2.1.7.1). The cells were then fixed and permeabilised with Cytofix/Cytoperm buffer (BD Biosciences), and then stained for the above mentioned cytokines/chemokine. Data were acquired using a Gallios flow cytometer (Beckman Coulter) and analyzed by FlowJo, V 8.5.2 (Tree Star) or Kaluza 1.3 software (Beckman Coulter). Positive

populations were defined setting the marker on Fluorescence minus one (FMO) control. The FMO control consists of the sample stained with all the antibodies included in the panel except the antibody specific for the marker under analysis. Here, we provide an example of the FMO for the detection of CD209⁺ myeloid cells. The antibodies contained in the panel are: anti-CD45, anti-CD11b, anti-CD14 and anti-CD209. The FMO control contained anti-CD45, anti-CD11b, anti-CD14, but not anti-CD209 (Figure 2.1.7.1).



2.1.7.1 Expression of CD209 in positive myeloid cells. Multiparametric flow cytometry analysis of live myeloid cells in the cell suspension of freshly dissociated HCC tumour tissues. Marker for CD209⁺ cells inside CD14⁺CD11b⁺CD45⁺ live cells was set based on the FMO control (dot plot on the left).

Table 2.1.7.1. List of antibodies used for multiparametric flow cytometry						
Marker	Cellular localization	Fluorochrome	Clone	Host species	Isotype	Company
CCL22	Intracellular	Alexa Fluor® 647	57203	mouse	monoclonal IgG2b	R&D Systems
CD3	Cell surface	PC7	UCHT1	mouse	monoclonal IgG1	Beckman Coulter
CD11b	Cell surface	PC7	Bear1	mouse	monoclonal IgG1	Beckman Coulter
CD14	Cell surface	APC-H7	MφP9	mouse	monoclonal IgG2b k	BD Biosciences
CD45	Cell surface	BV510	H130	mouse	monoclonal IgG1 k	BD Biosciences
CD163	Cell surface	PerCP-Cy5.5	6H1/61	mouse	monoclonal IgG1 k	BD Biosciences
CD209	Cell surface	Pe	DCN46	mouse	monoclonal IgG2b	BD Biosciences
IFNγ	Intracellular	Fitc	4S.B3	mouse	monoclonal IgG1	Biolegend
TNF	Intracellular	APC	Mab11	mouse	monoclonal IgG1	BD Biosciences
V-type proton ATPase subunit a isoform 1	Cell surface	Purified	/	rabbit	polyclonal	Santa Cruz Biotechnology
Secondary antibody:						
goat anti-rabbit		Alexa Fluor® 647	/	goat	/	Thermo Fischer Scientific
Note: /, not available						

2.1.8 Generation of the index score

The prognostic effect of the gene expression of *HIF1A*, *CA9*, *CA12 1*, *CA12 2/3*, *ATP6V0A1*, *ATP6V0C*, *ATP6V1A*, *ATP6V1C1*, *ATP6V1H*, *IL6*, *CD209*, *TWIST*, *CDH1*, *VIM*, *CD13*, *CD24*, *CD44*, *CD90*, *EpCAM*, *CD133*, *KRT19*, *OCT4*, *NANOG* and *SOX2* on relapse-free survival (RFS) was assessed by Dr. Luigi Mariani and Dr. Luca Lalli of Fondazione IRCCS Istituto Nazionale dei Tumori of Milan on the 57 HCC tissues analysed by qRT-PCR.

We performed univariate Cox proportional hazards regression analysis to assess the association between recurrence and our genes (see Table 3.4.2 in chapter 3.4). In addition, multivariate analysis based on a machine learning tool known as 'Adaptive Index Model' [166] was applied to generate the HCC index score (HIS). This method proceeds according to the following steps: 1) the genes were considered as variables; 2) a cut-off was assigned to each variable, so as to clearly separate (dichotomise) the expression of the genes in each patient analysed (Variable selection+dichotomisation); 3) enumeration of the altered genes, whereby each selected gene is considered as altered if the corresponding measure is above or below the cut-off value, depending on the existence of a positive or negative association with RFS (index score generation); 4) groups that are homogeneous in terms of number of altered genes are created (aggregation). The workflow of the HIS is reported in Figure 2.1.8. We investigated also the association of the HIS with the clinicopathological parameters by Mann-Whitney or Chi squared tests for continuous or categorical variables, respectively (see Table 3.4.2 in chapter 3.4).

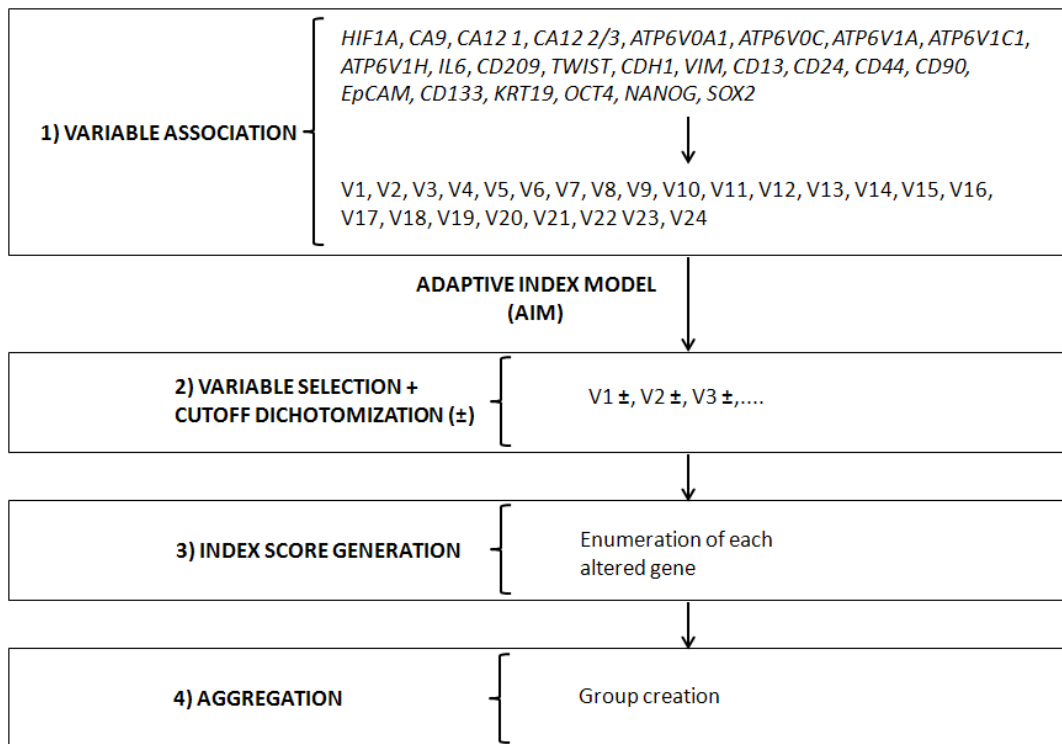


Figure 2.1.8. Generation of the HCC Index Score (HIS). This figure illustrates the workflow for the generation of the HIS.

2.2 *In vitro* experiments

2.2.1 Cell lines and culture conditions

Human HCC cell lines C3A, PLC/PRF/5, SNU-449 and the breast cancer cell line T-47D were purchased from American Type Culture Collection (ATCC). RPMI-1640 (Lonza) was used as a complete culture medium supplemented with 10% heat-inactivated foetal calf serum (FCS, Lonza), 100 U/ml penicillin, 100 U/ml streptomycin. Standard culturing condition (normoxia, N) was performed under 21% O₂, 5% CO₂, 37°C, 95% humidity. Incubation in hypoxia (H) was carried out at 1% O₂, 5% CO₂, 94% N₂ gas mix at 37°C, 95% humidity. The HCC

cell lines grown at 80-90% confluence were trypsinized, washed in 1x PBS (Lonza) and used for the analysis. The cell lines were routinely checked for their identity by STR profiling and were free of mycoplasma, as assessed using the N-GARDE Mycoplasma PCR reagent set (EMK-090020, Euroclone).

2.2.2 RNA extraction, reverse transcription and quantitative real-time PCR on HCC cell lines

The cells were seeded at a density of 2.5×10^5 cells/well on six-well plates with 3 ml RPMI+10% FCS and incubated under either normoxic or hypoxic conditions for 72h. The total RNA from the HCC cell lines grown was extracted using a NucleoSpin miRNA kit (Macherey-Nagel). To avoid changes in the oxygen content in the culture, the cells were removed from the normoxic or hypoxic specific incubators and, under sterile conditions, were removed from the medium from each well, washed two times with 1x PBS (Lonza) and 300 μ l of lysis buffer ML added (provided in the NucleoSpin miRNA kits). The cells were lysed immediately, and then the lysates were recovered to proceed with RNA extraction and cDNA synthesis as indicated in 2.1.4.

2.2.3 Western blotting on HCC cell lines

The HCC cell lines exposed to either normoxia or hypoxia were lysed in modified RIPA buffer (20 mM Tris-HCl, pH 7.4, 150 mM NaCl, 5 mM EDTA, 1% Nonidet P-40) in the presence of protease Inhibitors (Roche), 1 mM Na_3VO_4 and 1 mM PMSF. Protein samples were boiled in NuPAGE LDS sample buffer (Invitrogen) and separated on NuPAGE Novex 10% Bis-Tris gels (Invitrogen) in MES running buffer (Invitrogen), and then transferred onto nitrocellulose filters and

immunoblotted with the appropriate antibodies. The monoclonal mouse anti-human antibodies were directed against the following antigens: CAIX (clone M75, IgG2b, 1:2000 dilution, BioScience), vinculin (1:10000 dilution, cat. no.: V4505, Sigma-Aldrich) and α -tubulin (1:6000 dilution, cat. no.: T5168, Sigma-Aldrich). Rabbit monoclonal anti-human antibodies were directed against the following antigens: CAXII (clone D75C6, IgG, 1:500 dilution, cat. no.: 5864, Cell Signaling), β -actin (1:1000 dilution, cat. no.: A2066, Sigma-Aldrich), V-type proton ATPase subunit a isoform 1 (1:1000, cat. no.: HPA022144, Sigma-Aldrich), and V-type proton ATPase subunit C isoform 1 (1:1000, cat. no.: HPA023943, Sigma-Aldrich). The immuno-reactive bands were visualized using horseradish peroxidase (HRP)-conjugated secondary antibodies (Sigma-Aldrich), and the intensity of the signal was evaluated after incubation of the membranes with the HRP substrate (ECL Western Blotting Detection Reagent, Amersham) followed by exposure of the membranes to autoradiography film (Hyperfilm MP, Amersham Biosciences) and development using an automatic developer (Curix 60, AGFA).

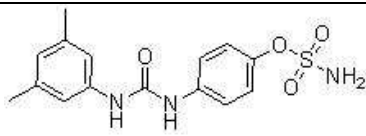
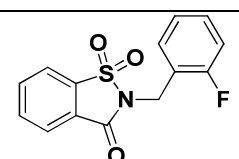
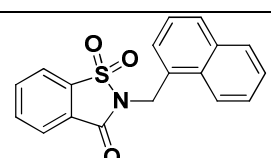
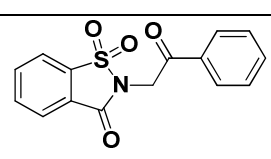
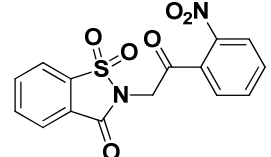
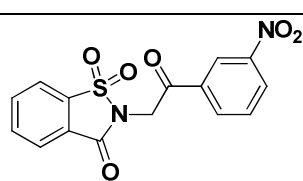
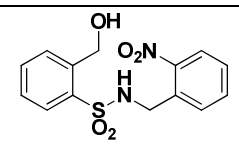
2.2.4 Flow cytometry on HCC cell lines

Anti-human CAIX and CAXII were purchased from BioScience and Cell Signaling, respectively. Cell surface staining was performed at RT. 1×10^6 cells were added in each assay tube. An anti-mouse FITC-conjugated secondary antibody (Dako) and anti-rabbit Alexa 647 (Thermo Fischer Scientific) was used for the detection of CAIX and CAXII, respectively. Data were acquired by Gallios (Beckman Coulter) and analyzed using FlowJo, V 8.5.2, (Tree Star).

2.2.5 Pharmacological inhibitors and cell viability assays

The selective CAIX inhibitor S4 and the selective CAXII inhibitor compound 25 were developed by the team of Professor Claudiu Supuran. See Table 2.2.5 for the chemical and biological details of the CAIX and CAXII inhibitors. These inhibitors have a sulfonamide group, which binds the catalytic zinc ion located in the active site of CAs. The synthesized compounds inhibit the *in vitro* CO₂ hydration activity of the recombinant CAIX and CAXII proteins evaluated by a colorimetric enzymatic assay using a Photophysics stopped-flow instrument. The selected compounds display specificity for CAIX and CAXII having no effect on the enzymatic activity of the ubiquitous off-target isoforms CA I and CA II, used as recombinant proteins, of in the above mentioned enzymatic assay [167-168]. Omeprazole was purchased from Sigma-Aldrich. Drugs were dissolved in DMSO (Sigma-Aldrich) and were stored at -20 °C. The HCC cells were plated at a density of 4 x 10³ cells/well on 96-well plates (Corning), drugs were added to fresh medium after 24 h from the seeding in the appropriate normoxic or hypoxic conditions, and the plates were incubated for an additional 72h in the appropriate growing conditions. The tested concentrations of the CAIX inhibitor S4 were 12.5 μM, 25 μM, 50 μM and 100 μM. The CAXII inhibitor compound 25 was used at concentrations of 12.5 μM, 25 μM, 50 μM, 100 μM and 200 μM, while omeprazole was used at concentrations of 25 μg/ml, 50 μg/ml, 100 μg/ml and 150 μg/ml. Prior to use, omeprazole was activated in acidified water at pH 3.7 for 30 min at RT in the dark and then diluted in culture medium. The activated omeprazole was used throughout the present study. The effects of

both CA inhibitors and activated omeprazole were tested in cell viability assays. As a vehicle control, the cells were treated with respective volumes of DMSO using the same approach. Treatment with the CA inhibitors was performed under normoxia (21% O₂) and hypoxia (1% O₂). Treatment with omeprazole was performed under normoxia (21% O₂) only. Cell viability was evaluated using the (3-(4,5)-dimethylthiazol-2-yl)-2,5-diphenyltetrazolium bromide (MTT) colorimetric assay (Sigma-Aldrich). Briefly, in each well, 50 µl of conditioned medium was replaced with 50 µl pre-warmed MTT solution (Sigma-Aldrich), and the plates were incubated at 37 °C for 2 h. When the purple precipitate of formazan crystals was clearly visible under the microscope, the total volume of each well was discarded by aspiration. Subsequently, 100 µl detergent solution was added to all the wells, and the plates were covered and incubated at RT on a shaker for 10 min in the dark. The absorbance was measured at 570 nm with a spectrophotometer (Infinite[®] M1000, Tecan). Data were reported as the average values from triplicate readings.

Table 2.2.5. Chemical details of selective CAIX and CAXII inhibitors				
Compound	Structure	Formula Weight	K_i (nM)	
			hCA IX	hCA XII
CAIX inhibitor				
S4		335.38	7	2
CAXII inhibitors				
12		291.30	> 50 000	2 520
16		323.37	> 50 000	2 540
18		301.32	> 50 000	1 780
19		346.31	> 50 000	970
20		346.31	> 50 000	2010
25		322.34	> 50 000	250

2.2.6 Cell proliferation assay

Cell proliferation was assessed using a BrdU Cell Proliferation Assay Kit (Cell Signaling). The cells were seeded at 4×10^3 cells/well in a 96-well plate and incubated overnight at 37°C. The cells were then treated with either 100 µM CAIX inhibitor (S4), 200 µM CAXII inhibitor (25), 100 µg/ml omeprazole or 5 µM doxorubicin for 48h. Finally, 10 µM BrdU was added to the plate, cells were incubated for 4h at 37 °C, and cell proliferation was assessed following the manufacturer's instruction. The assay was carried out under normoxia (21% O₂). The optical density was recorded using Infinite[®] M1000 (Tecan) at a reference wavelength of 450 nm.

2.2.7 Apoptosis assays

The cells were seeded at 8×10^5 cells/well in a T-75 cm² flask (Corning) and incubated overnight at 37°C. The cells were then treated with either 100 µM CAIX inhibitor (S4) or 1 µM staurosporine for 24h. Cell apoptosis was detected using a Caspase-3 Apoptosis Kit (Becton Dickinson) by a Gallios flow cytometer (Beckman Coulter) and analyzed by FlowJo, V 8.5.2 (Tree Star).

Caspase 3/7 activity was determined using a Caspase-Glo 3/7 assay kit (Promega, UK) according to the manufacturer's protocol. Briefly, the cells at 4×10^3 cells/well in an opaque-walled 96-well plate were incubated overnight at 37 °C. The cells were then treated with either 100 µM CAIX inhibitor (S4), 200 µM CAXII inhibitor (25), 100 µg/ml omeprazole or 1 µM staurosporine for 24 h. Then, 100 µl Caspase-Glo 3/7 reagent was added to the wells. The plates were gently shaken and then incubated in the dark at 37°C. The generated

luminescent signals were measured by Infinite[®] M1000 (Tecan). The apoptotic assays were performed under normoxia (21% O₂).

2.2.8 Necrosis assay

Necrosis induction was evaluated using the RealTime-Glo Annexin V Apoptosis and Necrosis Assay (Promega) according to the manufacturer's instructions. Briefly, the cells were seeded at 10×10^3 cells/well in an opaque-walled 96-well plate and incubated overnight at 37 °C. The cells were then treated with either 100 µM CAIX inhibitor (S4), 200 µM CAXII inhibitor (25), 100 µg/ml omeprazole or 50 µg/ml digitonin and, at the same time, 100 µl 2x Detection reagent was added. The plates were incubated in the dark at 37°C. The assay was carried out under normoxia (21% O₂). This assay is based on a fluorescent dye that is internalized in the cells when the cell membrane is compromised. The generated fluorescent signals at 485nm_{Ex}/530nm_{EM} were measured by Infinite[®] M1000 (Tecan) after 48h and 72h of treatment.

2.2.9 Confocal microscopy analysis on HCC cell lines

The HCC cell lines (C3A, PLC/PRF/5 and SNU-449) exposed or not to hypoxia (1% O₂) for 72h were collected by centrifugation, washed in 1x PBS (Lonza), fixed in 4% paraformaldehyde for 30 min, washed with 1x PBS and plated on glass slides. The confocal microscopy analysis was performed to evaluate the combined expression of CAXII, β-catenin and calnexin. The antibodies used are reported in Table 2.1.6. The immunofluorescence staining was performed as reported in 2.1.6.

2.3 Statistical analysis

Statistical analyses were performed using GraphPad Prism Software v.5 (GraphPad). The Wilcoxon matched pairs test was used to compare gene expression levels between matched non-tumour and tumour tissues, and the unpaired Mann-Whitney *U*-test was used to compare the gene expression levels between normal and non-tumour tissues and between unrelated normal and tumour tissues. p-values less than or equal to 0.05 were considered significant.

Spearman correlation analysis was performed on gene expression data ($\Delta Ct = Ct_{\text{target gene}} - Ct_{\text{GAPDH}}$) in the 57 liver tissues analyzed by qRT-PCR.

Fitted lines were generated using the four-parameter dose-response curve (variable slope), and the IC_{50} values for the inhibition of cell growth at 72 h of S4, compound 25 and omeprazole treatment were calculated. One-way analysis of variance (ANOVA) followed by Bonferroni correction was used to evaluate statistical significance.

One-way analysis of variance (ANOVA) followed by Dunnett correction was used to evaluate the statistical significance of the impact of S4, compound 25 and omeprazole on cell viability, BrdU incorporation, apoptosis and necrosis.

The paired t test was used to compare the expression of *MYC*, *CDH1*, *VIM*, *CCL22*, *IFNG* and *TNF* in HCC tumour explants treated with 100 $\mu\text{g/ml}$ omeprazole or the vehicle of the drug. To evaluate the modulation of IFN γ , TNF and CCL22 in fresh CD163⁺ and CD3⁺ cells isolated from HCC tissues due to the treatment with 100 $\mu\text{g/ml}$ omeprazole or the vehicle of the drug, paired t tests were used.

3. Results and discussion

3. pH regulatory molecules, intrinsic features and aggressiveness of HCC

HCC is one of the ten most frequent cancers in the world and it is the second leading cause of cancer-related death worldwide [60]. Although HCC is a hypervascular tumour, it arises in a hypoxic microenvironment due to the inflammation status of the surrounding tissue and the insufficient supply of oxygen to sustain the metabolic rate of HCC cells [84]. In conditions of hypoxia, tumour cells, including HCC cells, further exacerbate their dysfunctional metabolism and generate high quantities of CO₂ and acidic metabolites, such as lactate and H⁺, which leads to a decreased pHi. To cope with this acidity and to restore a physiological alkaline pHi, tumour cells overexpress pH regulatory molecules such as CAIX and CAXII that catalyse the reversible hydration of CO₂ and water to bicarbonate and H⁺, and V-ATPase complex that extrudes H⁺ out of the cells. This export leads to a reduction of the extracellular pH and acidification of the TME [97]. The hypoxic and acidic TME is pro-tumourigenic, because it favours immune evasion and local inflammation. Immunosuppressive/inflammatory cells, mainly by releasing soluble cytokine/chemokines, directly influence tumour aggressiveness [17]. However, the pH regulators *per se* are involved in the functional specification of suppressive cells such as M2 macrophages [169]. They also directly affect molecular pathways crucial in cancer cells [50, 100, 150, 152] and in CSC biology [116, 151]. Hence, pH regulatory molecules constitute a crucial hub of a

multimodal network resulting in tumour maintenance and progression. To the best of our knowledge, the relevance of these molecules in HCC is poorly defined. Thus, we investigated the expression of genes encoding for the pH regulatory molecules in patient-derived HCC tissues and their relationship with markers related to aggressiveness and immunosuppression of HCC with the final aim to discover any potential influence on patient prognosis.

3.1 mRNA expression of pH regulators in HCC patients

We collected 57 matched tumour (T) and non-tumour (NT) snap-frozen tissues from HCC patients undergoing curative resection from 2011 to 2015 at the Gastrointestinal Surgery and Liver Transplantation Unit of our Institute headed by the Professor Mazzaferro. The characteristics and medical information of the patients, including sex, age, liver status, aetiology of chronic liver disease, pathology results are reported in Table 3.1.1. The vast majority of the patients were male with a medium age ≥ 50 years, have a single HCC nodule in the liver with an intermediate grade of differentiation (grading 2 or G2) and have tumour invasion into minor vessels identified during macroscopic examination or radiological imaging, which is defined as micro vascular invasion. The patients are similarly distributed in the etiology subclasses, in the size of the tumour nodule, while 40.4% of patients recurred after surgical intervention.

Table 3.1.1. The clinicopathological characteristics of HCC patients

Clinical variable	N°	%
Age, mean \pm SD, years	72.0 \pm 9.9	
<50	2	3.5
\geq 50	55	96.5
Sex		
Male	44	77.2
Female	13	23.6
Etiology		
HBV	13	22.8
HCV	19	33.3
Others (NASH, POTUS, hemocromatosis)	16	28.1
Healthy liver	9	15.8
AFP, ng/mL*		
<20	35	63.6
20-100	9	16.4
100-400	5	9.1
\geq 400	6	10.9
Tumour number		
Single	49	86.0
Multiple	8	14.0
Tumour size, cm		
<3	20	35.1
3-5	17	29.8
\geq 5	20	35.1
Micro vascular invasion		
yes	35	61.4
no	22	38.6
Grading		
G1	3	5.3
G2	40	70.2
G3	14	24.6
Recurrence		
yes	23	40.4
no	34	59.6

Clinical and pathological features of the 57 matched tumour and non-tumour tissues collected from patients with HCC undergoing curative resection from 2011 to 2015 at the Gastrointestinal Surgery and Liver Transplantation Unit of our institute. * AFP, alpha-fetoprotein values not available for 2 patients

We evaluated the association between the clinicopathological parameters and recurrence of the 57 HCC patients by Cox's univariate proportional hazards model. The results reported in Table 3.1.2 indicated that gender is a prognostic factor for these patients (HR=4.193 for females versus males, 95% CI 1.827-9.627, $p < 0.001$). The other clinicopathological parameters were not significantly associated with tumour relapse (Table 3.1.2).

Table 3.1.2. Univariate analysis of clinicopathological parameters associated with recurrence of 57 HCC patients

Variables	Recurrence		
	Univariate analysis		
	HR	95% CI	P value
Age	0.691	0.421-1.1330	0.143
Sex (female versus male)	4.193	1.827-9.627	<0.001
Etiology			0.444
HBV versus healthy liver	0.954	0.256-3.563	
HCV versus healthy liver	1.284	0.408-4.041	
Others versus healthy liver	0.443	0.009-1.982	
AFP	1.201	0.884-1.633	0.241
Tumour number	1.134	0.173-7.419	0.896
Tumour size	1.348	0.991-1.834	0.058
Micro vascular invasion (yes versus no)	1.968	0.801-4.837	0.139
Grading G3 versus G2	1.167	0.459-2.966	0.870

Notes: HR, hazard ratio; CI, interval of confidence; AFP, alpha-fetoprotein

We started our analysis evaluating the positivity of the pH regulators CAIX, CAXII, V-ATPase subunits and HIF1- α at the gene expression level in the surgical tissue samples. CAIX, CAXII and HIF1- α are encoded by the genes *CA9*, *CA12* and *HIF1A*, respectively. Regarding *CA12*, alternative spliced

isoforms of *CA12* transcript have been described. One of these forms is present in astrocytic gliomas [147]. By alternative splicing, a single gene can generate multiple transcripts, ultimately leading to different proteins. In the splicing events, regulated by several splicing factors, which constitute the spliceosome machinery, one or more exons can be included or excluded during the maturation of the mRNA. The proteins generated from alternatively spliced mRNAs have differences in their amino acid sequence, which might be associated also to differences in their biological functions. In many cancer types, genes encoding splicing factors are frequently mutated and the generation of alternative splicing variants have been associated with cancer. Since hypoxia induces changes in gene transcription and it can also modulate the splicing of pre-mRNA molecules [170], we were interested in investigating the expression of the alternative splicing isoforms of *CA12* in HCC and its relationship with hypoxia.

Until now three transcripts of *CA12* mRNA are described, whose sequences are reported on the nucleotide database in the National Centre for Biotechnology Information (NCBI). The transcript variant #1, here called *CA12 1*, identified by the NCBI reference sequence: NM_001218.4 is 4209 bp in length contains 11 exons and encodes a protein of 354 aa. The NCBI reference sequence: NM_206925.2 coincides with the alternative transcript variant #2 of *CA12*, namely *CA12 2*, which lacks exon nine and encodes a protein of 343 aa. Finally, the alternative transcript variant #3, which is *CA12 3*, corresponds to the NCBI reference sequence: NM_001293642.1. It lacks exons three and nine and

encodes a protein of 284 aa. Figure 3.1.1 illustrates the graphical schematisation of *CA12* transcript variants. As described in Materials and Methods (chapter 2), TaqMan[®] gene expression assays exist for detecting *CA12* 1, and *CA12* 3 and the joint expression of *CA12* 2 and 3. No TaqMan[®] gene expression assay exists which uniquely detects the *CA12* 2 form. In the present thesis we checked the expression of the gene transcripts: NM_001218.4 (*CA12* 1) identified by the Hs01080910_m1 TaqMan[®] and NM_206925.2 and NM_001293642.1 evaluated by the same assay Hs01080911_m1.

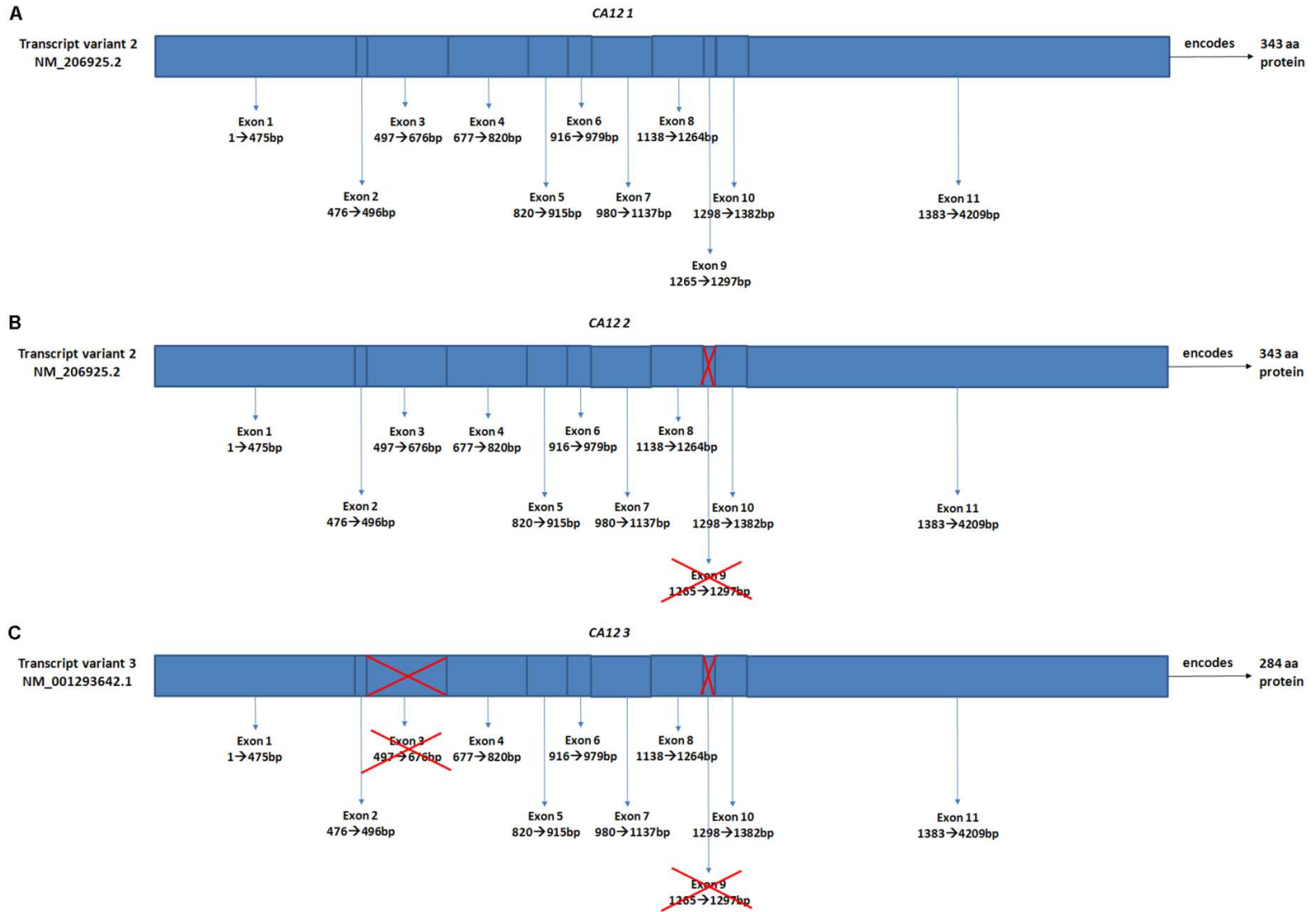


Figure 3.1.1 Schematic representation of CA12 transcript variants. Three transcript variant sequences of CA12 are reported in the nucleotide database National Centre for Biotechnology Information (NCBI) and the relative NCBI reference sequences are depicted in the figure **(A-C)**. **(A)** The transcript variant one of CA12 (NM_001218.4) has 11 exons and it encodes a protein of 354 amino acids (aa). **(B)** NM_206925.2 identifies the alternative transcript variant two of CA12, which is composed of ten exons. It loses the exon nine and it encodes a protein of 343 aa. **(C)** The alternative transcript variant three of CA12 (NM_001293642.1) loses exons three and nine and it is in total composed of nine exons. This transcript encodes a protein of 284 aa.

To investigate the expression of the V-ATPase complex, we chose to test the *ATP6V0A1*, *ATP6V0C*, *ATP6V1A*, *ATP6V1C1* and *ATP6V1H* genes that encode for the proteins a1, c, A1, C1 and H, respectively. Among the 14 subunits of the complex we studied these subunits because a1 contains the binding site for PPIs, while c, A1, C1 and H are involved in the regulation and the status of the whole complex [100].

Given that HCC arises from chronically inflamed liver tissue, samples from normal liver (N) obtained from patients undergoing an operation unrelated to cancer (cholecystectomy) (n=9) were included as a control group. qRT-PCR analysis showed that in comparison with N, both NT and T tissues displayed increased transcription of the *HIF1A* gene. NT and T tissues also exhibited an increase in the expression of *CA9* mRNA. Conversely, *CA12 1* was strongly positive in T samples, while it was barely detectable in N and NT tissues. Interestingly, the *CA12 2/3* was almost selectively expressed in T tissues. Concerning the V-ATPase complex, altogether all the subunits displayed an enhanced expression in T compared with NT or normal liver, with the differences reaching statistical significance for the *ATP6V1A*, *ATP6V1C1* and *ATP6V1H* genes. The *ATP6V0A1* and *ATP6V0C* genes were overexpressed in NT and T compared to N samples, but the differences were not statistically significant (Figure 3.1.2).

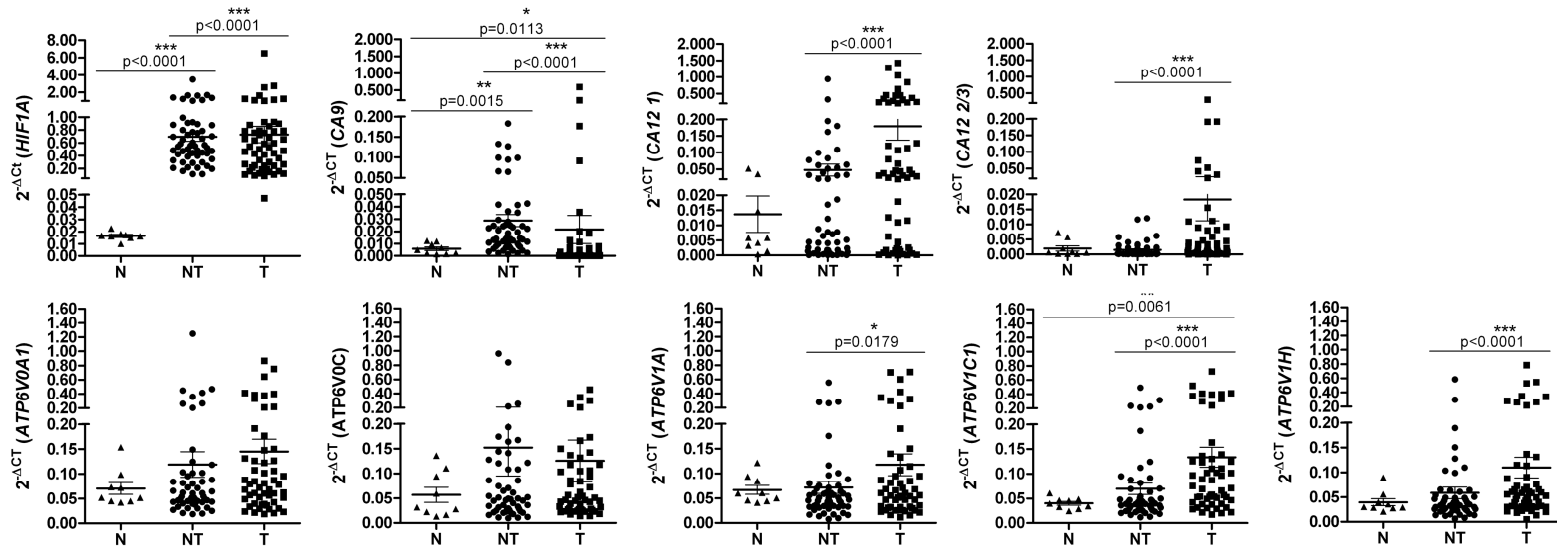


Figure 3.1.2. Gene expression of pH regulatory molecules in liver tissues. mRNA expression levels of *HIF1A*, *CA9*, *CA12 1*, *CA12 2/3*, *ATP6V0A1*, *ATP6V0C*, *ATP6V1A*, *ATP6V1C1* and *ATP6VIH*. The expression of the indicated genes was evaluated in nine normal (N) and 57 paired samples of adjacent non-tumour (NT) and tumour (T) liver tissues (see Materials and Methods for the statistical analyses used). The data are reported as $2^{-\Delta Ct}$ values ($\Delta Ct = Ct_{\text{target gene}} - Ct_{\text{GAPDH}}$).

To investigate any possible clinical relevance of the pH regulatory molecules, we evaluated the gene expression of the pH regulatory molecules in relationship to tumour number and size, presence or not of micro vascular invasion and grading. In our series, among the pH regulators analysed, *CA9*, *CA12* and *CA12 2/3* gene expression was associated with tumour grade of HCC, thus indicating their possible involvement in tumour malignancy (Figure 3.1.3). The other clinicopathological parameters tested did not show any significant relationship with the pH regulators.

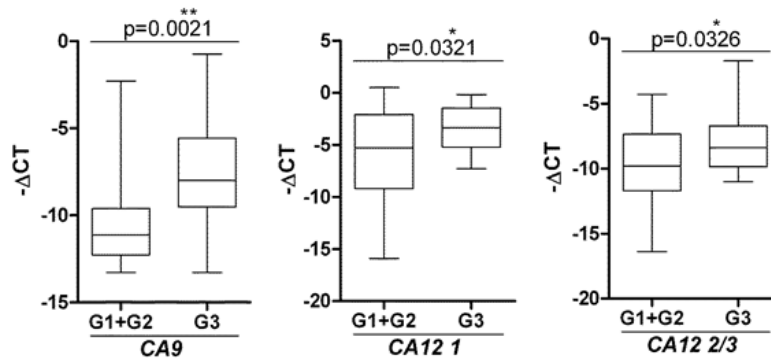


Figure 3.1.3. Expression of pH regulatory molecules in relationship to tumour differentiation. High expression of *CA9*, *CA12 1* and *CA12 2/3* was associated with poorly differentiated HCC (grading 3 or G3). Gene expression data of 57 tumour tissues analysed were reported as $-\Delta Ct$ values. The reported p-values were calculated by the unpaired t test.

3.2 Evaluation of genes related to HCC aggressiveness in HCC patients

In order to characterise the aggressive features of HCC, we evaluated the expression of EMT-, CSC- and inflammatory/immunosuppressive-related genes. As EMT-related genes, we explored the gene expression of *TWIST*, *CDH1* and *VIM*. We found that *TWIST* expression was much higher in NT and T than in N

tissues. The expression of *CDH1* in T samples was similar to N tissues, while T tissues showed lower *CDH1* expression compared to NT, in which *CDH1* was increased. We expected a high positivity of *VIM* in T tissues, but we observed the same expression level of *VIM* between NT and T samples. Nevertheless, this positivity was higher than that found in N samples (Figure 3.2.1).

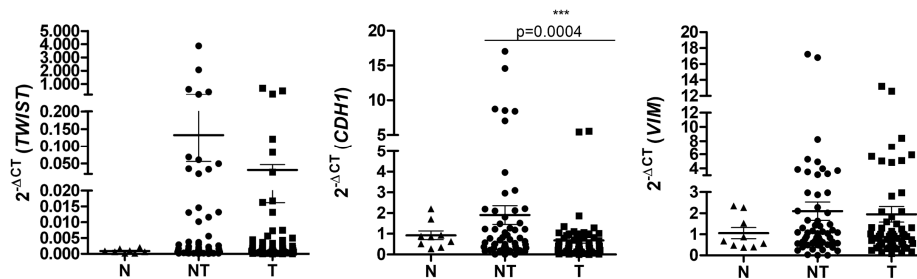


Figure 3.2.1. Gene expression of EMT-related genes in liver tissues. mRNA expression levels of *TWIST*, *CDH1* and *VIM*. The expression of the indicated genes was evaluated in nine normal (N) and 57 paired samples of adjacent non-tumour (NT) and tumour (T) liver tissues (see Materials and Methods for the statistical analyses used). The data are reported as $2^{-\Delta Ct}$ values ($\Delta Ct = Ct_{\text{target gene}} - Ct_{\text{GAPDH}}$).

In our liver tissues, we also investigated the expression of *CD13*, *CD24*, *CD44*, *CD90*, *EpCAM*, *CD133*, *KRT19*, *OCT4*, *NANOG* and *SOX2*, all genes encoding for markers described as associated to the putative CSCs of HCC [76]. These markers exhibited enhanced expression in T compared to N with the differences reaching statistical significance for the *CD24* and *CD90*. However, NT tissues exhibited high positivity of *CD13*, *PROM1* or *CD133*, *EpCAM*, *KRT19* and *OCT4*, suggesting an expansion of the stem cell compartment due to the inflammation and wound healing present in NT tissues (Figure 3.2.2).

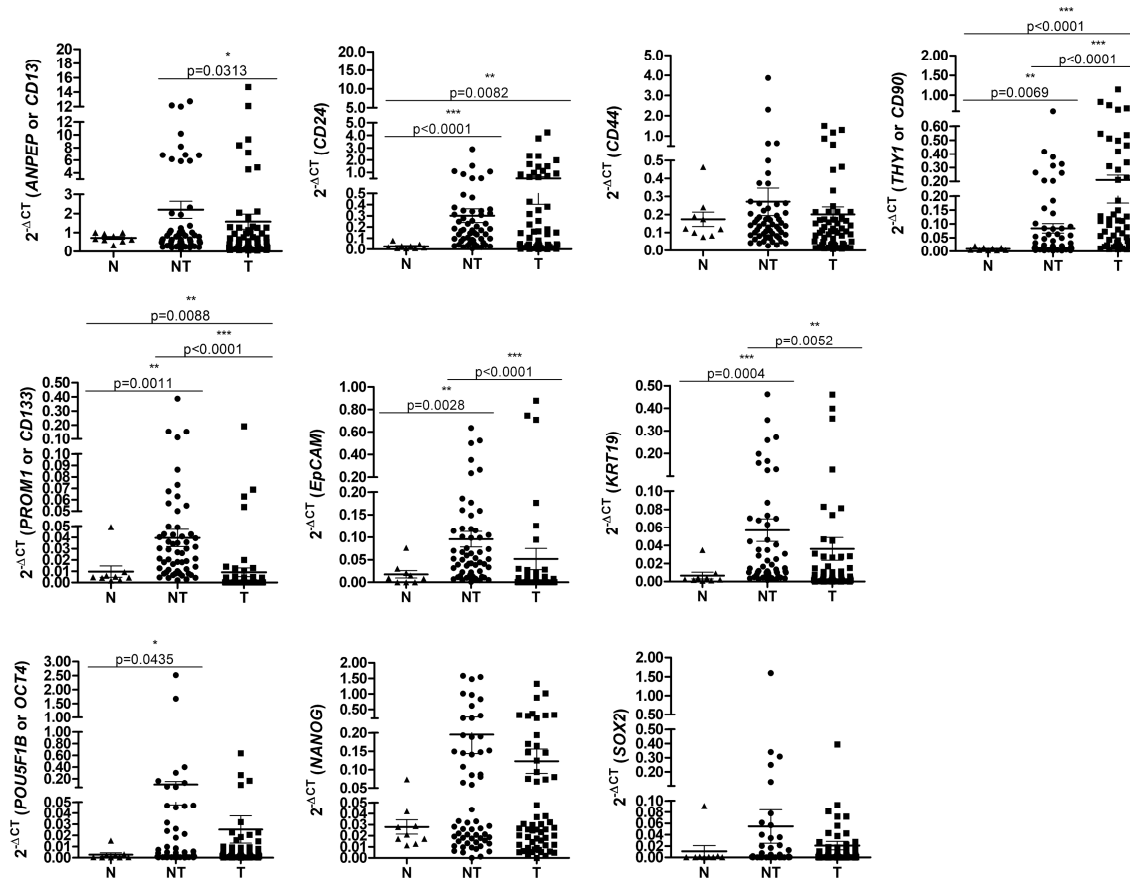


Figure 3.2.2. Gene expression of CSC-related genes in liver tissues. mRNA expression levels of ANPEP or CD13, CD24, CD44, THY1 or CD90, PROM1 or CD133, EpCAM, KRT19, NANOG, POU5F1B or OCT4 and SOX2. The expression of the indicated genes was evaluated in nine normal (N) and 57 paired samples of adjacent non-tumour (NT) and tumour (T) liver tissues (see Materials and Methods for the statistical analyses used). The data are reported as $2^{-\Delta Ct}$ values ($\Delta Ct = Ct_{\text{target gene}} - Ct_{\text{GAPDH}}$).

It is well known that IL-6 is a pro-tumourigenic cytokine that can be produced by TAMs and it can support the expansion of liver CSCs [80]. CD209 is a marker for myeloid cell-infiltration and it is considered as a TAM-associated marker [35]. Thus, we analysed the gene expression of *IL6* and *CD209* in our samples by qRT-PCR. *IL6* was significantly increased in T compared to NT samples, on the contrary *CD209* was significantly reduced in NT and T tissues compared to N samples (Figure 3.2.3).

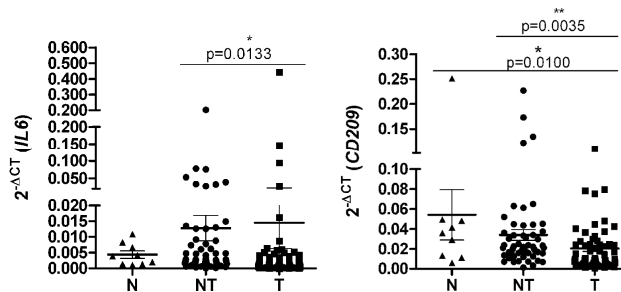


Figure 3.2.3. Gene expression of inflammatory/immunosuppressive-related genes in liver tissues. mRNA expression levels of *IL6* and *CD209*. The expression of the indicated genes was evaluated in nine normal (N) and 57 paired samples of adjacent non-tumour (NT) and tumour (T) liver tissues (see Materials and Methods for the statistical analyses used). The data are reported as $2^{-\Delta Ct}$ values ($\Delta Ct = Ct_{\text{target gene}} - Ct_{\text{GAPDH}}$).

3.3 Correlation between pH regulators and genes related to HCC

aggressiveness

To investigate if there was any connection among all the genes analysed, namely *HIF1A*, *CA9*, *CA12 1*, *CA12 2/3*, *ATP6V0A1*, *ATP6V0C*, *ATP6V1A*, *ATP6V1C1*, *ATP6V1H*, *IL6*, *CD209*, *TWIST*, *CDH1*, *VIM*, *CD13*, *CD24*, *CD44*, *CD90*, *EpCAM*, *CD133*, *KRT19*, *OCT4*, *NANOG* and *SOX2*, we performed Spearman's correlation analysis.

The results revealed a different significant degree of correlation among the studied genes (Figure 3.3). We noticed these most relevant correlations:

1. The genes encoding the different V-ATPase subunits were linked to each other. No correlation was found between genes of the V-ATPase family to those of the CA family (with the exclusion of a low degree of correlation linking *CA12 3/2* to *ATP6V1C1*), thus suggesting that CA and ATPase molecules are likely to exert non-redundant functions in HCC.
2. As expected from the literature data, the expression of *CA9* and of the spliced variants *CA12 2/3* were positively correlated to *HIF1A*. Likely because of their dependency on hypoxia, *CA9* and *CA12 2/3* gene expression was also partially correlated. Moreover, the expression of the transcript variant *CA12 2/3* was linked to the level of the main transcript *CA12 1*.
3. *HIF1A* positively correlated with the EMT-associated gene *TWIST*, with *CD44* and, although to a lower extent with *KRT19*, representative of CSC-related genes.
4. *CA9* expression was strongly correlated to *TWIST*, and to most of the CSC-related genes evaluated, including *CD24*, *EpCAM*, *CD133* and *KRT19*. *CA12 1* and *CA12 2/3* were both correlated to the expression of *VIM* and *CD44*.
5. The *IL6* gene expression was strongly correlated, as expected, to the myeloid marker *CD209* and to *CD133*, likely supporting the hypothesis that CSCs may directly produce IL-6 protein. Importantly, although with a

low degree of correlation, *IL6* was also associated to the expression of the pH regulatory genes, including *CA12 2/3*, *ATP6V1A* and *ATP6V1C1*. Moreover a link between *CA12 2/3* and *CD209* expression was also found.

Altogether, these data support our hypothesis that hypoxia and pH regulatory molecules are linked to the aggressive and the inflammatory/immunosuppressive status of HCC.

Spearman's correlation analysis																											
HIF1A																											
CA9	0.44																										
CA12 1																											
CA12 2/3	0.39	0.34	0.58																								
ATP6V0A1																											
ATP6V0C	0.29				0.66																						
ATP6V1A					0.86	0.65																					
ATP6V1C1				0.36	0.77	0.68	0.73																				
ATP6V1H					0.82	0.63	0.83																				
IL6				0.28			0.30	0.28																			
CD209			0.32							0.47																	
TWIST	0.46	0.40		0.40																							
CDH1		0.28								0.39	0.46	0.34															
VIM		0.29	0.42	0.38						0.38	0.39	0.41	0.64														
CD13					0.28						0.26		0.34														
CD24			0.45																								
CD44	0.48	0.28	0.38	0.51																							
CD90								0.28						0.47	0.34												
CD133		0.62								0.29			0.34														
EpCAM		0.65								0.40	0.29		0.32	0.33		0.55											
KRT19	0.36	0.56								0.36	0.40		0.45	0.47		0.56											
NANOG												0.74	0.28	0.29													
OCT4						0.31	0.28					0.35				0.74											
SOX2												0.65				0.30											
	HIF1A	CA9	CA12 1	CA12 2/3	ATP6V0A1	ATP6V0C	ATP6V1A	ATP6V1C1	ATP6V1H	IL6	CD209	TWIST	CDH1	VIM	CD13	CD24	CD44	CD90	CD133	EpCAM	KRT19	NANOG	OCT4	SOX2			
	Hypoxia and pH regulators									Inflammation /Immunosuppression			Epithelial-to-mesenchymal transition (EMT)			Cancer Stem Cells (CSCs)											
	NS		*** p<0.0001		** p<0.005		* p<0.0500																				

Figure 3.3. Analysis of correlation between genes related to hypoxia and pH regulatory molecules, epithelial-to-mesenchymal transition and HCC aggressiveness and inflammation/immunosuppression. Table shows results obtained from Spearman's correlation analysis for the gene expression levels of *HIF1A*, *CA9*, *CA12 1*, *CA12 2/3*, *ATP6V0A1*, *ATP6V0C*, *ATP6V1A*, *ATP6V1C1*, *ATP6V1H*, *IL6*, *CD209*, *TWIST*, *CDH1*, *VIM*, *ANPEP* or *CD13*, *CD24*, *CD44*, *THY1* or *CD90*, *EpCAM*, *PROM1* or *CD133*, *KRT19*, *POU5F1B* or *OCT4*, *NANOG* and *SOX2* in the malignant liver tissues obtained from 57 patients. In this analysis we used ΔCt values ($\Delta Ct = Ct_{\text{target genes}} - Ct_{\text{GAPDH}}$). The correlation coefficient R values are reported in the Table and are highlighted in white, olive-green, light green or pale green if their correspondent p-values are non-significant (NS), *** p<0.0001, ** p<0.005, * p<0.0500, respectively.

3.4 The development of a prognostic index score

Given that we showed that the pH regulators are associated with poor differentiation grade (G3) of the tumour and the expression of inflammatory/immunosuppressive-, EMT- and CSC-related genes, we investigated the prognostic effect in 57 HCC patients of the genes analysed in the previous paragraphs. The clinical endpoint of interest was relapse-free survival (RFS). The RFS was calculated as the time interval between the date of surgery and the date of diagnosis of any type of relapse (intrahepatic recurrence or extrahepatic metastasis). Firstly, we evaluated the effect of the genes on RFS by univariate analysis. As shown in Table 3.4.1, only *TWIST* and *EpCAM* genes were identified as prognostic factors for RFS (Table 3.4.1) in such analysis.

Table 3.4.1. Univariate analysis of genes associated with recurrence of 57 HCC patients

Genes	Recurrence		
	Univariate analysis		
	HR	95% CI	P value
<i>ATP6V0A1</i>	0.927	0.655-1.312	0.668
<i>ATP6V0C</i>	1.059	0.975-1.151	0.173
<i>ATP6V1A</i>	0.836	0.615-1.136	0.253
<i>ATP6V1H</i>	0.892	0.711-1.120	0.325
<i>ATP6V1C1</i>	1.035	0.819-1.310	0.772
<i>CA9</i>	0.999	0.993-1.005	0.677
<i>CA12 1</i>	1.215	0.938-1.574	0.139
<i>CA12 2/3</i>	1.025	0.974-1.079	0.341
<i>CD13</i>	0.955	0.812-1.122	0.574
<i>CD24</i>	1.201	0.971-1.485	0.092
<i>CD44</i>	1.062	0.910-1.238	0.446
<i>CD90</i>	0.859	0.509-1.446	0.567
<i>CD133</i>	1.033	0.967-1.103	0.334
<i>CD209</i>	1.063	0.999-1.131	0.051
<i>CDH1</i>	1.800	0.867-1.345	0.494
<i>EpCAM</i>	1.032	1.006-1.058	0.014
<i>HIF1A</i>	1.143	0.987-1.324	0.075
<i>IL6</i>	0.995	0.982-1.008	0.421
<i>KRT19</i>	1.034	0.938-1.140	0.507
<i>NANOG</i>	1.104	0.933-1.306	0.248
<i>OCT4</i>	1.019	0.996-1.041	0.084
<i>SOX2</i>	1.055	0.967-1.150	0.231
<i>TWIST</i>	1.018	1.007-1.029	0.001
<i>VIM</i>	0.961	0.792-1.166	0.684

Notes: HR, hazard ratio; CI, interval of confidence

Secondly, we evaluated if the combined expression of the genes impacts on the RFS of HCC patients. To this aim we used a machine-learning tool known as the 'Adaptive Index Model'. This tool allowed us to obtain a HCC Index Score (HIS) based on the following steps: 1) selection of the genes significantly associated with the RFS in a proportional-hazard Cox regression model; 2) definition of an optimal cut-off for each selected gene; 3) construction of the HIS, as an enumeration of altered genes. A gene is classified as altered if the corresponding measure is above or below the cut-off value, in cases of respectively positive or negative association with the endpoint. The HIS built with our data included four genes, namely *CD209*, *CA12 1*, *CA12 2/3* and *CDH1*, and the respective cut-offs were >0.0327 , >0.0653 , <0.0094 , <0.0665 . Hence, we could split the patient cohort into two groups based on HIS=0-1 (none or one gene with altered expression, "low risk" group) or HIS=2-3 (two or more genes with altered expression, "high risk" group). The low risk group included 29 patients with median a RFS >24 months, while the high risk group included 28 patients with a median RFS of 11.7 months. The corresponding RFS curves are shown in Figure 3.4, and their difference was statistically significant ($P<0.0001$).

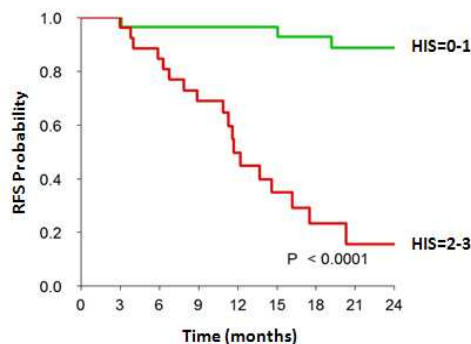


Figure 3.4. Prognostic significance of CA12 1, CA12 2/3, CDH1 and CD209 expression in the HCC training cohort. The graphs report the relationship between the expression of CA12 1, CA12 2/3, CDH1 and CD209 and relapse-free survival (RFS Probability). As shown in the graph, HIS=0-1 identified the “low risk” group in which none or one gene has an altered expression, while HIS=2-3 represented the group of patients with two or more genes with altered expression, namely “high risk” group. *This analysis was performed by the statisticians Dr. Luigi Mariani and Dr. Luca Lalli.*

We also investigated the possible association between the HIS and the clinicopathological parameters. As shown in Table 3.4.2, the only significant result was achieved for tumour size. Therefore, by not showing in general an association between HIS and clinicopathological parameters, it is possible to infer that HIS should retain an independent prognostic effect even in a multivariate analysis. The latter, however, could not be performed in our study because of the small patient series. A direct demonstration and unbiased quantification of the HIS prognostic effect would require an *ad hoc* validation study that is currently under way.

Table 3.4.2. Statistical analysis of HCC Index score (HIS) and clinicopathological parameters for recurrence of 57 HCC patients

Variables	*Mann-Whitney test (p value)
Age	0.307
AFP	0.086
Tumour size	0.045
	#Chi squared test (p value)
Sex	0.308
Etiology	0.344
Tumour number	0.271
Micro vascular invasion	0.325
Grading	0.704

Notes: *, this test was carried out on continuous variables; #, this analysis was performed on categorical variables; AFP, alpha-fetoprotein

In order to perform the validation of our HIS, we are sequentially collecting another series of matched tumour (T) and non-tumour (NT) snap-frozen tissues from patients with HCC undergoing curative resection at the Gastrointestinal Surgery and Liver Transplantation Unit of our Institute headed by the Professor Mazzaferro. So far 38 paired samples have been collected. The clinicopathological parameters associated with this cohort are reported in Table 7 and are similar to those reported for the training cohort (Table 3.4.3).

Table 3.4.3 The clinicopathological characteristics of HCC patients included in the validation cohort

Clinical variable	N°	%
Age, mean \pm SD, years	69.0 \pm 6.8	
<50	0	0
\geq 50	38	100
Sex		
Male	31	81.6
Female	7	18.4
Etiology		
HBV	8	21.1
HCV	17	44.7
Others (NASH, POTUS, haemochromatosis)	11	28.9
Healthy liver	2	5.3
AFP, ng/mL		
<20	26	68.4
20-100	5	13.2
100-400	2	5.3
\geq 400	5	13.2
Tumour number		
Single	36	94.7
Multiple	2	5.3
Tumour size, cm		
<3	15	39.5
3-5	15	39.5
\geq 5	8	21.1
Micro vascular invasion		
yes	29	76.3
no	9	23.7
Grading		
G1	2	5.3
G2	21	55.3
G3	15	39.5
Recurrence		
yes	14	36.9
no	24	63.2

Clinical and pathological features of the 38 matched tumour and non-tumour tissues collected from patients with HCC undergoing curative resection at the Gastrointestinal Surgery and Liver Transplantation Unit of our institute. AFP, alpha-fetoprotein.

The expression of all the genes analysed in the training cohort will be then assessed in this cohort of patients by qRT-PCR when we have reached the same number of samples as in the discovery cohort; a follow up of at least 24 months will be carried out. The obtained data will be then used by the statisticians to confirm the prognostic value of the HIS.

Discussion

The aims of this chapter were: - to characterise the expression of pH regulatory molecules *ex vivo* in HCC patients; – to evaluate the expression of genes involved in the aggressive features of HCC; - to assess whether genes related to pH regulatory molecules and HCC aggressiveness were associated; - to develop a prognostic index score comprising the simultaneous gene expression of pH regulators and aggressiveness.

Our *ex vivo* gene expression analysis revealed that HCC tissues express pH regulators, although with different levels of expression. Consistent with Wykoff and colleagues, who reported the dependency of CAIX expression on hypoxia in several human carcinomas [132], we found that also in HCC the gene expression of *CA9* was positively related to *HIF1A*. Furthermore, we demonstrated for the first time the presence of *CA12 1* in HCC and we showed that the alternative splicing variants *CA12 2/3* were expressed almost exclusively in the tumour hepatocytes. The expression of the alternative splicing variants *CA12 2/3* was correlated with the expression of *HIF1A* in line with the notion that hypoxia can modulate the splicing of pre-mRNA molecules [170]. Regarding the expression of V-ATPase in HCC, our study is the first describing

the expression of several subunits of the V-ATPase complex. We observed that all the V-ATPase subunits analysed were overexpressed in T samples compared to N and NT. The *ATP6V0C* and *ATP6V0A1* genes represented an exception to this rule. In fact, they certainly displayed a trend of overexpression in NT and T samples compared to normal liver, but without reaching statistical significance. We also observed that the gene expression of V-ATPase was not dependent on *HIF1A*, with perhaps the exception of *ATP6V0C* for which a small proportion of its expression was related to *HIF1A* ($r=0.29$).

We dissected the aggressive features of HCC in terms of genes related to EMT, CSCs and inflammation/immunosuppression. In the complex field of inflammation/immunosuppression status of the liver, we conducted an explorative study by investigating the gene expression of *IL6* and *CD209*. We chose these two genes, because IL-6 is involved in EMT in HCC [171] and because of its relevance for the survival and expansion of progenitor cells [68, 80]. *CD209*, also known as DC-SIGN, is expressed in the liver by cells exerting different functions. In fact, *CD209* is expressed by myeloid cells with different functional specifications. Moreover, *CD209* is expressed by DCs involved in antigen presentation and the generation of a positive anti-tumour immunity. Furthermore, it is also a marker of pro-tumour M2 macrophages. Our results showed that *IL6* was overexpressed in tumour tissues, in agreement with its supposed function in sustaining inflammation and CSC growth [68], while *CD209* was less expressed in non-tumour and tumour tissues as compared to normal liver. It should be mentioned that *CD209* is constitutively expressed by the

sinusoidal endothelial cells (SECs) and works as a receptor for HIV entry infection [172]. The diminished expression of *CD209* likely reflects the reduced presence of a normal sinusoidal organization, which characterises the normal liver and that is progressively lost in cirrhosis and in HCC.

Considering EMT, as expected, we observed a down-modulation in the gene expression of *CDH1* in tumour tissues, while we did not find the concomitant up-regulation of *TWIST* and *VIM*. *TWIST* and *VIM* are implicated in the metastasis of HCC [173, 174], and this could be the reason why the primary tumours in our samples lack a high expression of *TWIST* and *VIM*.

Several markers have been associated or used to identify CSCs in HCC, and this heterogeneous situation is true for the CSCs of other tumours as well. We studied the genes related to the most commonly utilised markers for HCC CSCs: *ANPEP* or *CD13*, *CD24*, *CD44*, *THY1* or *CD90*, *EpCAM*, *PROM1* or *CD133*, *KRT19*, *POU5F1B* or *OCT4*, *NANOG* and *SOX2* [76]. In our work, we observed that these genes were present both in tumour and non-tumour tissues with a level of expression increased with respect to normal liver tissues. Only the levels of *CD24* and *THY1* or *CD90* were found to be enriched in tumour samples compared to the normal and non-tumour ones, as already reported by Yang and colleagues for *CD24* [175] and by Yang and collaborators for *CD90* [176]. Moreover, the *ANPEP* or *CD13*, *EpCAM*, *KRT19* and *POU5F1B* or *OCT4* genes displayed higher expression levels in NT tissues, while *CD44*, *NANOG* and *SOX2* did not show any significant differences. This illustrates the heterogeneity and complex nature of CSC biology. The expression of CSC markers can be

considered as a sign of aggressiveness. In fact, HCC tumours with a stem cell signature, which includes the expression of these CSC related genes, are classified as having the worst prognosis [75]. We considered the CSCs in the context of the TME, and thus we looked for possible association/correlation with the other markers/genes we were studying, namely the pH regulators, hypoxia and immune-related genes.

Interestingly Spearman's correlation analysis outlined a link between CA9 and EMT (*TWIST*) and especially CSC (*CD24*, *CD133*, *EpCAM*, *KRT19*) genes thus suggesting a possible association of CA9 with HCC aggressiveness. In line with this hypothesis, we also found that CA9, and also CA12 1 and CA12 2/3 were associated with poorly differentiated HCCs, confirming a possible role of pH regulators in influencing HCC malignancy.

Since our analysis revealed other possible relationships between genes involved in inflammation/immunosuppression, EMT, CSCs and pH regulators, we investigated if the concomitant expression of the genes analysed in this chapter, or a subset of them, might have a prognostic significance in HCC.

By the machine learning tool known as 'Adaptive Index Model', the statisticians of our Institute developed an HCC Index Score (HIS). The HIS comprised the simultaneous gene expression of CA12 1, CA12 2/3, *CDH1* and *CD209*. The HIS showed that patients with two or more of these genes with altered expression were associated with a short RFS. This HIS is important for our study, because it was constructed based on the concomitant expression of pH regulators (CA12 1, CA12 2/3), EMT (*CDH1*) and

inflammation/immunosuppression (*CD209*). Thus, this result supports our hypothesis that all these players are important for HCC biology. An additional cohort of patients with similar clinicopathological features will be soon be available for validation purposes.

In conclusion, in HCC the pH regulators are widely -expressed and may have a non-redundant function. Furthermore, *CA9*, *CA12 1* and the alternative splicing variants *CA12 2/3* were associated with tumour malignancy. Moreover, the pro survival role V-ATPase has been demonstrated in different tumour models. Thus, to further and better explore whether these pH regulatory molecules indeed represent targetable molecules in HCC, in the next chapter, we assessed the *ex vivo* protein expression and distribution of pH regulators in patient-derived HCC tissues.

4. Results and discussion

4. Expression of pH regulatory molecules at the tumour site:

IHC analysis

In the previous chapter, we reported the expression of the pH regulatory molecules at the mRNA levels in HCC patients. We showed that *CA9*, *CA12 1*, *CA12 2/3* alternative splicing variants and genes encoding different V-ATPase subunits, crucial for the assembly of the functional enzymatic complex, were expressed in HCC tissues, although at different levels. We also observed their positive association with genes related to the aggressiveness of HCC such as inflammation/immunosuppression, EMT and CSCs. Moreover, the *CA9*, *CA12 1* and *CA12 2/3* mRNAs were associated with the HCC tumour grade, and *CA12 1* and *CA12 2/3* together with EMT-related gene *CDH1* and inflammation/immunosuppression-associated gene *CD209* had a prognostic significance in HCC. Thus, the pH regulators might affect tumour promotion, maintenance and progression of HCC and thus represent targets for therapeutic intervention.

To explore further this issue, we investigated at the protein level which cells in the HCC TME were positive for the pH regulatory molecules under our investigation. Unfortunately, no antibodies specific for the different *CA12* isoforms are currently available and thus, we were not able to dissect which *CAXII* protein variant was expressed.

4.1 Protein expression of CAs in HCC patients

To investigate the *ex vivo* distribution of CAs in HCC, we performed IHC analysis on a set of 23 formalin-fixed, paraffin-embedded (FFPE) pairs of tumour, non-tumour and peri-tumour samples obtained from the cohort of 57 HCC patients. Areas enriched in immune infiltrating cells adjacent to tumour nodules were found in the peri-tumour samples. *Ex vivo* analysis showed focal and intense plasma membrane immunoreactivity for CAIX located in discrete nests of hepatocytes inside the HCC lesions (Figure 4.1.1, upper panel).

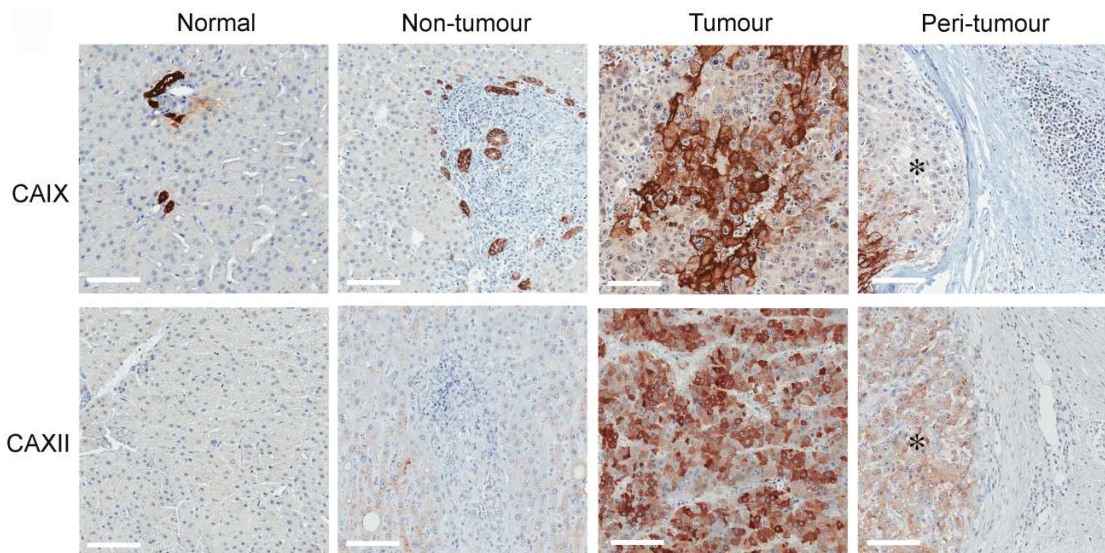


Figure 4.1.1. Expression and cellular distribution of CAIX and CAXII in liver tissues. Representative images of immunohistochemical staining for CAIX and CAXII in normal and matched non-tumour, tumour and peri-tumour liver tissues. Peri-tumour tissue was identified as areas adjacent to tumour nodules enriched in immune infiltrating cells. Membranous staining of CAIX was detectable in bile ductular cells in normal and non-tumour tissues and in malignant hepatocytes. CAXII was expressed in the cytoplasm of malignant hepatocytes. No positive staining was evident in the inflammatory cells infiltrating the peri-tumour areas. *Identifies tumour area in peri-tumour sections. Representative images with scale bars=100 μ m. *IHC analysis was performed by Consorzio Mia, University of Milan-Bicocca.*

This pattern of expression was found in approximately 50% of tumour samples, as illustrated in Table 4.1.1, in which we reported the score based on the intensity of the staining and the extent of stained cells as assessed by the pathologist Dr. Massimo Milione.

Table 4.1.1. Score categories for the expression of CAs in clinical HCC tissues (n=23) analysed by immunohistochemistry

Markers	Intensity of staining	Extent of stained cells			
		0	1	2	3
CAIX [#]	0	10 ^a	0	0	0
	2	0	3	0	10
CAXII [#]	2	0	0	0	23

Abbreviations: HCC, hepatocellular carcinoma.

Note: ^a, number of cases in each category; the expression of these markers was evaluated: # in tumour hepatocytes. Every tumour was given a score category according to the intensity of the membrane/cytoplasmic staining (0 = "negative" or 2 = "equal to the internal or experimental control") and to the extent of the stained cells (0 = 0-<5%, 1 = <10%, 2 = 10-50%, 3 = >50%). Bile duct cells were used as positive internal control for CAIX staining, while the glandular and superficial foveolar compartment in the stomach tissue were used as positive experimental control for CAXII staining. *The score was performed by the pathologist Milione M.*

The presence of CAIX was limited to the plasma membrane of cholangiocytes in normal and non-tumour tissues. No positivity of CAIX was detected in the inflammatory cells infiltrating the peri-tumour area.

In contrast to CAIX, CAXII was abundantly and selectively expressed in a large majority of the tumour hepatocytes, while hepatocytes in normal and non-tumour tissues were completely negative for CAXII. All the samples analysed shared this pattern of expression (Figure 4.1.1 and Table 4.1.1). Interestingly, in contrast with other tumour histotypes, such as breast cancer [177], in tumour hepatocytes the positivity of CAXII was mainly detected in the cytoplasm. No

positivity of CAXII was evident in the inflammatory cells infiltrating the peritumour area (Figure 4.1.1, lower panel).

As a positive control for a plasma membrane distribution of CAXII, IHC analysis was performed on breast cancer tissues. We confirmed that in this tumour CAXII was associated with the plasma membrane of malignant cells (Figure 4.1.2).

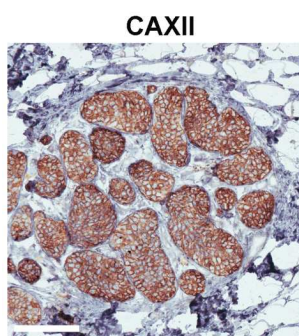


Figure 4.1.2. Cell surface expression of CAXII in *in situ* breast cancer tissues. Immunohistochemical staining for CAXII expression in *in situ* breast cancer tissues. Membranous staining of CAXII was detected in breast tumour cells. Representative image with scale bar = 100 μm . *IHC analysis was performed by Consorzio Mia, University of Milan-Bicocca.*

To define the cellular localization of CAXII in transformed hepatocytes, we performed immunofluorescence staining and confocal microscopy analysis of FFPE tumour tissue samples. As shown in Figure 4.1.3, left panel, confocal analysis revealed no co-localization between CAXII (green) and the cell surface-expressed β -catenin (red). Thus, these results confirm the lack of CAXII in the plasma membrane of malignant hepatocytes. In agreement with the IHC data shown in Figure 4.1.2, the same analysis performed on breast cancer tissue clearly showed CAXII and β -catenin co-localization (Figure 4.1.3, right panel).

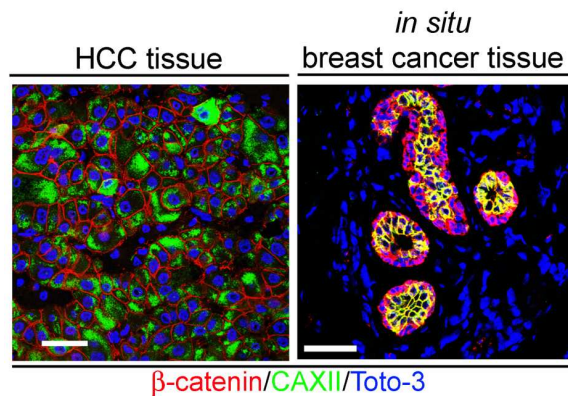


Figure 4.1.3. Cellular distribution of CAXII in tissues obtained from HCC and breast cancer patients. Confocal laser scanning micrographs of immunofluorescence staining with anti-CAXII (green) and anti- β -catenin (red). Nuclei were stained with TOTO-3 (blue). In HCC, CAXII displayed a cytoplasmic expression with no co-localization with the membranous staining of β -catenin (red) (left panel). Membrane CAXII and β -catenin co-expression was evident in *in situ* breast cancer tissue used as control (right panel, yellow staining). *Confocal analysis was performed by Consorzio Mia, University of Milan-Bicocca.*

To further analyse the cellular localization of CAXII, we evaluated the concomitant expression of CAXII and calnexin, a marker of ER. Interestingly, we observed that CAXII co-localized with calnexin thus indicating that CAXII was largely retained in the ER (Figure 4.1.4, left panel). This pattern of expression was not observed in *in situ* breast carcinoma cells (Figure 4.1.4, right panel).

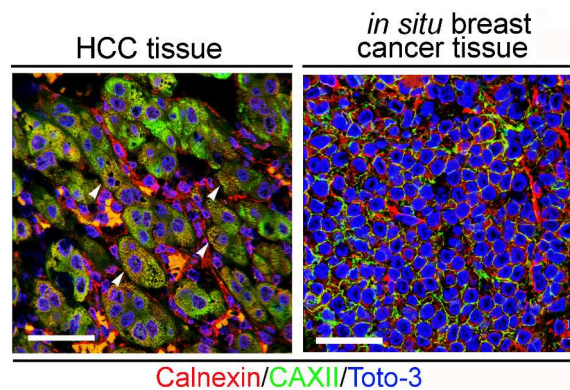


Figure 4.1.4. Cellular localization of CAXII in HCC and *in situ* breast tissues. Confocal laser scanning micrographs of immunofluorescence staining with anti-CAXII (green) and anti-calnexin (red). Nuclei were stained with TOTO-3 (blue). In HCC, CAXII partially co-localized with calnexin in malignant hepatocytes (left panel, yellow staining). The white triangle indicates the co-localization of CAXII and calnexin. This co-localization was not found in *in situ* breast cancer tissue used as control (right panel). Scale bars=50 μ m. *Confocal analysis was performed by Consorzio Mia, University of Milan-Bicocca.*

4.2 Protein expression of V-ATPase in HCC patients

We explored *ex vivo* the protein distribution of the V-ATPase subunits (*ATP6V0A1*, *ATP6V1C1* and *ATP6V1H*) that at mRNA level were overexpressed in tumour tissues. IHC analysis was performed using antibodies specific for the a1, C1 and H proteins encoded by *ATP6V0A1*, *ATP6V1C1* and *ATP6V1H*, respectively. a1 and C1 subunits were overexpressed in malignant hepatocytes with respect to non-tumour tissues and normal liver (Fig. 4.2.1).

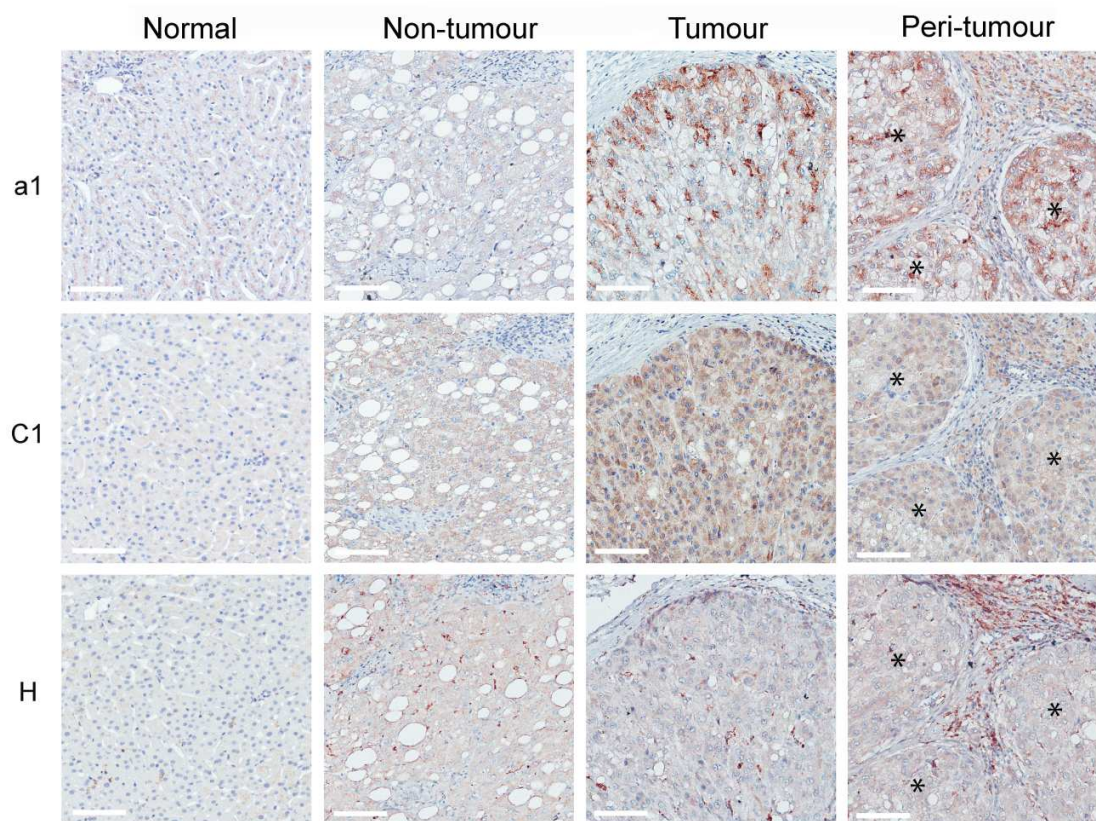


Figure 4.2.1. Expression pattern of V-ATPase subunits in liver tissues. The immunohistochemical expression of a1, C1 and H V-ATPase subunits was evaluated in normal and matched non-tumour, tumour and peri-tumour liver tissues. Peri-tumour tissues were identified as areas adjacent to tumour nodules enriched in immune infiltrating cells. The membranous/cytoplasmic expression of a1 and C1 subunits was detected in malignant hepatocytes. The H subunit was mainly expressed in the Kupffer cells present in non-tumour and tumour tissues. The a1 and H subunits were also expressed by infiltrating immune cells in the peri-tumour areas of the liver. *Identifies a tumour area in the peri-tumour sections. Representative images with scale bars = 100 μ m. *IHC analysis was performed by Consorzio Mia, University of Milan-Bicocca.*

This expression pattern was detectable in approximately 90% of HCC cases, although a heterogeneous frequency of positive cells and staining intensity was observed (Table 4.2.1).

Table 4.2.1. Score categories for the expression of V-ATPase in clinical HCC tissues (n=23) analysed by immunohistochemistry

Markers	Intensity of staining	Extent of stained cells			
		0	1	2	3
a1 [#]	0	3 ^a	0	0	0
	1	0	5	1	0
	2	0	2	6	6
C1 [#]	0	2	0	0	0
	1	0	4	3	0
	2	0	1	10	3
a1 [*]	0	17	0	0	0
	1	0	4	2	0
	2	0	0	0	0
H [*]	0	13	0	0	0
	1	0	5	2	0
	2	0	0	3	0

Abbreviations: HCC, hepatocellular carcinoma.

Note: ^a, number of cases in each category; the expression of these markers was evaluated: [#] in tumour hepatocytes and ^{*} in immune infiltrating cells in peri-tumour areas. Every tumour was given a score category according to the intensity of the membrane/cytoplasmic staining (0 = "negative"; 1 = "lower than the internal or experimental control"; 2 = "equal to the internal or experimental control") and to the extent of the stained cells (0 = 0-<5%, 1 = <10%, 2 = 10-50%, 3 = >50%). The islets of Langerhans in the human pancreas and the glandular compartment in stomach tissues were used as positive experimental controls for a1 and H staining, respectively. Subunit H of V-ATPase was not expressed by malignant hepatocytes, except for 4 of 23 HCC lesions that displayed strong staining in the Golgi (see Figure 4.2.2). The score was performed by the pathologist Milione M.

The H subunit was not detected in tumours and normal hepatocytes, as shown by the IHC staining of tumour and non-tumour tissues (Figure 4.2.1) except for 4 HCC cases (Figure 4.2.2). In these samples, the V-ATPase subunit H was intracellularly expressed in malignant hepatocytes, with a pattern suggesting its accumulation in the Golgi apparatus.

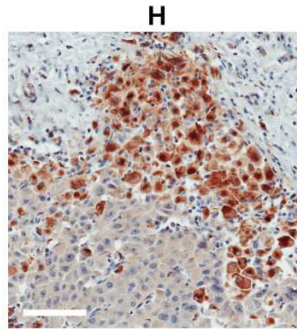


Figure 4.2.2. Expression of V-ATPase subunit H in malignant hepatocytes of HCC. Representative immunohistochemical staining for the V-ATPase subunit H which was found in four of the 23 HCC tissues analyzed. The H subunit displayed an intracellular expression pattern, suggesting its accumulation in the Golgi apparatus of malignant hepatocytes. Scale bars=100 μ m. *IHC analysis was performed by Consorzio Mia, University of Milan-Bicocca.*

The H subunit was also detectable in cells infiltrating non-tumour and tumour tissues, likely to be Kupffer cells, the liver's macrophages lining the walls of the sinusoids. Notably, in approximately half of the cases analysed, marked expression of the V-ATPase α 1 and H subunits could also be detected in the HCC inflammatory infiltrate in the peri-tumour area of the HCC samples (Figure 4.2.1 and Table 4.2.1).

Discussion

The aim of this chapter was to characterise protein expression and cellular localisation of pH regulatory molecules in the TME of HCC patients.

Our IHC analysis complemented the results obtained by gene expression analysis and added new important information on the heterogeneity of intra-tumour and intra-cellular distribution of these crucial molecules affecting the metabolic status of the tumour and its microenvironment. The IHC analysis shed

light on the tissue distribution of CAIX and CAXII molecules in HCC and the corresponding non-tumour tissues.

Importantly, we found that both CAIX and CAXII were expressed by transformed, but not normal hepatocytes thus qualifying them as proteins acquired during the transformation process, a feature crucial for their definition as targetable molecules.

Inside the transformed hepatocytes, CAIX displayed a focal distribution and it was expressed within discrete tumour nests that may represent areas of tumour with a particularly low O₂ tension. This hypothesis is in line with the data we discussed in chapter 3, which showed a positive significant correlation between the expression of *CA9* and *HIF1A*. Furthermore, it is possible that the hypoxic niches, defined by CAIX expression, host HCC cells with stem cell-like features and that thus CAIX targeting would likely control the most aggressive portion of the tumour. In support of this hypothesis, Lock and collaborators demonstrated that CAIX was associated with stemness features in breast cancer [151]. We think that this association can occur in HCC as well, in line with the results of the previous chapter illustrating a positive association between *CA9* and several genes related to CSCs.

However, analysis of CAIX expression revealed that this protein is also expressed in the bile ducts of normal liver and in non-tumour adjacent tissues, likely in relation to their secretory functions. This may pose a limit to its clinical utilization as a therapeutic target.

In contrast to CAIX, the IHC analysis revealed that CAXII was expressed by a large majority of tumour cells and it was not detectable in any of the cells of normal tissue. This pattern of expression is clearly a great advantage for effective therapeutic targeting. IHC also demonstrated that CAXII was hardly detectable at the plasma membrane of the tumour hepatocytes, while this protein was instead mainly accumulated in the cytoplasm, likely retained in the ER of HCC cells. These data are partially in agreement with that of Haapasalo and colleagues showing that astrocytic gliomas express CAXII not only at the plasma membrane, but also in the cytoplasm of tumour cells. These authors interpreted this cytoplasmic accumulation of CAXII as the result of the elevated production of new enzyme. However, it should be noted that astrocytic gliomas also expressed the alternative splicing variant of *CA12 2* [147], as we also found in HCC. Although it is well recognized that altered glycosylation or alternative splicing events, known to occur in cancer under certain conditions [178, 179] might play a role in determining the abnormal intracellular localization of proteins, neither we, nor Haapasalo and colleagues in astrocytic gliomas, could formally define which isoforms of CAXII were retained in the ER.

Our data concerning the V-ATPase expression described the precise distribution of several subunits that are involved in the function of the V-ATPase complex. We demonstrated a significant up-regulation of the *ATP6V0A1*, *ATP6V1C1* and *ATP6V1H1* genes in tumour tissues at the mRNA level. Furthermore, malignant hepatocytes expressed the a1 and C1 subunits in the plasma membrane with a strong or moderate intensity. Interestingly, these pH regulators, namely a1 and

H V-ATPase subunits, were also detectable in immune cells infiltrating HCC tissue, and thus they might also have immunomodulating functions.

In conclusion, the data we collected about pH regulatory molecule distribution in HCC patients, their relationship with the aggressive features of the tumour and their prognostic significance, concur to define these molecules as promising therapeutic targets for HCC. Thus, taking advantage of HCC cell lines representative of the epithelial and mesenchymal phenotypes of HCC, in the next chapter we explored the effects of pH regulator inhibitors on HCC viability.

5. Results and discussion

5. pH regulators as targets for pharmacological intervention in

HCC: *in vitro* data

The data described in chapter 3 and 4 suggests that the pH regulatory molecules are potential targetable molecules. In fact, we showed that their expression at the mRNA level correlated with the aggressive features of the tumour and that at the protein levels they were enriched in cancer tissues. Moreover, we found that the CAIX and CAXII proteins were expressed by transformed but not by normal hepatocytes.

Based on these results, the aims of this chapter were: - to characterise the expression of the pH regulatory molecules in HCC cell lines and the role of hypoxia in the modulation of their expression; – to assess whether drugs inhibiting the function of pH regulatory molecules affected the *in vitro* growth of HCC cells.

5.1 *In vitro* characterisation of CAs in HCC cell lines

To explore the effects of pH regulator inhibitors on HCC viability, we selected from the ATCC[®] cell bank three different HCC cell lines representative of the tumour subtypes present in HCC [169, 180] and we characterized them for the expression of the pH regulatory molecules. These cell lines have been previously described as epithelial or mesenchymal types. PLC/PRF/5 and C3A were defined as epithelial since they are highly positive for E-cadherin (CDH1) and EpCAM and CD133, (two epithelial stem cell markers), and display a low level of vimentin (VIM), CD44 and CD90 (mesenchymal markers). On the

contrary, SNU-449 cells were annotated as mesenchymal, because they showed a higher expression of the mesenchymal markers vimentin and CD44 [171, 180].

Since it is well known that CAIX and CA XII are induced by hypoxia in tumours [132] and our *ex vivo* data showed a correlation between CA9 and CA12 2/3 in HCC tissues, we explored the gene and protein expression of these molecules in these commercially available HCC cell lines. Although no studies have measured the exact level of hypoxia in human HCC, it should be considered that 5% O₂ characterizes the normal liver and it is thus considered as the normal physiological condition (normoxia) [85]. Hence, we decided to set the *in vitro* hypoxia level for HCC cell lines at 1% O₂.

Cells cultured for 72h in either normoxic (21% O₂) or hypoxic (1% O₂) conditions were evaluated for the hypoxia-induced CA expression. Figure 5.1.1 shows that the mRNA level of CA9 was normally expressed by the PLC/PRF/5 and C3A cells and significantly augmented under hypoxia. In contrast, the SNU-449 cells did not express CAIX in any culture conditions.

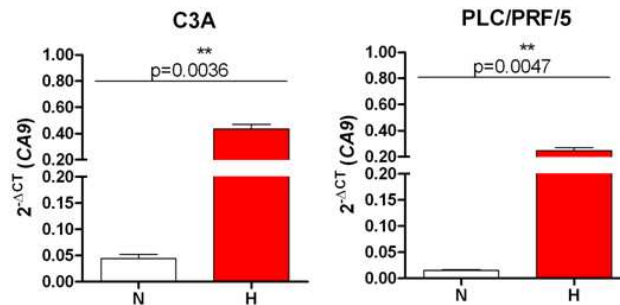


Figure 5.1.1 Gene expression of CA9 in HCC cell lines. mRNA level of CA9 was evaluated in HCC cell lines grown in either normoxia (N=21% O₂, white column) or hypoxia (H=1% O₂, red column) for 72 h. Data are reported as $2^{-\Delta Ct}$ values ($\Delta Ct = Ct_{\text{target gene}} - Ct_{\text{GAPDH}}$) of three biological replicates in C3A and PLC/PRF/5. SNU-449 did not express CA9 in any of the tested conditions. The unpaired *t*-test was used to compare CA9 gene expression between cells exposed to N or H.

In the PLC/PRF/5, we found that the expression of CA12 1 and CA12 2/3 was significantly increased by hypoxia, with the latter displaying a stronger up-regulation. The C3A and SNU-449 cell lines expressed CA12 1 although at lower levels compared to the PLC/PRF/5 cells and this expression was not modified by hypoxia. Furthermore, hypoxia did not influence the low expression of CA12 2/3 in the SNU-449 cells (Figure 5.1.2). The analysis of these different CA12 isoforms is unfeasible at the protein level, because no antibodies specific for each of these three forms are currently available.

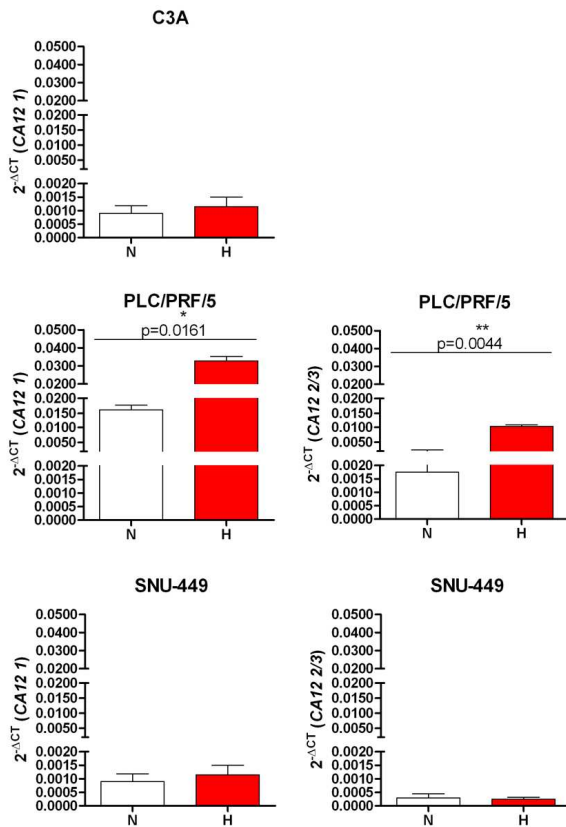


Figure 5.1.2 Gene expression of CA12 isoforms in HCC cell lines. mRNA level of CA12 1 and CA 12 2/3 was evaluated in HCC cell lines grown in either normoxia (N=21% O₂, white column) or hypoxia (H=1% O₂, red column) for 72 h. Data are reported as 2^{-ΔCt} values (ΔCt=Ct_{target gene}-Ct_{GAPDH}) of three biological replicates in C3A and PLC/PRF/5. Graph related to the expression of CA12 2/3 in C3A cells was not shown, because these cells were negative for these isoform genes. The unpaired *t*-test was used to compare CA12 gene expression isoforms between cells exposed to N or H.

To confirm these mRNA data at the protein level, we performed western blot and flow cytometry analyses for the corresponding CA molecules. A marked up-regulation of CAIX was detected in the C3A and PLC/PRF/5 cell lines upon hypoxia exposure. In contrast, the SNU-449 cells were completely negative for CAIX independently from the cell culture conditions (Figure 3.1.4A). CAXII was expressed by all the HCC cell lines, but up-regulated after 72h of hypoxia

exposure exclusively in the PLC/PRF/5 cells (Figure 5.1.3A). Flow cytometry confirmed the plasma membrane expression of CAIX in the PLC/PRF/5 and SNU-449 cell lines and this expression was enhanced when the cells were exposed to hypoxia for 72h (Figure 5.1.3B). A very low level of cell surface expression of CAXII was observed in all our cell lines, and this expression was not modulated by hypoxia (Figure 5.1.3B).

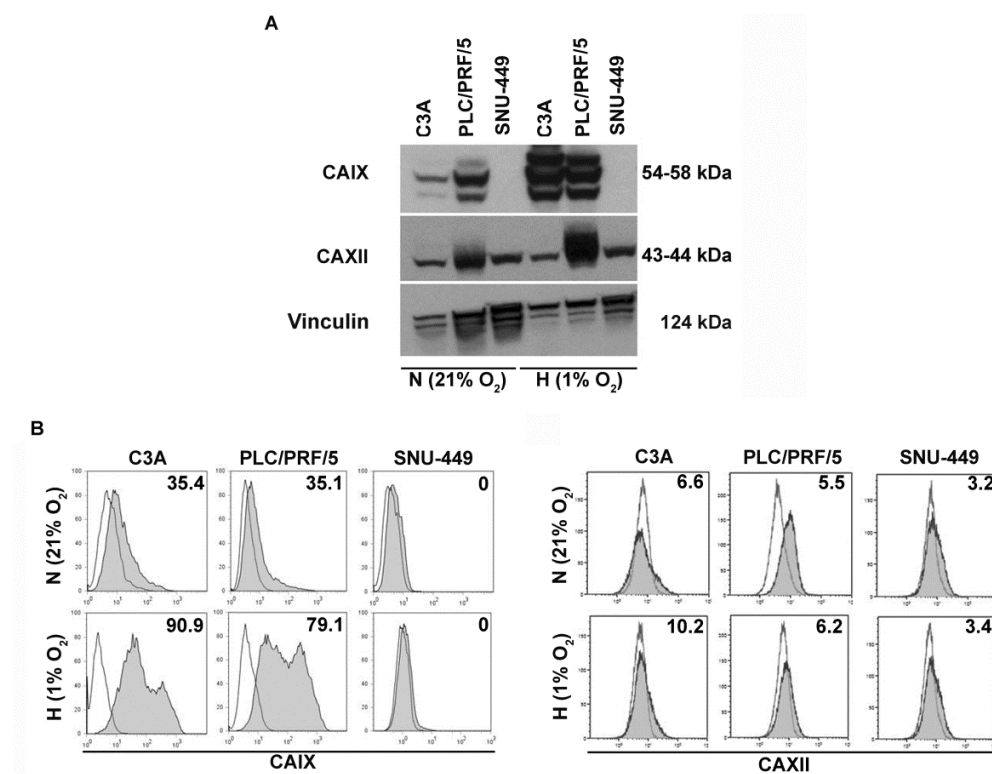


Figure 5.1.3 Protein expression of carbonic anhydrases (CAs) in HCC cell lines. CA protein expressions were analysed in HCC cell lines grown in either normoxia (N=21% O₂) or hypoxia (H=1% O₂) for 72 h. **(A)** CAIX, CAXII and vinculin was measured in cell lysates of C3A, PLC/PRF/5 and SNU-449 by western blot. **(B)** The cell surface expression of CAIX and CAXII was evaluated by flow cytometry. The percentages of cells positive for the indicated markers (filled histograms) evaluated with respect to the corresponding secondary antibody (black line) were reported in each histogram plot. *These analyses were performed in collaboration with my colleague Olga Kuchuk.*

As already observed in HCC tissues, we detected only weak membranous expression of CAXII despite a strong protein signal revealed by western blot. In order to evaluate if CAXII in the cultured HCC cell lines was also retained in the ER, we performed immunofluorescence staining for CAXII (green) in combination with wheat germ agglutinin (WGA, red) which marks the plasma membrane and calnexin. Confocal analysis revealed that CAXII was mainly detected in the cytoplasm when cells were grown in normoxia (Figure 5.1.4, left panels), while the protein appeared to be largely retained in the ER after 72h of hypoxia exposure, as indicated by the co-localization with calnexin, defined by the appearance of an azure colour (Figure 5.1.4, right panels).

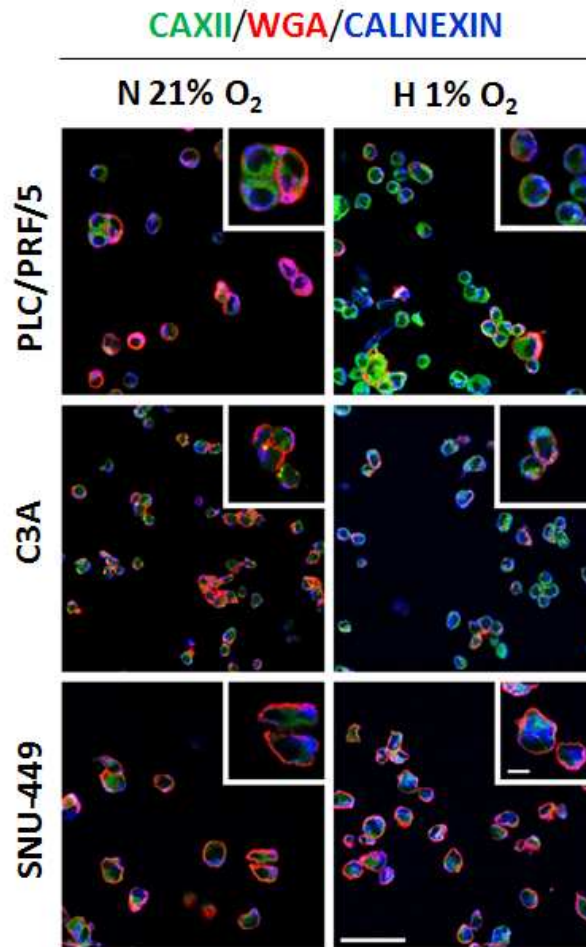


Figure 5.1.4 Cellular distribution of CAXII in HCC cell lines. Confocal laser scanning microscopy of triple immunofluorescence staining with anti-CAXII (in green), anti-WGA (in red, detecting cell membrane) and anti-calnexin (in blue, detecting the ER compartment) performed on the indicated HCC cell lines grown in either normoxic (N 21% O₂, left panels) or hypoxic (H 1% O₂, right panels) conditions for 72 h. HCC cells grown in normoxia mainly display cytoplasmic expression of CAXII as shown by the green staining with no or very little overlap with the membranous staining of WGA (red) or with the calnexin staining of ER (blue) (left panels). Co-localization of CAXII and calnexin in the ER was evident by the appearance of an azure colour in HCC cell lines exposed to hypoxia (right panels). *Confocal analysis was performed by Consorzio Mia, University of Milan-Bicocca.*

5.2 *In vitro* characterisation of V-ATPase in HCC cell lines

Since data from HCC patients (see chapter 3) showed no correlations between the gene expression of the V-ATPase subunits and *HIF1A*, we evaluated the expression of V-ATPase only in cells maintained *in vitro* under normoxic conditions. We analysed the protein expression of the a1 and C1 subunits, which we found to be expressed by malignant hepatocytes of HCC patients. We observed that all the HCC cell lines displayed a prominent expression level of the a1 and C1 V-ATPase subunits (Figure 5.2.1).

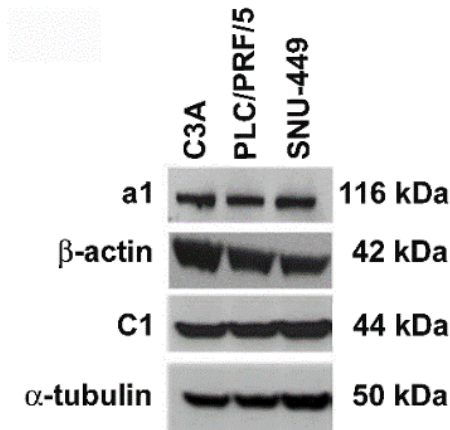


Figure 5.2.1 Protein expression of V-ATPase subunits in the HCC cell lines. The protein expression of a1 and C1 V-ATPase subunits, β-actin and tubulin was assessed by Western Blot in cell lysates of C3A, PLC/PRF/5 and SNU-449 grown under normoxic conditions.

Altogether, these results show that the commercially available HCC cell lines expressed the pH regulatory molecules, thus representing a suitable model to study the pH regulatory molecules in the HCC biology.

5.3 Effect of pH regulatory molecule inhibitors on the cell viability of HCC cell lines

To assess whether the inhibition of the pH regulatory molecules influences the viability of HCC cells, we treated the HCC cell lines with CAIX, CAXII and V-ATPase inhibitors. The CAIX and CAXII inhibitors, namely S4 and compound 25, respectively, were provided by Professor Supuran's group from the University of Florence. The chemical details of these small molecules are described in Materials and Methods section of this thesis (see chapter 2). To inhibit V-ATPase we used omeprazole (Sigma) belonging to the PPI class of molecules. Omeprazole has shown anti-tumour effects in several cancers [124]. We evaluated the effect of these drugs in affecting HCC cell viability using the MTT assay.

The CAIX-positive C3A and PLC/PRF/5 cell lines were susceptible to the S4 drug with an IC_{50} value around 100 μ M, when cultured under normoxia. Exposed to S4 in hypoxia, the C3A and PLC/PRF/5 cell viability rapidly decreased and IC_{50} values were equal to 57.4 and 53.9 for C3A and PLC/PRF/5, respectively. The specificity of the drug was confirmed by the lack of any S4-mediated effect on the CAIX-negative SNU-449 cells ($IC_{50} >100 \mu$ M) under both normoxic and hypoxic conditions (Figure 5.3.1).

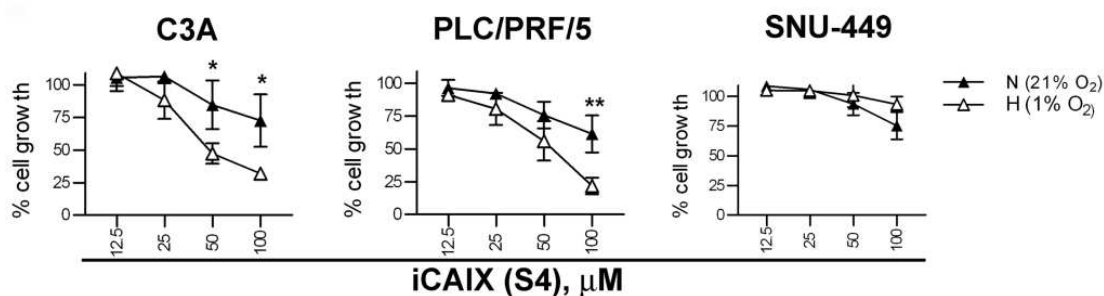


Figure 5.3.1. The effect of S4 (CAIX inhibitor) treatment on HCC cell viability. Graphs show the viability of the three HCC cell lines treated with different doses of S4 (μM) under normoxic (N=21% O₂, black triangles) or hypoxic (H= 1% O₂, white triangles) conditions for 72h. The cell viability was evaluated using the MTT assay. The data are expressed as mean values of six replicates. *This analysis was performed in collaboration with my colleague Olga Kuchuk.*

The breast cancer cell line T-47D, which was negative for CAIX, but expressed high levels of CAXII in the plasma membrane (Figure 5.3.2A), was used as a positive control to screen for the effects of several CAXII inhibitors. Among the six compounds (12, 16, 18, 19, 20 and 25) tested by the MTT assay, compound 25 showed the highest, dose-dependent inhibition of cell viability of the T-47D cell line (Figure 5.3.2B).

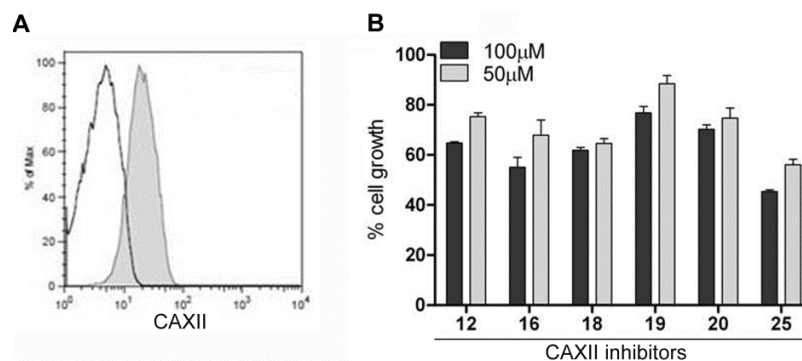


Figure 5.3.2 CAXII expression in the T-47D cells and cell growth inhibition by CAXII specific compounds. (A) The cell surface expression of CAXII was evaluated by flow cytometry. The expression of CAXII (filled histograms) was evaluated with respect to the corresponding secondary antibody (black line) reported in the histogram plot. (B) The T-47D cell line was treated with 100 μM (dark columns) and 50 μM (gray columns) of several CAXII inhibitors (compound 12, 16, 18, 19, 20 and 25) and the cell viability was assessed by MTT assay. The data are expressed as mean values of six replicates. *These analyses were performed in collaboration with my colleague Olga Kuchuk.*

Based on the degree of growth inhibition of the breast cancer cell line, compound 25 was selected and tested on the three HCC cell lines, all of which expressed CAXII, although with different levels of positivity. As shown in Figure 5.3.3, the viability of HCC cells was affected by the drug under normoxic conditions, with an IC_{50} of 198.5 and 142.9 μM in the C3A and PLC/PRF/5 cell lines, respectively. Unexpectedly, all the HCC cell lines were less sensitive to compound 25 when exposed to hypoxia as shown by the clear increase in the IC_{50} (> 200 μM for all cell lines). The SNU-449 cells appeared rather resistant to the drug (IC_{50} > 200 μM) independently from the culture conditions.

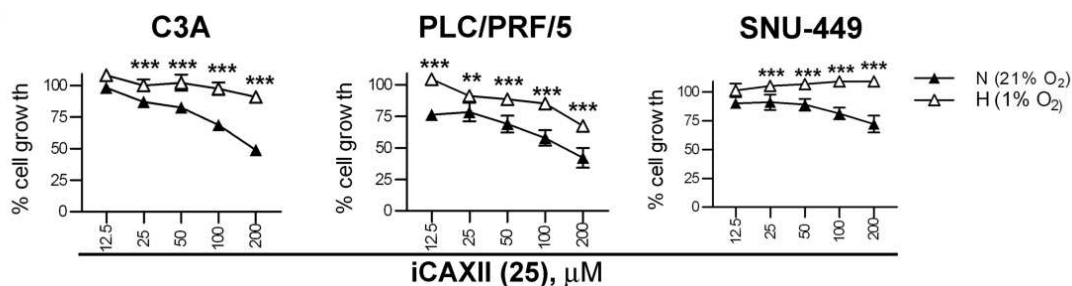


Figure 5.3.3 The effect of compound 25 (CAXII inhibitor) treatment on HCC cell viability. Graphs show the viability of the three HCC cell lines treated with different doses of compound 25 (μM) under normoxic (N=21% O_2 , black triangles) or hypoxic (H= 1% O_2 , white triangles) conditions for 72h. The cell viability was evaluated using the MTT assay. The data are expressed as mean values of six replicates. *This analysis was performed in collaboration with my colleague Olga Kuchuk.*

All the HCC cell lines were sensitive to omeprazole under normoxic conditions (Figure 5.3.4), with IC_{50} values of 39.4 $\mu\text{g/ml}$ for PLC/PRF/5 cells and of 100.9 $\mu\text{g/ml}$ for the C3A cells. As for the CA inhibitors, the SNU-449 cells displayed the lowest sensitivity to omeprazole (IC_{50} values of 128.4 $\mu\text{g/ml}$).

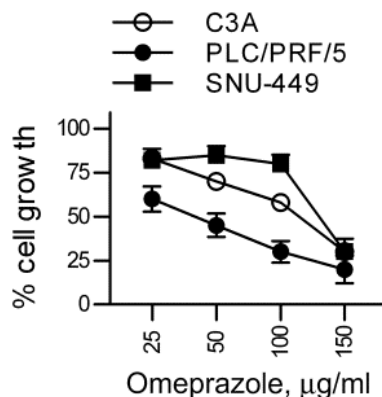


Figure 5.3.4 Treatment of HCC cell lines with omeprazole. Graphs show the viability of the three HCC cell lines treated with different doses of omeprazole ($\mu\text{g/ml}$) under normoxic (N=21% O_2) conditions for 72h. The data are expressed as mean values of six replicates. *This analysis was performed in collaboration with my colleague Olga Kuchuk.*

5.4 Mechanisms of cell death induced by pH regulatory molecule inhibitors

Our data demonstrated that the pH regulatory inhibitors (CAIX, CAXII and V-ATPase inhibitors) affect the viability of HCC cells grown in either 21% O₂ or hypoxic 1% O₂ conditions. We next sought to determine which mechanisms of cell death these inhibitors induced in the HCC cell lines. Firstly, we evaluated if the drugs interfere with the proliferation of HCC cell lines. To this aim, we performed an ELISA to quantify changes in BrdU incorporation under drug exposure. We observed that the CAIX inhibitor and omeprazole limited the cell proliferation of C3A and PLC/PRF/5 cell lines. Conversely, the CAXII inhibitor did not affect the proliferation of any of the HCC cell lines tested. In agreement with the MTT assay, which defined the SNU-449 cells as quite resistant to all the used drugs, no variation in proliferation was detected in the SNU-449 cells treated with S4 or compound 25. Significant inhibition of SNU-449 cell proliferation was only detected in omeprazole treated cells. Of note, the SNU-449 cells were resistant to doxorubicin and as a positive control, staurosporine was used as an anti-proliferative drug (Figure 5.4.1).

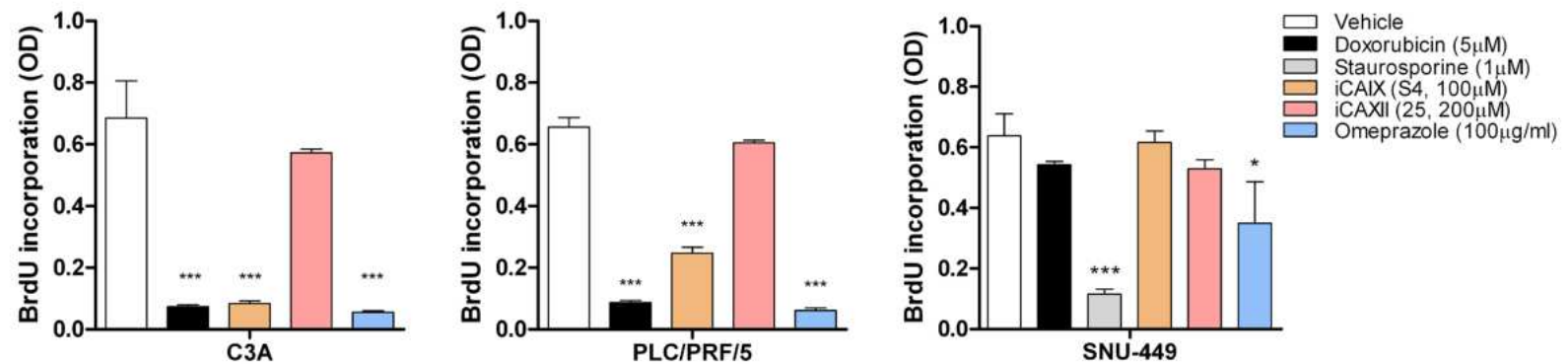


Figure 5.4.1 The impact of pH regulatory inhibitors on the proliferation of HCC cell lines. HCC cell lines were exposed to either 100 µM CAIX inhibitor (S4), 200 µM CAXII inhibitor (compound 25) or 100 µg/ml omeprazole and subjected to evaluation of proliferation (BrdU incorporation assay, OD: optical density). Data are the mean of three replicates \pm SD. BrdU incorporation was evaluated after 24h of drug treatment. As positive control compounds, 5 µM doxorubicin and 1 µM staurosporine were used. * $p < 0.05$ and *** $p < 0.001$ values were calculated using one-way analysis of variance (ANOVA) followed by Dunnett correction comparing cells treated with the drugs or the vehicle.

To investigate whether these drugs induce apoptosis and necrosis in our cell lines we used the RealTime-Glo Annexin V Apoptosis and Necrosis Assay. In this assay, the translocation of phosphatidylserine to the outer cell membrane during the apoptotic process is measured by a luminescent signal. Cell necrosis is detected by a dye that becomes fluorescent when internalized in the cells with a compromised membrane. Unfortunately, measurement of apoptosis by this kit was not feasible in cells treated with the pH regulatory inhibitors due to an unexpected interference of these drugs with the enzymatic luminescent reaction of the test. Both S4 and omeprazole significantly induced necrosis in our HCC cell lines after 48h and 72h of treatment. No effect was recorded for the CAXII inhibitor (Figure 5.4.2).

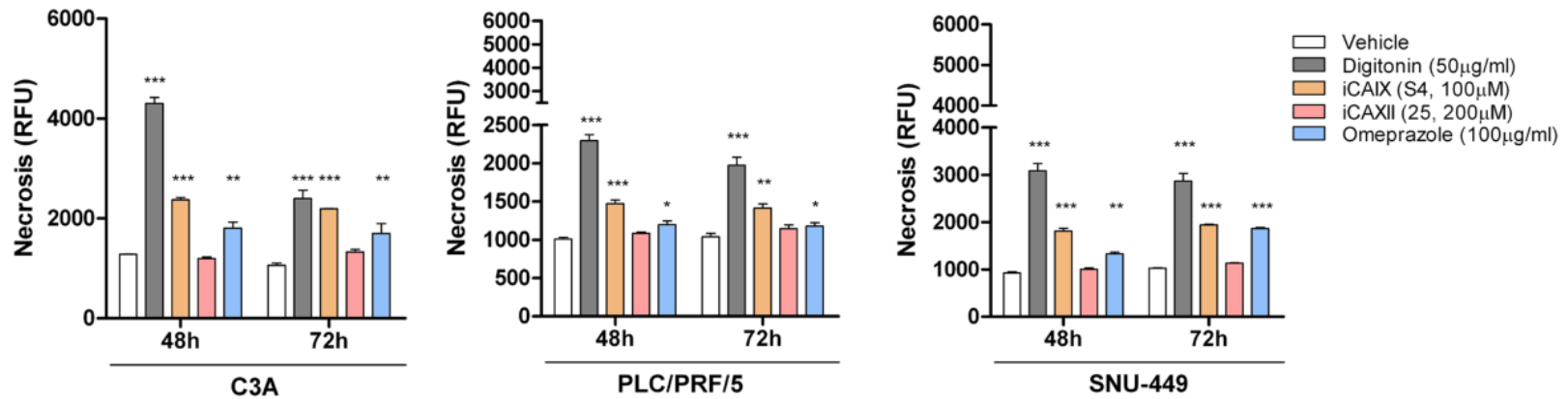


Figure 5.4.2 Necrosis detection in HCC cell lines. HCC cell lines were exposed to 100 µM CAIX inhibitor (S4), 200 µM CAXII inhibitor (25) or 100 µg/ml omeprazole and subjected to evaluation of necrosis (fluorescence emission upon internalization of a specific dye, RFU: relative fluorescence units). Data shown in the graphs are the mean of three replicates \pm SD. Necrosis was evaluated after 48h and 72h of drug treatment. As a positive control 50 µg/ml digitonin was used to evaluate the necrosis. *p<0.05, **p<0.01 and ***p<0.001 values were calculated using one-way analysis of variance (ANOVA) followed by Dunnett correction comparing cells treated with the drugs or the vehicle.

To detect apoptosis induced by our drugs, we also used the Caspase-Glo 3/7 assay that measures Caspase 3/7 activity. This assay is based on an enzymatic reaction that generates a luminescent signal recorded by a luminometer. We observed that neither the CAXII inhibitor nor omeprazole were able to induce apoptotic death in our cells compared to cells treated with the apoptosis inducer staurosporine (Figure 5.4.3A). Unfortunately, measurement of caspase 3/7 activity was not possible in S4-treated cells due to the interference of S4 with the enzymatic reaction of the test. For this reason, we grew the HCC cell lines in the presence or not of 100 μ M S4 for 24h and then we evaluated the percentage of activated caspase 3 by flow cytometry. However, no activation of caspase 3 was found in our cells exposed to S4 (Figure 5.4.3B).

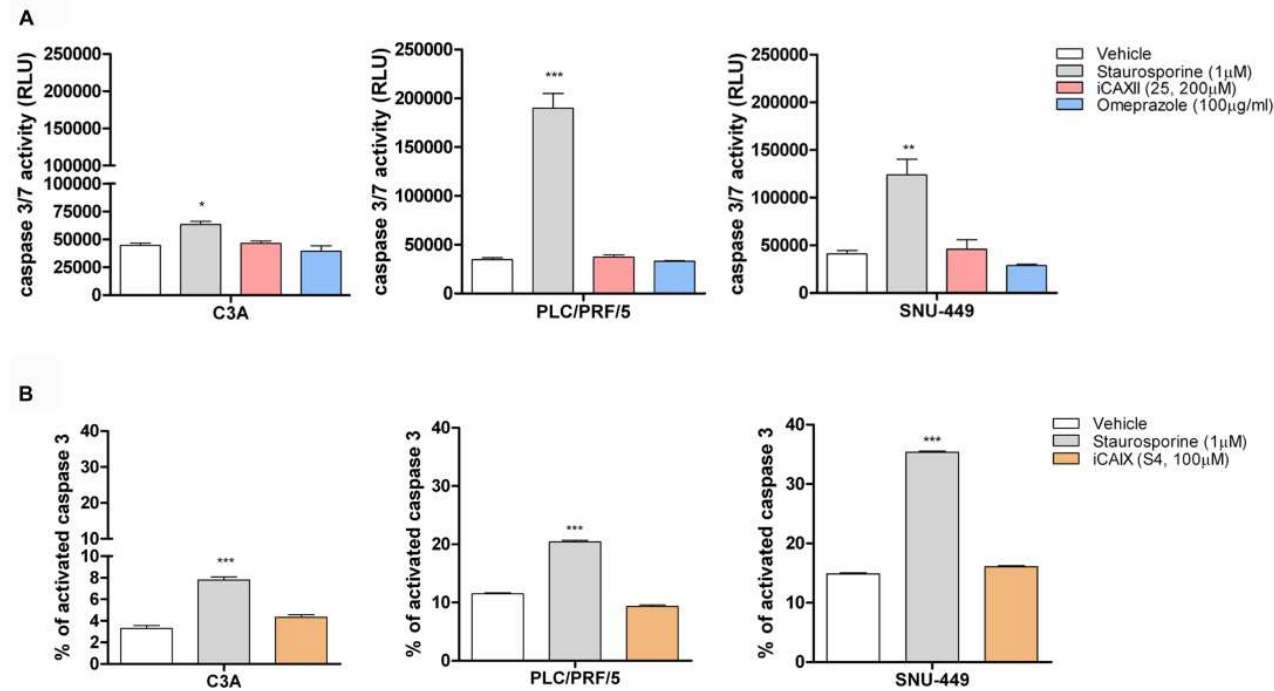


Figure 5.4.3 Apoptosis measurement in HCC cell lines. HCC cell lines were exposed to 100 μM CAIX inhibitor (S4), 200 μM CAXII inhibitor (25) or 100 μg/ml omeprazole and subjected to evaluation of **(A)** apoptosis in compound 25 and omeprazole drug-treated cells (caspase 3/7 activity, RLU: relative luminescence units) and **(B)** apoptosis in S4-treated cells (percentage of cells positive for activated caspase 3 evaluated by flow cytometry). Data shown in the graphs are the mean of three replicates ±SD. Apoptosis was evaluated after 24h of drug treatment. Positive control: cells treated with 1 μM staurosporine. *p<0.05 and ***p<0.001 values were calculated using one-way analysis of variance (ANOVA) followed by Dunnett correction comparing cells treated with the drugs or the vehicle.

Discussion

The aims of this chapter were: - to characterise the expression of pH regulatory molecules in HCC cell lines and the role of hypoxia in the modulation of their expression; – to assess whether drugs inhibiting the function of pH regulatory molecules affected the *in vitro* growth of HCC cells.

Regarding CAIX, we observed that in normoxic conditions CAIX was expressed in two epithelial HCC cell lines (PLC/PRF/5 and C3A) and its expression was incrementally increased upon 1% O₂ exposure. Our data are in agreement with Hyuga and colleagues that showed hypoxia-mediated up-regulation of CAIX in two different epithelial HCC cell lines (Huh-7 and HepG2). They also reported that CAIX induced by hypoxia promotes EMT in epithelial HCC cells [140]. Thus, CAIX is involved in the induction of EMT in epithelial cells, but its expression is probably not necessary for the maintenance of the mesenchymal phenotype. In fact, we noticed that the SNU-449 cells, with evident mesenchymal traits, were constitutively negative for CAIX and hypoxia did not induce EMT.

To inhibit CAIX function, we used a sulphonamide drug whose anti-proliferative and-metastatic effect is well-characterized in breast cancer by *in vitro* and *in vivo* experiments [151, 154]. Consistent with these data, we observed an anti-proliferative effect of the CAIX inhibitor in the CAIX-positive HCC cell lines (C3A and PLC/PRF/5). In our setting, this drug failed to induce apoptosis, but instead it directly caused necrotic death in the HCC cells lines after 48h and 72h of exposure. The anti-tumour effect of this inhibitor might be dependent on the tumour type. In fact, in laryngeal tumours the CAIX inhibitor did not affect

proliferation, apoptosis or necrosis [181]. Moreover, in breast cancer and in HCC, CAIX expression is associated with stemness features [95, 151]. Thus, CAIX likely represents a promising targetable molecule to suppress aggressive tumours, although its clinical benefit needs to be further demonstrated. The CAIX inhibitor (SLC-0111) has entered a phase I clinical trial in patients with advanced solid tumours (NCT02215850), but data about the anti-tumour effects and toxicity of this drug are not yet available.

While investigated in other tumours such as kidney, breast and ovarian cancers, CAXII expression remains poorly explored in HCC. All our studied HCC cell lines constitutively expressed the CAXII protein as shown by Western blot analysis, while hypoxia up-regulated CAXII both at gene and protein levels. Interestingly, qRT-PCR analysis showed that hypoxia induced the up-regulation of different transcript variants of *CA12*, including the transcript *CA12 1* and the *CA12* alternative transcripts variants *CA12 2/3*. Unfortunately, the currently available anti-CAXII antibody does not discriminate between the different CAIX protein isoforms. Thus, we cannot verify whether the alternative CAXII transcripts were indeed translated into their corresponding CAXII protein. In astrocytic gliomas, CAXII was expressed not only at the plasma membrane, but also in the cytoplasm of tumour cells [147]. These results in part parallel our data. In fact, we found that CAXII was poorly detectable at the plasma membrane of the HCC cells, and that this protein mainly accumulated in the cytoplasm of HCC cells. Moreover, we found that hypoxia induced the retention of CAXII in the ER. Collectively these data suggest an altered protein folding of CAXII mediated by

hypoxia preventing its transport to the cell membrane. The ER retention and the expression of the different splicing variants of *CA12* might somehow explain the poor anti-tumour effect exerted by the CAXII inhibitor compound 25 in our cell lines. This poor activity was indeed further exacerbated when the cells were grown in hypoxia. Thus, we formulated the following hypotheses: a) CAXII retained in the ER loses its activity and/or its function is not crucial for the *in vitro* growth of HCC cell lines; b) compound 25 does not gain access to the ER and thus, it is not able to block CAXII function; c) compound 25 has no effect against the spliced variant of CAXII strongly up-regulated under hypoxia. Further experiments should be designed to address all these open questions, but certainly the discovery of novel and selective drugs effectively targeting CAXII and its spliced variants are mandatory to further explore any possible clinical application.

Regarding the expression of V-ATPase in HCC, we found that some subunits of the V-ATPase complex were expressed by HCC cell lines including the $\alpha 1$ subunit, in which the binding site for PPIs is located. The study developed by Xu and collaborators used bafilomycin as a V-ATPase inhibitor in HCC [107]. Since bafilomycin show prohibitive toxicity [182] we used omeprazole. Omeprazole is a PPI which reduces gastric acid secretion and has recently been reported to exert broad antitumor effects at preclinical and clinical levels [183, 184]. PPIs were designed to bind to gastric H^+ , K^+ -ATPase, but they can also cross-react with V-ATPase, albeit with lower affinity [100]. In our setting, omeprazole efficiently inhibited the cell viability and proliferation of HCC cell lines. Contrary to what has

been reported in human B-cell tumours, omeprazole did not induce apoptosis in our HCC cell lines. Nevertheless, necrotic death occurred in the omeprazole treated HCC cells, probably as a secondary event following caspase-dependent apoptosis. The production of reactive oxygen species (ROS), as described previously in melanoma by De Milito and colleagues [125], might have played a role, but additional studies are required to precisely dissect the type of events induced by omeprazole and leading to HCC cell death. Omeprazole and its S-enantiomer esomeprazole have shown low toxicity and side effects in pre-clinical settings [125, 126]. In addition, esomeprazole was used in a clinical study for osteosarcoma patients showing low hepatic toxicity [184]. Thus, we think that this class of PPIs might also have a promising clinical potential in HCC.

The V-ATPase $\alpha 1$ and H subunits were expressed not only in transformed hepatocytes, but also in the tumour immune infiltrating cells (see chapter 4), thus we designed additional experiments: 1) to precisely locate the expression of V-ATPase in the immune components of the HCC microenvironment and 2) to evaluate whether inhibiting V-ATPase exerts any immune modulating activity in the HCC microenvironment.

6. Results and discussion

6. V-ATPase as a modulator of the tumour microenvironment

In the previous chapter we showed that V-ATPase blockage with omeprazole exerted an anti-tumour activity *in vitro* in the HCC cell lines by inducing blockage of proliferation and necrosis of tumour cells. In addition, we also reported (chapter 4) that in HCC tissues V-ATPase was not only expressed by the tumour cells, but also by the immune infiltrating cells.

Several studies have reported the expression of V-ATPase subunits in cells belonging to both the adaptive and innate immune systems, as we summarised in recent reviews [15, 183]. Indeed, V-ATPase is an important component in DCs, monocytes, macrophages and lymphocytes. Specifically, the A1 subunit is involved in the maturation process of DCs; the B2 subunit, expressed by macrophages, is crucial for the maintenance of an optimal pHi in inflammatory conditions. Moreover, the cleaved isoform of the $\alpha 2$ subunit is expressed by ovarian and breast cancer cells and is involved in the differentiation of monocytes into TAMs. The $\alpha 2$ subunit is present on the plasma membrane of activated lymphocytes, while the $\alpha 3$ subunit is expressed by activated T cells [15]. This chapter aims were: - to further investigate the *ex vivo* expression of V-ATPase in immune cells infiltrating the HCC microenvironment; - to evaluate the effects of V-ATPase blockage on the TME of HCC, considering both the tumour and immune components. To accomplish these tasks, we used IHC, immunofluorescence staining and confocal analysis together with flow cytometry of single cell suspensions obtained by the enzymatic digestion of HCC

specimens. We also took advantage of human primary HCC tissue explants, which preserve the intercellular network operating in local tissue.

6.1 Expression of V-ATPase in the immune components of the HCC microenvironment

We started our analysis characterising the type of immune cells infiltrating the HCC tissues. By IHC we evaluated the expression of markers related to myeloid cells, which included markers for monocytes/macrophages (CD14), macrophages (CD68) and M2 macrophages (CD163, CD209). For cells belonging to the adaptive immune response, we checked for the presence of T cells using the CD3 marker. Our results, reported in Figure 6.1.1 indicated an abundant presence of both myeloid and T cells in the peri-tumour areas of HCC tissues.

To investigate which type of immune cells expressed the V-ATPase subunits, we performed confocal microscopy analysis in HCC tissues stained with anti-a1 (red), anti-H (red), anti-CD163 (green), anti-CD209 (green) and anti-CD3 (green). As shown in Figure 6.1.2, in the peri-tumour region of HCC tissues, the V-ATPase a1 and H were co-expressed with the M2-like macrophage markers CD163 and CD209. In addition, we found that CD3⁺ cells also expressed the a1 subunits of the V-ATPase complex. No co-staining was observed for the CD3 and H subunits (Figure 6.1.2, next page).

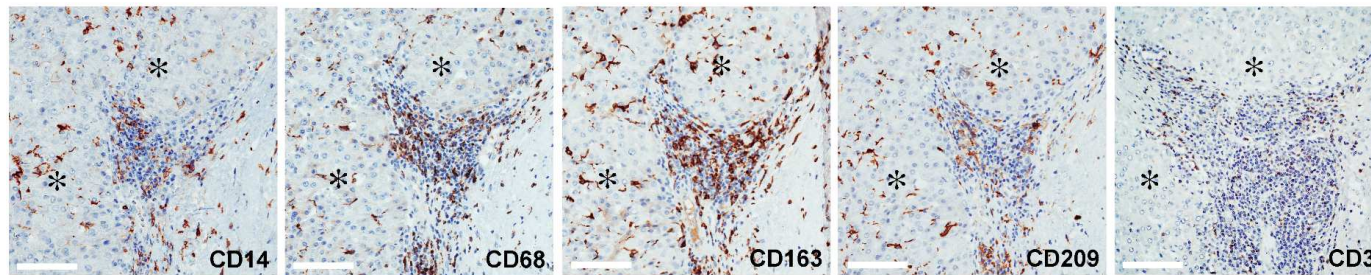


Figure 6.1.1. Expression of V-ATPase in immune cells infiltrating HCC tissues. Representative images of immunohistochemical staining for the myeloid-associated markers CD14, CD68, CD163, CD209 and T cell marker CD3 in HCC tissues. Scale bars = 100 μm are shown. *Identifies the tumour area. *IHC analysis was performed by Consorzio Mia, University of Milan-Bicocca.*

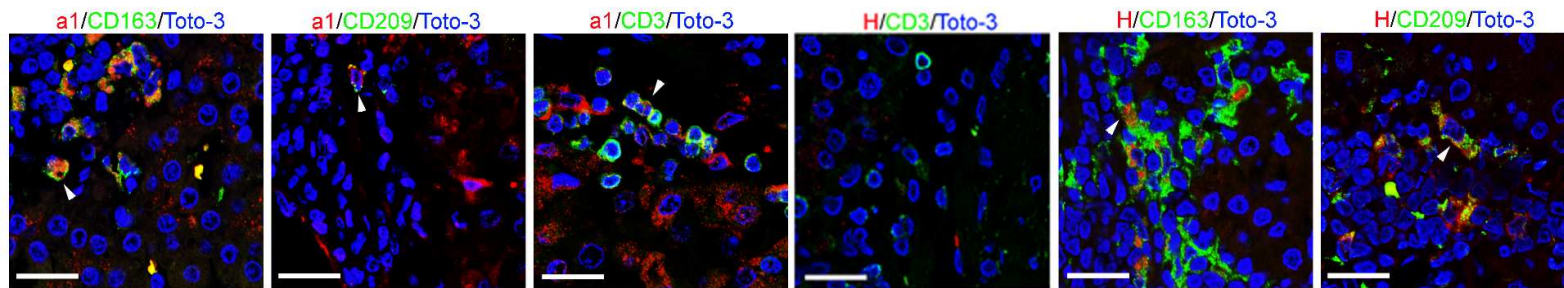


Figure 6.1.2. Expression of V-ATPase in M2-like macrophages infiltrating HCC tissues. Triple-labeled immunofluorescence staining for $\alpha 1$ and H subunits of the V-ATPase complex (red) and CD163 (green), CD209 (green) or CD3 (green) in HCC tissues. Nuclei were stained with Toto-3 (blue). White arrows indicate the co-expression of the analysed markers. Representative images with scale bars = 25 μm . *Confocal analysis was performed by Consorzio Mia, University of Milan-Bicocca.*

These data suggest that the expanding edge of HCC is enriched in immunosuppressive M2 macrophages and CD3 T cells, which both express the V-ATPase complex.

To confirm these findings, single-cell suspensions, obtained from surgical resected HCC tissue by enzymatic digestion, were analysed by multiparametric flow cytometry. The frequencies of myeloid cells, defined as CD11b⁺CD14⁺CD163⁺ or CD11b⁺CD14⁺CD209⁺, and that of T lymphocytes, characterized as CD3⁺, were assessed in the CD45⁺ gated population. The expression of the a1 V-ATPase, for which a specific antibody working in flow cytometry is available, was evaluated inside the above mentioned immune cells. Figure 6.1.3A and B report the gating strategy. The CD209 and CD163 positive populations, as well as the positivity for V-ATPase a1, have been defined by setting the markers on the corresponding FMO control. For FMO definition and examples see Materials and Methods. HCC patients had different frequencies of myeloid (CD14⁺, CD163⁺, CD209⁺) and lymphocytic (CD3⁺) cells as illustrated in Figure 6.1.3C which reports cumulative results obtained from the analysis of six independent samples. The expression of the a1 V-ATPase marker was evaluated inside the above mentioned immune cells and interestingly, we found that a1 was mainly expressed in macrophages expressing M2-related markers (Figure 6.1.3D). CD3⁺ cells evaluated in the gate of CD45⁺ cells were also positive for a1, although only a small fraction of a1 positive cells was detectable (Figure 6.1.3E). Figure 6.1.3D illustrates the cumulative results of the percentage of a1 V-ATPase-positive cells in the CD14⁺, CD163^{+/-}, CD209^{+/-} and

CD3⁺ gated populations of six independent samples analysed. A higher percentage of a1⁺ cells was found in the CD163⁺ and CD209⁺ M2-like macrophages.

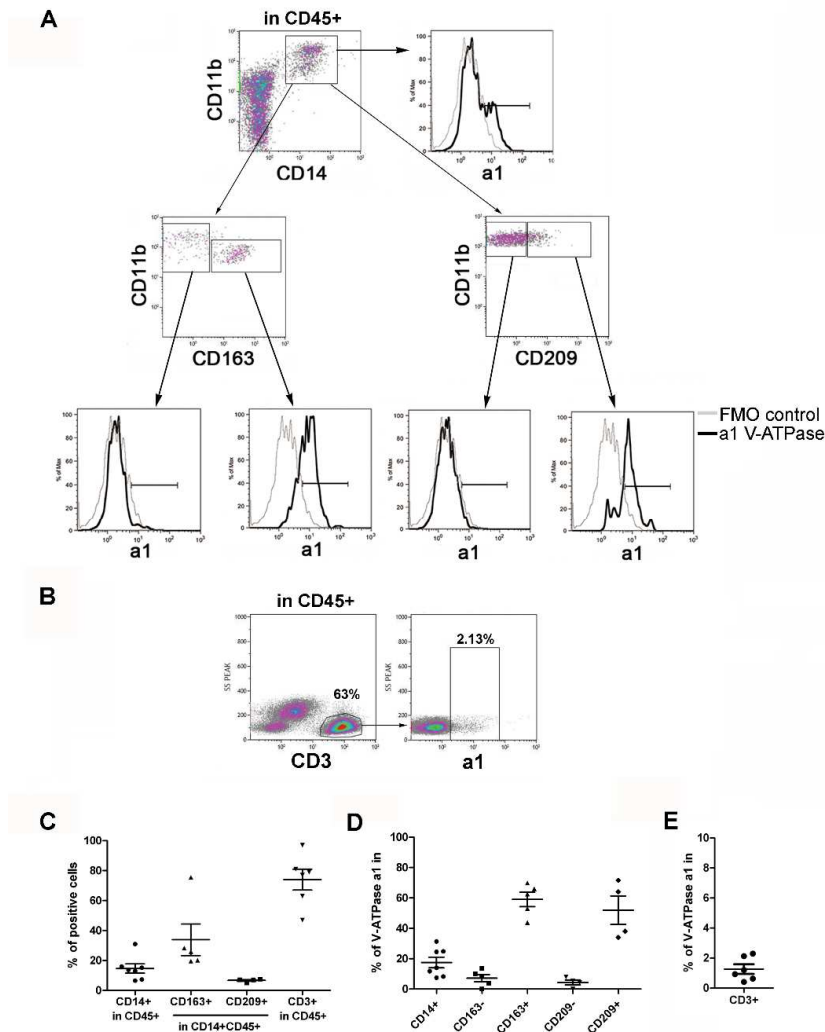


Figure 6.1.3. Expression of V-ATPase a1 in immune cells infiltrating HCC tissues. Multiparametric flow cytometry analysis of live myeloid and lymphocytic cells in cell suspensions of freshly dissociated HCC surgical specimens. **(B-C)** The cell surface expression of V-ATPase a1 was evaluated in CD14⁺CD11b⁺, CD11b⁺CD163⁻, CD11b⁺CD163⁺ CD11b⁺CD209⁻, CD11b⁺CD209⁺ **(A)** and CD45⁺CD3⁺ cells **(B)**. **(C)** The graph summarizes the percentages of CD14⁺, CD163⁺, CD209⁺ and CD3⁺ cells found in the analysed HCC samples. **(D)** The graph illustrates the percentages of V-ATPase a1⁺ cells assessed in the indicated myeloid cell populations and in **(E)** CD3⁺ cells for all the analysed samples.

6.2 In the tumour microenvironment, V-ATPase inhibition modulated cancer and immune cell features: *ex vivo* analysis

In the chapter 5 using HCC cell lines, we showed that V-ATPase blockage with omeprazole exerted anti-tumour activity. Since here we showed that, besides tumour cells, the V-ATPase was also expressed by innate and adaptive immune components infiltrating HCC, we asked whether interfering with V-ATPase activity with omeprazole could modulate the HCC microenvironment in both the tumour and immune cells. Thus, we used two different *ex vivo* approaches: HCC tissue explants and single-cell suspensions from HCC tissues.

We applied drug treatment to primary human HCC tissue explants (n=8), which preserve the complex network of the tumour, linking tumour cells and cells of the local microenvironment, including inflammatory infiltrating cells (see chapter 2 for further technical details). Inflammation/immune evasion and EMT are linked by bidirectional interactions [186, 187], and they both confer aggressive traits to human carcinomas, including HCC [169]. Thus, to evaluate whether the V-ATPase blockage by omeprazole may impact these phenotypic HCC features, HCC tissue fragments, cultured for 24h in omeprazole-conditioned medium or in control medium, were assessed by qRT-PCR for the mRNA expression of *MYC*, *CDH1* and *VIM*, all genes associated with EMT [188, 189]. Data reported in Figure 6.2.1 upper panel show that *MYC* and *VIM* were down-modulated in parallel with an increased *CDH1* expression in HCC tissue explants treated with omeprazole. Omeprazole treatment induced also a reshaping in the TME cytokine milieu characterized by a down-regulation of genes encoding for the

immune-suppressive cytokine *CCL22* (Figure 6.2.1, lower panel) and up-regulation of the antitumor, Th1 associated *IFNG* and *TNF* genes (Figure 6.2.1, lower panel).

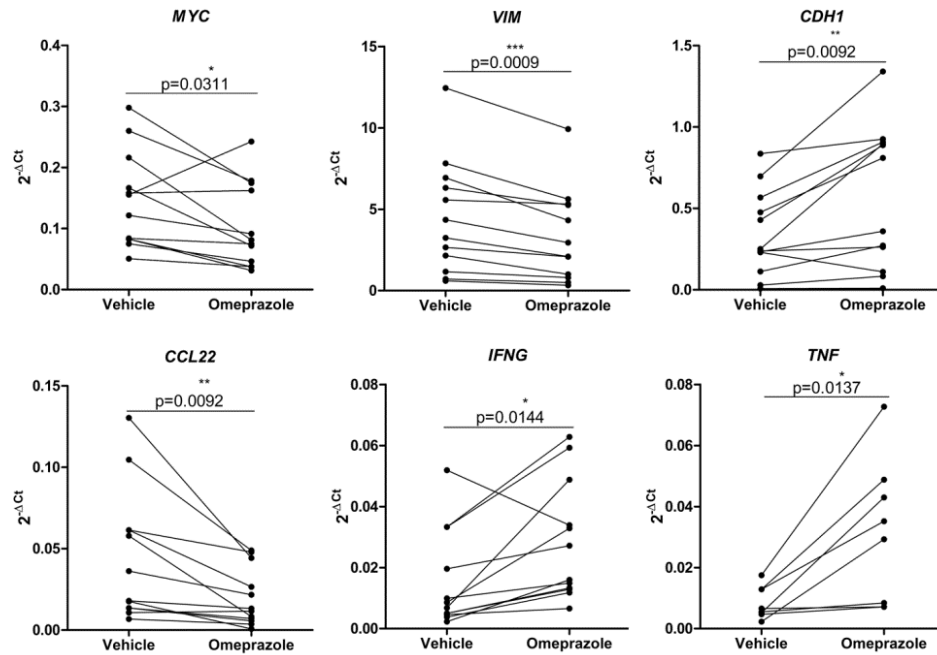


Figure 6.2.1. Omeprazole affects the expression of genes conferring EMT and suppressive features at HCC TME. Graphs illustrate the expression levels of the indicated genes in HCC tissue explants (*MYC*, *VIM*, *CDH1*, *CCL22*, *IFNG* n=12; *TNF*, n=8) cultured *ex vivo* in the presence of 100 μ g/ml omeprazole or the vehicle of the drug for 24h. The gene expression data are reported as $2^{-\Delta Ct}$ values. The p-values are calculated by the paired t test comparing cells treated with omeprazole or the vehicle.

To define whether cytokine modulation also occurred at the protein level and to assess if omeprazole interferes with the production of inflammatory and immunosuppressive molecules in specific immune cell populations of the HCC TME, single cell suspensions obtained from HCC specimens were exposed *ex vivo* to omeprazole or vehicle for 24h (see Materials and Methods on chapter 2

for further details). To assess the cytokine/chemokine secretion by the different immune cell compartments, the single-cell suspensions treated or not with the drug were subjected to intracellular staining in multiparametric flow cytometry. Interestingly, compared to cells exposed to the vehicle of the drug, omeprazole decreased the production of CCL22, whereas it significantly increased IFN γ and TNF expression in M2-like macrophages, identified by their positivity for CD11b and CD163 in the gate of CD45⁺CD3⁻ cells (Figure 6.2.2).

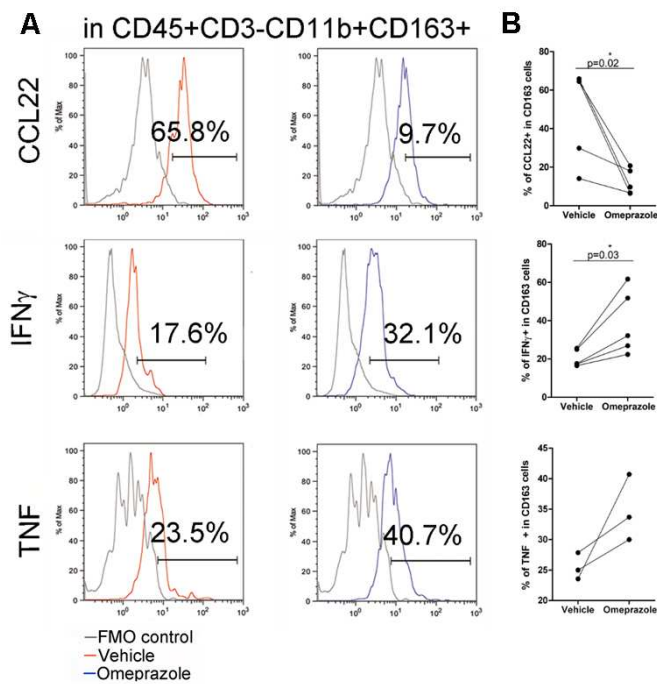


Figure 6.2.2. Modulation of the cytokine profile in M2-like macrophages by omeprazole treatment. (A) Multiparametric flow cytometry of live cells in freshly dissociated HCC tumours treated with the drug vehicle (red line) or with omeprazole (100 μ g/ml, blue line) for 24 h. IFN γ , TNF and CCL22 production was evaluated by intracellular staining in CD163⁺ myeloid cells gated inside the live CD45⁺CD3⁻ cells. FMO control for each cytokine (gray line) is reported in the histogram plot. FMO control consists of the same cells as those of the sample stained with all the antibodies of the sample, minus the antibody for which the positivity is evaluated. (B) The graphs show the percentages of IFN γ -, TNF- and CCL22-positive cells in the CD163⁺ cells. The p-values are calculated by the paired t test comparing cells treated with omeprazole or the vehicle.

Interestingly, the same immunomodulating activities of omeprazole were evident in the in CD3⁺ T cells (Figure 6.2.3).

Altogether, these data indicate pleiotropic modulating functions of omeprazole and that V-ATPase blockage affects the TME both at the tumour and at the immune cellular levels.

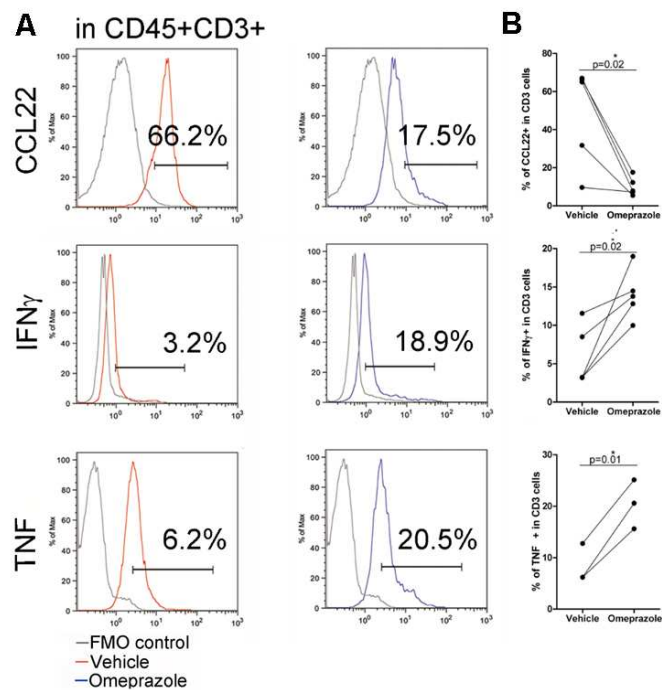


Figure 6.2.3. Modulation of the cytokine profile in CD3⁺ T cells by omeprazole treatment. (A) Multiparametric flow cytometry of live cells in freshly dissociated HCC tumours treated with the drug vehicle (red line) or with omeprazole (100 μ g/ml, blue line) for 24h. IFN γ , TNF and CCL22 production was evaluated by intracellular staining in CD3⁺ T cells gated inside the live CD45⁺ cells. FMO control for each cytokine (gray line) is reported in the histogram plot. FMO control consists of the same cells as those of the sample stained with all the antibodies of the sample, minus the antibody for which the positivity is evaluated. (B) The graphs show the percentages of IFN γ -, TNF- and CCL22-positive cells in the CD3⁺ cells. The p-values are calculated by the paired t test comparing cells treated with omeprazole or the vehicle.

Discussion

The aims of this chapter were: - to characterise the immune infiltrate of HCC TME; - to evaluate the expression of V-ATPase in the immune components of HCC TME; - to assess the effects of omeprazole on tumour and immune cells of HCC TME.

Our results showed that CD163⁺ and CD209⁺ M2-like macrophages and CD3⁺ T cells infiltrated HCC tissues and these cells were the prevalent immune components in the HCC TME. Interestingly, our data revealed the detection of V-ATPase in the majority of the malignant hepatocytes and in the infiltrating immune cells. Thus, in the HCC TME, V-ATPase represents the most broadly and highly expressed pH regulator among those analysed in this thesis. Importantly, M2-like TAMs, located within tumour nests or in the peri-tumour area at the boundary between tumour and adjacent non-tumour tissue, expressed V-ATPase. It is well-known that *ATP6V1B2* encoding for the B2 V-ATPase subunit is up-regulated in human monocytic cells during macrophage differentiation [169]. Furthermore, as previously reported by Brisseau and collaborators the expression of V-ATPase on the plasma membrane of murine macrophages is essential for maintaining the optimal pHi that becomes acid in an inflammatory microenvironment. Specifically, the authors demonstrated that IL-1, released in the microenvironment, boosts the activity of V-ATPase and consequently increases the pHi in macrophages [190]. Recently, Kimura and colleagues demonstrated that M2 polarization requires the activation of the mTORC1/mTOR pathway through V-ATPase [118]. Hence, it is conceivable that

HCC-associated macrophages might exploit V-ATPase expression to survive the acidic TME and possibly to exert their immunosuppressive effects. Indeed our data showed that targeting V-ATPase *ex vivo* by omeprazole in patient-derived HCC tissue explants and cell suspensions interfered with TAM activity, by decreasing CCL22 expression and concomitantly increasing IFN γ and TNF. Thus, omeprazole possibly limits the immunosuppressive function of TAM and favours the conversion of pro-tumour M2-like myeloid cells into antitumor M1-like cells

In our setting, the $\alpha 1$ V-ATPase subunit was also expressed by CD3⁺ T cells. Other studies have already demonstrated a physiological expression of $\alpha 2$ and $\alpha 3$ subunits in lymphocytes and activated T cells [191, 192]. Bulwin and collaborators showed that $\alpha 3$ expression co-localizes with CTLA-4 in human T cells and is involved in the control of T cell proliferation [193]. This opens the way for possible combinatorial therapeutic approaches between PPIs and anti-CTLA-4 therapy (ipilimumab). Furthermore, we observed that CD3⁺ T cells infiltrating HCC tissues can be targeted by omeprazole and this inhibition caused the modulation of the same cytokines modulated in the M2-like macrophages. These results may indicate a reactivation of a Th1 anti-tumour response. Thus, our data indicate a broad impact of omeprazole in creating a less immunosuppressive HCC microenvironment involving both innate and adaptive effector T cells. Although we have not demonstrated a direct effect of omeprazole on tumour or stromal cells, our data (Fig. 6.2.1) showed a down-regulation of the oncogenes *MYC* and *VIM*, while an up-regulation of *CDH1*.

These results point to a block in EMT, a process that can be also sustained by myeloid cells [92, 194]; the anti-tumour effect of reverting EMT has already been described in melanoma cells treated with esomeprazole, an S-enantiomer of omeprazole [127].

In conclusion, our data indicate that targeting V-ATPase could reduce the viability and aggressive features of tumour cells, while concomitantly interfering with the pro-tumour and immunosuppressive functions exerted by the myeloid cell infiltrate in HCC, likely favouring an anti-tumour response mediated by T cells.

7. General Discussion

7.1 Overall summary

The metabolism of tumour cells is the focus of a new wave of studies aimed to better understand cancer biology and to develop new therapeutic interventions. Metabolic dysfunction of cancer cells not only determines the survival and aggressiveness of transformed cells, but it also directly influences the TME [17]. In the present thesis we showed that in HCC, whose metabolism adapts to a highly hypoxic environment, the pH regulators CAIX, CAXII and V-ATPase are overexpressed at the gene and protein levels in tumour tissues. Proton extrusion and pHi regulation are the physiological functions of these proteins and in tumour cells they exert detoxification functions ensuring tumour cell survival. The pH regulatory molecules alkalinise the pHi and simultaneously they contribute to microenvironment acidification [17]. Our *in vitro* data indicated that the inhibition of CAIX, CAXII and V-ATPase with specific drugs affected the growth and cell viability of HCC cell lines, chosen to represent the known HCC heterogeneity [171, 180]. Thus, our findings suggest a strong pro-survival role of these molecules in HCC biology and qualify CAIX, CAXII and V-ATPase as possible targets for anti-tumour therapy. However, our *ex vivo* analysis performed on a series of autologous adjacent, non-tumour and HCC tissues, showed that HCC displays a complex expression pattern for these molecules in terms of inter- and intra-tumour variability and cellular distribution. Hepatocytes in normal and in the inflamed non-tumour liver tissues were CAIX negative, thus, the CAIX expression in HCC is possibly *de novo* acquired during neoplastic

transformation. We observed a focal distribution of CAIX in discrete nests of tumour hepatocytes, which is probably associated to areas of the tumour with low oxygen tension and high aggressive features. In support of this observation, we found that the expression of the *CA9* gene positively correlated in tumour tissues with that of hypoxia inducible factor 1 α (*HIF1A*). Moreover, our *ex vivo* analysis in HCC specimens also revealed an enhanced expression of *CA9* in poorly differentiated tumours (grading 3) and a relationship between *CA9*, *TWIST* and the majority of CSC-related genes. Our data are in agreement with the findings obtained in other solid malignancies highlighting the association of CAIX to stemness [95, 151], cell migration and invasion [140]. Thus, our results indicate an association of *CA9* with malignancies, and stemness in HCC and suggest that, targeting CAIX might also possibly result in the inhibition of the most aggressive HCC cancer cells.

However, we found that CAIX was also highly positive in the bile ducts of normal liver and in non-tumour tissues, likely in relation to their secretory functions. This expression pattern in normal liver cells indeed poses worries for the utilization of CAIX as therapeutic target in HCC. *In vivo* studies, that showed the selective and anti-metastatic activity of CAIX inhibitors, have shown that these drugs are well tolerated and do not cause any toxic and cachectic effects in treated mice. However, these studies did not specifically investigate liver toxicity caused by inhibiting CAIX functions [154-157]. Thus, additional pre-clinical studies are warranted to exclude any adverse events due to liver toxicity, especially in HCC patients, who display already partially compromised liver functions.

Our *ex vivo* analysis revealed for the first time the presence of CAXII in HCC. We observed that tumour hepatocytes also expressed the alternative splicing variant *CA12 2/3* which unlike the normal transcript *CA12 1*, was positively associated to *HIF1A*. Furthermore, this association was further supported by our *in vitro* results, in which we demonstrated a clear induction of *CA12 2/3* in HCC cell lines mediated by hypoxia. These results are in line with the reported observation that indeed hypoxia can modulate the splicing of pre-mRNA molecules [170]. The *ex vivo* protein distribution of CAXII in HCC patients showed a selective and homogeneous expression in tumour hepatocytes, while no positivity of CAXII was found in normal or peri-tumour tissues. Moreover, as we have already reported for CAIX, CAXII was also implicated in the aggressiveness of HCC. Specifically, we found that poorly differentiated HCC also have high gene expression levels of *CA12 1* and *CA12 2/3*. Thus, these results support a possible role of CAXII in influencing HCC malignancy. This conclusion was supported by our HCC index score (HIS), which comprised the concomitant gene expression levels of a number of pH regulators (*CA12 1*, *CA12 2/3*), plus the EMT-related *CDH1* and the inflammation/immunosuppression-related gene (*CD209*). Based on the alteration of two or more of these genes, this HIS identified patients with a short RFS. For these reasons, CAXII represents an ideal targetable molecule in HCC patients. However, our data also showed that *ex vivo*, unexpectedly, CAXII was mainly localised in the cytoplasm and in the ER with no or a paucity of expression at the cell surface. This intracellular distribution was also seen in the HCC cell lines, in

which hypoxia further accentuated the retention of CAXII in the ER. Of note, in hypoxic conditions, HCC cells became partially refractory to the action of the CAXII specific inhibitor compound 25, probably because CAXII displayed limited availability to the drug. It remains to be assessed whether and how this peculiar cellular distribution affects CAXII-mediated biological functions, but it likely hampers the clinical targeting of this protein in the context of the highly hypoxic HCC. Nevertheless, with compound 25 being highly specific, modifications might be incorporated to make this drug able to target CAXII inside the cell and increase its efficacy in a hypoxic environment that is a main feature of human HCC [85].

In contrast to CAIX and CAXII, whose expression was restricted to malignant hepatocytes, we observed that not only were the vast majority of malignant hepatocytes positive for V-ATPase subunits but, importantly, myeloid and lymphocytic cells, infiltrating the tumour nodule or localized at the expanding edge of the tumour also expressed V-ATPase. This expression was found in CD163⁺ and CD209⁺ M2-like macrophages and CD3⁺ T cells in HCC tissues. It is already reported that in macrophages the V-ATPase is expressed to maintain the optimal pHi in an inflammatory microenvironment [190]. Thus, it can be speculated that in the hypoxic/acidic TME the enzymatic activity of V-ATPase protects M2 macrophages with suppressive and pro-tumour functions. Our data suggest that by V-ATPase blockade we may inhibit tumour and pro-tumorigenic/immunosuppressive immune cells. In support of this hypothesis, our data obtained by short-term treatment of HCC tissue explants with omeprazole,

actually demonstrated that omeprazole exerted important effects on TME, reducing *CCL22* together with increasing *IFNG* and *TNF* transcription. Importantly, this drug affected the aggressiveness of malignant cells inducing a down-modulation of EMT-associated genes *VIM* and *MYC*, while increasing the transcription of *CDH1*. By the usage of cell suspensions obtained from HCC tissues, we clearly demonstrated that V-ATPase inhibition induced a reshaping of the cytokine pool, specifically by decreasing *CCL22* production and concomitantly increasing IFN γ and TNF in M2-like macrophages and CD3⁺ T cells. Omeprazole possibly limits the immunosuppressive function of TAMs favouring the conversion of pro-tumour M2-like cells into anti-tumour M1-like myeloid cells, while it stimulates an anti-tumour response mediated by boosting the T cell subset (Th1).

While it is already known that the buffering of the external pH by bicarbonate treatment favours anti-tumour immunity and potentiates the efficacy of ICIs in a pre-clinical model [59], the mechanism by which omeprazole induces these pleiotropic modifications at the TME remains to be fully addressed. Interestingly, emerging evidence indicate that infiltrating M2 polarized macrophages might function as a bridge between EMT and immunosuppression [92]. In our *ex vivo* experiments, the relief in immune suppression induced by V-ATPase blockage was associated with a change in the EMT features of the tumour cells. Thus, we speculate that this effect can be mediated by the direct targeting of tumour cells, which express V-ATPase, or by the inhibition of the pro-tumourigenic functions of TAMs. The anti-tumour effect of omeprazole has been demonstrated at

preclinical and clinical levels [183, 184], but not in HCC. Furthermore, omeprazole is a safe drug, well-tolerated by mice and esomeprazole, the S-enantiomer of omeprazole, showed low hepatic toxicity in a clinical study enrolling osteosarcoma patients [184]. These observations support the usage of a V-ATPase inhibitor in HCC. Particularly, in advanced HCC patients in which a randomized study comparing TACE versus TACE plus the local administration of bicarbonate has clearly shown that the cohort of patients receiving the combination therapy had a strong improvement in the objective response rate, thus indicating that local normalization of acidosis improves tumour control [96].

7.2 Conclusions

The present work supports the belief that the TME acidity can be an important target to counteract the pro-tumourigenic features of the HCC TME. Specifically, inhibition of pH regulators in HCC can be useful to block the most aggressive cancer cells. However, considering the expression and distribution of CAIX and CAXII in HCC, the usage of CAIX and CAXII inhibitors in this setting requires additional pre-clinical studies and the development of more selective drugs efficiently targeting the different isoforms of CAXII. Nevertheless, on the basis of the data contained in this thesis, the inhibition of V-ATPase in HCC should be considered a multi-task strategy which restrains tumour growth and aggressiveness by simultaneously inhibiting cancer cells and immunosuppressive cells, while also stimulating an anti-tumour immune response. Figure 7 summarises this discussion.

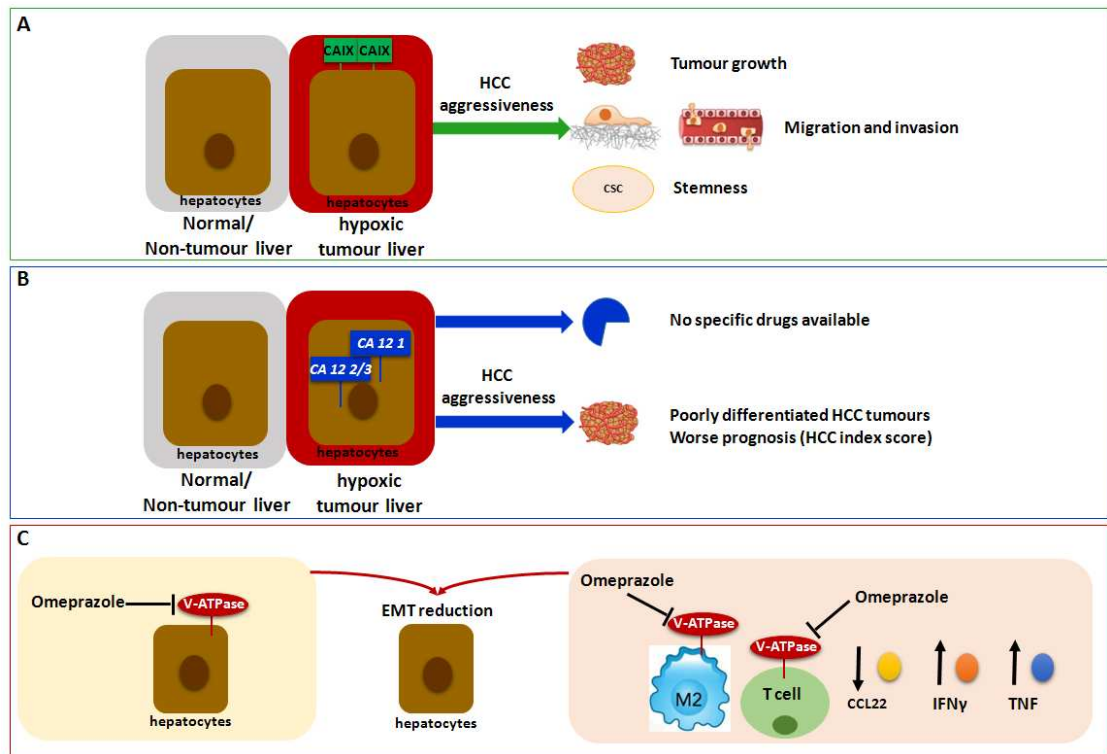


Figure 7. The schematic representation of the discussion and conclusions of this thesis. (A) CAIX is selectively expressed by malignant hepatocytes and its expression is increased by hypoxia. It is involved in the aggressive features of HCC. **(B)** Malignant hepatocytes express the CA12 1 and the splicing variants CA12 2/3 that are up-regulated by hypoxia. These CA12 isoforms at the moment can not be targeted by specific drugs. CA12 1 and CA12 2/3 are associated with the aggressiveness of HCC. **(C)** V-ATPase is expressed by tumour and immune cells (M2-like macrophages and T cells). Targeting V-ATPase in HCC reduces the immunosuppressive cytokine (CCL22) and increases the anti-tumour-associated cytokines (IFN γ and TNF), while reverting EMT in malignant hepatocytes. The reduction of EMT could be related to the inhibition of V-ATPase in cancer cells or to the control of immunosuppression.

7.3 Future perspectives

Regarding this study, there are many issues that remain to be investigated for elucidating the connections between pH regulatory molecules and the immunosuppressive and aggressive status of HCC.

With this work, we have demonstrated that the pH regulators are well expressed in HCC and they display different expression patterns. Several issues related to the precise functions exerted by CAIX, CAXII and V-ATPase in HCC biology still remain open to investigation.

Concerning CAIX, our *ex vivo* analyses showed a peculiar expression of CAIX in discrete nests of hepatocytes inside the hypoxic areas of HCC lesions, along with its apparent association with tumour aggressiveness, invasive features and stemness of HCC. In order to further dissect the functions of CAIX in HCC, CAIX-positive and CAIX-negative adjacent areas from FFPE HCC samples will be microdissected, and we will perform genome-wide transcriptional analyses to identify pathways regulated by CAIX and hence likely to be involved in tumour aggressiveness.

We think that many aspects of CAXII biology still deserve attention. Our data showed the presence of different spliced variants of the *CA12* gene transcripts, and all of them were associated with hypoxia and HCC malignancy. Several issues are still open regarding the protein encoded by each of these spliced variants and the role they may play in the intracellular distribution of the CAXII proteins and in affecting HCC behaviour. We thus plan to use the CRISPR/Cas9 genome editing technology to generate stable HCC cell lines that express separately *CA12 1* and *CA12 2/3*. Then, we will evaluate whether these genome-edited cells acquire a more aggressive

behaviour (decreased cell-cell adhesion and increased cell motility, enhanced invasiveness into the surrounding tissues, greater ability to self-renew and to form tumours in immunodeficient mice, influencing the pro-tumourigenic functions of immunosuppressive cells). Moreover, in collaboration with Professor Supuran's group we will develop novel and selective drugs able to target the different isoforms of CAXII expressed in HCC, that then will be tested *in vitro* and *ex vivo* for their biological activity in HCC.

Intriguingly, we have also observed that V-ATPase is an important modulator of tumour cells and of the HCC microenvironment. Specifically, V-ATPase inhibition changed the anti-tumour immune profile that involved both innate and adaptive immune cells, but also suggested that it reversed the expression levels of some genes associated with the EMT of malignant hepatocytes. One of our objectives will be to define which molecular pathways are modulated in HCC tumour cells by V-ATPase inhibition and evaluate whether these pathways are also involved in the shaping of the immune-related features of HCC. As a first step in this analysis, we will perform genome-wide transcriptional analyses on HCC cell lines treated with omeprazole and the vehicle to identify genes differentially expressed. Particular interest will be focused on genes encoding for immunomodulating molecules. Then, we will apply Ingenuity Pathway Analysis (IPA) to identify signaling pathways and biological functions induced by V-ATPase in tumour cells. Since we have already obtained good quality RNA samples from HCC tissue explants treated with omeprazole and the vehicle, as a second step of this analysis, we will perform genome-wide transcriptional analysis on these

samples and then we will apply CIBERSORT software for studying the immune cell composition of our HCC tissue explants.

References

1. Vander Heiden MG, Cantley LC, Thompson CB. Understanding the warburg effect: The metabolic requirements of cell proliferation. *Science* 2009;324:1029-33.
2. Ward PS, Thompson CB. Metabolic reprogramming: A cancer hallmark even warburg did not anticipate. *Cancer Cell* 2012;21:297-308.
4. Masoud GN, Li W. HIF-1alpha pathway: Role, regulation and intervention for cancer therapy. *Acta Pharm Sin B* 2015;5:378-89.
3. Nagarajan A, Malvi P, Wajapeyee N. Oncogene-directed alterations in cancer cell metabolism. *Trends Cancer* 2016;2:365-77.
5. Doe MR, Ascano JM, Kaur M, Cole MD. Myc posttranscriptionally induces HIF1 protein and target gene expression in normal and cancer cells. *Cancer Res* 2012;72:949-57.
6. Marchiq I, Pouyssegur J. Hypoxia, cancer metabolism and the therapeutic benefit of targeting lactate/H(+) symporters. *J Mol Med (Berl)* 2016;94:155-71.
7. Eales KL, Hollinshead KE, Tennant DA. Hypoxia and metabolic adaptation of cancer cells. *Oncogenesis* 2016;5:e190.
8. Parks SK, Pouyssegur J. Targeting pH regulating proteins for cancer therapy-progress and limitations. *Semin Cancer Biol* 2017;43:66-73.
9. Peppicelli S, Andreucci E, Ruzzolini J, Laurenzana A, Margheri F, Fibbi G, et al. The acidic microenvironment as a possible niche of dormant tumor cells. *Cell Mol Life Sci* 2017;74:2761-71.
10. Schito L, Semenza GL. Hypoxia-inducible factors: Master regulators of cancer progression. *Trends Cancer* 2016;2:758-70.
11. Carnero A, Leonart M. The hypoxic microenvironment: A determinant of cancer stem cell evolution. *Bioessays* 2016;38 Suppl 1:S65-74.
12. Chen DS, Mellman I. Elements of cancer immunity and the cancer-immune set point. *Nature* 2017;541:321-30.
13. Triner D, Shah YM. Hypoxia-inducible factors: A central link between inflammation and cancer. *J Clin Invest* 2016;126:3689-98.
14. Nagarsheth N, Wicha MS, Zou W. Chemokines in the cancer microenvironment and their relevance in cancer immunotherapy. *Nat Rev Immunol* 2017;17:559-72.

15. Huber V, Camisaschi C, Berzi A, Ferro S, Lugini L, Triulzi T, et al. Cancer acidity: An ultimate frontier of tumor immune escape and a novel target of immunomodulation. *Semin Cancer Biol* 2017;43:74-89.
16. Lyssiotis CA, Kimmelman AC. Metabolic interactions in the tumor microenvironment. *Trends Cell Biol* 2017;27:863-75.
17. McDonald PC, Chafe SC, Dedhar S. Overcoming hypoxia-mediated tumor progression: Combinatorial approaches targeting pH regulation, angiogenesis and immune dysfunction. *Front Cell Dev Biol* 2016;4:27.
18. McIntyre A, Hulikova A, Ledaki I, Snell C, Singleton D, Steers G, et al. Disrupting hypoxia-induced bicarbonate transport acidifies tumor cells and suppresses tumor growth. *Cancer Res* 2016;76:3744-55.
19. Sarosi GA, Jr, Jaiswal K, Herndon E, Lopez-Guzman C, Spechler SJ, Souza RF. Acid increases MAPK-mediated proliferation in barrett's esophageal adenocarcinoma cells via intracellular acidification through a $\text{Cl}^-/\text{HCO}_3^-$ exchanger. *Am J Physiol Gastrointest Liver Physiol* 2005;289:G991-7.
20. Amith SR, Wilkinson JM, Fliegel L. Na^+/H^+ exchanger NHE1 regulation modulates metastatic potential and epithelial-mesenchymal transition of triple-negative breast cancer cells. *Oncotarget* 2016;7:21091-113.
21. Estrella V, Chen T, Lloyd M, Wojtkowiak J, Cornnell HH, Ibrahim-Hashim A, et al. Acidity generated by the tumor microenvironment drives local invasion. *Cancer Res* 2013;73:1524-35.
22. Martinez-Zaguilan R, Seftor EA, Seftor RE, Chu YW, Gillies RJ, Hendrix MJ. Acidic pH enhances the invasive behavior of human melanoma cells. *Clin Exp Metastasis* 1996;14:176-86.
23. Cox TR, Rumney RMH, Schoof EM, Perryman L, Hoye AM, Agrawal A, et al. The hypoxic cancer secretome induces pre-metastatic bone lesions through lysyl oxidase. *Nature* 2015;522:106-10.
24. Shi Q, Abbruzzese JL, Huang S, Fidler IJ, Xiong Q, Xie K. Constitutive and inducible interleukin 8 expression by hypoxia and acidosis renders human pancreatic cancer cells more tumorigenic and metastatic. *Clin Cancer Res* 1999;5:3711-21.
25. Rofstad EK, Mathiesen B, Kindem K, Galappathi K. Acidic extracellular pH promotes experimental metastasis of human melanoma cells in athymic nude mice. *Cancer Res* 2006;66:6699-707.
26. Peppicelli S, Bianchini F, Contena C, Tombaccini D, Calorini L. Acidic pH via NF-kappaB favours VEGF-C expression in human melanoma cells. *Clin Exp Metastasis* 2013;30:957-67.

27. Shibue T, Weinberg RA. EMT, CSCs, and drug resistance: The mechanistic link and clinical implications. *Nat Rev Clin Oncol* 2017;14:611-29.
28. Krishnamachary B, Zagzag D, Nagasawa H, Rainey K, Okuyama H, Baek JH, et al. Hypoxia-inducible factor-1-dependent repression of E-cadherin in von hippel-lindau tumor suppressor-null renal cell carcinoma mediated by TCF3, ZFHX1A, and ZFHX1B. *Cancer Res* 2006;66:2725-31.
29. Peppicelli S, Bianchini F, Torre E, Calorini L. Contribution of acidic melanoma cells undergoing epithelial-to-mesenchymal transition to aggressiveness of non-acidic melanoma cells. *Clin Exp Metastasis* 2014;31:423-33.
30. Ulmschneider B, Grillo-Hill BK, Benitez M, Azimova DR, Barber DL, Nystul TG. Increased intracellular pH is necessary for adult epithelial and embryonic stem cell differentiation. *J Cell Biol* 2016;215:345-55.
31. Mathieu J, Zhang Z, Zhou W, Wang AJ, Heddleston JM, Pinna CM, et al. HIF induces human embryonic stem cell markers in cancer cells. *Cancer Res* 2011;71:4640-52.
32. Merk H, Messer P, Ardelt MA, Lamb DC, Zahler S, Muller R, et al. Inhibition of the V-ATPase by archazolid A: A new strategy to inhibit EMT. *Mol Cancer Ther* 2017;16:2329-39.
33. Filatova A, Seidel S, Bogurcu N, Graf S, Garvalov BK, Acker T. Acidosis acts through HSP90 in a PHD/VHL-independent manner to promote HIF function and stem cell maintenance in glioma. *Cancer Res* 2016;76:5845-56.
34. Hjelmeland AB, Wu Q, Heddleston JM, Choudhary GS, MacSwords J, Lathia JD, et al. Acidic stress promotes a glioma stem cell phenotype. *Cell Death Differ* 2011;18:829-40.
35. Mantovani A, Marchesi F, Malesci A, Laghi L, Allavena P. Tumour-associated macrophages as treatment targets in oncology. *Nat Rev Clin Oncol* 2017;14:399-416.
36. Movahedi K, Laoui D, Gysemans C, Baeten M, Stange G, Van den Bossche J, et al. Different tumor microenvironments contain functionally distinct subsets of macrophages derived from Ly6C(high) monocytes. *Cancer Res* 2010;70:5728-39.
37. Laoui D, Van Overmeire E, Di Conza G, Aldeni C, Keirsse J, Morias Y, et al. Tumor hypoxia does not drive differentiation of tumor-associated macrophages but rather fine-tunes the M2-like macrophage population. *Cancer Res* 2014;74:24-30.

38. Murdoch C, Giannoudis A, Lewis CE. Mechanisms regulating the recruitment of macrophages into hypoxic areas of tumors and other ischemic tissues. *Blood* 2004;104:2224-34.
39. Casazza A, Laoui D, Wenes M, Rizzolio S, Bassani N, Mambretti M, et al. Impeding macrophage entry into hypoxic tumor areas by Sema3A/Nrp1 signaling blockade inhibits angiogenesis and restores antitumor immunity. *Cancer Cell* 2013;24:695-709.
40. Harney AS, Arwert EN, Entenberg D, Wang Y, Guo P, Qian BZ, et al. Real-time imaging reveals local, transient vascular permeability, and tumor cell intravasation stimulated by TIE2hi macrophage-derived VEGFA. *Cancer Discov* 2015;5:932-43.
41. Tripathi C, Tewari BN, Kanchan RK, Baghel KS, Nautiyal N, Shrivastava R, et al. Macrophages are recruited to hypoxic tumor areas and acquire a pro-angiogenic M2-polarized phenotype via hypoxic cancer cell derived cytokines oncostatin M and eotaxin. *Oncotarget* 2014;5:5350-68.
42. Doedens AL, Stockmann C, Rubinstein MP, Liao D, Zhang N, DeNardo DG, et al. Macrophage expression of hypoxia-inducible factor-1 alpha suppresses T-cell function and promotes tumor progression. *Cancer Res* 2010;70:7465-75.
43. Colegio OR, Chu NQ, Szabo AL, Chu T, Rhebergen AM, Jairam V, et al. Functional polarization of tumour-associated macrophages by tumour-derived lactic acid. *Nature* 2014;513:559-63.
44. Zhang H, Lu H, Xiang L, Bullen JW, Zhang C, Samanta D, et al. HIF-1 regulates CD47 expression in breast cancer cells to promote evasion of phagocytosis and maintenance of cancer stem cells. *Proc Natl Acad Sci U S A* 2015;112:E6215-23.
45. Veglia F, Perego M, Gabrilovich D. Myeloid-derived suppressor cells coming of age. *Nat Immunol* 2018;19:108-19.
46. Zhu G, Tang Y, Geng N, Zheng M, Jiang J, Li L, et al. HIF-alpha/MIF and NF-kappaB/IL-6 axes contribu
47. Corzo CA, Condamine T, Lu L, Cotter MJ, Youn JI, Cheng P, et al. HIF-1alpha regulates function and differentiation of myeloid-derived suppressor cells in the tumor microenvironment. *J Exp Med* 2010;207:2439-53.
48. Noman MZ, Desantis G, Janji B, Hasmim M, Karray S, Dessen P, et al. PD-L1 is a novel direct target of HIF-1alpha, and its blockade under hypoxia enhanced MDSC-mediated T cell activation. *J Exp Med* 2014;211:781-90.
49. Sceneay J, Chow MT, Chen A, Halse HM, Wong CS, Andrews DM, et al. Primary tumor hypoxia recruits CD11b+/Ly6Cmed/Ly6G+ immune

suppressor cells and compromises NK cell cytotoxicity in the premetastatic niche. *Cancer Res* 2012;72:3906-11.

50. Chafe SC, Lou Y, Sceneay J, Vallejo M, Hamilton MJ, McDonald PC, et al. Carbonic anhydrase IX promotes myeloid-derived suppressor cell mobilization and establishment of a metastatic niche by stimulating G-CSF production. *Cancer Res* 2015;75:996-1008.

51. Tanaka A, Sakaguchi S. Regulatory T cells in cancer immunotherapy. *Cell Res* 2017;27:109-18.

52. Clambey ET, McNamee EN, Westrich JA, Glover LE, Campbell EL, Jedlicka P, et al. Hypoxia-inducible factor-1 alpha-dependent induction of FoxP3 drives regulatory T-cell abundance and function during inflammatory hypoxia of the mucosa. *Proc Natl Acad Sci U S A* 2012;109:E2784-93.

53. Deng B, Zhu JM, Wang Y, Liu TT, Ding YB, Xiao WM, et al. Intratumor hypoxia promotes immune tolerance by inducing regulatory T cells via TGF-beta1 in gastric cancer. *PLoS One* 2013;8:e63777.

54. Angelin A, Gil-de-Gomez L, Dahiya S, Jiao J, Guo L, Levine MH, et al. Foxp3 reprograms T cell metabolism to function in low-glucose, high-lactate environments. *Cell Metab* 2017;25:1282,1293.e7.

55. Li J, Wang L, Chen X, Li L, Li Y, Ping Y, et al. CD39/CD73 upregulation on myeloid-derived suppressor cells via TGF-beta-mTOR-HIF-1 signaling in patients with non-small cell lung cancer. *Oncoimmunology* 2017;6:e1320011.

56. Young A, Mittal D, Stagg J, Smyth MJ. Targeting cancer-derived adenosine: New therapeutic approaches. *Cancer Discov* 2014;4:879-88.

57. Facciabene A, Peng X, Hagemann IS, Balint K, Barchetti A, Wang LP, et al. Tumour hypoxia promotes tolerance and angiogenesis via CCL28 and T(reg) cells. *Nature* 2011;475:226-30.

58. Ren L, Yu Y, Wang L, Zhu Z, Lu R, Yao Z. Hypoxia-induced CCL28 promotes recruitment of regulatory T cells and tumor growth in liver cancer. *Oncotarget* 2016;7:75763-73.

59. Pilon-Thomas S, Kodumudi KN, El-Kenawi AE, Russell S, Weber AM, Luddy K, et al. Neutralization of tumor acidity improves antitumor responses to immunotherapy. *Cancer Res* 2016;76:1381-90.

60. Torre LA, Siegel RL, Ward EM, Jemal A. Global cancer incidence and mortality rates and trends--an update. *Cancer Epidemiol Biomarkers Prev* 2016;25:16-27.

61. Mazzaferro V, Lencioni R, Majno P. Early hepatocellular carcinoma on the procrustean bed of ablation, resection, and transplantation. *Semin Liver Dis* 2014;34:415-26.
62. Forner A, Reig M, Bruix J. Hepatocellular carcinoma. *Lancet* 2018;391:1301-14.
63. Llovet JM, Zucman-Rossi J, Pikarsky E, Sangro B, Schwartz M, Sherman M, et al. Hepatocellular carcinoma. *Nat Rev Dis Primers* 2016;2:16018.
64. Kudo M. Immune checkpoint inhibition in hepatocellular carcinoma: Basics and ongoing clinical trials. *Oncology* 2017;92 Suppl 1:50-62.
65. Pitt JM, Vetizou M, Daillere R, Roberti MP, Yamazaki T, Routy B, et al. Resistance mechanisms to immune-checkpoint blockade in cancer: Tumor-intrinsic and -extrinsic factors. *Immunity* 2016;44:1255-69.
66. Luedde T, Kaplowitz N, Schwabe RF. Cell death and cell death responses in liver disease: Mechanisms and clinical relevance. *Gastroenterology* 2014;147:765,783.e4.
67. Pusterla T, Nemeth J, Stein I, Wiechert L, Knigin D, Marhenke S, et al. Receptor for advanced glycation endproducts (RAGE) is a key regulator of oval cell activation and inflammation-associated liver carcinogenesis in mice. *Hepatology* 2013;58:363-73.
68. He G, Dhar D, Nakagawa H, Font-Burgada J, Ogata H, Jiang Y, et al. Identification of liver cancer progenitors whose malignant progression depends on autocrine IL-6 signaling. *Cell* 2013;155:384-96.
69. Villanueva A and Luedde T. The transition from inflammation to cancer in the liver. *Clinical Liver Disease* 2016 <https://doi.org/10.1002/cld.578>
70. Cancer Genome Atlas Research Network. Electronic address: wheeler@bcm.edu, Cancer Genome Atlas Research Network. Comprehensive and integrative genomic characterization of hepatocellular carcinoma. *Cell* 2017;169:1327,1341.e23.
71. Sia D, Jiao Y, Martinez-Quetglas I, Kuchuk O, Villacorta-Martin C, Castro de Moura M, et al. Identification of an immune-specific class of hepatocellular carcinoma, based on molecular features. *Gastroenterology* 2017;153:812-26.
72. Sia D, Llovet JM. Liver cancer: Translating '-omics' results into precision medicine for hepatocellular carcinoma. *Nat Rev Gastroenterol Hepatol* 2017;14:571-2.
73. Lin S, Nascimento EM, Gajera CR, Chen L, Neuhofer P, Garbuzov A, et al. Distributed hepatocytes expressing telomerase repopulate the liver in homeostasis and injury. *Nature* 2018;556:244-8.

74. Miyajima A, Tanaka M, Itoh T. Stem/progenitor cells in liver development, homeostasis, regeneration, and reprogramming. *Cell Stem Cell* 2014;14:561-74.
75. Sia D, Villanueva A, Friedman SL, Llovet JM. Liver cancer cell of origin, molecular class, and effects on patient prognosis. *Gastroenterology* 2017;152:745-61.
76. Nio K, Yamashita T, Kaneko S. The evolving concept of liver cancer stem cells. *Mol Cancer* 2017;16:4,016-0572-9.
77. Oikawa T. Cancer stem cells and their cellular origins in primary liver and biliary tract cancers. *Hepatology* 2016;64:645-51.
78. Tschaharganeh DF, Xue W, Calvisi DF, Evert M, Michurina TV, Dow LE, et al. p53-dependent nestin regulation links tumor suppression to cellular plasticity in liver cancer. *Cell* 2016;165:1546-7.
79. Hoshida Y, Villanueva A, Kobayashi M, Peix J, Chiang DY, Camargo A, et al. Gene expression in fixed tissues and outcome in hepatocellular carcinoma. *N Engl J Med* 2008;359:1995-2004.
80. Wan S, Zhao E, Kryczek I, Vatan L, Sadovskaya A, Ludema G, et al. Tumor-associated macrophages produce interleukin 6 and signal via STAT3 to promote expansion of human hepatocellular carcinoma stem cells. *Gastroenterology* 2014;147:1393-404.
81. Song YJ, Zhang SS, Guo XL, Sun K, Han ZP, Li R, et al. Autophagy contributes to the survival of CD133+ liver cancer stem cells in the hypoxic and nutrient-deprived tumor microenvironment. *Cancer Lett* 2013;339:70-81.
82. Buonaguro L, Petrizzo A, Tagliamonte M, Tornesello ML, Buonaguro FM. Challenges in cancer vaccine development for hepatocellular carcinoma. *J Hepatol* 2013;59:897-903.
83. Nishida N, Kudo M. Immunological microenvironment of hepatocellular carcinoma and its clinical implication. *Oncology* 2017;92 Suppl 1:40-9.
84. Wilson GK, Tennant DA, McKeating JA. Hypoxia inducible factors in liver disease and hepatocellular carcinoma: Current understanding and future directions. *J Hepatol* 2014;61:1397-406.
85. Vaupel P, Hockel M, Mayer A. Detection and characterization of tumor hypoxia using pO₂ histography. *Antioxid Redox Signal* 2007;9:1221-35.
86. Liu XB, Cheng Q, Geng W, Ling CC, Liu Y, Ng KT, et al. Enhancement of cisplatin-based TACE by a hemoglobin-based oxygen carrier in an orthotopic rat HCC model. *Artif Cells Nanomed Biotechnol* 2014;42:229-36.

87. Qu A, Taylor M, Xue X, Matsubara T, Metzger D, Chambon P, et al. Hypoxia-inducible transcription factor 2alpha promotes steatohepatitis through augmenting lipid accumulation, inflammation, and fibrosis. *Hepatology* 2011;54:472-83.
88. Copple BL, Bai S, Burgoon LD, Moon JO. Hypoxia-inducible factor-1alpha regulates the expression of genes in hypoxic hepatic stellate cells important for collagen deposition and angiogenesis. *Liver Int* 2011;31:230-44.
89. Hochst B, Schildberg FA, Sauerborn P, Gabel YA, Gevensleben H, Goltz D, et al. Activated human hepatic stellate cells induce myeloid derived suppressor cells from peripheral blood monocytes in a CD44-dependent fashion. *J Hepatol* 2013;59:528-35.
90. Chiu DK, Xu IM, Lai RK, Tse AP, Wei LL, Koh HY, et al. Hypoxia induces myeloid-derived suppressor cell recruitment to hepatocellular carcinoma through chemokine (C-C motif) ligand 26. *Hepatology* 2016;64:797-813.
91. Chiu DK, Tse AP, Xu IM, Di Cui J, Lai RK, Li LL, et al. Hypoxia inducible factor HIF-1 promotes myeloid-derived suppressor cells accumulation through ENTPD2/CD39L1 in hepatocellular carcinoma. *Nat Commun* 2017;8:517,017-00530-7.
92. Ye LY, Chen W, Bai XL, Xu XY, Zhang Q, Xia XF, et al. Hypoxia-induced epithelial-to-mesenchymal transition in hepatocellular carcinoma induces an immunosuppressive tumor microenvironment to promote metastasis. *Cancer Res* 2016;76:818-30.
93. Liu L, Zhu XD, Wang WQ, Shen Y, Qin Y, Ren ZG, et al. Activation of beta-catenin by hypoxia in hepatocellular carcinoma contributes to enhanced metastatic potential and poor prognosis. *Clin Cancer Res* 2010;16:2740-50.
94. Xu W, Zhou W, Cheng M, Wang J, Liu Z, He S, et al. Hypoxia activates Wnt/beta-catenin signaling by regulating the expression of BCL9 in human hepatocellular carcinoma. *Sci Rep* 2017;7:40446.
95. Lai JP, Conley A, Knudsen BS, Guindi M. Hypoxia after transarterial chemoembolization may trigger a progenitor cell phenotype in hepatocellular carcinoma. *Histopathology* 2015;67:442-50.
96. Chao M, Wu H, Jin K, Li B, Wu J, Zhang G, et al. A nonrandomized cohort and a randomized study of local control of large hepatocarcinoma by targeting intratumoral lactic acidosis. *Elife* 2016;5:10.7554/eLife.15691.
97. Neri D, Supuran CT. Interfering with pH regulation in tumours as a therapeutic strategy. *Nat Rev Drug Discov* 2011;10:767-77.

98. Iessi E, Logozzi M, Mizzone D, Di Raimo R, Supuran CT, Fais S. Rethinking the combination of proton exchanger inhibitors in cancer therapy. *Metabolites* 2017;8:10.3390/metabo8010002.
99. Cotter K, Stransky L, McGuire C, Forgac M. Recent insights into the structure, regulation, and function of the V-ATPases. *Trends Biochem Sci* 2015;40:611-22.
100. Stransky L, Cotter K, Forgac M. The function of V-ATPases in cancer. *Physiol Rev* 2016;96:1071-91.
101. Lim JH, Park JW, Kim SJ, Kim MS, Park SK, Johnson RS, et al. ATP6V0C competes with von hippel-lindau protein in hypoxia-inducible factor 1alpha (HIF-1alpha) binding and mediates HIF-1alpha expression by bafilomycin A1. *Mol Pharmacol* 2007;71:942-8.
102. Miles AL, Burr SP, Grice GL, Nathan JA. The vacuolar-ATPase complex and assembly factors, TMEM199 and CCDC115, control HIF1alpha prolyl hydroxylation by regulating cellular iron levels. *Elife* 2017;6:10.7554/eLife.22693.
103. Hendrix A, Sormunen R, Westbroek W, Lambein K, Denys H, Sys G, et al. Vacuolar H⁺ ATPase expression and activity is required for Rab27B-dependent invasive growth and metastasis of breast cancer. *Int J Cancer* 2013;133:843-54.
104. Feng S, Zhu G, McConnell M, Deng L, Zhao Q, Wu M, et al. Silencing of *atp6v1c1* prevents breast cancer growth and bone metastasis. *Int J Biol Sci* 2013;9:853-62.
105. Liu P, Chen H, Han L, Zou X, Shen W. Expression and role of V1A subunit of V-ATPases in gastric cancer cells. *Int J Clin Oncol* 2015;20:725-35.
106. Lu X, Qin W, Li J, Tan N, Pan D, Zhang H, et al. The growth and metastasis of human hepatocellular carcinoma xenografts are inhibited by small interfering RNA targeting to the subunit ATP6L of proton pump. *Cancer Res* 2005;65:6843-9.
107. Xu J, Xie R, Liu X, Wen G, Jin H, Yu Z, et al. Expression and functional role of vacuolar H⁽⁺⁾-ATPase in human hepatocellular carcinoma. *Carcinogenesis* 2012;33:2432-40.
108. Kuchuk O, Tuccitto A, Citterio D, Huber V, Camisaschi C, Milione M, Vergani B, Villa A, Alison MR, Carradori S, Supuran CT, Rivoltini L, Castelli C and Mazzaferro V. pH regulators to target the tumor immune microenvironment in human hepatocellular carcinoma. *Oncol Immunology* 2018. <https://doi.org/10.1080/2162402X.2018.1445452>.

109. Nishisho T, Hata K, Nakanishi M, Morita Y, Sun-Wada GH, Wada Y, et al. The $\alpha 3$ isoform vacuolar type H(+)-ATPase promotes distant metastasis in the mouse B16 melanoma cells. *Mol Cancer Res* 2011;9:845-55.
110. Lozupone F, Borghi M, Marzoli F, Azzarito T, Matarrese P, Iessi E, et al. TM9SF4 is a novel V-ATPase-interacting protein that modulates tumor pH alterations associated with drug resistance and invasiveness of colon cancer cells. *Oncogene* 2015;34:5163-74.
111. Kulshrestha A, Katara GK, Ibrahim S, Pamarthy S, Jaiswal MK, Gilman Sachs A, et al. Vacuolar ATPase ' $\alpha 2$ ' isoform exhibits distinct cell surface accumulation and modulates matrix metalloproteinase activity in ovarian cancer. *Oncotarget* 2015;6:3797-810.
112. Garcia-Garcia A, Perez-Sayans Garcia M, Rodriguez MJ, Antunez-Lopez J, Barros-Angueira F, Somoza-Martin M, et al. Immunohistochemical localization of C1 subunit of V-ATPase (ATPase C1) in oral squamous cell cancer and normal oral mucosa. *Biotech Histochem* 2012;87:133-9.
113. Perut F, Avnet S, Fotia C, Baglio SR, Salerno M, Hosogi S, et al. V-ATPase as an effective therapeutic target for sarcomas. *Exp Cell Res* 2013.
114. Michel V, Licon-Munoz Y, Trujillo K, Bisoffi M, Parra KJ. Inhibitors of vacuolar ATPase proton pumps inhibit human prostate cancer cell invasion and prostate-specific antigen expression and secretion. *Int J Cancer* 2013;132:E1-10.
115. Lange C, Prenninger S, Knuckles P, Taylor V, Levin M, Calegari F. The H(+) vacuolar ATPase maintains neural stem cells in the developing mouse cortex. *Stem Cells Dev* 2011;20:843-50.
116. Di Cristofori A, Ferrero S, Bertolini I, Gaudioso G, Russo MV, Berno V, et al. The vacuolar H⁺ ATPase is a novel therapeutic target for glioblastoma. *Oncotarget* 2015;6:17514-31.
117. McGuire C, Cotter K, Stransky L, Forgac M. Regulation of V-ATPase assembly and function of V-ATPases in tumor cell invasiveness. *Biochim Biophys Acta* 2016;1857:1213-8.
118. Kimura T, Nada S, Takegahara N, Okuno T, Nojima S, Kang S, et al. Polarization of M2 macrophages requires Lamtor1 that integrates cytokine and amino-acid signals. *Nat Commun* 2016;7:13130.
119. Costa GA, de Souza SB, da Silva Teixeira LR, Okorokov LA, Arnholdt ACV, Okorokova-Facanha AL, et al. Tumor cell cholesterol depletion and V-ATPase inhibition as an inhibitory mechanism to prevent cell migration and invasiveness in melanoma. *Biochim Biophys Acta* 2018;1862:684-91.

120. Schneider LS, von Schwarzenberg K, Lehr T, Ulrich M, Kubisch-Dohmen R, Liebl J, et al. Vacuolar-ATPase inhibition blocks iron metabolism to mediate therapeutic effects in breast cancer. *Cancer Res* 2015;75:2863-74.
121. Was H, Barszcz K, Czarnecka J, Kowalczyk A, Bernas T, Uzarowska E, et al. Bafilomycin A1 triggers proliferative potential of senescent cancer cells in vitro and in NOD/SCID mice. *Oncotarget* 2017;8:9303-22.
122. Wiedmann RM, von Schwarzenberg K, Palamidessi A, Schreiner L, Kubisch R, Liebl J, et al. The V-ATPase-inhibitor archazolid abrogates tumor metastasis via inhibition of endocytic activation of the rho-GTPase Rac1. *Cancer Res* 2012;72:5976-87.
123. Schempp CM, von Schwarzenberg K, Schreiner L, Kubisch R, Muller R, Wagner E, et al. V-ATPase inhibition regulates anoikis resistance and metastasis of cancer cells. *Mol Cancer Ther* 2014;13:926-37.
124. Spugnini EP, Sonveaux P, Stock C, Perez-Sayans M, De Milito A, Avnet S, et al. Proton channels and exchangers in cancer. *Biochim Biophys Acta* 2015;1848:2715-26.
125. De Milito A, Iessi E, Logozzi M, Lozupone F, Spada M, Marino ML, et al. Proton pump inhibitors induce apoptosis of human B-cell tumors through a caspase-independent mechanism involving reactive oxygen species. *Cancer Res* 2007;67:5408-17.
126. De Milito A, Canese R, Marino ML, Borghi M, Iero M, Villa A, et al. pH-dependent antitumor activity of proton pump inhibitors against human melanoma is mediated by inhibition of tumor acidity. *Int J Cancer* 2010;127:207-19.
127. Peppicelli S, Bianchini F, Toti A, Laurenzana A, Fibbi G, Calorini L. Extracellular acidity strengthens mesenchymal stem cells to promote melanoma progression. *Cell Cycle* 2015;14:3088-100.
128. Calcinotto A, Filipazzi P, Grioni M, Iero M, De Milito A, Ricupito A, et al. Modulation of microenvironment acidity reverses anergy in human and murine tumor-infiltrating T lymphocytes. *Cancer Res* 2012;72:2746-56.
129. Supuran CT. Carbonic anhydrase inhibition and the management of hypoxic tumors. *Metabolites* 2017;7:10.3390/metabo7030048.
130. Pastorek J, Pastorekova S. Hypoxia-induced carbonic anhydrase IX as a target for cancer therapy: From biology to clinical use. *Semin Cancer Biol* 2015;31:52-64.
131. Tafreshi NK, Lloyd MC, Proemsey JB, Bui MM, Kim J, Gillies RJ, et al. Evaluation of CAIX and CAXII expression in breast cancer at varied O₂

levels: CAIX is the superior surrogate imaging biomarker of tumor hypoxia. *Mol Imaging Biol* 2016;18:219-31.

132. Wykoff CC, Beasley NJ, Watson PH, Turner KJ, Pastorek J, Sibtain A, et al. Hypoxia-inducible expression of tumor-associated carbonic anhydrases. *Cancer Res* 2000;60:7075-83.

133. Ivanov S, Liao SY, Ivanova A, Danilkovitch-Miagkova A, Tarasova N, Weirich G, et al. Expression of hypoxia-inducible cell-surface transmembrane carbonic anhydrases in human cancer. *Am J Pathol* 2001;158:905-19.

134. Granja S, Tavares-Valente D, Queiros O, Baltazar F. Value of pH regulators in the diagnosis, prognosis and treatment of cancer. *Semin Cancer Biol* 2017;43:17-34.

135. Pinheiro C, Sousa B, Albergaria A, Paredes J, Dufloth R, Vieira D, et al. GLUT1 and CAIX expression profiles in breast cancer correlate with adverse prognostic factors and MCT1 overexpression. *Histol Histopathol* 2011;26:1279-86.

136. Ilie M, Mazure NM, Hofman V, Ammadi RE, Ortholan C, Bonnetaud C, et al. High levels of carbonic anhydrase IX in tumour tissue and plasma are biomarkers of poor prognostic in patients with non-small cell lung cancer. *Br J Cancer* 2010;102:1627-35.

137. Pinheiro C, Granja S, Longatto-Filho A, Faria AM, Fragoso MC, Lovisolo SM, et al. Metabolic reprogramming: A new relevant pathway in adult adrenocortical tumors. *Oncotarget* 2015;6:44403-21.

138. Choschzick M, Oosterwijk E, Muller V, Woelber L, Simon R, Moch H, et al. Overexpression of carbonic anhydrase IX (CAIX) is an independent unfavorable prognostic marker in endometrioid ovarian cancer. *Virchows Arch* 2011;459:193-200.

139. Huang WJ, Jeng YM, Lai HS, Fong IU, Sheu FY, Lai PL, et al. Expression of hypoxic marker carbonic anhydrase IX predicts poor prognosis in resectable hepatocellular carcinoma. *PLoS One* 2015;10:e0119181.

140. Hyuga S, Wada H, Eguchi H, Otsuru T, Iwagami Y, Yamada D, et al. Expression of carbonic anhydrase IX is associated with poor prognosis through regulation of the epithelial-mesenchymal transition in hepatocellular carcinoma. *Int J Oncol* 2017;51:1179-90.

141. Kang HJ, Kim IH, Sung CO, Shim JH, Yu E. Expression of carbonic anhydrase 9 is a novel prognostic marker in resectable hepatocellular carcinoma. *Virchows Arch* 2015;466:403-13.

142. van Kuijk SJ, Yaromina A, Houben R, Niemans R, Lambin P, Dubois LJ. Prognostic significance of carbonic anhydrase IX expression in cancer patients: A meta-analysis. *Front Oncol* 2016;6:69.
143. Watson PH, Chia SK, Wykoff CC, Han C, Leek RD, Sly WS, et al. Carbonic anhydrase XII is a marker of good prognosis in invasive breast carcinoma. *Br J Cancer* 2003;88:1065-70.
144. Yoo CW, Nam BH, Kim JY, Shin HJ, Lim H, Lee S, et al. Carbonic anhydrase XII expression is associated with histologic grade of cervical cancer and superior radiotherapy outcome. *Radiat Oncol* 2010;5:101,717X-5-101.
145. Ilie MI, Hofman V, Ortholan C, Ammadi RE, Bonnetaud C, Havet K, et al. Overexpression of carbonic anhydrase XII in tissues from resectable non-small cell lung cancers is a biomarker of good prognosis. *Int J Cancer* 2011;128:1614-23.
146. Kobayashi M, Matsumoto T, Ryuge S, Yanagita K, Nagashio R, Kawakami Y, et al. CAXII is a sero-diagnostic marker for lung cancer. *PLoS One* 2012;7:e33952.
147. Haapasalo J, Hilvo M, Nordfors K, Haapasalo H, Parkkila S, Hyrskyluoto A, et al. Identification of an alternatively spliced isoform of carbonic anhydrase XII in diffusely infiltrating astrocytic gliomas. *Neuro Oncol* 2008;10:131-8.
148. Ilie M, Hofman V, Zangari J, Chiche J, Mouroux J, Mazure NM, et al. Response of CAIX and CAXII to in vitro re-oxygenation and clinical significance of the combined expression in NSCLC patients. *Lung Cancer* 2013;82:16-23.
149. Swayampakula M, McDonald PC, Vallejo M, Coyaud E, Chafe SC, Westerback A, et al. The interactome of metabolic enzyme carbonic anhydrase IX reveals novel roles in tumor cell migration and invadopodia/MMP14-mediated invasion. *Oncogene* 2017;36:6244-61.
150. Kim BR, Shin HJ, Kim JY, Byun HJ, Lee JH, Sung YK, et al. Dickkopf-1 (DKK-1) interrupts FAK/PI3K/mTOR pathway by interaction of carbonic anhydrase IX (CA9) in tumorigenesis. *Cell Signal* 2012;24:1406-13.
151. Lock FE, McDonald PC, Lou Y, Serrano I, Chafe SC, Ostlund C, et al. Targeting carbonic anhydrase IX depletes breast cancer stem cells within the hypoxic niche. *Oncogene* 2013;32:5210-9.
152. Hsieh MJ, Chen KS, Chiou HL, Hsieh YS. Carbonic anhydrase XII promotes invasion and migration ability of MDA-MB-231 breast cancer cells through the p38 MAPK signaling pathway. *Eur J Cell Biol* 2010;89:598-606.

153. Gul HI, Yamali C, Sakagami H, Angeli A, Leitans J, Kazaks A, et al. New anticancer drug candidates sulfonamides as selective hCA IX or hCA XII inhibitors. *Bioorg Chem* 2018;77:411-9.
154. Lou Y, McDonald PC, Oloumi A, Chia S, Ostlund C, Ahmadi A, et al. Targeting tumor hypoxia: Suppression of breast tumor growth and metastasis by novel carbonic anhydrase IX inhibitors. *Cancer Res* 2011;71:3364-76.
155. Pacchiano F, Carta F, McDonald PC, Lou Y, Vullo D, Scozzafava A, et al. Ureido-substituted benzenesulfonamides potently inhibit carbonic anhydrase IX and show antimetastatic activity in a model of breast cancer metastasis. *J Med Chem* 2011;54:1896-902.
156. Gieling RG, Babur M, Mamnani L, Burrows N, Telfer BA, Carta F, et al. Antimetastatic effect of sulfamate carbonic anhydrase IX inhibitors in breast carcinoma xenografts. *J Med Chem* 2012;55:5591-600.
157. Touisni N, Maresca A, McDonald PC, Lou Y, Scozzafava A, Dedhar S, et al. Glycosyl coumarin carbonic anhydrase IX and XII inhibitors strongly attenuate the growth of primary breast tumors. *J Med Chem* 2011;54:8271-7.
158. Lounnas N, Rosilio C, Nebout M, Mary D, Griessinger E, Neffati Z, et al. Pharmacological inhibition of carbonic anhydrase XII interferes with cell proliferation and induces cell apoptosis in T-cell lymphomas. *Cancer Lett* 2013;333:76-88.
159. Battke C, Kremmer E, Mysliwietz J, Gondi G, Dumitru C, Brandau S, et al. Generation and characterization of the first inhibitory antibody targeting tumour-associated carbonic anhydrase XII. *Cancer Immunol Immunother* 2011;60:649-58.
160. Gondi G, Mysliwietz J, Hulikova A, Jen JP, Swietach P, Kremmer E, et al. Antitumor efficacy of a monoclonal antibody that inhibits the activity of cancer-associated carbonic anhydrase XII. *Cancer Res* 2013;73:6494-503.
161. Boyd NH, Walker K, Fried J, Hackney JR, McDonald PC, Benavides GA, et al. Addition of carbonic anhydrase 9 inhibitor SLC-0111 to temozolomide treatment delays glioblastoma growth in vivo. *JCI Insight* 2017;2:10.1172/jci.insight.92928.
162. McIntyre A, Patiar S, Wigfield S, Li JL, Ledaki I, Turley H, et al. Carbonic anhydrase IX promotes tumor growth and necrosis in vivo and inhibition enhances anti-VEGF therapy. *Clin Cancer Res* 2012;18:3100-11.
163. Dubois L, Peeters S, Lieuwes NG, Geusens N, Thiry A, Wigfield S, et al. Specific inhibition of carbonic anhydrase IX activity enhances the in vivo therapeutic effect of tumor irradiation. *Radiother Oncol* 2011;99:424-31.

164. Doyen J, Parks SK, Marcie S, Pouyssegur J, Chiche J. Knock-down of hypoxia-induced carbonic anhydrases IX and XII radiosensitizes tumor cells by increasing intracellular acidosis. *Front Oncol* 2013;2:199.
165. Muthuswamy R, Berk E, Junecko BF, Zeh HJ, Zureikat AH, Normolle D, et al. NF-kappaB hyperactivation in tumor tissues allows tumor-selective reprogramming of the chemokine microenvironment to enhance the recruitment of cytolytic T effector cells. *Cancer Res* 2012;72:3735-43.
166. Tian L, Tibshirani R. Adaptive index models for marker-based risk stratification. *Biostatistics* 2011;12:68-86.
167. Winum JY, Carta F, Ward C, Mullen P, Harrison D, Langdon SP, et al. Ureido-substituted sulfamates show potent carbonic anhydrase IX inhibitory and antiproliferative activities against breast cancer cell lines. *Bioorg Med Chem Lett* 2012;22:4681-5.
168. D'Ascenzio M, Bizzarri B, De Monte C, Carradori S, Bolasco A, Secci D, et al. Design, synthesis and biological characterization of thiazolidin-4-one derivatives as promising inhibitors of toxoplasma gondii. *Eur J Med Chem* 2014;86:17-30.
169. Lee BS, Krits I, Crane-Zelkovic MK, Gluck SL. A novel transcription factor regulates expression of the vacuolar H⁺-ATPase B2 subunit through AP-2 sites during monocytic differentiation. *J Biol Chem* 1997;272:174-81.
170. Moller-Levet CS, Betts GN, Harris AL, Homer JJ, West CM, Miller CJ. Exon array analysis of head and neck cancers identifies a hypoxia related splice variant of LAMA3 associated with a poor prognosis. *PLoS Comput Biol* 2009;5:e1000571.
171. Yamada S, Okumura N, Wei L, Fuchs BC, Fujii T, Sugimoto H, et al. Epithelial to mesenchymal transition is associated with shorter disease-free survival in hepatocellular carcinoma. *Ann Surg Oncol* 2014;21:3882-90.
172. Lai WK, Sun PJ, Zhang J, Jennings A, Lalor PF, Hubscher S, et al. Expression of DC-SIGN and DC-SIGNR on human sinusoidal endothelium: A role for capturing hepatitis C virus particles. *Am J Pathol* 2006;169:200-8.
173. Hu L, Lau SH, Tzang CH, Wen JM, Wang W, Xie D, et al. Association of vimentin overexpression and hepatocellular carcinoma metastasis. *Oncogene* 2004;23:298-302.
174. Yang MH, Chen CL, Chau GY, Chiou SH, Su CW, Chou TY, et al. Comprehensive analysis of the independent effect of twist and snail in promoting metastasis of hepatocellular carcinoma. *Hepatology* 2009;50:1464-74.

175. Yang XR, Xu Y, Yu B, Zhou J, Li JC, Qiu SJ, et al. CD24 is a novel predictor for poor prognosis of hepatocellular carcinoma after surgery. *Clin Cancer Res* 2009;15:5518-27.
176. Yang ZF, Ngai P, Ho DW, Yu WC, Ng MN, Lau CK, et al. Identification of local and circulating cancer stem cells in human liver cancer. *Hepatology* 2008;47:919-28.
177. Parkkila S, Parkkila AK, Saarnio J, Kivela J, Karttunen TJ, Kaunisto K, et al. Expression of the membrane-associated carbonic anhydrase isozyme XII in the human kidney and renal tumors. *J Histochem Cytochem* 2000;48:1601-8.
178. Oliveira-Ferrer L, Legler K, Milde-Langosch K. Role of protein glycosylation in cancer metastasis. *Semin Cancer Biol* 2017;44:141-52.
179. Venables JP. Aberrant and alternative splicing in cancer. *Cancer Res* 2004;64:7647-54.
180. Yamashita T, Ji J, Budhu A, Forgues M, Yang W, Wang HY, et al. EpCAM-positive hepatocellular carcinoma cells are tumor-initiating cells with stem/progenitor cell features. *Gastroenterology* 2009;136:1012-24.
181. Meijer TW, Bussink J, Zatovicova M, Span PN, Lok J, Supuran CT, et al. Tumor microenvironmental changes induced by the sulfamate carbonic anhydrase IX inhibitor S4 in a laryngeal tumor model. *PLoS One* 2014;9:e108068.
182. Niikura K. Vacuolar ATPase as a drug discovery target. *Drug News Perspect* 2006;19:139-44.
183. Taylor S, Spugnini EP, Assaraf YG, Azzarito T, Rauch C, Fais S. Microenvironment acidity as a major determinant of tumor chemoresistance: Proton pump inhibitors (PPIs) as a novel therapeutic approach. *Drug Resist Updat* 2015;23:69-78.
184. Ferrari S, Perut F, Fagioli F, Brach Del Prever A, Meazza C, Parafioriti A, et al. Proton pump inhibitor chemosensitization in human osteosarcoma: From the bench to the patients' bed. *J Transl Med* 2013;11:268,5876-11-268.
185. Camisaschi C, Vallacchi V, Vergani E, Tazzari M, Ferro S, Tuccitto A, et al. Targeting immune regulatory networks to counteract immune suppression in cancer. *Vaccines (Basel)* 2016;4:10.3390/vaccines4040038.
186. Chockley PJ, Keshamouni VG. Immunological consequences of epithelial-mesenchymal transition in tumor progression. *J Immunol* 2016;197:691-8.

187. Datar I, Schalper KA. Epithelial-mesenchymal transition and immune evasion during lung cancer progression: The chicken or the egg? *Clin Cancer Res* 2016;22:3422-4.
188. Cao Z, Fan-Minogue H, Bellovin DI, Yevtdiyenko A, Arzeno J, Yang Q, et al. MYC phosphorylation, activation, and tumorigenic potential in hepatocellular carcinoma are regulated by HMG-CoA reductase. *Cancer Res* 2011;71:2286-97.
189. Smith AP, Verrecchia A, Faga G, Doni M, Perna D, Martinato F, et al. A positive role for myc in TGFbeta-induced snail transcription and epithelial-to-mesenchymal transition. *Oncogene* 2009;28:422-30.
190. Brisseau GF, Dackiw AP, Cheung PY, Christie N, Rotstein OD. Posttranscriptional regulation of macrophage tissue factor expression by antioxidants. *Blood* 1995;85:1025-35.
191. Derks RA, Beaman KD. Regeneration and tolerance factor prevents bystander T-cell death associated with human immunodeficiency virus infection. *Clin Diagn Lab Immunol* 2004;11:835-40.
192. Utku N, Heinemann T, Tullius SG, Bulwin GC, Beinke S, Blumberg RS, et al. Prevention of acute allograft rejection by antibody targeting of TIRC7, a novel T cell membrane protein. *Immunity* 1998;9:509-18.
193. Bulwin GC, Heinemann T, Bugge V, Winter M, Lohan A, Schlawinsky M, et al. TIRC7 inhibits T cell proliferation by modulation of CTLA-4 expression. *J Immunol* 2006;177:6833-41.
194. Fan QM, Jing YY, Yu GF, Kou XR, Ye F, Gao L, et al. Tumor-associated macrophages promote cancer stem cell-like properties via transforming growth factor-beta1-induced epithelial-mesenchymal transition in hepatocellular carcinoma. *Cancer Lett* 2014;352:160-8.

List of abbreviations

5'-AMP	5'-adenosine monophosphate
AFP	Alpha-fetoprotein
Akt	RAC-alpha serine/threonine-protein kinase
Arg 1	Arginase 1
ATP	Adenosine triphosphate
BCL9	B-cell CLL/lymphoma 9 protein
BCLC	Barcelona Clinic Liver Cancer
BrdU	5-bromo-2'-deoxyuridine
CAFs	Cancer-associated fibroblasts
CAIX	Carbonic anhydrase nine
CAXII	Carbonic anhydrase twelve
CCL-2	C-C motif chemokine 2
CCL-20	C-C motif chemokine 20
CCL22	C-C motif chemokine 22
CCL-26	C-C motif chemokine 26
CCL-28	C-C motif chemokine 28
CCR10	C-C chemokine receptor type 10
CD13	Aminopeptidase N
CD133	Prominin 1
CD14	Monocyte differentiation antigen CD14
CD163	Scavenger receptor cysteine-rich type 1 protein M130
CD209	CD209 antigen
CD209/DC-SIGN	Dendritic Cell-Specific Intercellular adhesion molecule-3-Grabbing Non-integrin
CD24	Signal transducer CD24
CD3	T-cell surface glycoprotein CD3

CD34	Hematopoietic progenitor cell antigen CD34
CD39	Ectonucleoside triphosphate diphosphohydrolase 1
CD44	CD44 antigen, cell-surface glycoprotein
CD47	Leukocyte surface antigen CD47
CD68	Macrosialin
CD73	5'-nucleotidase
CD90	Thy-1 membrane glycoprotein
CDH1	Cadherin 1
CO ₂	Carbon dioxide
CoA	Acetyl-Coenzyme A
c-RAF	Proto-oncogene serine/threonine-protein kinase
CSCs	Cancer stem cells
CTLA-4	Cytotoxic T-lymphocyte protein 4
CX ₃ CR1	CX3C chemokine receptor 1
CXCR4	C-X-C chemokine receptor type 4
DAB/H ₂ O ₂	3,3'-diaminobenzidine/tetrahydrochloride
DAMPS	Damage-associated molecular patterns
DCs	Dendritic cells
DMSO	Dimethylsulfoxide
DNA	Deoxyribonucleic acid
ECM	Extracellular matrix
EDTA	Ethylenediaminetetraacetic acid
EMT	Epithelial-to-mesenchymal transition
ENTPD2	Ectonucleoside triphosphate diphosphohydrolase 2
EpCAM	Epithelial cell adhesion molecule
ER	Endoplasmic reticulum
FAK	Focal adhesion kinase 1

FDA	Food and drug administration
FFPE	Formalin-fixed, paraffin-embedded
FMO	Fluorescence minus one
Foxp3	Forkhead box transcription factor 3
G2	Grading 2
G3	Grading 3
G-CSF	Granulocyte colony-stimulating factor
GLUT1	Solute carrier family 2, facilitated glucose transporter member 1
gMDSC	Granulocytic myeloid-derived suppressor cells
GPCR	G-protein coupled receptors
GPCR	Non-G-protein coupled receptors
GSCs	Glioma stem cells
GSK-3 β	Glycogen synthase kinase-3 beta
H ⁺	Hydrogen ion/proton
H ⁺ /K ⁺ ATPase	Hydrogen/potassium ATP-ase
HBV	Hepatitis virus B
HCC	Hepatocellular carcinoma
HCO ₃ ⁻	Bicarbonate
HCV	Hepatitis virus C
HGDNs	High-grade dysplastic nodules
HIF-1 α	Hypoxia-inducible factor 1 α
HIF-2 α	Hypoxia-inducible factor 2 α
HIS	HCC Index Score
HMGB1	High mobility group protein B1
HRE	Hypoxia-response element
HSCs	Hepatic stellate cells
ICIs	Immune checkpoint inhibitors

IDH1	Isocitrate dehydrogenase [NADP] cytoplasmic
IDH2	Isocitrate dehydrogenase [NADP], mitochondrial
IDO	indoleamine-pyrrole 2,3-dioxygenase
IFN γ	Interferon gamma
IHC	Immunohistochemistry
IL-10	Interleukin-10
IL1 β	Interleukin-1 beta
IL-6	Interleukin-6
IL-8	Interleukin-8
iNos	nitric oxide synthase
IPA	Ingenuity Pathway Analysis
KRT19	Keratin, type I cytoskeletal 19
LDHA	Lactate dehydrogenase A
LDS	Lithium Dodecyl Sulfate
LGDNs	Low-grade dysplastic nodules
LOX	Lysyl oxidases
LPR6	Low-density lipoprotein receptor-related protein 6
MAPK	Mitogen-activated protein kinase
MCTs	Monocarboxylate transporters
MDM4	MDM4, P53 Regulator
MDSCs	Myeloid-derived suppressor cells
Mek	Mitogen-Activated Protein Kinase Kinase 1
mMDSC	Monocytic myeloid-derived suppressor cells
MMP-2	Metalloprotease 2
MMP-9	Metalloprotease 9
MMP-14	Metalloprotease 14
mTOR/mTORC1	Mechanistic Target Of Rapamycin Kinase

MTT	(3-(4,5)-dimethylthiazol-2-yl)-2,5-diphenyltetrazolium bromide
Myc	MYC Proto-Oncogene, BHLH Transcription Factor
Na ₃ VO ₄	Sodium orthovanadate
NaCl	Sodium chloride
NAFLD	Non-alcoholic fatty liver disease
NANOG	Homeobox protein NANOG
NASH	Non-alcoholic steatohepatitis
NF-κB	Nuclear Factor Of Kappa Light Polypeptide Gene Enhancer In B-Cells
NHE1	Na ⁺ /H ⁺ exchanger 1
NOTCH	Neurogenic locus notch homolog protein 1
NSCLC	Non-small cell lung cancer
O ₂	Oxygen
OCT4	POU Class 5 Homeobox 1
PDGF	Platelet-derived growth factor
PD-L1	Programmed cell death ligand 1
PG	Proteoglycan domain
PHDs	HIF prolyl hydroxylases
pHe	Extracellular pH
pHi	Intracellular pH
PI3K	Phosphatidylinositol 4,5-bisphosphate 3-kinase
PMSF	Phenylmethane sulfonyl fluoride or phenylmethylsulfonyl fluoride
pO ₂	Partial pressure of oxygen
PPIs	Proton pump inhibitors
PRR	Prorenin receptor
qRT-PCR	Quantitative real-time PCR
RAGE	Triggering of advanced glycation end product
RFS	Relapse-free survival

RIPK1-3	Receptor-interacting protein kinases1 and 3
RNA	Ribonucleic acid
RNS	Reactive nitrogen species
ROS	Reactive oxygen species
RT	Room temperature
S100	S100 Calcium Binding Protein
SECs	Sinusoidal endothelial cells
SNAIL1	Snail Family Transcriptional Repressor 1
SOX2	SRY (Sex Determining Region Y)-Box 2
STAT3	Signal Transducer And Activator Of Transcription 3
TACE	Transarterial chemoembolization
TAMs	Tumour-associated macrophages
TCA	Mitochondrial tricarboxylic acid
TERT	Telomerase Reverse Transcriptase
TGF- β 1	Transforming Growth Factor Beta 1
Th17 cells	T helper 17 cells
Th1 cells	T helper 1 cells
TICs	Tumour initiating cells
TIE2	Angiopoietin-1 receptor
TIMP-1	Metalloproteinase inhibitor 1
TME	Tumour microenvironment
TNF	Tumour necrosis factor α
TP53	Cellular tumor antigen p53
Tregs	T regulatory cells
TWIST	Twist Family BHLH Transcription Factor
V-ATPase	Vacuolar ATPase
VEGF-A	Vascular endothelial growth factor A

VEGF-C	Vascular endothelial growth factor C
VHL	Von Hippel-Lindau Tumor Suppressor
VIM	Vimentin
WGA	Wheat germ agglutinin
WNT	Wingless-Type MMTV Integration Site Family
β -catenin	Catenin (Cadherin-Associated Protein), Beta 1

List of figures

Figure 1.1.2. Schematic representation of oxidative phosphorylation, anaerobic glycolysis, and aerobic glycolysis (Warburg effect) in differentiated tissue, proliferating tissue and tumour	6
Figure 1.1.3. Signaling pathways and oncogenes involved in the metabolic reprogramming of cancer cells	8
Figure 1.1.4 Model of hypoxia, cancer metabolism and acidity in tumour cells	10
Figure 1.1.5. Tumour hypoxia and acidic tumour microenvironment can influence tumour aggressiveness and immunosuppression	12
Figure 1.2.2. HCC development in the setting of a chronic inflammation	21
Figure 1.2.5. The main players in the development of HCC	28
Figure 1.3. Hypoxic and acidic cancer cells express pH regulators	31
Figure 1.3.1.1. Graphic representation of structure and mechanism of the V-ATPase complex	32
Figure 1.3.1.2. The role of V-ATPase inhibition in cancer	35
Figure 1.3.2. Anti-cancer effect of CAIX and CAXII inhibition	39
Figure 2.1.7.1 Expression of CD209 in positive myeloid cells	56
Figure 2.1.8. Generation of the HCC Index Score (HIS)	59
Figure 3.1.1 Schematic representation of <i>CA12</i> transcript variants	74
Figure 3.1.2. Gene expression of pH regulatory molecules in liver tissues	77
Figure 3.1.3. Expression of pH regulatory molecules in relationship to tumour differentiation	78
Figure 3.2.1. Gene expression of EMT-related genes in liver tissues	79
Figure 3.2.2. Gene expression of CSC-related genes in liver tissues	80
Figure 3.2.3. Gene expression of inflammatory/immunosuppressive-related genes in liver tissues	81
Figure 3.3. Analysis of correlation between genes related to hypoxia and pH regulatory molecules, epithelial-to mesenchymal transition and	84

HCC aggressiveness and inflammation/immunosuppression

Figure 3.4. Prognostic significance of <i>CA12 1</i> , <i>CA12 2/3</i> , <i>CDH1</i> and <i>CD209</i> expression in the HCC training cohort	88
Figure 4.1.1. Expression and cellular distribution of CAIX and CAXII in liver tissues	97
Figure 4.1.2. Cell surface expression of CAXII in <i>in situ</i> breast cancer tissues	99
Figure 4.1.3. Cellular distribution of CAXII in tissues obtained from HCC and breast cancer patients	100
Figure 4.1.4. Cellular localization of CAXII in HCC and <i>in situ</i> breast tissues	101
Figure 4.2.1. Expression pattern of V-ATPase subunits in liver tissues	102
Figure 4.2.2. Expression of V-ATPase subunit H in malignant hepatocytes of HCC	104
Figure 5.1.1 Gene expression of <i>CA9</i> in HCC cell lines	110
Figure 5.1.2 Gene expression of <i>CA12</i> isoforms in HCC cell lines	111
Figure 5.1.3 Protein expression of carbonic anhydrases (CAs) in HCC cell lines	112
Figure 5.1.4 Cellular distribution of CAXII in HCC cell lines	114
Figure 5.2.1 Protein expression of V-ATPase subunits in the HCC cell lines	115
Figure 5.3.1. The effect of S4 (CAIX inhibitor) treatment on HCC cell viability	117
Figure 5.3.2 CAIX expression in the T-47D cells and cell growth inhibition by CAXII specific compounds	118
Figure 5.3.3 The effect of compound 25 (CAXII inhibitor) treatment on HCC cell viability	119
Figure 5.3.4 Treatment of HCC cell lines with omeprazole	119
Figure 5.4.1 The impact of pH regulatory inhibitors on the proliferation of HCC cell lines	121
Figure 5.4.2 Necrosis detection in HCC cell lines	123

Figure 5.4.3 Apoptosis measurement in HCC cell lines	125
Figure 6.1.1. Expression of V-ATPase in immune cells infiltrating HCC tissues	132
Figure 6.1.2. Expression of V-ATPase in M2-like macrophages infiltrating HCC tissues	132
Figure 6.1.3. Expression of V-ATPase a1 in immune cells infiltrating HCC tissues	134
Figure 6.2.1. Omeprazole affects the expression of genes conferring EMT and suppressive features at HCC TME	136
Figure 6.2.2. Modulation of the cytokine profile in M2-like macrophages by omeprazole treatment	137
Figure 6.2.3. Modulation of the cytokine profile in CD3 ⁺ T cells by omeprazole treatment	138
Figure 7. The schematic representation of the discussion and conclusions of this thesis	148

List of tables

Table 2.1.4. Panel of TaqMan [®] gene expression assays	46
Table 2.1.5. Antibodies used for immunohistochemistry (IHC) analysis	51
Table 2.1.6. Antibodies used for immunofluorescence (IF) analysis	54
Table 2.1.7. List of antibodies used for multiparametric flow cytometry	57
Table 2.2.5. Chemical details of selective CAIX and CAXII inhibitors	64
Table 3.1.1. The clinicopathological characteristics of HCC patients	70
Table 3.1.2. Univariate analysis of clinicopathological parameters associated with recurrence of 57 HCC patients	71
Table 3.4.1 Univariate analysis of genes associated with recurrence of 57 HCC patients	86
Table 3.4.2. Statistical analysis of HCC Index score (HIS) and clinicopathological parameters for recurrence of 57 HCC patients	89
Table 3.4.3. The clinicopathological characteristics of HCC patients included in the validation cohort	90
Table 4.1.1. Score categories for the expression of CAs in clinical HCC tissues (n=23) analysed by immunohistochemistry	98
Table 4.2.1. Score categories for the expression of V-ATPase in clinical HCC tissues (n=23) analysed by immunohistochemistry	103

Publications

Part of data contained in this thesis have been published in:

Kuchuk O[‡], **Tuccitto A**[‡], Citterio D[‡], Huber V, Camisaschi C, Milione M, Vergani B, Villa A, Alison MR, Carradori S, Supuran CT, Rivoltini L, Castelli C[&] and Mazzaferro V[&]. pH regulators to target the tumor immune microenvironment in human hepatocellular carcinoma. *Oncolmunology* 2018. <https://doi.org/10.1080/2162402X.2018.1445452>.

^{‡, &}These authors contributed equally to this work.

Publications related to the field of my PhD project:

1. Ponziani FR, Bhoori S, Castelli C, Putignani L, Rivoltini L, Del Chierico F, Sanguinetti M, Morelli D, Paroni Sterbini F, Petito V, Reddel S, Calvani R, Camisaschi C, Picca A, **Tuccitto A**, Gasbarrini A, Pompili M, Mazzaferro V. Hepatocellular Carcinoma is Associated with Gut Microbiota Profile and Inflammation in Non-Alcoholic Fatty Liver Disease. *Hepatology* 2018.

2. Huber V, Camisaschi C, Berzi A, Ferro S, Lugini L, Triulzi T, **Tuccitto A**, Tagliabue E, Castelli C, Rivoltini L: Cancer acidity: An ultimate frontier of tumor immune escape and a novel target of immunomodulation. *Semin Cancer Biol* 2017, 43:74-89.

3. Camisaschi C, Vallacchi V, Vergani E, Tazzari M, Ferro S, **Tuccitto A**, Kuchuk O, Shahaj E, Sulsenti R, Castelli C, Rodolfo M, Rivoltini L, Huber V: Targeting Immune Regulatory Networks to Counteract Immune Suppression in Cancer. *Vaccines (Basel)* 2016, 4:10.3390/vaccines4040038.

4. **Tuccitto A**, Tazzari M, Beretta V, Rini F, Miranda C, Greco A, Santinami M, Patuzzo R, Vergani B, Villa A, Manenti G, Cleris L, Giardiello D, Alison M, Rivoltini L, Castelli C, Perego M: Immunomodulatory Factors Control the Fate of Melanoma Tumor Initiating Cells. *Stem Cells* 2016, 34:2449-2460.

Acknowledgements

I would like to express my sincere gratitude to my Director of Studies Dr. Chiara Castelli for the continuous support of my PhD study, for feeding my curiosity on science, for her patience, motivation and immense knowledge.

Her guidance helped me in all the time of research and writing of this thesis. I am also grateful to my External Supervisor Dr. Malcolm Ronald Alison for his supervision and support during my PhD period.

My sincere thank also goes to Dr. Licia Rivoltini, who gave me the access to her laboratory and research facilities. I thank all the members of the Unit of Immunotherapy of Human Tumours, past and present, each of which has taught me anything. Expecially, Marcella who passed me her passion for science. Elisabetta, Viviana and Eriomina for their patience and daily support. Francesca, Valeria and Barbara for giving me their technical help.

I thank also Prof. Mazzaferro and Dr. Davide Citterio for providing me the clinical samples and helping me to understand the complexity of hepatocellular carcinoma. Dr. Luigi Mariani and Luca Lalli for their support in statistical analysis.

I would also express my gratitude to all the patients enrolled in my study, to Associazione Italiana per la Ricerca sul Cancro (AIRC) and to Ministry of Health for funding my studies.

I am very grateful to my husband Alberto, my father, my mother, my sister and my grandparents for always believing in me and in my work.

*“Science is not only a disciple of reason but, also, one of romance and passion” -**Stephen Hawking**-*

Appendix

Original publication: pH regulators to target the tumor immune microenvironment in human hepatocellular carcinoma. Kuchuk O *et al.*

OncolImmunology 2018, <https://doi.org/10.1080/2162402X.2018.1445452>

pH regulators to target the tumor immune microenvironment in human hepatocellular carcinoma

Olga Kuchuk, Alessandra Tuccitto, Davide Citterio, Veronica Huber, Chiara Camisaschi, Massimo Milione, Barbara Vergani, Antonello Villa, Malcolm Ronald Alison, Simone Carradori, Claudiu T Supuran, Licia Rivoltini, Chiara Castelli & Vincenzo Mazzaferro

To cite this article: Olga Kuchuk, Alessandra Tuccitto, Davide Citterio, Veronica Huber, Chiara Camisaschi, Massimo Milione, Barbara Vergani, Antonello Villa, Malcolm Ronald Alison, Simone Carradori, Claudiu T Supuran, Licia Rivoltini, Chiara Castelli & Vincenzo Mazzaferro (2018): pH regulators to target the tumor immune microenvironment in human hepatocellular carcinoma, *Oncoimmunology*, DOI: [10.1080/2162402X.2018.1445452](https://doi.org/10.1080/2162402X.2018.1445452)

To link to this article: <https://doi.org/10.1080/2162402X.2018.1445452>



© 2018 The Author(s). Published with license by Taylor & Francis Group, LLC
Olga Kuchuk, Alessandra Tuccitto, Davide Citterio, Veronica Huber, Chiara Camisaschi, Massimo Milione, Barbara Vergani, Antonello Villa, Malcolm Ronald Alison, Simone Carradori, Claudiu T Supuran, Licia Rivoltini, Chiara Castelli, and Vincenzo Mazzaferro



[View supplementary material](#)



Accepted author version posted online: 01 Mar 2018.
Published online: 26 Mar 2018.



[Submit your article to this journal](#)



Article views: 149



[View related articles](#)



[View Crossmark data](#)

pH regulators to target the tumor immune microenvironment in human hepatocellular carcinoma

Olga Kuchuk ^{a,b,†††}, Alessandra Tuccitto^{a,b,††}, Davide Citterio^{c,††}, Veronica Huber^{a,b}, Chiara Camisaschi^{a,b}, Massimo Milione^d, Barbara Vergani^e, Antonello Villa^e, Malcolm Ronald Alison^f, Simone Carradori ^g, Claudiu T Supuran ^h, Licia Rivoltini^{a,b}, Chiara Castelli^{a,b,†††}, and Vincenzo Mazzaferro^{c,i,†††}

^aUnit of Immunotherapy of Human Tumors, Fondazione IRCCS Istituto Nazionale dei Tumori, Milan, Italy; ^bDepartment of Experimental Oncology and Molecular Medicine, Fondazione IRCCS Istituto Nazionale dei Tumori, Milan, Italy; ^cHepatology and Liver Transplantation Unit, Department of Surgery, Fondazione IRCCS Istituto Nazionale dei Tumori, Milan, Italy; ^dAnatomic Pathology, Department of Pathology and Laboratory Medicine, Fondazione IRCCS Istituto Nazionale dei Tumori, Milan, Italy; ^eConsorzio MIA (Microscopy and Image Analysis), University of Milano-Bicocca, Milan, Italy; ^fCentre for Tumour Biology, Barts Cancer Institute, Charterhouse Square, London, EC1M 6BQ, United Kingdom; ^gDepartment of Pharmacy, "G. D'Annunzio" University of Chieti-Pescara, Chieti, Italy; ^hPolo Scientifico, Department of Pharmaceutical Sciences, Sesto Fiorentino, Firenze, Italy; ⁱUniversity of Milan, Italy

ABSTRACT

Interfering with tumor metabolism is an emerging strategy for treating cancers that are resistant to standard therapies. Featuring a rapid proliferation rate and exacerbated glycolysis, hepatocellular carcinoma (HCC) creates a highly hypoxic microenvironment with excessive production of lactic and carbonic acids. These metabolic conditions promote disease aggressiveness and cancer-related immunosuppression. The pH regulatory molecules work as a bridge between tumor cells and their surrounding milieu. Herein, we show that the pH regulatory molecules CAIX, CAXII and V-ATPase are overexpressed in the HCC microenvironment and that interfering with their pathways exerts antitumor activity. Importantly, the V-ATPase complex was expressed by M2-like tumor-associated macrophages. Blocking *ex vivo* V-ATPase activity established a less immune-suppressive tumor microenvironment and reversed the mesenchymal features of HCC. Thus, targeting the unique cross-talk between tumor cells and the tumor microenvironment played by pH regulatory molecules holds promise as a strategy to control HCC progression and to reduce the immunosuppressive pressure mediated by the hypoxic/acidic metabolism, particularly considering the potential combination of this strategy with emerging immune checkpoint-based immunotherapies.

ARTICLE HISTORY

Received 1 August 2017
Revised 16 February 2018
Accepted 20 February 2018

KEYWORDS



hepatocellular carcinoma; pH regulatory molecules; therapy; tumor microenvironment; immunosuppressive cells

Introduction

Hepatocellular carcinoma (HCC) is the second leading cause of cancer death worldwide.¹ Surgical resection and ablation, depending on tumor burden and intra-hepatic location, are the sole curative, non-transplant treatments; nevertheless, relapse occurs in approximately 70% of patients within five years,² with a dismal prognosis when eligibility criteria for salvage transplantation are not met.³ Promising results are emerging with immunotherapy based on immune checkpoint inhibition,⁴ but tumor-intrinsic and -extrinsic resistance points in metabolic and immunosuppressive pathways are the major obstacles to effective immune-mediated cancer control.⁵

HCC is a highly hypoxic tumor due to its rapid growth rate and the surrounding fibrotic tissue produced by chronic inflammation.⁶ In cancer cells, hypoxia is associated with


metabolic reprogramming based on anaerobic glycolysis, leading to the overproduction of pyruvate, lactate and carbonic acids.⁷ A hypoxic/acidic microenvironment is the hallmark of invasive tumors,^{8,9} the aggressiveness of which is also driven by the ability to escape adaptive immune surveillance and contribute to local inflammation.¹⁰⁻¹³ To cope with hypoxic stress and acidity, tumor cells overexpress different pH regulators, including carbonic anhydrase (CA) IX and XII.¹⁴ CAs are zinc metalloenzymes that catalyze the reversible hydration of carbon dioxide to carbonic acid and are involved in respiration and acid-base equilibrium.¹⁴ V-ATPase is also a key protein in the regulation of the tumor acidic microenvironment and is one of the most studied pH regulators in cancer.¹⁵ V-ATPase consists of multiple subunits assembled in two domains: the membrane-associated domain V0 transports protons across the

CONTACT Licia Rivoltini  Licia.Rivoltini@istitutotumori.mi.it  Unit of Immunotherapy of Human Tumors, Fondazione IRCCS Istituto Nazionale dei Tumori, Via G. Venezian 1, Milan, 20133, Italy.

[†]Present address: Tisch Cancer Institute, Department of Medicine, Icahn School of Medicine at Mount Sinai, Madison Avenue 1425, 11 F-70, Box 1123, New York, New York 10029, USA

^{††}These authors contributed equally to this work.

^{†††}These authors contributed equally to this work.

 Supplemental data for this article can be accessed on the [publisher's website](#).

© 2018 Olga Kuchuk, Alessandra Tuccitto, Davide Citterio, Veronica Huber, Chiara Camisaschi, Massimo Milione, Barbara Vergani, Antonello Villa, Malcolm Ronald Alison, Simone Carradori, Claudiu T Supuran, Licia Rivoltini, Chiara Castelli, and Vincenzo Mazzaferro. Published with license by Taylor & Francis Group, LLC

This is an Open Access article distributed under the terms of the Creative Commons Attribution-NonCommercial-NoDerivatives License (<http://creativecommons.org/licenses/by-nc-nd/4.0/>), which permits non-commercial re-use, distribution, and reproduction in any medium, provided the original work is properly cited, and is not altered, transformed, or built upon in any way.

membrane, while the cytoplasmic domain V1 hydrolyses ATP.¹⁶ Each V-ATPase subunit displays several splice variants, conferring specific intracellular localization and tissue specificity.¹⁷

The main function of pH regulators is to counteract the intracellular accumulation of protons caused by tumor energy metabolic dysfunction, expelling protons into the extracellular milieu, leading in turn to its acidification.¹⁴ Additionally, CAs and V-ATPase are crucial components of signal transduction cascades associated with neoplastic transformation.¹⁸ Because of their pivotal role in tumor survival, pH regulators are receiving attention as promising therapeutic targets, and pharmacological strategies to disrupt their function have recently been developed and tested in early clinical trials.¹⁹

In the present study, we investigated the expression and role of pH regulators in the tumor microenvironment of HCC patients, focusing on CAIX, CAXII and V-ATPase because of the availability of specific inhibitors with potential clinical use. Interestingly, we found that interfering with these pathways may represent a pleiotropic strategy to influence tumor survival, aggressiveness and the immunological properties of HCC.

Results

pH regulatory molecules are expressed in HCC

Matched tumor (T) and adjacent non-tumor (NT) snap-frozen tissues from patients with HCC undergoing curative resection (n = 57, see Table 1 for the pathological features of these tumors) were profiled for the expression of CA9 and CA12, encoding for CAIX and CAXII proteins respectively, and *ATP6V0A1*, *ATP6V1A*, *ATP6VIC1* and *ATP6V1H* encoding for

the $\alpha 1$, A1, C1 and H subunits of the V-ATPase. These subunits were chosen for analysis because $\alpha 1$ contains the binding site for proton pump inhibitors (PPIs), while A1, C1 and H encompass the V1 domain involved in the regulation and stator of the whole encoded complex.¹⁶ The level of *HIF1A* mRNA was also assessed. Given that HCC arises from chronically inflamed liver tissue, samples from normal liver obtained from patients undergoing an operation unrelated to cancer (cholecystectomy) (n = 9) were included as a control group. In line with the literature data,²⁰ qRT-PCR analysis showed that in comparison with normal liver, both NT and T tissues displayed increased transcription of the *HIF1A* gene. NT and T tissues also displayed an increase in the expression of CA9 mRNA (Fig. 1A). CA9 and *HIF1A* expression was positively correlated both in NT and T tissues, thus highlighting the dependence of CA9 on hypoxia also in the HCC setting²¹ (Supplementary Fig. S1). NT tissues displayed higher CA9 mRNA levels, likely due to their enrichment in bile ducts with cholangiocytes positive for CAIX.²² Conversely, CA12 was strongly positive in T samples, while it was barely detectable in normal liver and NT tissues (Fig. 1A). Concerning the V-ATPase complex, all the subunits exhibited enhanced expression in T compared with NT or normal liver, with the differences reaching statistical significance for the *ATP6V1A*, *ATP6VIC1* and *ATP6V1H* genes (Fig. 1A).

In the tumor tissues, the expression of *ATP6V0A1*, *ATP6VIC1* and *ATP6V1H* genes was positively associated, in agreement with the notion that they encode for ATPase subunits essential in the functional activity of the V-ATPase molecular complex.¹⁶ No other significant correlation was found, suggesting that the CA and ATPase molecules are likely to exert non-redundant functions in HCC (Supplementary Fig. S1). Moreover, in our series, CA9 and CA12 gene expression was associated with tumor grading, thus indicating their possible role in tumor malignancy (Fig. 1B).

Selective expression of CAIX and CAXII in HCC tumor cells

The distribution of pH regulatory molecules in the HCC microenvironment was assessed by IHC analysis performed on a set of formalin-fixed, paraffin-embedded (FFPE) pairs of T, NT and peri-tumor (PT) samples (n = 23). PT corresponds to FFPE HCC sections, which include areas enriched in immune infiltrating cells adjacent to tumor nodules.

In normal liver and NT tissues, the presence of CAIX was limited to the plasma membrane of cholangiocytes, while normal hepatocytes were completely negative for the protein (Fig. 2A). In contrast, approximately 50% of the T samples exhibited scattered foci of HCC cells that were strongly positive for CAIX at the plasma membrane level; these cells were evenly distributed within discrete tumor nests (Fig. 2A and Table 2). Conversely, CAXII was abundantly and homogeneously expressed in most tumor cells, but was largely undetectable in NT tissue and normal liver. This expression pattern was shared by all the analyzed samples (Fig. 2A and Table 2). In contrast to reports using other tumor histotypes,²³ in the present study, CAXII was mainly confined to the cytoplasm of HCC cells. We confirmed the paucity of CAXII expression at the plasma membrane by immunofluorescence staining and confocal analysis of tumor tissue samples, revealing no

Table 1. The clinicopathological characteristics of HCC patients.

Clinical variable	N°	%
Age, mean \pm SD, years	72.0 \pm 9.9	
<50	2	3.5
\geq 50	55	96.5
Sex		
Male	44	77.2
Female	13	23.6
Etiology		
HBV	13	22.8
HCV	19	33.3
Others (NASH, potus, hemochromatosis)	16	28.1
healthy liver	9	15.8
Tumor number		
Single	49	86.0
Multiple	8	14.0
Tumor size, cm		
<3	20	35.1
3–5	17	29.8
\geq 5	20	35.1
Microvascular invasion		
Yes	35	61.4
no	22	38.6
Grading		
G1	3	5.3
G2	40	70.2
G3	14	24.6

Clinical and pathological features of 57 paired tumor and adjacent non-tumor liver tissues collected from patients with HCC who underwent curative resection from 2011 to 2015 at the Gastrointestinal Surgery and Liver Transplantation Unit of our institute.

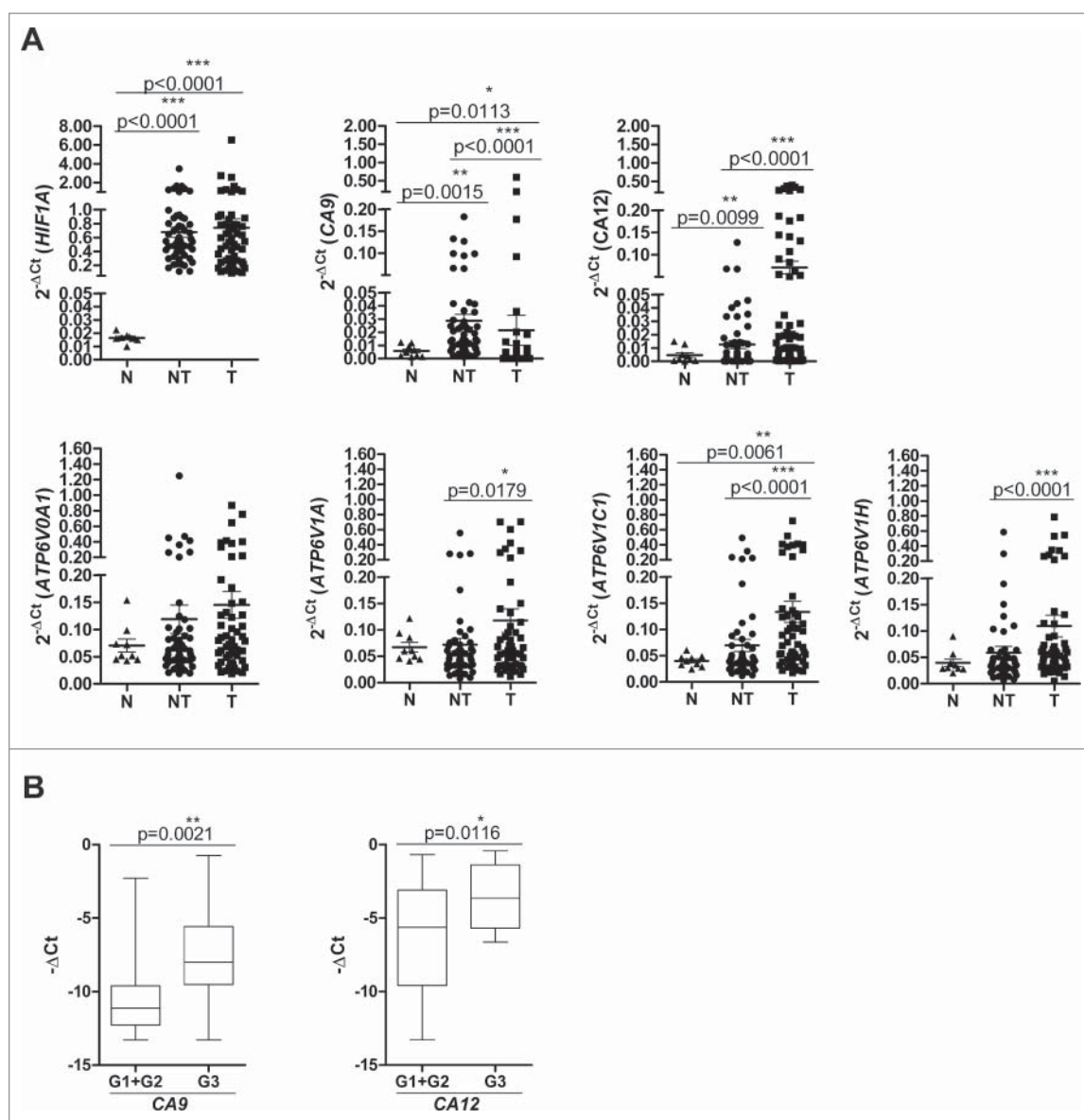


Figure 1. Gene expression of pH regulatory molecules in liver tissues. (A) mRNA expression levels of *HIF1A*, *CA9*, *CA12*, *ATP6V0A1*, *ATP6V1A*, *ATP6V1C1* and *ATP6V1H*. The expression of the indicated genes was evaluated in 9 normal (N) and 57 paired samples of adjacent non-tumor (NT) and tumor (T) liver tissues (see Materials and Methods for the statistical analyses used). The data are reported as $2^{-\Delta Ct}$ values ($\Delta Ct = Ct_{\text{target gene}} - Ct_{\text{GAPDH}}$). (B) High expression of *CA9* and *CA12* was associated with poorly differentiated HCC (G3). Gene expression data of 57 tumor tissues analyzed were reported as $-\Delta Ct$ values. The reported p-values were calculated by the unpaired t test.

detectable co-localization between CAXII and cell surface-expressed β -catenin. Interestingly, the majority of CAXII co-localized with calnexin, indicating that the protein was likely retained in the endoplasmic reticulum (ER) (Fig. 2B). This pattern of expression was specific to HCC since breast carcinoma cells displayed conventional CAXII membranous expression and β -catenin co-localization (Supplementary Fig. S2 A and S2B). For both CAIX and CAXII, no positivity was detected in the inflammatory cells infiltrating the PT areas (Fig. 2A).

Modulation of CA expression and distribution by hypoxia

HCC cell lines, representative of HCC subtypes,^{24,25} were profiled for the expression of CAs and were subsequently tested for their sensitivity to selective inhibitors. As detected by western blotting, we observed that the PLC/PRF/5 and C3A cell lines

expressed CAIX under normoxia ($N = 21\% O_2$), which was significantly up-regulated upon exposure to hypoxia ($H = 1\% O_2$) for 72 h. In contrast, SNU-449 cells did not express CAIX irrespective of the culture conditions (Fig. 3A).

CAXII was expressed by all HCC cell lines but only up-regulated under hypoxia in the PLC/PRF/5 cell line (Fig. 3A and Supplementary Fig. S3). Flow cytometric analysis confirmed the membrane-bound expression of CAIX in C3A and PLC/PRF/5 cells cultured under normoxia (approximately 35% positive cells), which was markedly enhanced by 72 h of hypoxia, while the SNU-449 cell line was completely negative, consistent with the qRT-PCR data (Fig. 3B). Conversely, all HCC cell lines grown under either 21% or 1% O_2 expressed very low levels of CAXII at the cell surface (Fig. 3C), in agreement with the expression patterns observed in HCC samples. To further explore the cellular distribution of CAXII, immunofluorescence staining of HCC cell

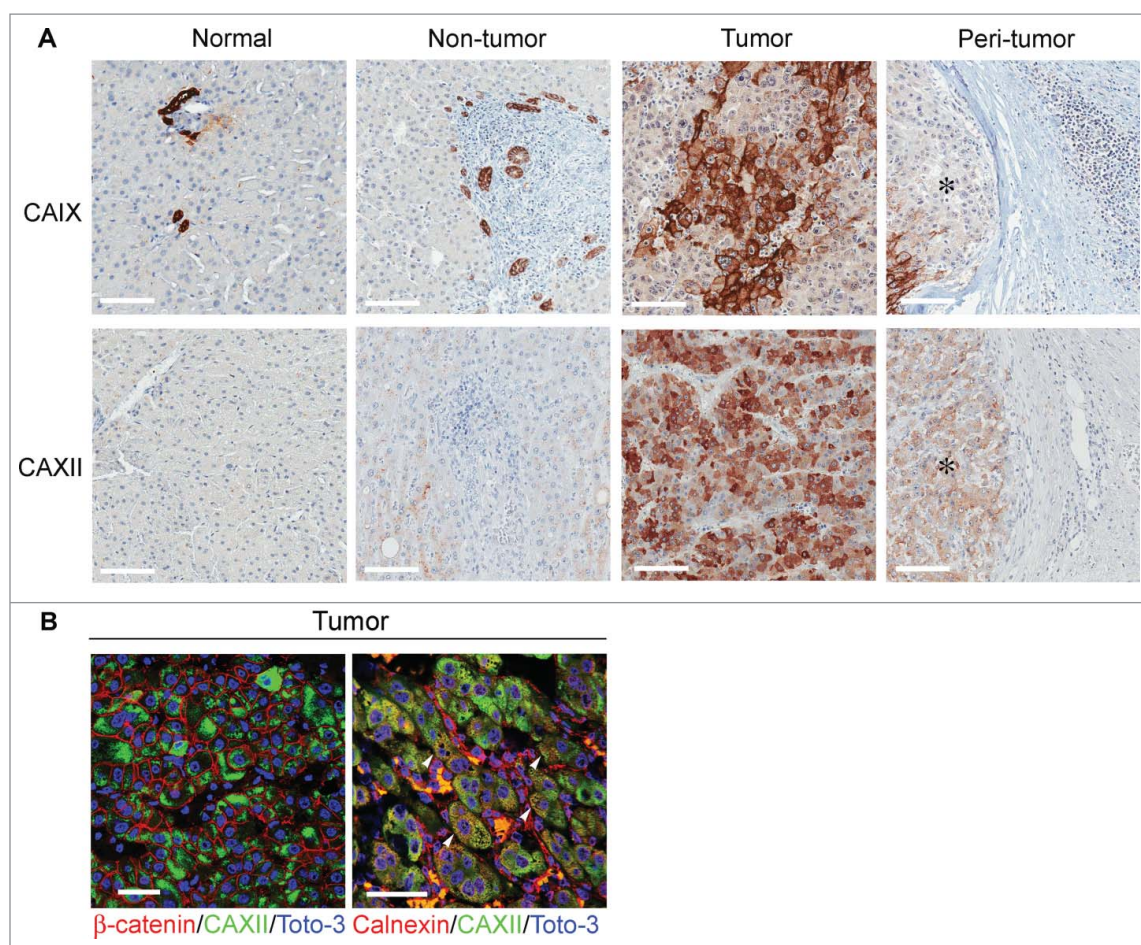


Figure 2. Expression and cellular distribution of CAIX and CAXII in liver tissues. (A) Representative images of immunohistochemical staining for CAIX and CAXII in normal and matched non-tumor, tumor and peri-tumor liver tissues. Peri-tumor tissue was identified as areas adjacent to tumor nodules enriched in immune infiltrating cells. Membranous staining of CAIX was detectable in bile ductular cells in normal and non-tumor tissues and in malignant hepatocytes. CAXII was expressed in the cytoplasm of malignant hepatocytes. No positive staining was evident in the inflammatory cells infiltrating the peri-tumor areas. *Identifies tumor area in peri-tumor sections. Representative images with scale bars = 100 μm . (B) Confocal laser scanning micrographs of immunofluorescent staining with anti-CAXII (green), anti- β -catenin (red) and anti-calnexin (red) in formalin-fixed, paraffin-embedded HCC tissues. Nuclei were stained with Toto-3 (blue). In the left panel, CAXII displays cytoplasmic expression without any co-localization with the membranous staining of β -catenin (red). In the right panel, the white triangle indicates the co-localization of CAXII and calnexin. Scale bars = 50 μm .

lines was performed for CAXII (green) in combination with wheat germ agglutinin (WGA, red) and an anti-calnexin monoclonal antibody (blue) to mark the plasma membrane and ER respectively. Confocal analysis confirmed that CAXII was mainly localized in the cytoplasm when the cells were grown under normoxia, while the protein was largely retained in the ER after 72 h of hypoxia exposure, indicated by the co-staining with calnexin defined by the appearance of an azure color (Fig. 3D). Hence, HCC cell lines reacted to hypoxia in a similar fashion to the *in vivo* setting, i.e., with hypoxia causing intracellular retention of CAXII, primarily localized in the ER.

Sensitivity of HCC to CA inhibitors and the consequences of sub-cellular target localization

To investigate whether pH regulators may serve as effective therapeutic targets in HCC, the effect of CA blockade on HCC cell lines was investigated by inhibiting CAIX with the specific inhibitor S4, known to exert antitumor activity in breast cancer models.^{26,27} CAXII was blocked using the inhibitor compound 25, a molecule belonging to a new series of N-substituted saccharin derivatives, displaying a K_i of 0.25 μM for human

CAXII while being largely inactive against other human carbonic anhydrase isoforms, including CAIX ($K_i > 50 \mu\text{M}$)²⁸ (Supplementary Table S1). Among the saccharin-based derivatives, compound 25 was selected for its *in vitro* activity in blocking the growth of the breast cancer cell line T-47D, a cell displaying membrane positivity for CAXII in the absence of CAIX expression (Supplementary Fig. S4 A and B).

The CAIX-positive HCC cell lines C3A and PLC/PRF/5 had a low sensitivity to S4 under normoxia ($\text{IC}_{50} > 100 \mu\text{M}$), but they exhibited rapidly decreased cell viability under 1% O_2 (down to 30% for C3A and 20% for PLC/PRF/5, with IC_{50} values of 57.4 and 53.9 respectively) (Fig. 3E). The lack of any antitumor effect of S4 on SNU-449 cells ($\text{IC}_{50} > 100 \mu\text{M}$), which were negative for CAIX under both normoxic and hypoxic conditions, confirmed the specificity of the drug (Fig. 3E).

The CAXII inhibitor compound 25 was tested on the three HCC cell lines, all of which expressed CAXII. As depicted in Fig. 3F, the drug affected the viability of HCC cells under normoxic conditions, with an IC_{50} of 198.5 and 142.9 μM in the C3A and PLC/PRF/5 cell lines, respectively, while the SNU-449 cells appeared rather resistant to the drug ($\text{IC}_{50} > 200 \mu\text{M}$). Unexpectedly, all the HCC cell lines showed a significantly

Table 2. Score categories for the expression of pH regulatory molecules and CD163 in clinical HCC tissues (n = 23) analyzed by immunohistochemistry.

Markers	Intensity of staining	Extent of stained cells			
		0	1	2	3
CAIX [#]	0	10 ^a	0	0	0
	2	0	3	0	10
CAXII [#]	2	0	0	0	23
a1 [#]	0	3	0	0	0
	1	0	5	1	0
	2	0	2	6	6
C1 [#]	0	2	0	0	0
	1	0	4	3	0
	2	0	1	10	3
a1 [*]	0	7	0	0	0
	1	6	7	1	0
	2	0	2	0	0
H [*]	0	3	0	0	0
	1	8	7	0	0
	2	0	3	2	0
CD163 [*]	2	2	5	8	8

Abbreviations: HCC, hepatocellular carcinoma.

Note: ^a, number of cases in each category; the expression of these markers was evaluated: [#] in tumor hepatocytes and ^{*} in immune infiltrating cells in peri-tumor areas. Every tumor was given a score category according to the intensity of the membrane/cytoplasmic staining (0 = negative; 1 = lower than the internal or experimental control; 2 = equal to the internal or experimental control) and to the extent of the stained cells (0 = 0–<5%, 1 = <10%, 2 = 10–50%, 3 = >50%). Bile duct cells and the glandular and superficial foveolar compartment in the stomach tissue were used as control for CAIX and CAXII staining, respectively. The islets of Langerhans in the human pancreas and the glandular compartment in stomach tissues were used as controls for a1 and H staining, respectively. Subunit H of V-ATPase was not expressed by malignant hepatocytes, except for 4 of 23 HCC lesions that displayed strong staining in the Golgi (see Supplementary Fig. S6). Kupffer cells of the liver were used as an internal control for CD163 staining.

decreased sensitivity to compound 25 when cultured under hypoxic conditions, with a consequential marked increase in the IC₅₀ (> 200 μM for all cell lines) (Fig. 3F). These data suggest that CAXII sequestration in the ER under hypoxia hampered the activity of compound 25, indicating that drug modifications or alternative pharmacological strategies need to be applied for the effective targeting of CAXII in HCC.

CA inhibitors affected HCC cell viability, and we found that blockage of CAIX activity limited the proliferative capacity of the CAIX-positive cell lines (C3A and PLC/PRF/5) and induced necrosis. However, our experiments failed to depict a clear mechanism of drug-induced cell death common to CAIX and CAXII inhibitors in the HCC cell lines (Supplementary Fig. S5). In agreement with data from the literature, the cell death pathway induced by CAs is reminiscent of the ‘metabolic catastrophe’ occurring in cancer cells upon disruption of proton dynamics and energy metabolism.²⁹

Expression of the V-ATPase complex in the HCC microenvironment

We then explored the *in vivo* distribution of the V-ATPase complex. IHC analyses showed selective overexpression of the V-ATPase subunits a1 and C1 in T in comparison with NT tissues and normal liver (Fig. 4). This pattern was detectable in approximately 90% of HCC cases, although a heterogeneous frequency of positive cells and staining intensity could be observed (Table 2). The H subunit was not detected in tumors and normal hepatocytes, as observed by the IHC staining of T and NT tissues (Fig. 4) except for 4 HCC cases. In these samples, V-ATPase subunit H was intracellularly expressed in malignant hepatocytes, with a pattern suggesting its accumulation in the Golgi apparatus

(Supplementary Fig. S6). The H subunit was detectable in cells infiltrating NT and T tissues, likely to be Kupffer cells, the liver’s macrophages lining the walls of the sinusoids. Notably, in approximately half of the cases analyzed, marked expression of the V-ATPase a1 and H subunits could also be detected in the HCC inflammatory infiltrate in the PT area of the HCC samples (Fig. 4 and Table 2). IHC analysis defined these immune cells as being composed of myeloid cells, expressing the CD14, CD68, CD163 and CD209 markers, and of CD3⁺ lymphocytes (Fig. 5A). Confocal microscopic analysis showed that V-ATPase a1 and H were co-expressed with CD163 and CD209, known markers of M2 macrophages (Fig. 5B and Supplementary Fig. S7 A). In addition, a fraction of CD3⁺ cells were positive for the V-ATPase a1 subunit (Fig. 5B and Supplementary Fig. S7B), while no co-staining with the V-ATPase H subunit was detectable (data not shown). Flow cytometry analysis of cell suspensions obtained from HCC surgical specimens confirmed that myeloid cells expressing CD163 and CD209 markers were clearly present, although with different frequencies, along with the presence of CD3⁺ cells (Fig. 5C–E). A fraction of CD14⁺CD11b⁺ cell population was V-ATPase a1 positive, and in agreement with confocal microscopy analysis, V-ATPase a1 was preferentially expressed by myeloid cells expressing the M2-associated marker CD163⁺ or CD209⁺ (Fig. 5C, F). Flow cytometry also confirmed that a small fraction of CD3⁺ lymphocytes expressed V-ATPase a1 (Fig. 5D, G).

Pleiotropic effects of V-ATPase inhibition by omeprazole in the HCC microenvironment

C3A, PLC/PRF/5 and SNU-449 cells displayed significant levels of the V-ATPase a1 and C1 subunits (Fig. 6A), corroborating the expression data observed in the HCC specimens. To test

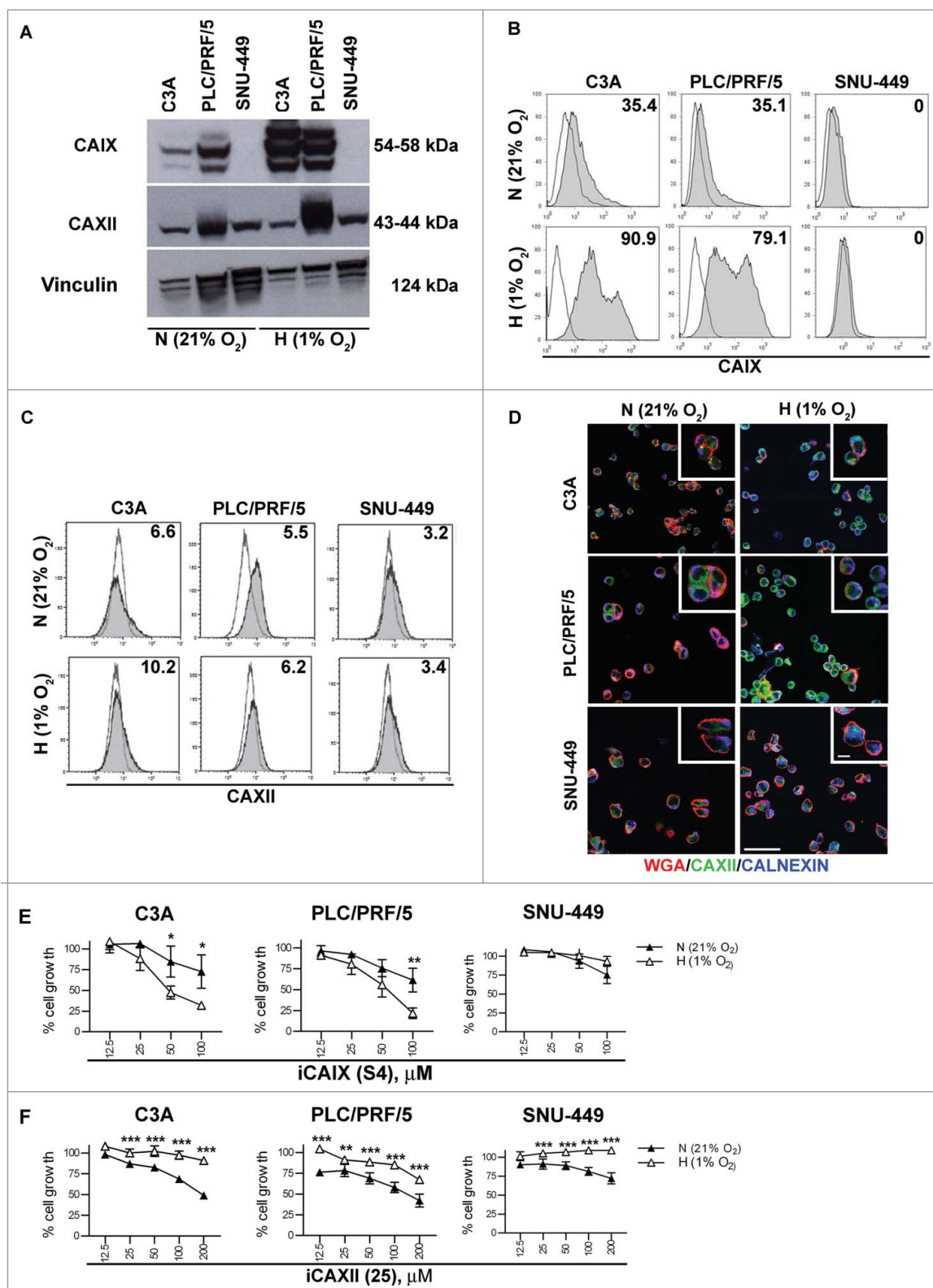


Figure 3. CAIX and CAXII expression and functional inhibition in HCC cell lines. The indicated HCC cell lines were cultured under either normoxic (N = 21% O₂) or hypoxic (H = 1% O₂) conditions for 72 h and were analyzed as indicated below. (A) The protein expression of CAIX, CAXII and vinculin was assessed by western blotting in cell lysates of the C3A, PLC/PRF/5 and SNU-449 cell lines. The cell surface expression of CAIX (B) and CAXII (C) was evaluated by flow cytometry. The number in each histogram plot shows the percentage of cells positive for the indicated markers (filled histograms) evaluated with respect to the corresponding secondary antibody (black line). Representative histograms from three independent experiments are shown. (D) The cellular distribution of CAXII was assessed by confocal laser scanning microscopy under the indicated conditions. Representative micrographs of triple immunofluorescence staining with anti-CAXII (green), anti-WGA (red, detecting the cell membrane) and anti-calnexin (blue, detecting the ER compartment) are reported. Scale bars = 50 μ m and = 5 μ m for the lower and higher magnification respectively. The cell viability of the HCC cell lines treated with different doses of S4 (μ M) (E) and compound 25 (μ M) (F) under normoxia (N = 21% O₂, black triangles) or hypoxia (H = 1% O₂, white triangles) for 72 h was evaluated using the MTT assay. The data show the percentage of viable cells of the untreated control and represent the mean of six replicate reactions from 3 independent experiments. IC₅₀ values for S4 were >100 μ M for all HCC cell lines grown under normoxic conditions and 57.4, 53.9 and >100 μ M for C3 A, PLC/PRF/5 and SNU-449 exposed to hypoxia respectively. For compound 25, C3 A, PLC/PRF/5 and SNU-449 cells grown under normoxia displayed IC₅₀ values of 198.5, 142.9 and >200 μ M respectively. All the HCC cell lines exposed to hypoxia displayed IC₅₀ values >200 μ M for compound 25.

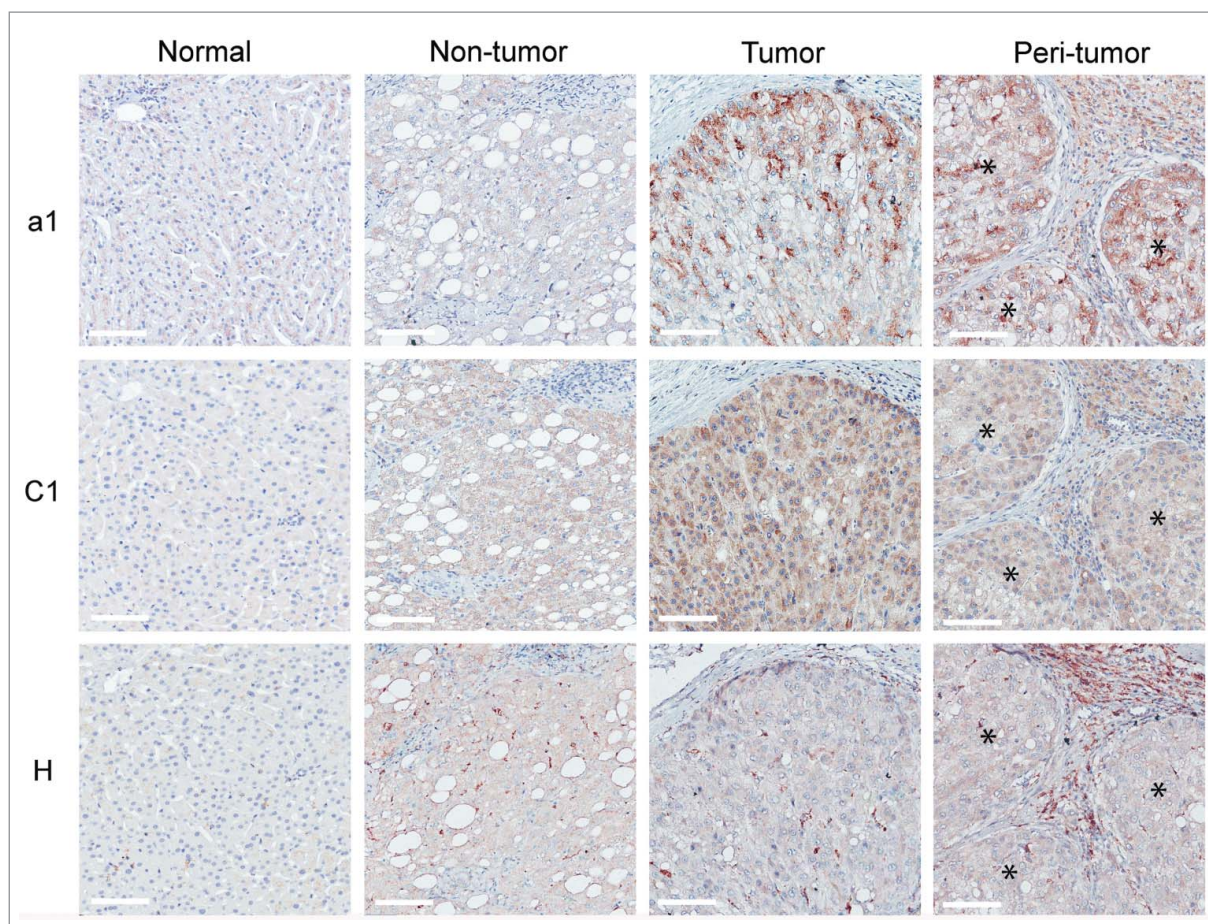


Figure 4. Expression pattern of V-ATPase subunits in liver tissues. The immunohistochemical expression of a1, C1 and H V-ATPase subunits was evaluated in normal and matched non-tumor, tumor and peri-tumor liver tissues. Peri-tumor tissues were identified as areas adjacent to tumor nodules enriched in immune infiltrating cells. The membranous/cytoplasmic expression of a1 and C1 subunits was detected in malignant hepatocytes. The H subunit was mainly expressed in the Kupffer cells present in non-tumor and tumor tissues. The a1 and H subunits were also expressed by infiltrating immune cells in the peri-tumor areas of the liver. *Identifies a tumor area in the peri-tumor sections. Representative images with scale bars = 100 μm .

the antitumor potential of V-ATPase targeting, we chose omeprazole, a selective inhibitor of proton pumps that is broadly used to block acid secretion by gastric parietal cells through inhibition of the H⁺/K⁺ ATPase system.³⁰ Omeprazole has been shown to cross-react with V-ATPase and mediate antitumor properties in a preclinical setting¹⁵. As shown in Fig. 6B, all HCC cells showed a significantly blocked growth response to omeprazole, with IC₅₀ values ranging from 39.4 $\mu\text{g}/\text{ml}$ for PLC/PRF/5 cells to 100.9 $\mu\text{g}/\text{ml}$ for C3A cells. SNU-449 cells again displayed the lowest sensitivity (IC₅₀ values of 128.4 $\mu\text{g}/\text{ml}$), in accordance with the relative resistance observed with CA inhibitors (Fig. 3E and F) and described for other drugs, including sorafenib.³¹ No difference in the sensitivity to omeprazole treatment was found in hypoxic conditions for any of the HCC cell lines (Supplementary Fig. S8). These experiments suggested that omeprazole affected the proliferative capacity of all the HCC cell lines tested and induced necrosis, but the mechanisms leading to drug-induced HCC cell death remain to be elucidated, as discussed for the CA inhibitors (Supplementary Fig. S5).

V-ATPase was expressed not only in tumor cells but also in the infiltrating immune cells. To evaluate whether interfering with V-ATPase activity could modulate the HCC microenvironment in both the tumor and immune components, human

primary HCC tissue explants (n = 12), preserving the intercellular networks of local tissue,³² were cultured for 24 h with omeprazole or drug vehicle and were then analyzed for the modulated expression of selected tumor and immune genes.

MYC and VIM, expressed by tumor cells and associated with epithelial-to-mesenchymal transition (EMT),^{33,34} were down-regulated in HCC tissue explants, in parallel with increased CDH1, indicating a reduced aggressiveness of the tumor component (Fig. 6C). Omeprazole treatment also induced a reshaping of the cyto/chemokine milieu, including a down-regulation of CCL22 and a concomitant up-regulation of the IFNG and TNF genes (Fig. 6C). The expression of other immune genes, including CCL2 and IL6, was not consistently detectable by qRT-PCR.

To gain further evidence of the functional role of V-ATPase in the modulation of the cytokine profile of the HCC TME and to assess whether the cytokine modulation in the HCC TME also occurred at the protein level, cell suspensions obtained from HCC surgical specimens were treated for 24 h with omeprazole or vehicle and monitored by multiparametric flow cytometry for cyto/chemokine secretion by the different immune cell subsets. In CD11b⁺CD163⁺ myeloid cells and in CD3⁺ T cells, omeprazole treatment was associated with a decreased production of CCL22, paralleled by a significant

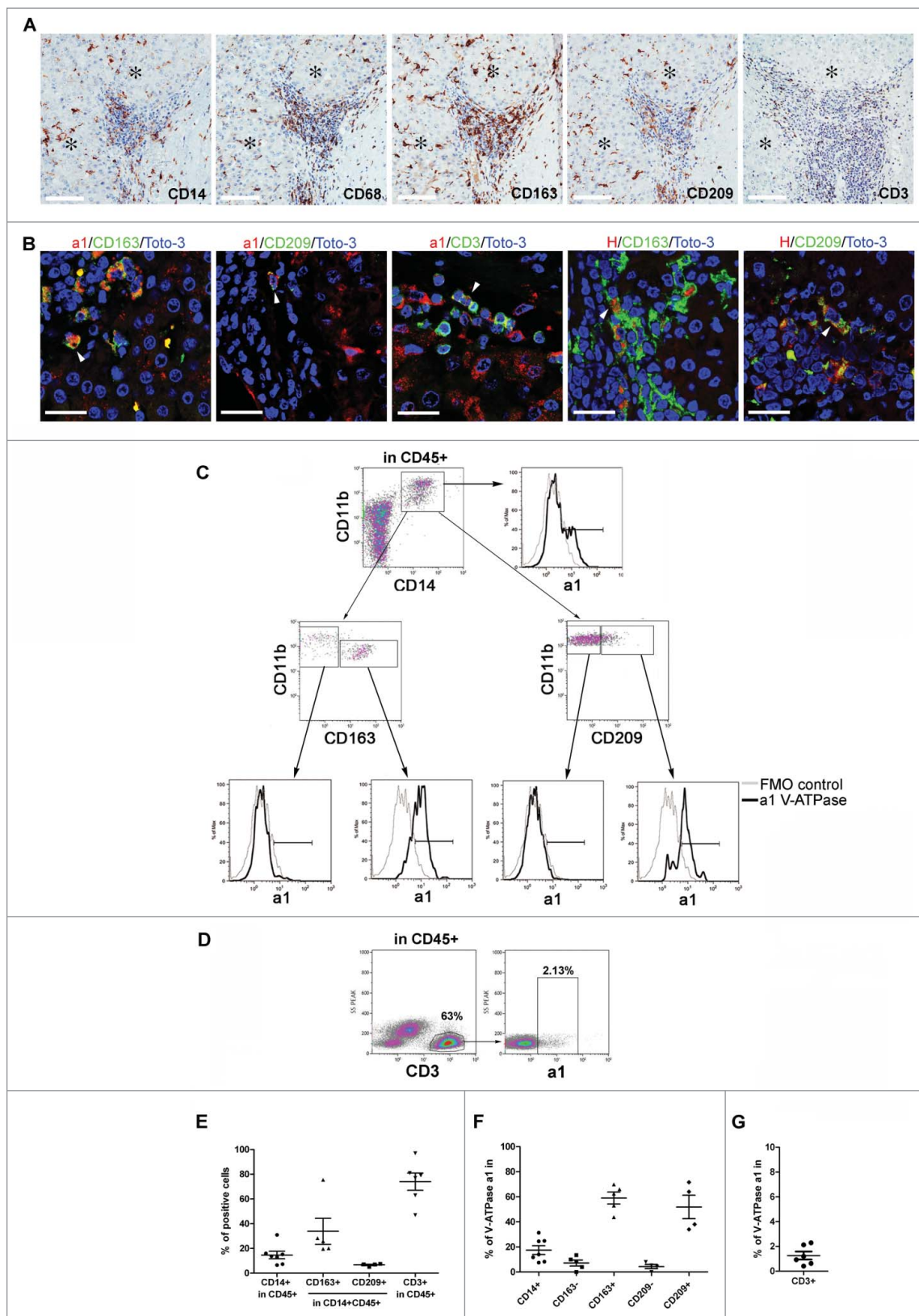


Figure 5. Expression of V-ATPase in immune cells infiltrating HCC tissues. (A) Representative images of immunohistochemical staining for the myeloid-associated markers CD14, CD68, CD163, CD209 and the CD3 T cell marker in HCC tissues. Scale bars = 100 μ m are shown. *Identifies the tumor area. (B) Triple-labeled immunofluorescence staining for a1 and H1 subunits of the V-ATPase complex (red) and CD163 (green), CD209 (green) or CD3 (green) in HCC tissues. Nuclei were stained with Toto-3 (blue). White triangles indicate the co-expression of the analyzed markers. Representative images with scale bars = 25 μ m. No co-staining was found for CD3 and V-ATPase H1 (data not shown). (C) Multi-parametric flow cytometry analysis of live myeloid cells in cell suspensions of freshly dissociated HCC surgical specimens. The CD209 and CD163 positive population has been defined by setting the marker on the corresponding FMO control. The cell surface expression of V-ATPase a1 was evaluated within the CD14⁺CD11b⁺, CD11b⁺CD163⁺, CD11b⁺CD163⁺CD11b⁺CD209⁻ and CD11b⁺CD209⁺ cell populations and the corresponding histograms are reported (black line). FMO control is shown (gray line). (D) Multi-parametric flow cytometry analysis of cell surface V-ATPase a1 expression in live CD3⁺ cells in cell suspensions of freshly dissociated HCC tumors. V-ATPase a1 positive cells have been defined using the FMO control. (E) The graph summarizes the percentages of CD14⁺, CD163⁺, CD209⁺ and CD3⁺ cells found in the analyzed HCC samples. (F-G) The percentages of V-ATPase a1-positive cells assessed in the indicated myeloid cell populations and within the CD3⁺ cells for all the analyzed samples.

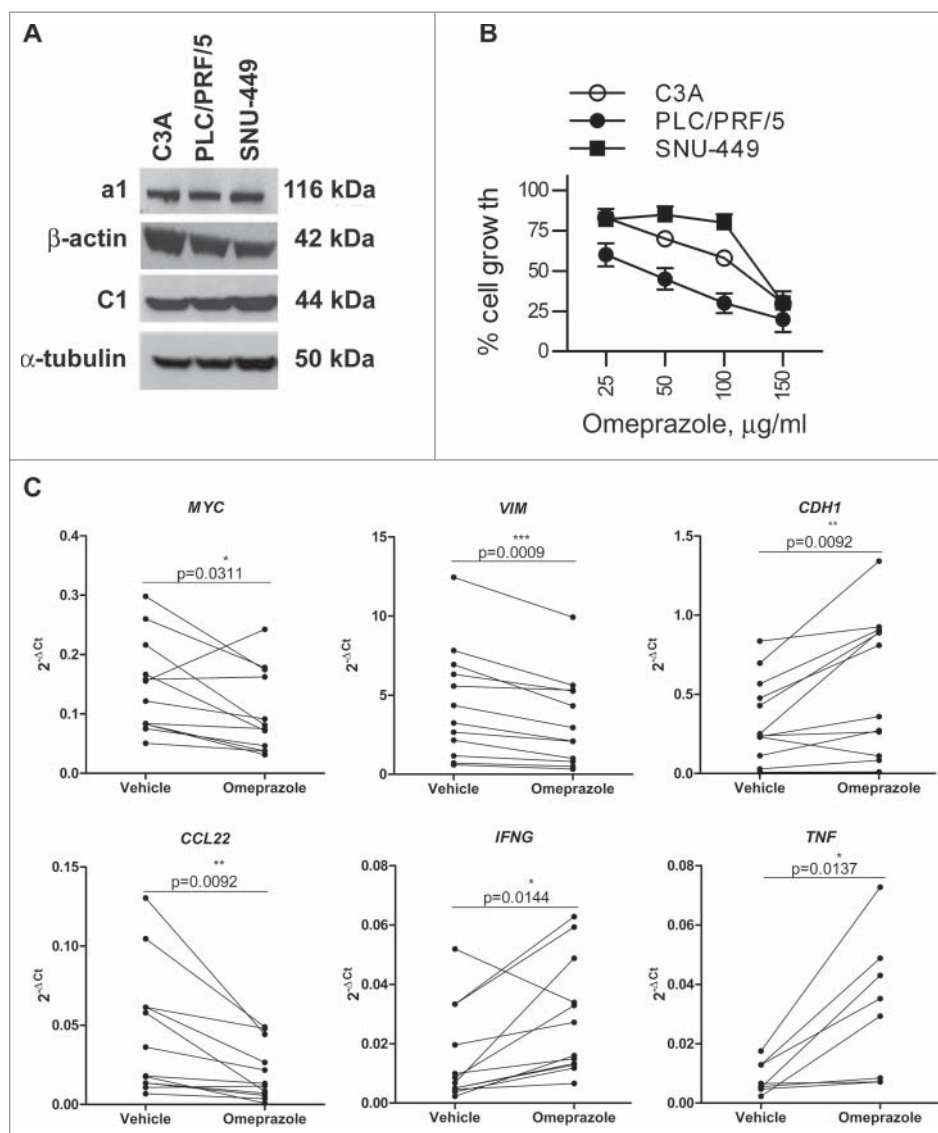


Figure 6. Effects of omeprazole on HCC cell line viability and on the tumor microenvironment of HCC tissue explants. (A) The protein expression of a1, C1, β -actin and α -tubulin was assessed by western blotting in cell lysates of the C3A, PLC/PRF/5 and SNU-449 cell lines. (B) The HCC cell lines were treated with different doses of omeprazole, and cell viability was evaluated using the MTT assay. The data on the y-axes report the percentage of viable cells of the untreated control and represent the mean of six replicate reactions from 3 independent experiments. The calculated IC_{50} values for omeprazole are 100.9, 39.4, and 128.4 μ g/ml for C3A, PLC/PRF/5 and SNU-449 respectively. (C) Expression levels of the indicated genes in HCC tissue explants (MYC, VIM, CDH1, CCL22, IFNG N = 12; TNF, N = 8) cultured *ex vivo* in the presence of 100 μ g/ml omeprazole or the vehicle of the drug for 24 h. The gene expression data are reported as $2^{-\Delta Ct}$ values. The p-values are calculated by the paired t test comparing cells treated with omeprazole or the vehicle.

increase in IFN γ and TNF Representative flow cytometry histograms are shown (Fig. 7A, B), and cumulative data obtained from all the HCC cell suspensions are summarized (Fig. 7C, D). Altogether, these data indicate that omeprazole promotes a rapid modulation of the HCC TME involving a relief of immunosuppression and a potential gain of a more antitumor or immune profile that involved both innate and adaptive immune cells.

Discussion

Tumor metabolism is the focus of a new wave of studies aimed at a better understanding of cancer biology and for developing novel tools for therapeutic intervention.^{35,36} In the present work, we show that HCC, the dysfunctional metabolism of which promotes a highly hypoxic and acidic environment,⁷

selectively overexpress molecules such as V-ATPase, CAIX and CAXII that are in charge of proton extrusion and intracellular pH regulation. The pharmacological inhibition of these pH regulators greatly decreased tumor cell viability, suggesting a strong pro-survival role of these transporters in HCC biology. Moreover, in our HCC series, CA9 and CA12 gene expression was associated with tumor grading, thus indicating their possible involvement in tumor malignancy *in vivo* in HCC patients. Overexpression of these pH regulatory molecules is a biological feature common to many human tumors, and data in the literature show that their blockage exerts strong antitumor activity *in vivo* in human tumor xenografts.^{27, 37-39} However, to fully qualify these pH regulatory molecules as therapeutic targets for HCC patients, the *in vivo* antitumor effects of their specific antagonistic drugs in human HCC xenografts have still to be demonstrated.

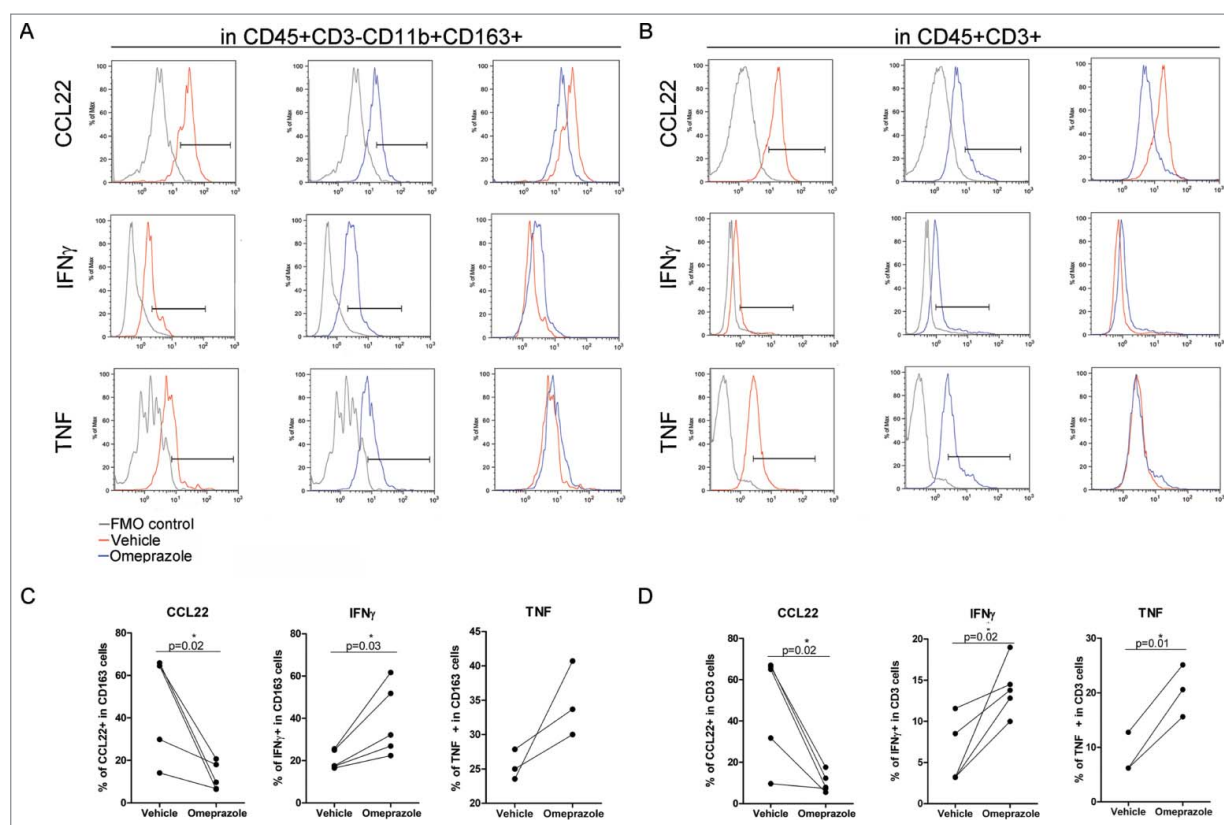


Figure 7. Modulation of the cytokine profile in HCC immune-infiltrating cells by omeprazole treatment. (A–D) Multiparametric flow cytometry of live cells in freshly dissociated HCC tumors treated with the drug vehicle (red line) or with omeprazole (100 μ g/ml, blue line) for 24 h. IFN γ , TNF and CCL22 production was evaluated by intracellular staining (A) in CD163⁺ myeloid cells gated inside live CD45⁺CD3⁻ cells and (B) in CD3⁺ T cells gated inside live CD45⁺ cells. FMO control for each cytokine (gray line) is reported in the histogram plot. The percentages of IFN γ -, TNF- and CCL22-positive cells in the CD163⁺ and in the CD3⁺ cells are shown in C and D respectively. The p-values are calculated by the paired t test comparing cells treated with omeprazole or the vehicle.

Although selectively associated with the neoplastic transformation of hepatocytes, the expression patterns of V-ATPase, CAIX and CAXII in HCC showed non-redundant functions and thus diverse potentials as druggable targets. The focal distribution of CAIX within discrete tumor nests indicates that this transporter, promptly induced by hypoxia, might identify tumor areas with particularly low O₂ tension. Given that CAIX is associated with stemness and enhanced malignancy in other solid cancers^{40,41} and that acidity may promote *per se* cell pluripotency,⁴² it is possible that hypoxic niches may host HCC cells with stem-like features and that CAIX targeting may control the most aggressive cancer cells. These data also identify CAIX as a potential HCC prognostic biomarker, in accordance with a recent meta-analysis identifying that CAIX tumor expression is associated with a higher risk of locoregional failure and metastatic spread in multiple cancers.^{22,43}

On the other hand, CAXII showed a homogeneous expression pattern in transformed hepatocytes, which is clearly a great advantage for effective therapeutic targeting. However, this pH regulator was unexpectedly retained intracellularly in both the HCC specimens and cell lines. Of note, the ER localization of CAXII was exacerbated by hypoxia and was seemingly specific to this tumor histotype, being undetectable in other solid cancers.²³ Although the molecular mechanism underlying this phenomenon is presently unknown, it could be that altered CAXII glycosylation or alternative splicing events, known to occur in cancer under certain conditions^{44,45} might play a role in determining the

intracellular localization of CAXII. Nevertheless, since HCC cell lines became partially refractory to CAXII inhibitor compound 25 under hypoxic conditions, it suggests that either the protein loses its function when retained in the ER or the drug has no access to this intracellular compartment. Modifications of compound 25 to allow binding to ER-retained CAXII, or the use of “intrabodies” designed to target splice variants,⁴⁶ could increase the efficacy of CAXII-specific targeting in liver cancer.

Our results show that V-ATPase was positive in most malignant hepatocytes, was detectable in infiltrating immune cells and was thus the most broadly and highly expressed pH regulator in the HCC microenvironment among those tested. These observations are consistent with data reported for melanoma and breast cancer, for which V-ATPase overexpression has also been associated with more aggressive disease and multi-drug resistance.⁴⁷ Selective V-ATPase inhibitors for clinical use are presently unavailable, and those developed for *in vitro* studies (e.g., bafilomycin) have exhibited prohibitive toxicity.⁴⁸ Hence, the functional analysis of the role of V-ATPase in HCC has been performed with omeprazole, a proton pump inhibitor (PPI) that is widely used to reduce gastric acid secretion³⁰ and has recently been reported to exert broad antitumor effects at preclinical and clinical levels.^{47,49} PPIs were designed to bind to gastric H⁺, K⁺-ATPase, but they can also cross-react with V-ATPase, albeit with lower affinity.¹⁶ In our hands, omeprazole displayed antitumor activity in the HCC cell lines, suggesting promising clinical potential. Nevertheless, novel V-ATPase

inhibitors that have recently been introduced, such as enoxacin and other small molecules, will potentially provide additional tools for therapeutic intervention in HCC.⁵⁰

Importantly, our data indicated that in contrast to the other pH regulators, V-ATPase was also markedly expressed by both the resident myeloid Kupffer cells and by the HCC immune cell infiltrate. Specifically, V-ATPase expression occurred in myeloid cells, most likely M2-like TAMs located within tumor nests or in the peri-tumor area at the boundary between tumor and adjacent non-tumor tissue. Transcriptional up-regulation of V-ATPase genes has been reported to occur in monocytic cells during macrophage differentiation in association with phagocytic activity.⁵¹ Hence, it is conceivable that HCC-associated macrophages might exploit V-ATPase expression to survive the acidic tumor microenvironment and possibly exert their immunosuppressive effects. Data from HCC tissue explants, likely preserving the intercellular network operating *in vivo*, and the analysis of cell suspensions obtained from HCC specimens indicate that V-ATPase blockade via omeprazole can interfere with TAM activity, possibly favoring the conversion of protumor M2-like myeloid cells into antitumor M1-like cells, as indicated by the decrease in CCL22 expression and the concomitant significant increase of IFN γ and TNF. This cytokine modulation also occurred in the adaptive CD3⁺ cell population. Whether the immune cells were direct targets of the drugs or their functional modulation was the result of the drug-induced modification in tumor or other stromal cells remains to be addressed. Nevertheless, these data indicate a broad impact of omeprazole in creating a less immune-suppressive HCC microenvironment involving both innate and adaptive effector T cells. Indeed, omeprazole changed the tumor cell phenotype; V-ATPase inhibition in HCC explants by omeprazole down-regulated the *MYC* oncogene and induced an inverse modulation of E-cadherin and vimentin expression, thus implying a block of the EMT, a process that is also sustained by myeloid cells^{9,52} and which drives disease progression in HCC.²⁴ Thus, targeting V-ATPase could achieve the twin goals of reducing the viability and aggressive features of tumor cells while concomitantly interfering with the protumor and immunosuppressive functions exerted by the myeloid cell infiltrate in HCC.⁵³

The precise molecular mechanisms underlying these effects remain to be fully elucidated. Tumor pH buffering mediated by omeprazole administration can certainly play a role in both tumor growth and associated immune dysfunctions.¹¹ Consistent with this opinion is the evidence that bicarbonate can be beneficial in HCC patients receiving locoregional therapy⁵⁴ and in mice undergoing tumor immunotherapy.⁵⁵ Nevertheless, it should be underlined that blockade of pH regulators might also directly interfere with downstream signaling pathways, including Wnt/ β -catenin, Notch and mTOR,^{16,18} and with genes involved in the so called “metabolic catastrophe”²⁹ both in tumor cells and immune cells.

In conclusion, drugs that inhibit pH regulation might represent a promising therapeutic strategy in HCC patients, endowed with the novelty of simultaneously interfering with metabolic pathways of tumors and the associated immunosuppressive cell populations. In this era of immune checkpoint-based immunotherapy, not only showing promising efficacy in

HCC patients⁴ but also underscoring the key role of myeloid cells in primary and acquired resistance,^{56,57} the identification of drugs that may potentially induce a less-aggressive and immunosuppressive tumor microenvironment could provide further therapeutic benefit when used in combination therapy.

Materials and methods

Ethical statement

This study was conducted in compliance with the Helsinki Declaration of 1975 and was approved by the review board of Fondazione IRCCS Istituto Nazionale dei Tumori of Milan (protocol number: INT 110/13). Written informed consent was obtained from the patients.

Patients, tissue samples and clinical data

Tumor (T) and adjacent non-tumor liver tissue (NT), sampled within 2 cm proximal to the tumor margin, were collected from resected HCC in patients with well-compensated cirrhosis (n = 57). Nine non-cirrhotic, normal (N) liver tissue samples were obtained from patients who underwent operations unrelated to cancer (cholecystectomy). Liver tissue specimens were snap-frozen in RNAlaterTM solution (Thermo Fisher Scientific) for RNA analyses and stored at -80°C until use. See Table 1 for the tumor pathology features. Formalin-fixed, paraffin-embedded (FFPE) samples corresponding to the liver tissues stored in the RNAlater solution were also prepared for immunostaining. Breast cancer samples were used as a control (n = 3) and were obtained from a pathology archive. To obtain single-cell suspensions, HCC tissues were enzymatically and mechanically digested using the gentleMACS Dissociator (Miltenyi Biotec) and were stored in liquid nitrogen until use.

Cell lines and culture conditions

The human HCC cell lines C3A, PLC/PRF/5 and SNU-449 and the breast cancer cell line T-47D (ATCC, Manassas, Virginia, USA) were cultured in complete culture medium (RPMI-1640, Lonza) supplemented with 10% heat-inactivated fetal calf serum (FCS, Lonza), 100 U/ml penicillin and 100 U/ml streptomycin under normoxia (N = 21% O₂) or hypoxia (H = 1% O₂) as indicated. HCC cell lines grown at 80–90% confluence were trypsinized, washed in 1x PBS and used for the analysis. Cell lines were routinely checked for their identity by STR profiling and were free of mycoplasma, as assessed using the N-GARDE Mycoplasma PCR reagent set (EMK-090020, Euroclone).

Ex vivo treatment of HCC tissue explants

Culturing of *ex vivo* HCC tissue explants was performed as previously described.³² Fresh HCC tissues (n = 5) were cut into 3 mm³ pieces using a biopsy puncher under sterile conditions and were cultured for 24 h in a 48-well plate (Corning) in the presence of 300 μl RPMI 1640 with 1% FCS (Lonza) and 100 $\mu\text{g/ml}$ omeprazole (Sigma-Aldrich) or drug vehicle (dimethylsulfoxide, DMSO, Sigma-Aldrich).

RNA extraction, reverse transcription and quantitative real-time PCR

Total RNA was extracted using a NucleoSpin miRNA kit (Macherey-Nagel). cDNA was generated using a High-Capacity cDNA reverse transcription kit (Thermo Fisher Scientific). In addition, cDNA obtained from HCC tissue explants was also pre-amplified using the TaqMan® Preamp Master Mix Kit (Thermo Fisher Scientific). cDNA was used to perform real-time PCR (qRT-PCR) with TaqMan® gene expression assays and the primers/probes reported in Supplementary Table S2. qRT-PCR assays were conducted using an ABI 7900HT instrument (Thermo Fisher Scientific). Data analysis was performed with SDS 2.2.2 software (Thermo Fisher Scientific).

Immunohistochemistry

Serial sections of 1–2- μm -thickness FFPE HCC ($n = 23$) and normal liver ($n = 9$) samples were processed for immunohistochemical staining. For each HCC case, the FFPE section slides of non-tumor, (NT) tumor (T) and peri-tumor (PT) tissues were analyzed. PT corresponds to the FFPE HCC sections, which include areas enriched in immune infiltrating cells adjacent to tumor nodules. The antibodies used are reported in Supplementary Table S3. Stained whole-section slides were scanned using Aperio Scanscope Cs (Aperio Technologies). Images were visualized and annotated with ImageScope software (Aperio Technologies).

Confocal analysis

Confocal microscopic analyses were performed using FFPE samples and HCC cell lines that were exposed or not to hypoxia (1% O_2) for 72 h. The antibodies used are reported in Supplementary Table S3. The nuclei were stained with Toto-3 (Thermo Fisher Scientific). Confocal microscopy was performed using a Radiance 2100 microscope (Bio-Rad Laboratories) equipped with a krypton/argon laser and a red laser diode.

Flow cytometry

Antibodies used in flow cytometry are reported in Supplementary Table S4. CAIX and CAXII were detected at the cell surface. Multiparametric flow cytometry was performed on cell suspensions obtained from clinical HCC tissues and stored in liquid nitrogen. The cells were stained for cell surface markers, including V-ATPase a1, fixed and permeabilized with Cytofix/Cytoperm buffer (BD Biosciences), and stained with the intracellular markers (CCL22, $\text{IFN}\gamma$ and TNF). CCL22, $\text{IFN}\gamma$ and TNF production was measured after treatment with 100 $\mu\text{g}/\text{ml}$ omeprazole or the vehicle of the drug (DMSO) for 24 h. Golgi Stop (0.7 $\mu\text{l}/\text{ml}$) was added after 1.5 h of treatment

Dead cells were identified using the LIVE/DEAD Fixable Violet Dead Cell Stain Kit (ThermoFisher Scientific) and were excluded from the analysis. Data were acquired using a Gallios flow cytometer (Beckman Coulter) and were analyzed by FlowJo, V 8.5.2 (Tree Star) or Kaluza 1.3 software (Beckman Coulter).

Pharmacological inhibitors and cell viability assays

The selective CAIX inhibitor S4 (4-(3'-(3'',5''-dimethylphenyl)ureido)phenyl sulfamate) and the selective CAXII inhibitor compound 25 were developed by the team of Dr. CT Supuran. See Supplementary Table S1 for the chemical and biological details of the CAXII inhibitors. Omeprazole was purchased from Sigma-Aldrich. Drugs were dissolved in DMSO (Sigma-Aldrich) and were stored at -20°C . Prior to use, omeprazole was activated in acidified water at pH 3.7 for 30 min at RT in the dark and then diluted in culture medium. Activated omeprazole was used throughout the present study. HCC cells were plated at a density of $4\text{--}5 \times 10^3$ cells/well in 96-well plates (Corning), drugs were added to fresh medium after 24 h, and plates were incubated for an additional 72 h. Cell viability was evaluated using the (3-(4,5)-dimethylthiazol-2-yl)-2,5-diphenyl-tetrazolium bromide (MTT) colorimetric assay (Sigma-Aldrich). Absorbance was measured at 570 nm with a spectrophotometer (Infinite® M1000, Tecan), and the average values from triplicate readings were calculated.

Statistical analysis

Statistical analyses were performed using GraphPad Prism Software v.5 (GraphPad, La Jolla). The Wilcoxon signed-rank test was used to compare gene expression levels between non-tumor and tumor tissues, and the Mann-Whitney U -test was used to compare the gene expression levels between normal and non-tumor tissues and between normal and tumor tissues. p -values less than or equal to 0.05 were considered significant. Fitted lines were generated using the four-parameter dose-response curve (variable slope), and the IC_{50} values for inhibition of cell growth at 72 h of S4, compound 25 and omeprazole treatment were calculated. One-way analysis of variance (ANOVA) followed by Bonferroni correction was used to evaluate statistical significance. The paired t test was used to compare the expression of *MYC*, *CDH1*, *VIM*, *CCL22*, *IFNG* and *TNF* in HCC tumor explants treated with 100 $\mu\text{g}/\text{ml}$ omeprazole or the vehicle of the drug. To evaluate the modulation of $\text{IFN}\gamma$, TNF and CCL22 in fresh $\text{CD}163^+$ and $\text{CD}3^+$ cells isolated from HCC tissues due to the treatment with 100 $\mu\text{g}/\text{ml}$ omeprazole or the vehicle of the drug, paired t tests were used.

Disclosure of potential conflicts of interest

No potential conflicts of interest were disclosed.

Acknowledgments

The authors are grateful to Francesca Rini, Valeria Beretta, Agata Cova, Martina Filugelli and Paola Squarcina (Unit of Immunotherapy of Human Tumors, Fondazione IRCCS Istituto Nazionale dei Tumori, Milan, Italy) for technical help, Paola Frati for data management and Grazia Convertino for administrative support.

Financial support

This study was supported by the Associazione Italiana Ricerca sul Cancro (CC IG-15192; LR IG-14285) and the Italian Ministry of Health grant 52/RF-2010-2312620. O.K. is supported by a Prometeo Association fellowship. Fellowship provided by Prometeo Association.

Funding

Associazione Italiana Ricerca sul Cancro ID: CC IG-15192, Italian Ministry of Health ID: 52/RF-2010-2312620, Associazione Italiana Ricerca sul Cancro ID: LR IG-14285. Fellowship provided by Prometeo Association.

ORCID

Olga Kuchuk  <http://orcid.org/0000-0001-7301-0347>
 Simone Carradori  <http://orcid.org/0000-0002-8698-9440>
 Claudiu T Supuran  <http://orcid.org/0000-0003-4262-0323>

References

- Torre LA, Siegel RL, Ward EM, Jemal A. Global cancer incidence and mortality rates and trends—an update. *Cancer Epidemiol. Biomarkers Prev.* 2016;25(1):16–27. doi:10.1158/1055-9965.EPI-15-0578. PMID:26667886
- Mazzaferro V, Lencioni R, Majno P. Early hepatocellular carcinoma on the procrustean bed of ablation, resection, and transplantation. *Semin. Liver Dis.* 2014;34(4):415–26. doi:10.1055/s-0034-1394365. PMID:25369303
- Bruix J, Gores GJ, Mazzaferro V. Hepatocellular carcinoma: Clinical frontiers and perspectives. *Gut.* 2014;63(5):844–55. doi:10.1136/gutjnl-2013-306627. PMID:24531850
- Kudo M. Immune checkpoint inhibition in hepatocellular carcinoma: Basics and ongoing clinical trials. *Clinical Trials. Oncology.* 2017;92 Suppl 1:50–62. doi:10.1159/000451016.
- Pitt JM, Vetzou M, Daillere R, Roberti MP, Yamazaki T, Routy B, Lepage P, Boneca IG, Chamaillard M, Kroemer G, et al. Resistance mechanisms to immune-checkpoint blockade in cancer: Tumor-intrinsic and -extrinsic factors. *Immunity.* 2016;44(6):1255–69. doi:10.1016/j.immuni.2016.06.001. PMID:27332730
- Vaupel P, Hockel M, Mayer A. Detection and characterization of tumor hypoxia using pO₂ histography. *Antioxid. Redox Signal.* 2007;9(8):1221–35. doi:10.1089/ars.2007.1628. PMID:17536958
- Pavlova NN, Thompson CB. The emerging hallmarks of cancer metabolism. *Cell. Metab.* 2016;23(1):27–47. doi:10.1016/j.cmet.2015.12.006. PMID:26771115
- Webb BA, Chimenti M, Jacobson MP, Barber DL. Dysregulated pH: A perfect storm for cancer progression. *Nat. Rev. Cancer.* 2011;11(9):671–7. doi:10.1038/nrc3110. PMID:21833026
- Ye LY, Chen W, Bai XL, Xu XY, Zhang Q, Xia XF, Sun X, Li GG, Hu QD, Fu QH, et al. Hypoxia-induced epithelial-to-mesenchymal transition in hepatocellular carcinoma induces an immunosuppressive tumor microenvironment to promote metastasis. *Cancer Res.* 2016;76(4):818–30. doi:10.1158/0008-5472.CAN-15-0977. PMID:26837767
- Brand A, Singer K, Koehl GE, Kolitzus M, Schoenhammer G, Thiel A, Matos C, Bruss C, Klobuch S, Peter K, et al. LDHA-associated lactic acid production blunts tumor immunosurveillance by T and NK cells. *Cell. Metab.* 2016;24(5):657–71. doi:10.1016/j.cmet.2016.08.011. PMID:27641098
- Calcinotto A, Filipazzi P, Grioni M, Iero M, De Milito A, Ricupito A, Cova A, Canese R, Jachetti E, Rossetti M, et al. Modulation of microenvironment acidity reverses anergy in human and murine tumor-infiltrating T lymphocytes. *Cancer Res.* 2012;72(11):2746–56. doi:10.1158/0008-5472.CAN-11-1272. PMID:22593198
- Huber V, Camisaschi C, Berzi A, Ferro S, Lugini L, Triulzi T, Tuccitto A, Tagliabue E, Castelli C, Rivoltini L. Cancer acidity: An ultimate frontier of tumor immune escape and a novel target of immunomodulation. *Semin. Cancer Biol.* 2017; 43:74–89. Epub 2017/3/6. doi:10.1004-579X(17)30036-6. doi:10.1016/j.semcancer.2017.03.001. PMID:28267587
- Corzo CA, Condamine T, Lu L, Cotter MJ, Youn JI, Cheng P, Cho HI, Celis E, Quiceno DG, Padhya T, et al. HIF-1 α regulates function and differentiation of myeloid-derived suppressor cells in the tumor microenvironment. *J. Exp. Med.* 2010;207(11):2439–53. doi:10.1084/jem.20100587. PMID:20876310
- Supuran CT. Carbonic anhydrases: Novel therapeutic applications for inhibitors and activators. *Nat. Rev. Drug Discov.* 2008;7(2):168–81. doi:10.1038/nrd2467. PMID:18167490
- Fais S, De Milito A, You H, Qin W. Targeting vacuolar H⁺-ATPases as a new strategy against cancer. *Cancer Res.* 2007;67(22):10627–30. doi:10.1158/0008-5472.CAN-07-1805. PMID:18006801
- Stransky L, Cotter K, Forgac M. The function of V-ATPases in cancer. *Physiol. Rev.* 2016;96(3):1071–91. doi:10.1152/physrev.00035.2015. PMID:27335445
- Toei M, Saum R, Forgac M. Regulation and isoform function of the V-ATPases. *Biochemistry.* 2010;49(23):4715–23. doi:10.1021/bi100397s. PMID:20450191
- Sun-Wada GH, Wada Y. Role of vacuolar-type proton ATPase in signal transduction. *Biochim. Biophys. Acta.* 2015;1847(10):1166–72. doi:10.1016/j.bbabi.2015.06.010. PMID:26072192
- Neri D, Supuran CT. Interfering with pH regulation in tumours as a therapeutic strategy. *Nat. Rev. Drug Discov.* 2011;10(10):767–77. doi:10.1038/nrd3554. PMID:21921921
- Wilson GK, Tennant DA, McKeating JA. Hypoxia inducible factors in liver disease and hepatocellular carcinoma: Current understanding and future directions. *J. Hepatol.* 2014;61(6):1397–406. doi:10.1016/j.jhep.2014.08.025. PMID:25157983
- Wykoff CC, Beasley NJ, Watson PH, Turner KJ, Pastorek J, Sibtain A, Wilson GD, Turley H, Talks KL, Maxwell PH, et al. Hypoxia-inducible expression of tumor-associated carbonic anhydrases. *Cancer Res.* 2000;60(24):7075–83. PMID:11156414
- Huang WJ, Jeng YM, Lai HS, Fong IU, Sheu FY, Lai PL, Yuan RH. Expression of hypoxic marker carbonic anhydrase IX predicts poor prognosis in resectable hepatocellular carcinoma. *PLoS One.* 2015;10(3):e0119181. doi:10.1371/journal.pone.0119181. PMID:25738958
- Parkkila S, Parkkila AK, Saarnio J, Kivela J, Karttunen TJ, Kaunisto K, Waheed A, Sly WS, Tureci O, Virtanen I, et al. Expression of the membrane-associated carbonic anhydrase isozyme XII in the human kidney and renal tumors. *J. Histochem. Cytochem.* 2000;48(12):1601–08. doi:10.1177/002215540004801203. PMID:11101628
- Yamada S, Okumura N, Wei L, Fuchs BC, Fujii T, Sugimoto H, Nomoto S, Takeda S, Tanabe KK, Kodera Y. Epithelial to mesenchymal transition is associated with shorter disease-free survival in hepatocellular carcinoma. *Ann. Surg. Oncol.* 2014;21(12):3882–90. doi:10.1245/s10434-014-3779-2. PMID:24833103
- Yamashita T, Ji J, Budhu A, Forgues M, Yang W, Wang HY, Jia H, Ye Q, Qin LX, Wauthier E, et al. EpCAM-positive hepatocellular carcinoma cells are tumor-initiating cells with stem/progenitor cell features. *Gastroenterology.* 2009;136(3):1012–24. doi:10.1053/j.gastro.2008.12.004. PMID:19150350
- Winum JY, Carta F, Ward C, Mullen P, Harrison D, Langdon SP, Cecchi A, Scozzafava A, Kunkler I, Supuran CT. Ureido-substituted sulfamates show potent carbonic anhydrase IX inhibitory and anti-proliferative activities against breast cancer cell lines. *Bioorg. Med. Chem. Lett.* 2012;22(14):4681–85. doi:10.1016/j.bmcl.2012.05.083. PMID:22721713
- Gielsing RG, Babur M, Mamnani L, Burrows N, Telfer BA, Carta F, Winum JY, Scozzafava A, Supuran CT, Williams KJ. Antimetastatic effect of sulfamate carbonic anhydrase IX inhibitors in breast carcinoma xenografts. *J. Med. Chem.* 2012;55(11):5591–600. doi:10.1021/jm300529u. PMID:22621623
- D'Ascenzio M, Carradori S, Secchi D, Vullo D, Ceruso M, Akdemir A, Supuran CT. Selective inhibition of human carbonic anhydrases by novel amide derivatives of probenecid: synthesis, biological evaluation and molecular modelling studies. *Bioorg. Med. Chem.* 2014;22(15):3982–88. doi:10.1016/j.bmc.2014.06.003. PMID:25027802
- Parks SK, Chiche J, Pouyssegur J. Disrupting proton dynamics and energy metabolism for cancer therapy. *Nat. Rev. Cancer.* 2013;13(9):611–23. doi:10.1038/nrc3579. PMID:23969692
- Suzuki M, Suzuki H, Hibi T. Proton pump inhibitors and gastritis. *J. Clin. Biochem. Nutr.* 2008;42(2):71–75. doi:10.3164/jcfn.2008012. PMID:18385822
- Fornari F, Pollutri D, Patrizi C, La Bella T, Marinelli S, Casadei Gardini A, Marisi G, Baron Toaldo M, Baglioni M, et al. In Hepatocellular Carcinoma miR-221 Modulates Sorafenib Resistance through

- Inhibition of Caspase-3-Mediated Apoptosis. *Clin. Cancer Res.* **2017**;23(14):3953–3965. Epub 2017/1/17. doi:10.1158/1078-0432.CCR-16-1464. PMID:28096271
32. Breunig C, Mueller BJ, Umansky L, Wahl K, Hoffmann K, Lehner F, Manns MP, Bantel H, Falk CS. BRAF and MEK inhibitors differentially regulate cell fate and microenvironment in human hepatocellular carcinoma. *Clin. Cancer Res.* **2014**;20(9):2410–23. doi:10.1158/1078-0432.CCR-13-1635. PMID:24573550
33. Cao Z, Fan-Minogue H, Bellovin DI, Yevtdiyenko A, Arzeno J, Yang Q, Gambhir SS, Felsner DW. MYC phosphorylation, activation, and tumorigenic potential in hepatocellular carcinoma are regulated by HMG-CoA reductase. *Cancer Res.* **2011**;71(6):2286–97. doi:10.1158/0008-5472.CAN-10-3367. PMID:21262914
34. Smith AP, Verrecchia A, Faga G, Doni M, Perna D, Martinato F, Guccione E, Amati B. A positive role for Myc in TGFbeta-induced Snail transcription and epithelial-to-mesenchymal transition. *Oncogene.* **2009**;28(3):422–30. doi:10.1038/onc.2008.395. PMID:18978814
35. Sun Y, Shi Z, Lian H, Cai P. Energy metabolic dysfunction as a carcinogenic factor in cancer cells. *Clin. Transl. Med.* **2016**;5(1):14-016-0094-5. Epub 2016 Apr 6. doi:10.1186/s40169-016-0094-5.
36. Lim S, Phillips JB, Madeira da Silva L, Zhou M, Fodstad O, Owen LB, Tan M. Interplay between Immune Checkpoint Proteins and Cellular Metabolism. *Cancer Res.* **2017**;77(6):1245–49. doi:10.1158/0008-5472.CAN-16-1647. PMID:28246276
37. Lou Y, McDonald PC, Oloumi A, Chia S, Ostlund C, Ahmadi A, Kyle A, Auf dem Keller U, Leung S, Huntsman D, et al. Targeting tumor hypoxia: Suppression of breast tumor growth and metastasis by novel carbonic anhydrase IX inhibitors. *Cancer Res.* **2011**;71(9):3364–76. doi:10.1158/0008-5472.CAN-10-4261. PMID:21415165
38. Gondi G, Mysliwicz J, Hulikova A, Jen JP, Swietach P, Kremmer E, Zeidler R. Antitumor efficacy of a monoclonal antibody that inhibits the activity of cancer-associated carbonic anhydrase XII. *Cancer Res.* **2013**;73(21):6494–503. doi:10.1158/0008-5472.CAN-13-1110. PMID:24030978
39. De Milito A, Canese R, Marino ML, Borghi M, Iero M, Villa A, Venturi G, Lozupone F, Iessi E, Logozzi M, et al. pH-dependent antitumor activity of proton pump inhibitors against human melanoma is mediated by inhibition of tumor acidity. *Int. J. Cancer.* **2010**;127(1):207–19. doi:10.1002/ijc.25009. PMID:19876915
40. Currie MJ, Beardsley BE, Harris GC, Gunningham SP, Dachs GU, Dijkstra B, Morrin HR, Wells JE, Robinson BA. Immunohistochemical analysis of cancer stem cell markers in invasive breast carcinoma and associated ductal carcinoma in situ: relationships with markers of tumor hypoxia and microvasculature. *Hum. Pathol.* **2013**;44(3):402–11. doi:10.1016/j.humpath.2012.06.004. PMID:23036368
41. Lock FE, McDonald PC, Lou Y, Serrano I, Chafe SC, Ostlund C, Aparicio S, Winun JY, Supuran CT, Dedhar S. Targeting carbonic anhydrase IX depletes breast cancer stem cells within the hypoxic niche. *Oncogene.* **2013**;32(44):5210–19. doi:10.1038/onc.2012.550. PMID:23208505
42. Hjelmeland AB, Wu Q, Heddleston JM, Choudhary GS, MacSwords J, Lathia JD, McLendon R, Lindner D, Sloan A, Rich JN. Acidic stress promotes a glioma stem cell phenotype. *Cell Death Differ.* **2011**;18(5):829–40. doi:10.1038/cdd.2010.150. PMID:21127501
43. van Kuijk SJ, Yaromina A, Houben R, Niemans R, Lambin P, Dubois LJ. Prognostic Significance of Carbonic Anhydrase IX Expression in Cancer Patients: A Meta-Analysis. *Front. Oncol.* **2016**;6:69. doi:10.3389/fonc.2016.00069. PMID:27066453
44. Venables JP. Aberrant and alternative splicing in cancer. *Cancer Res.* **2004**;64(21):7647–54. doi:10.1158/0008-5472.CAN-04-1910. PMID:15520162
45. Oliveira-Ferrer L, Legler K, Milde-Langosch K. Role of protein glycosylation in cancer metastasis. *Semin. Cancer Biol.* **2017**;44:141–152. Epub 2017/3/16. doi:10.1016/j.semcancer.2017.03.002. PMID:28673608
46. Marschall AL, Dubel S. Antibodies inside of a cell can change its outside: Can intrabodies provide a new therapeutic paradigm? *Comput. Struct. Biotechnol. J.* **2016**;14:304–8. doi:10.1016/j.csbj.2016.07.003.
47. Taylor S, Spugnini EP, Assaraf YG, Azzarito T, Rauch C, Fais S. (2015) Microenvironment acidity as a major determinant of tumor chemoresistance: Proton pump inhibitors (PPIs) as a novel therapeutic approach. *Drug Resist Updat.* **2015**;23:69–78. doi:10.1016/j.drug.2015.08.004. PMID:26341193
48. Niikura K. Vacuolar ATPase as a drug discovery target. *Drug News. Perspect.* **2006**;19(3):139–44. doi:10.1358/dnp.2006.19.3.977442. PMID:16804565
49. Ferrari S, Perut F, Fagioli F, Brach Del Prever A, Meazza C, Parafioriti A, Picci P, Gambarotti M, Avnet S, Baldini N, et al. Proton pump inhibitor chemosensitization in human osteosarcoma: from the bench to the patients' bed. *J. Transl. Med.* **2013**;11:268-5876-11-268. doi:10.1186/1479-5876-11-268.
50. Toro EJ, Ostrov DA, Wronski TJ, Holliday LS. Rational identification of enoxacin as a novel V-ATPase-directed osteoclast inhibitor. *Curr. Protein Pept. Sci.* **2012**;13(2):180–91. doi:10.2174/138920312800493151. PMID:22044158
51. Wang SP, Krits I, Bai S, Lee BS. Regulation of enhanced vacuolar H⁺-ATPase expression in macrophages. *Biol. Chem.* **2002**;277(11):8827–34. doi:10.1074/jbc.M111959200.
52. Fan QM, Jing YY, Yu GF, Kou XR, Ye F, Gao L, Li R, Zhao QD, Yang Y, Lu ZH, et al. Tumor-associated macrophages promote cancer stem cell-like properties via transforming growth factor-beta1-induced epithelial-mesenchymal transition in hepatocellular carcinoma. *Cancer Lett.* **2014**;352(2):160–8. doi:10.1016/j.canlet.2014.05.008. PMID:24892648
53. Yeung OW, Lo CM, Ling CC, Qi X, Geng W, Li CX, Ng KT, Forbes SJ, Guan XY, Poon RT, et al. Alternatively activated (M2) macrophages promote tumor growth and invasiveness in hepatocellular carcinoma. *J. Hepatol.* **2015**;62(3):607–16. doi:10.1016/j.jhep.2014.10.029. PMID:25450711
54. Chao M, Wu H, Jin K, Li B, Wu J, Zhang G, Yang G, Hu X. A non-randomized cohort and a randomized study of local control of large hepatocarcinoma by targeting intratumoral lactic acidosis. *Elife* **2016**;e15691. doi:10.7554/eLife.15691. doi:10.7554/eLife.15691.
55. Pilon-Thomas S, Kodumudi KN, El-Kenawi AE, Russell S, Weber AM, Luddy K, Damaghi M, Wojtkowiak JW, Mule JJ, Ibrahim-Hashim A, et al. Neutralization of Tumor Acidity Improves Antitumor Responses to Immunotherapy. *Cancer Res.* **2016**;76(6):1381–90. doi:10.1158/0008-5472.CAN-15-1743. PMID:26719539
56. Gebhardt C, Sevko A, Jiang H, Lichtenberger R, Reith M, Tarnanidis K, Holland-Letz T, Umansky L, Beckhove P, Sucker A, et al. Myeloid Cells and Related Chronic Inflammatory Factors as Novel Predictive Markers in Melanoma Treatment with Ipilimumab. *Clin. Cancer Res.* **2015**;21(24):5453–59. doi:10.1158/1078-0432.CCR-15-0676. PMID:26289067
57. Antonios JP, Soto H, Everson RG, Moughon D, Orpilla JR, Shin NP, Sedighim S, Treger J, Odesa S, Tucker A, et al. Immunosuppressive tumor-infiltrating myeloid cells mediate adaptive immune resistance via a PD-1/PD-L1 mechanism in glioblastoma. *Neuro Oncol.* **2017**;19(6):796–807. doi:10.1093/neuonc/now287. PMID:28115578

SUPPLEMENTARY MATERIALS

SUPPLEMENTARY MATERIALS AND METHODS

RNA extraction, reverse transcription and quantitative real-time PCR

To maintain RNA integrity and to enhance the yield, the specimens were placed in liquid nitrogen and then homogenized with a TissueLyser Homogenizer (Qiagen) in the presence of lysis buffer ML (provided in the NucleoSpin miRNA kits) and tungsten carbide beads (Qiagen) for 2 min at a frequency of 30/sec. After the addition of ethanol, DNA and RNA were bound to the NucleoSpin RNA columns. The DNA was digested on the columns by RNase-free recombinant DNase. Subsequently, RNA was washed and eluted with RNase-free water. The purity of the RNA samples was assessed by measuring the OD₂₆₀/OD₂₈₀ ratio on a Picodrop spectrometer (Picodrop). A ratio of 1.8-2.0 was generally accepted as “pure” for RNA in all cases. The reverse transcription polymerase chain reaction (RT-PCR) was conducted in the GeneAmp PCR System 9700 instrument (Thermo Fisher Scientific) using the following settings: 25 °C for 10 min and 60 °C for 120 min. cDNA obtained from the HCC tissue explants was pre-amplified using the TaqMan[®] Preamp Master Mix Kit (Thermo Fisher Scientific) by combining 188 ng cDNA with TaqMan[®] Preamp Master Mix and pooling the TaqMan[®] gene expression assays (Thermo Fisher Scientific) at a final concentration of 0.2X, according to the manufacturer’s instructions. qRT-PCR assays were run in the ABI 7900HT instrument (Thermo Fisher Scientific) with the standard qRT-PCR settings: 50 °C for 2 min, 95 °C for 10 min, and 40 cycles of 95 °C for 15 s and 60 °C for 1 min. The relative levels of templates in each sample were determined through relative quantification (RQ) using the comparative Ct ($\Delta\Delta CT$) method ($RQ=2^{-\Delta\Delta CT}$, where $\Delta CT=CT_{\text{target gene}}-CT_{\text{GAPDH}}$, and $\Delta\Delta CT=\Delta CT_{\text{sample}} - \Delta CT_{\text{calibrator}}$).

Immunohistochemistry

After xylene deparaffinization and rehydration, the sections were incubated in a 3% H₂O₂ solution for 10 min to block endogenous peroxidase. Antigen retrieval was performed by heating the sample in 1 mM EDTA at pH 8 or 5 mM citrate buffer solution in a high-pressure cooker for 10-15 or 20 min and cooled for 15 min prior to immunostaining. A peroxidase-labeled polymer (UltraVision Quanto Detection System HRP Polymer, Thermo Fisher Scientific) was used for detection according to the manufacturer's instructions and was visualized using 3,3'-diaminobenzidinetetrahydrochloride (DAB)/H₂O₂. The immunostaining intensity was evaluated with a scoring system performed by the pathologist (MM). The intensity (I) of the nuclear or membrane/cytoplasmic staining was scored as I = 0 negative, I = 1 lower than the internal or experimental control, and I = 2 equal to the internal or experimental control. The extent of the cell staining was scored as 0 (0-<5%), 1 (<10%), 2 (10-50%), and 3 (>50%). The score categories are shown in Table 2.

Confocal analysis

Serial sections of 1-2- μ m-thick FFPE paired tumor and adjacent non-tumor liver tissues (n = 3) and breast cancer tissues (n = 3) were processed for deparaffinization and antigen retrieval. The HCC cell lines (C3A, PLC/PRF/5 and SNU-449) were fixed in 4% paraformaldehyde for 30 min, washed with 1x PBS and plated on glass slides. The samples were washed and incubated for 1 h with dye-conjugated secondary antibodies (see Supplementary Table S3). The sections were treated briefly with 0.1 M glycine in PBS, pH 7.4 followed by 0.3% Triton X-100 in 1x PBS (Sigma-Aldrich) and incubated overnight at 4 °C with the primary antibodies. Following a final wash, the stained tissue sections were mounted on glass slides with 95% glycerol in 1x PBS.

Pharmacological inhibitors and cell viability assays

The tested concentrations of the CAIX inhibitor S4 were 12.5 μM , 25 μM , 50 μM and 100 μM . The CAXII inhibitor compound 25 was used at concentrations of 12.5 μM , 25 μM , 50 μM , 100 μM and 200 μM , while omeprazole was used at concentrations of 72.4 μM , 144.8 μM , 299.5 μM and 434.3 μM . As a pro-drug, omeprazole was activated in acidified water at pH = 3.7 for 30 min at RT in the dark prior to use. The effects of both CA inhibitors and activated omeprazole were tested. As a vehicle control, cells were treated with respective volumes of DMSO using the same approach. Treatment with CA inhibitors was performed under normoxia (21% O₂) and hypoxia (1% O₂). Treatment with omeprazole was performed under normoxia (21% O₂) only. Cell viability assay: briefly, in each well, 50 μl of conditioned medium was replaced with 50 μl pre-warmed MTT solution (Sigma-Aldrich), and the plates were incubated at 37 °C for 2 h. When the purple precipitate of formazan crystals was clearly visible under the microscope, the total volume of each well was discarded by aspiration. Subsequently, 100 μl detergent solution was added to all the wells, and the plates were covered and incubated at RT on a shaker for 10 min in the dark.

Cell proliferation assay

Cell proliferation was assessed using a BrdU Cell Proliferation Assay Kit (Cell Signaling). The cells were seeded at 4×10^3 cells/well in a 96-well plate and incubated overnight at 37 °C. Cells were then treated with either 100 μM CAIX inhibitor (S4), 200 μM CAXII inhibitor (25), 100 $\mu\text{g/ml}$ omeprazole or 5 μM doxorubicin for 48 h. Finally, 10 μM BrdU was added to the plate, cells were incubated for 4 h at 37 °C, and cell proliferation was assessed following the manufacturer's instruction. The assay was carried out under normoxia (21% O₂). The optical density was recorded using Infinite[®] M1000 (Tecan) at a reference wavelength of 450 nm.

Apoptosis assays

The cells were seeded at 8×10^5 cells/well in a T-75 cm² flask (Corning) and incubated overnight at 37 °C. Cells were then treated with either 100 μM CAIX inhibitor (S4) or 1 μM staurosporine for 24 h. Cell apoptosis was detected using a Caspase-3 Apoptosis Kit (Becton Dickinson) by a Gallios flow cytometer (Beckman Coulter) and analyzed by FlowJo, V 8.5.2 (Tree Star).

Caspase 3/7 activity was determined using a Caspase-Glo 3/7 assay kit (Promega, UK) according to the manufacturer's protocol. Briefly, the cells at 4×10^3 cells/well in an opaque-walled 96-well plate were incubated overnight at 37 °C. The cells were then treated with either 100 μM CAIX inhibitor (S4), 200 μM CAXII inhibitor (25), 100 μg/ml omeprazole or 1 μM staurosporine for 24 h. Then, 100 μl Caspase-Glo 3/7 reagent was added to the wells. The plates were gently shaken and then incubated in the dark at 37 °C. The generated luminescent signals were measured by Infinite[®] M1000 (Tecan). The apoptotic assays were performed under normoxia (21% O₂).

Necrosis assay

Necrosis induction was evaluated using the RealTime-Glo Annexin V Apoptosis and Necrosis Assay (Promega) according to the manufacturer's instructions. Briefly, the cells were seeded at 10×10^3 cells/well in an opaque-walled 96-well plate and incubated overnight at 37 °C. The cells were then treated with either 100 μM CAIX inhibitor (S4), 200 μM CAXII inhibitor (25), 100 μg/ml omeprazole or 50 μg/ml digitonin and, at the same time, 100 μl 2X Detection reagent was added. The plates were incubated in the dark at 37 °C. The assay was carried out under normoxia (21% O₂). This assay is based on a fluorescent dye that is internalized in the cells when the cell membrane is compromised. The generated fluorescent signals at 485nm_{EX}/530nm_{EM} were measured by Infinite[®] M1000 (Tecan) after 48 h and 72 h of treatment.

HCC tumor dissociation

HCC tissues were enzymatically and mechanically digested using the gentleMACS Dissociator (Miltenyi). Briefly, tumor specimens were minced under sterile conditions into small pieces and digested for 1 h at 37 °C following the gentleMACS Dissociator protocol (Miltenyi). The obtained cell suspension was filtered through a 70- μ m mesh (BD Biosciences), the red blood cells were lysed, and the cell suspension was washed with RPMI 1640. The cells were stored in liquid nitrogen until use.

Western blotting

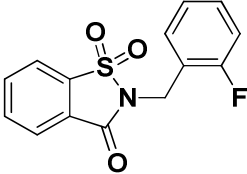
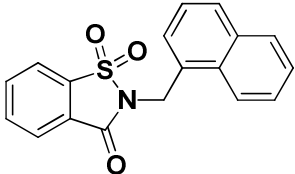
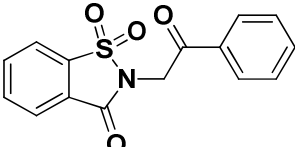
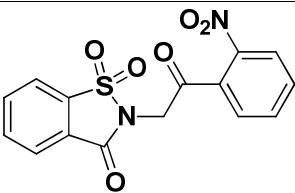
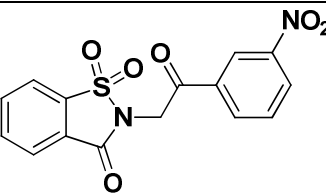
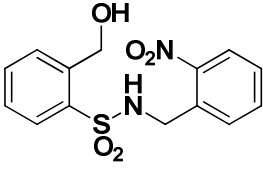
HCC cell lines exposed to either normoxia (21% O₂) or hypoxia (1% O₂) were lysed in modified RIPA buffer (20 mM Tris-HCl, pH 7.4, 150 mM NaCl, 5 mM EDTA, 1% Nonidet P-40) in the presence of protease Inhibitors (Roche), 1 mM Na₃VO₄ and 1 mM PMSF. Protein samples were boiled in NuPAGE LDS sample buffer (Invitrogen) and separated on NuPAGE Novex 10% Bis-Tris gels (Invitrogen) in MES running buffer (Invitrogen), and then transferred onto nitrocellulose filters and immunoblotted with the appropriate antibodies. The monoclonal mouse anti-human antibodies were directed against the following antigens: CAIX (clone M75, IgG2b, 1:2000 dilution, BioScience), vinculin (1:10000 dilution, cat. no.: V4505, Sigma-Aldrich) and α -tubulin (1:6000 dilution, cat. no.: T5168, Sigma-Aldrich). Rabbit monoclonal anti-human antibodies were directed against the following antigens: CAXII (clone D75C6, IgG, 1:500 dilution, cat. no.: 5864, Cell Signaling), β -actin (1:1000 dilution, cat. no.: A2066, Sigma-Aldrich), V-type proton ATPase subunit a isoform 1 (1:1000, cat. no.: HPA022144, Sigma-Aldrich), and V-type proton ATPase subunit C isoform 1 (1:1000, cat. no.: HPA023943, Sigma-Aldrich). The immuno-reactive bands were visualized using horseradish peroxidase (HRP)-conjugated secondary antibodies (Sigma-Aldrich), and the intensity of the signal was evaluated after incubation of the membranes with the HRP substrate (ECL Western Blotting Detection

Reagent, Amersham) followed by exposure of the membranes to autoradiography film (Hyperfilm MP, Amersham Biosciences) and development using an automatic developer (Curix 60, AGFA).

Statistical analysis

Statistical analyses were performed with GraphPad Prism Software (GraphPad). Spearman correlation analysis was performed on gene expression data ($\Delta Ct = Ct_{\text{target gene}} - Ct_{\text{GAPDH}}$) for *HIF1A*, *CA9*, *ATP6V0A1*, *ATP6VIC1* and *ATP6VIH* in 57 liver tissues analyzed by qRT-PCR. One-way analysis of variance (ANOVA) followed by Dunnett correction was used to evaluate the statistical significance of the impact of S4, compound 25 and omeprazole on cell viability, BrdU incorporation, apoptosis and necrosis.

SUPPLEMENTARY TABLES

Table S1. Chemical details of selective CAXII inhibitors				
Compound ^a	Structure	FW	<i>K_i</i> (nM)	
			hCA IX	hCA XII
12		291.30	> 50 000	2 520
16		323.37	> 50 000	2 540
18		301.32	> 50 000	1 780
19		346.31	> 50 000	970
20		346.31	> 50 000	2 010
25		322.34	> 50 000	250

Note: ^a These compounds were provided by Professor CT Supuran's group; solubility in DMSO. FW: formula weight.

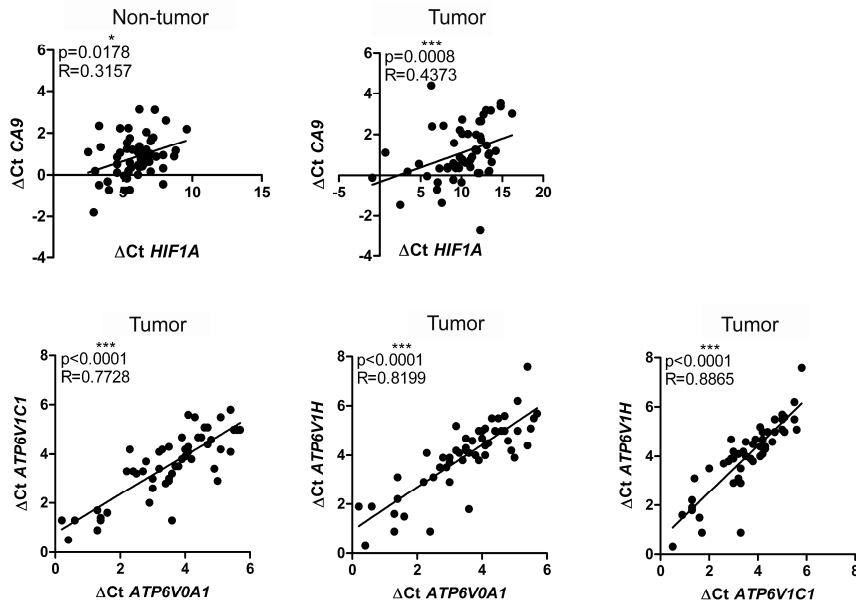
Table S2. Panel of gene expression assays					
Gene name	Gene symbol	RefSeq (NM)	Assay ID^a	Amplicon length	Protein name
ATPase H+ transporting V0 subunit a1	<i>ATP6V0A1</i>	NM_001130020.1 NM_001130021.1 NM_005177.3	Hs00193110_m1	62	V-ATPase subunit a isoform 1
ATPase H+ transporting V1 subunit A1	<i>ATP6V1A1</i>	NM_001690.3	Hs01097169_m1	66	V-ATPase subunit A isoform 1
ATPase H+ transporting V1 subunit C1	<i>ATP6VIC1</i>	NM_001695.4	Hs00940702_m1	67	V-ATPase subunit C isoform 1
ATPase H+ transporting V1 subunit H	<i>ATP6VIH</i>	NM_015941.3 NM_213619.2 NM_213620.2	Hs00977521_m1	103	V-ATPase subunit H
cadherin 1	<i>CDH1</i>	NM_001317184.1 NM_001317185.1 NM_001317186.1 NM_004360.4	Hs01023894_m1	61	cadherin 1
carbonic anhydrase 9	<i>CA9</i>	NM_001216.2	Hs00154208_m1	78	CAIX
carbonic anhydrase 12	<i>CA12</i>	NM_001218.4 NM_206925.2	Hs01080902_m1	60	CAXII
c-c motif chemokine ligand 22	<i>CCL22</i>	NM_002990.4	Hs01574247_m1	88	C-C motif chemokine 22
glyceraldehyde-3-phosphate dehydrogenase	<i>GAPDH</i>	NM_001289746.1 NM_002046.5	Hs99999905_m1	122	Glyceraldehyde-3-phosphate dehydrogenase
interleukin 6	<i>IL6</i>	NM_000600.4	Hs00985639_m1	66	interleukin-6
interferon gamma	<i>IFNG</i>	NM_000619.2	Hs00989291_m1	73	Interferon gamma
v-myc avian myelocytomatosis viral oncogene homolog	<i>MYC</i>	NM_002467.4	Hs00153408_m1	107	Myc proto-oncogene protein
tumor necrosis factor	<i>TNF</i>	NM_000594.3	Hs00174128_m1		tumor necrosis factor
vimentin	<i>VIM</i>	NM_003380.3	Hs00958111_m1	65	vimentin
Note: ^a TaqMan [®] Gene Expression Assays purchased from Thermo Fisher Scientific					

Table S3. Antibodies used for immunohistochemistry (IHC)/immunofluorescence (IF) analysis					
Antibody	Clone	Isotype	Company	Dilution	Antigen retrieval
Primary antibodies:					
β-catenin	6B3	rabbit monoclonal IgG	Cell Signaling	1:200 IHC/1:20 IF	EDTA buffer 15 min
Calnexin	1C2.2D11	mouse monoclonal IgG2b k	Novus Biological	1:200 IF	EDTA buffer 15 min
CAIX	M75	mouse monoclonal IgG2b	BioScience	1:100 IHC	EDTA buffer 15 min
CAXII	D-2	mouse monoclonal IgG1	Santa Cruz Biotechnology	1:50 IHC/1:5 IF	EDTA buffer 15 min
CD3	PS1	mouse monoclonal IgG2a	Abcam	1:50 IHC/1:10 IF	Citrate buffer 15 min
CD14	7	mouse monoclonal IgG2a	Thermo Fisher Scientific	1:50 IHC	EDTA buffer 20 min
CD34	QBEnd-10	mouse monoclonal IgG1	Dako	1:100 IHC	Citrate buffer 15 min
CD68	KP1	mouse monoclonal IgG1 k	Leica Microsystems	1:200 IHC	EDTA buffer 10 min
CD163	10D6	mouse monoclonal IgG1	Leica Microsystems	1:100 IHC/1:10 IF	Citrate buffer 15 min
CD209	DCN46	mouse monoclonal IgG2b	BD	1:20 IHC/1:10 IF	Citrate buffer 15 min
V- ATPase subunit a isoform 1	/	rabbit polyclonal	Sigma-Aldrich	1:200 IHC/1:20 IF	EDTA and Triton buffer 15 min
V- ATPase subunit C isoform 1	/	rabbit polyclonal	Sigma-Aldrich	1:200 IHC	EDTA buffer 15 min
V- ATPase subunit H	/	rabbit polyclonal	Novus Biological	1:50 IHC/IF	EDTA buffer 15 min
Note: /, not available					

Table S4. Flow cytometry antibodies				
Marker	Clone	Isotype		Company
CAIX	M75	mouse	monoclonal	BioScience
		IgG2b		
CAXII	D-2	rabbit	monoclonal IgG	Cell Signaling
CCL22	57203	mouse	monoclonal	R&D Systems
		IgG2b		
CD3	UCHT1	mouse	monoclonal IgG1	Beckman Coulter
CD11b	Bear1	mouse	monoclonal IgG1	Beckman Coulter
CD14	MφP9	mouse	monoclonal	BD Biosciences
		IgG2b k		
CD45	H130	mouse	monoclonal IgG1	BD Biosciences
		k		
CD163	6H1/61	mouse	monoclonal IgG1	BD Biosciences
		k		
CD209	DCN46	mouse	monoclonal	BD Biosciences
		IgG2b		
IFNγ	4S.B3	mouse	monoclonal IgG1	Biolegend
TNF	Mab11	mouse	monoclonal IgG1	BD Biosciences
V-type proton ATPase subunit a isoform 1	/	rabbit	polyclonal	Santa Cruz Biotechnology
Secondary antibodies:				
goat anti-mouse	/	polyclonal	IgG	Dako
goat anti-rabbit	/	polyclonal	IgG H+L	Thermo Scientific Fisher
Note: /, not available				

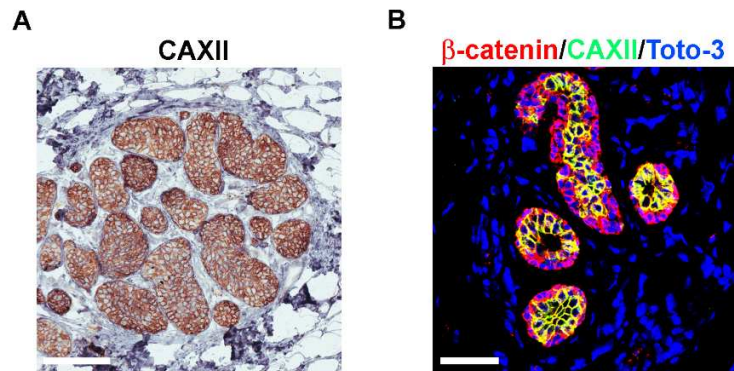
SUPPLEMENTARY FIGURES AND LEGENDS

Supplementary Figure S1



Supplementary Figure S1. Correlations between pH regulatory molecules under hypoxia in liver tissues. *HIF1A/CA9*, *ATP6V0A1/ATP6V1C1*, *ATP6V0A1/ATP6V1H* and *ATP6V1C1/ATP6V1H* correlations were analyzed by Spearman's correlation test in non-tumor and tumor liver tissues (n=57). The R values, Spearman's correlation coefficient, and p-values are reported.

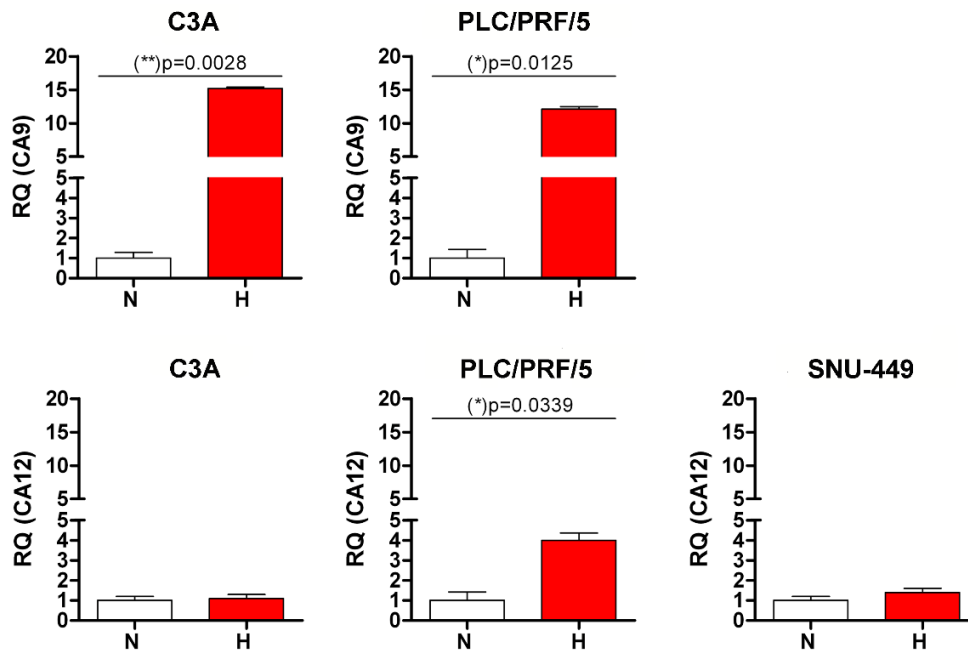
Supplementary Figure S2



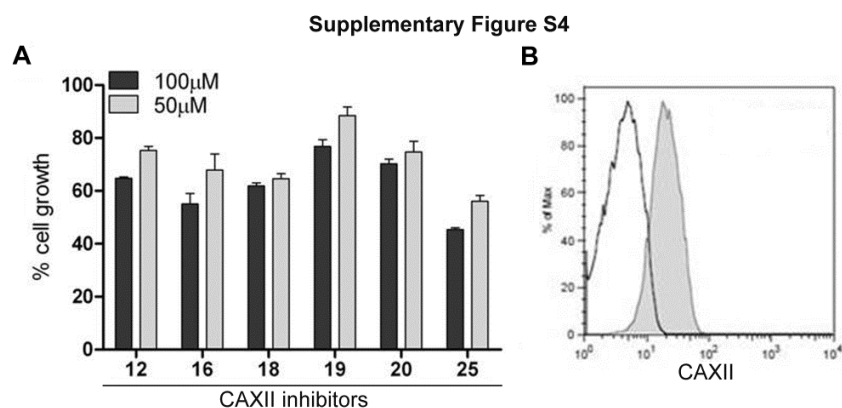
Supplementary Figure S2. Cell surface expression of CAXII in *in situ* breast cancer tissues.

(A) Immunohistochemical staining for CAXII expression in *in situ* breast cancer tissues. Membranous staining of CAXII was detected in breast tumor cells. Representative image with scale bar = 100 μm . (B) Confocal laser scanning micrographs of immunofluorescent staining with anti-CAXII (green) and anti- β -catenin (red). Nuclei were stained with Toto-3 (blue). CAXII co-localized with β -catenin in the membrane of breast tumor cells as indicated by the yellow staining. Representative image with scale bar = 50 μm .

Supplementary Figure S3



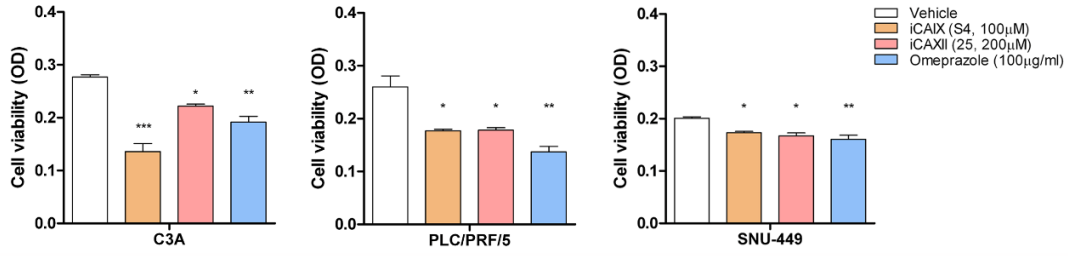
Supplementary Figure S3. Gene expression of CAIX and CAXII in HCC cell lines cultured under normoxic and hypoxic conditions. HCC cell lines were grown under normoxic (N=21% O₂) or hypoxic (H=1% O₂) conditions for 72 h. The mRNA levels of CA9 and CA12 were evaluated in the indicated HCC cell lines and reported as the relative quantity (RQ) using cells exposed to normoxia as calibrators. The p-values reported in the graphs were calculated using the paired t test.



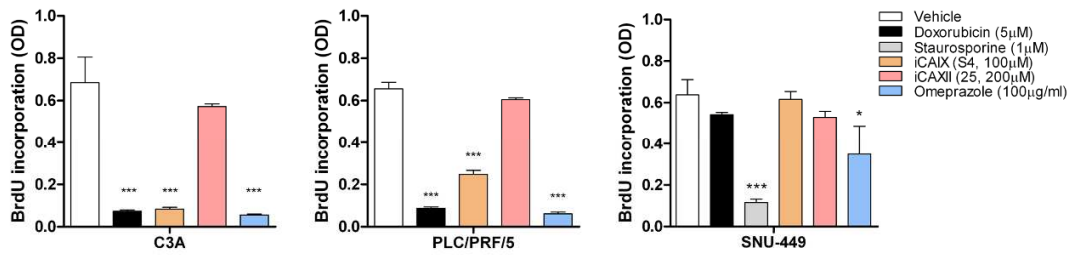
Supplementary Figure S4. CAXII expression and functional activity in the breast cancer cell line T-47D. (A) Screening of the biological activity of CAXII inhibitors in limiting the tumor growth of the T-47D cell line was assessed by the MTT assay. The T-47D cells were treated with 100 μ M (dark columns) and 50 μ M (gray columns) of the different CAXII inhibitors (compounds 12, 16, 18, 19, 20 and 25). The data are expressed as the mean values of six replicates. The chemical structures of these compounds are reported in Table S1. (B) The cell surface expression of CAXII was evaluated by flow cytometry in T-47D cells. Representative histograms from three independent experiments are shown.

Supplementary Figure S5

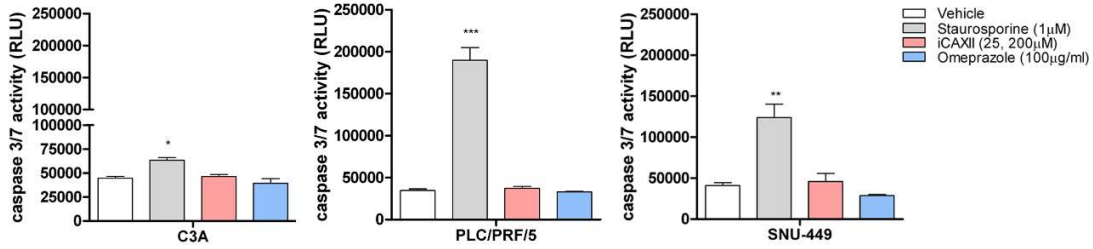
A



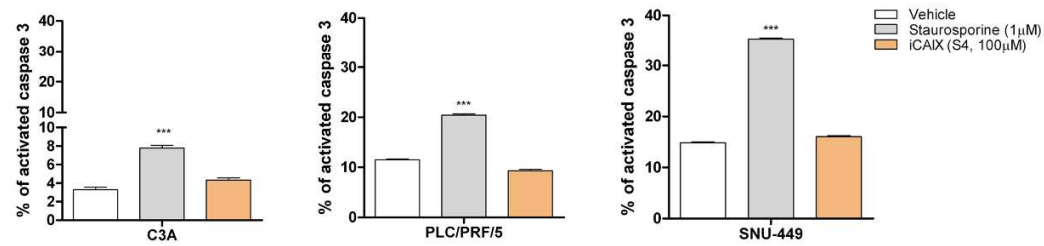
B



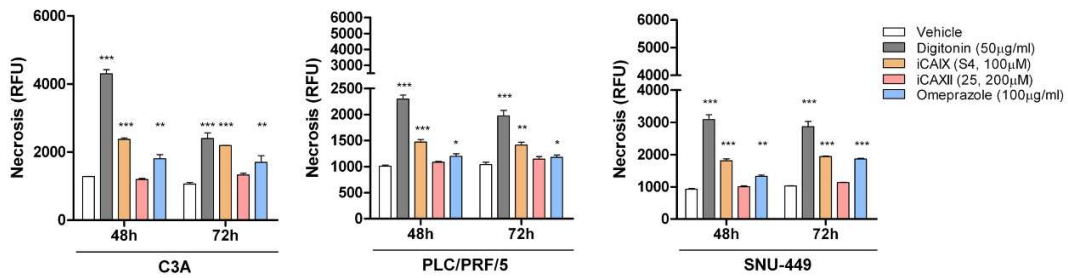
C



D



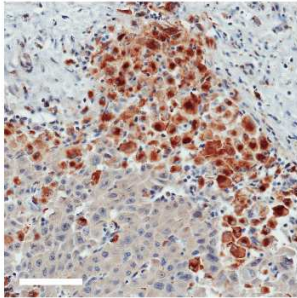
E



Supplementary Figure S5. Mechanisms of drug-induced cell death in HCC cell lines. HCC cell lines were exposed to either 100 μ M CAIX inhibitor (S4), 200 μ M CAXII inhibitor (compound 25) or 100 μ g/ml omeprazole and subjected to evaluation of **(A)** cell viability (MTT assay, OD: optical density), **(B)** proliferation (BrdU incorporation assay, OD: optical density), **(C)** apoptosis in compound 25 and omeprazole drug-treated cells (caspase 3/7 activity, RLU: relative luminescence units) and **(D)** apoptosis in S4-treated cells (percentage of cells positive for activated caspase 3 evaluated by flow cytometry). Measurement of caspase 3/7 activity was not feasible in S4-treated cells due to the interference of S4 with the enzymatic assay of the test. **(E)** Necrosis (fluorescence emission upon internalization of a specific dye, RFU: relative fluorescence units). Data are the mean of 3 replicates \pm SD. Cell viability, BrdU incorporation, apoptosis and necrosis were evaluated after 48 h, 24 h, 48 h and 72 h of drug treatment, respectively. As positive control compounds, 5 μ M doxorubicin, 1 μ M staurosporine and 50 μ g/ml digitonin were used to evaluate the BrdU incorporation, apoptosis and necrosis respectively. * p <0.05, ** p <0.01 and *** p <0.001 values were calculated using one-way analysis of variance (ANOVA) followed by Dunnett correction comparing cells treated with the drugs or the vehicle.

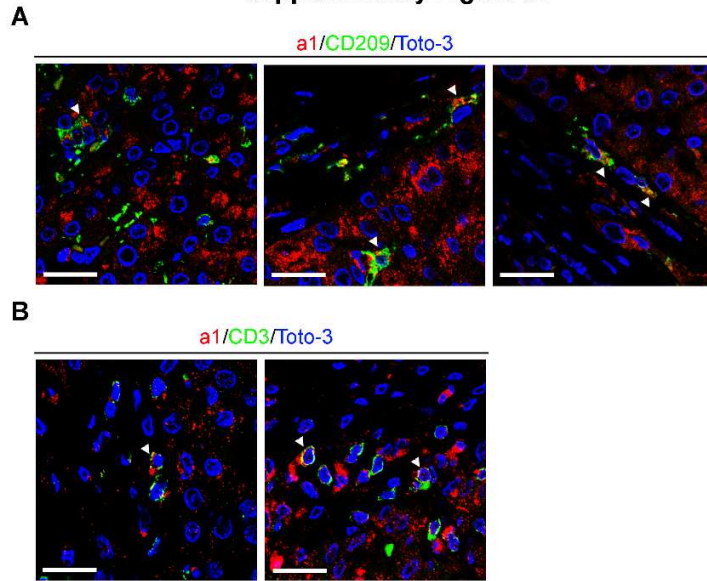
Supplementary Figure 6

H



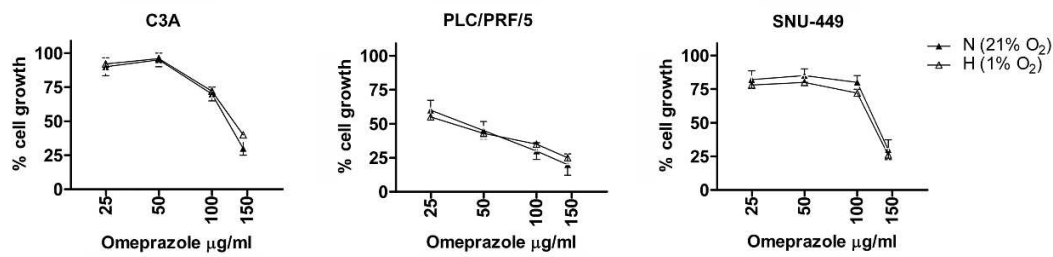
Supplementary Figure S6. Expression of V-ATPase subunit H in malignant hepatocytes of HCC. Representative immunohistochemical staining for the V-ATPase subunit H which was found in 4 of the 23 HCC tissues analyzed. The H subunit displayed an intracellular expression pattern, suggesting its accumulation in the Golgi of malignant hepatocytes. Scale bars=100 μ m.

Supplementary Figure S7



Supplementary Figure S7. Confocal microscopy of V-ATPase a1 in CD209⁺ myeloid cells and in CD3⁺ T cells. Immunofluorescence staining for a1 subunits of the V-ATPase complex (red), CD209 (green) (**A**) and CD3 (green) (**B**) of the HCC peri-tumor area. Nuclei were stained with Toto-3 (blue). Additional representative images of the case reported in Fig. 5 are reported here. White triangles indicate the co-expression of the analyzed markers. Scale bars=25 μ m.

Supplementary Figure S8



Supplementary Figure S8. Omeprazole treatment of HCC cell lines exposed to either normoxia or hypoxia. The HCC cell lines grown under normoxia (N=21% O₂, black triangles) or hypoxia (H=1% O₂, white triangles) were treated with different doses of omeprazole for 72 h. The cell viability was evaluated using the MTT assay. The data on the y-axes report the percentage of viable cells of the untreated control and represent the mean of 6 replicate reactions from 3 independent experiments.